The Hong Kong Polytechnic University

Department of Civil and Structural Engineering

THE CHARACTERISTICS AND SOURCE IDENTIFICATION OF AIRBORNE PARTICLES AT THE ROADSIDE OF HONG KONG - POLYU (PU) SUPERSITE

by:

CHENG Yan

A thesis submitted in partial fulfillment of the requirements for the Degree of Doctor of Philosophy

November, 2006

Certificate of Originality

I hereby declare that this thesis is my own work and that, to the best of my knowledge and belief, it reproduces no material previously published or written nor material which has been accepted for the award of any other degree or diploma, expect where due acknowledgement has been made in the text.

_____(Signed)

Cheng Yan _____(Name of student)

Abstract

With the rising environmental and resultant health awareness, there are increasing concerns on particulate emissions due to the continuously growing vehicle numbers and kilometers driven in Hong Kong. Thus, investigation on particulate emissions related to vehicles is needed in order to improve urban air quality. This thesis is aimed to explore the characteristics and sources of airborne particles in ultrafine (D_p<0.1 μm), fine (D_p<2.5 μm), and coarse (2.5 μm <D_p<10 μm) size ranges in the urban roadside environment.

Investigation on the chemical compositions and abundance of aerosols shows distinct differences between ultrafine, fine and coarse particles at PU (PolyU) Supersite, a typical roadside site with heavy traffic. Aerosol mass and number concentrations are studied in different scenarios (daily cycles, large-scale weather systems and aerosol episodes). Distinct variations are shown on a daily basis in the number concentrations of ultrafine particles. In addition, high number concentrations of ultrafine particles are found in winter and low in summer. The diurnal cycles of fine particle mass concentrations track the fluctuations of the local vehicle numbers, on the other hand, the seasonal cycles are influenced by East Asia monsoons, which bring pollutants from

upwind areas. For coarse particles, a good relationship is found between the hourly mean mass concentration and wind speed. The study of aerosol chemical compositions in each scenario indicates substantial variations for each fraction. Due to unfavorable synoptic systems, particulate episodes are observed in both summer and winter. The PSCF (Potential Source Contribution Function) receptor model identifies the coastal areas of southeastern China and the PRD (Pearl River Delta) region as the source areas of regional pollution in cold and warm seasons respectively.

By analyzing the emissions from vehicles in the Shing Mun tunnel, a higher emission rate for diesel-fueled vehicle and unique chemical profiles for vehicles with different fuels are found. To better understand the sources of particles at PU Supersite, various techniques, including OC/EC ratios, linear/multilinear regression, PMF (Positive Matrix Factorization) and CMB (Chemical Mass Balance) receptor model, are applied in this study. Vehicle exhaust is identified as the major source for both ultrafine and fine particles, while resuspensions being the main source for coarse particles. Regional-scale pollution is another important source for fine particles. The contributions from regional pollution can increase to nearly half of the total fine particulate mass when air masses are from Mainland China.

Publications

International journal

Cheng, Y., Lee, S. C., Ho, K. F., Wang, Y. Q., Cao, J. J., Chow, J. C., Watson, J. G. 2006. Black carbon measurement in a coastal area of South China, *Journal of Geophysical Research*, 111, D12310, doi:10.1029/2005JD006663.

Cheng, Y., Lee, S. C., Ho, K. F., Louie, P. K-K. 2006. On-road particulate matter ($PM_{2.5}$) and gaseous emissions in the Shing Mun tunnel, Hong Kong. *Atmospheric Environment*, 40 (23), 4235-4245.

Cheng, Y., Lee, S. C., Cao, J. J., Ho, K. F., Chow, J. C., Watson, J. G., and Ao, C. H. 2006. Elemental composition of airborne aerosols at a traffic site and a suburban site in Hong Kong. *International Journal of Environment and Pollution*, in press.

Lee, S. C., **Cheng, Y.**, Ho, K. F., Cao, J. J., Louie, P. K-K., Chow, J. C., and Watson, J. G. 2006. $PM_{1.0}$ and $PM_{2.5}$ characteristics in the roadside environment of Hong Kong. *Aerosol Science and Technology*, 40:157-165.

Ho, K. F., Ho, S. S. H., **Cheng, Y.**, Lee, S. C., and Yu, J. Z. 2007. Real-world emission of carbonyl compounds from a tunnel study in Hong Kong. *Atmospheric Environment*, 41 (8): 1747-1758.

Ho, K. F., Lee, S. C., Cao, J. J., Kawamura, K., Watanabe, T., **Cheng Y.** and Chow, J.

2006. Dicarboxylic acids, ketocarboxylic acids and dicarbonyls in the urban roadside area of Hong Kong. *Atmospheric Environment*, 40(17), 3030-3040.

Cao, J. J., Lee, S. C., Chow, J. C., **Cheng, Y.**, Ho, K. F., Fung, K., Liu, S. X., Watson, J. G. 2005. Indoor/outdoor relationships for $PM_{2.5}$ and associated carbonaceous pollutants at residential homes in Hong Kong. *Indoor Air*, 15 (3): 197-204.

Fang, G. C., Lee, S. C., Lee, W. J., **Cheng, Y.**, and Lin, I. C. 2007. Characteristics of carbonaceous aerosol at Taichung Harbor, Taiwan during summer and autumn period of 2005. *Environmental Monitoring and Assessment*, DOI 10.1007/s10661-006-9495-z.

Cheng, Y., Lee, S. C., Ho, K. F., Fung, K. Positive sampling artifacts in particulate organic carbon measurements in roadside environment. *Aerosol Science and Technology*, revised.

International conference paper

Cheng, Y., Lee, S. C. 2006. Ultrafine particle emissions near a heavily trafficked road in Hong Kong, *Healthy Buildings 2006*, Lisbon, Portugal, 3-8 June, 2006.

Cheng, Y., Lee, S. C. 2005. Atmospheric aerosols during pollution episodes in Hong Kong, *The International Association of Meteorology and Atmospheric Sciences 2005*, Beijing, China, 2-11 August, 2005.

Acknowledgements

I would like to express my sincere thanks to my supervisor, Prof. S. C. Lee, for his unanimous and sincere support and supervision throughout this project. Without his guidance and advice, the completion of this thesis would be unachievable. Dr. L. Y. Chan, my co-supervisor, is also acknowledged for his support and valuable comments. Thanks go to our laboratory technician, Mr. W. F. Tam, his technical support is invaluable. Sincere gratitude is expressed for the precious suggestions of Dr. J. C. Chow, Dr. J. G. Watson, Dr. P. K. K. Louie, Dr. K. F. Ho and Dr. J. J. Cao towards completing this project. Finally, I would like to express my deepest appreciation to my parents and husband, for their understanding, support and encouragement during the last three years.

Table of Contents

List of Figures

List of Tables

Chapter 1 Introduction

1.1 Background information of air quality in Hong Kong

On-road emission is a major source of air pollution in mega-cities. Among those emissions, particulate matter (PM) is one of the major pollutants present in vehicle exhausts and urban air (MAGE et al. 1996). In addition to the minor sources from ambient areas, on-road emissions occur in three categories: (i) vehicle exhausts (both fuel and lubricating oil combustion); (ii) vehicle-related particles from tire and brake wear, and (iii) fugitive dust from paved and unpaved dust caused by the vehicle-generated turbulence and winds. PM adversely affects human health through the cardiovascular and respiratory systems and is associated with premature mortality as well as sickness (http://www.epa.gov/).

As a result of city development and urbanization, Hong Kong has been experiencing serious air pollution problems for decades. These problems are largely due to high emission motor vehicles that are coupled with high kilometer traveled. There were 540641 licensed vehicles in Hong Kong at the end of 2005 (The Annual Traffic Census, 2005), representing an increase of 16% when compared with the corresponding figure in 1995. New vehicles are added each year to the existing large

vehicle population and the inadequate street and roadways networks. The vehicle density in Hong Kong has ranked one of the highest in the world, with 540641 vehicles on only 1900 km of road.

Hong Kong is one of the most populated cities in Asia, containing seven million people within its 1100 km^2 of territory. Consequently, streets with heavy traffic are close to public and buildings. The on-road pollutants are often trapped in between the very tall buildings along the streets, indicating poor dispersion of pollutants and high human exposure. Thus, particulate matters associated with vehicles pose risks to the environment and human health in Hong Kong.

Although the Government has been working for years to control emissions from motor vehicles, improvements from those measures have tended to be offset by the increasing emission levels from the continuously growing vehicle numbers and kilometers driven. Nonetheless, there has been limited air quality studies related to real-world emissions at the roadside environment in Hong Kong.

Besides the particulate matter due to local vehicles, the regional or remote pollution can also influence air quality in Hong Kong because of its location and climate scheme. The PM_{10} concentrations in urban ambient areas of Hong Kong have shown a primarily downward trend between 1995 and 2002 but have rebounded afterwards

(The Annual Air Quality Report, 2004). Such territory-wide rise in PM_{10} concentrations reflects an increase in regional background PM_{10} levels in recent years.

1.2 The location of Hong Kong and the climate scheme

Hong Kong is located on the southeastern coast of the Asian continent with marked spatial variations in relief and topography. Surrounding Hong Kong's east and south sides is the South China Sea, the PRD region on the northwest, and mainland China to its north (Figure 1.1). There are few industries inside the territory of Hong Kong since the industries have been moved to the PRD region. Only a few fossil-fuel fired power plants are located in the south edge of Hong Kong Island and the northwest of Kowloon Peninsula.

The climate of Hong Kong is governed by the East Asia monsoons, and it is dominated by the Asian continental high pressure system, which builds up in the autumn and winter, collapses in the spring and then become a low-pressure system in the summer (Chin, 1986). This seasonal cycle of wind fields gives rise to a marked alteration in the properties of the air masses reaching Hong Kong. During the autumn and winter, a northwesterly wind prevails in north China, Korea and Japan while a northeasterly wind prevails in South China, South China Sea and Hong Kong. The cool and dry air masses that originate from the Asian continent as far as Siberia

usually travel over the Asian continent. Therefore, the air masses carry a number of continental pollutants during its transport to downwind area, like Hong Kong and the South China Sea. In summer, the southwesterly wind becomes the prevalent wind in South China, South China Sea and Hong Kong. The warm and humid marine air masses that originate from the South China Sea are carried to Hong Kong by a southwesterly wind, bringing clean air to Hong Kong. Moreover, spring is the season where the northeasterly monsoon changes into southwesterly monsoon.

1.3 Limitation of previous PM studies in Hong Kong

The air quality standards must protect human health. However, the current standards of air quality in Hong Kong are for the Total Suspended Particulates (TSP) and Respirable Suspended Particulates (RSP/PM_{10}, particles with aerodynamic diameter less than 10 μm), which do not provide a total picture of human exposure to pollution and the effects of exposure on health and welfare since fine particles (or $PM_{2.5}$, particles with aerodynamic diameter less than 2.5 μm) have closer relationship with health effect when compared with coarse particles (or PM_{coarse}, particles with aerodynamic diameters between 2.5 and 10 μm).

Previously, individual aerosol studies in Hong Kong include the studies on chemical characteristics of 24-hr integrated TSP, PM_{10}, and $PM_{2.5}$ (e.g., Qin et al. 1997; Lam et

al. 1999; Cheng et al. 2000; Zheng et al. 2000), and a few studies on mass size distribution (e.g., Zhuang et al. 1999a,b; Yu et al. 2004a). The main research fields have focused on temporal and spatial variations of PM in ambient areas of Hong Kong (e.g., Qin et al. 1997; Lam et al. 1999; Cao et al. 2003; Louie et al. 2002; 2005a), but few characterize the PM at a source-dominated site, namely the roadside environment. Obtaining city-specific data related to on-road vehicles is important since the fundamental knowledge on particles near sources can help us to better understand of the factors that influence air qualities, and further find a solution to particulate pollutions. In addition, the size range over the impactors operating in the studies of the size distribution does not extend to the very small sizes, such as ultrafine particles (or $PM_{0.1}$, particles with aerodynamic diameters less than 0.1 μm), which have strong effects on human health even in a low concentration (Ferin et al. 1992; Oberdörster et al. 1995; Donaldson et al. 1998; Oberdörster et al. 2001). Finally, source profiles for different air pollutant sources are still unavailable for Hong Kong, which are needed for the purpose of source identification in ambient particulate pollution.

1.4 Objectives

To fill in those gaps mentioned above, the main objectives in this thesis were to:

1. Explore the characteristics of particulate matters at PU Supersite through the

measurements of the ultrafine particles, $PM_{2.5}$, PM_{10}, and PM_{coarse}, and size distribution of particle mass;

2. Understand the particulate origin and regular evolution on a daily and seasonal basis;
3. Evaluate the changes of particles in chemical compositions during pollution episodes and identify the source areas for the long-range-transported pollution;
4. Determine the emission factors and chemical profiles of fine particles for vehicles with different fuels;
5. Apportion source contributions for fine and coarse particles observed at PU Supersite using PMF and CMB receptor model.

The objectives of this study have been introduced above. In the next chapter, the background literature will be reviewed and then the subject methodology will be explained. Chapters 4 and 6 in particular will report the results of the investigation of the chemical and physical characteristics of particles in various size fractions. The pollution episodes will be studied in Chapter 5. The emission factors and chemical profiles of vehicle emissions will be presented in Chapter 7, followed by the estimation of various source contributions for fine and coarse particles in the next chapter. Finally, the thesis will end with a brief conclusion.

Chapter 2 Literature Review

In this chapter the background literature on particulate emissions will be discussed. First I will look at the nature of atmospheric particles, followed by a description of tunnel studies and modeling. The chapter ends with a brief discussion of previous investigations of aerosol.

2.1 Physics and chemistry of atmospheric particles

Airborne particles, a mixture of solid particles and liquid droplets found in the air (http://www.epa.gov), are also called PM in scientific communities. PM includes dust, dirt, soot, smoke, and liquid droplets. They embrace a very wide range of sizes, the smallest being only a few nanometers in diameter whilst the largest range up to more than 100 μm in diameter. Particles can be suspended in the air for long periods of time and are present in virtually all tropospheric air masses.

Knowledge of the physical and chemical properties of particles in the urban area is important because of its role in climate change and health effects on human beings. Particles can be characterized by their physical properties, such as size, shape, color, number, gas/particle phase equilibrium, as well as be classified by chemical characterizations, e.g. chemical composition and origin. TSP, PM_{10}, PM_{coarse}, $PM_{2.5}$

and $PM_{1.0}$ commonly are used in scientific communities.

2.1.1 Air quality standards for particulate matter

In recognition of the important role of particles to human health, the US Environmental Protection Agency (EPA) established the national ambient air quality standards for PM_{10} in 1987 and for $PM_{2.5}$ in 1997 (http://www.epa.gov). The long-term standard specifies an expected annual arithmetic mean not to exceed 15 $\mu g\ m^{-3}$ averaged over three years for $PM_{2.5}$. Due to a lack of evidence linking health problems to long-term exposure to coarse particle pollution, the agency revoked the annual PM_{10} standard in 2006 (effective December 17, 2006). The short-term (24-hr) standard of 150 $\mu g\ m^{-3}$ for PM_{10} and 35 $\mu g\ m^{-3}$ for $PM_{2.5}$ is not to be exceeded more than once per year on an average over three years. TSP, PM_{10}, and $PM_{2.5}$ are widely monitored by air quality agencies in recent years. Over the next few months, the US EPA will be finalizing its proposal to revise the NAAQS for fine and coarse particulate matter in recognition of different health effects that may be associated with different particle components.

To protect Hong Kong's air quality, in 1989, the entire territory was declared as air control zones with a set of Air Quality Objectives (AQOs) for seven pollutants. TSP and RSP were included as two air standards. The AQOs set target concentrations for

these pollutants at levels which are consistent with international health standards. The annual AQOs are 80 μg m^{-3} for TSP and for 55 μg m^{-3} RSP; the 24-hr AQOs are 260 μg m^{-3} for TSP and 180 μg m^{-3} for RSP.

2.1.2 Particle size

Particle size is the most important parameter for characterizing the behavior of aerosols. Not only do aerosol properties depend on particle size, but also the nature of the laws governing these properties may change with particle size. As measured by various investigators, particle size mass distributions usually show four typical modes: nucleation mode (e.g., Whitby, 1978; Fitzgerald et al. 1991; Oberdörster et al. 1995), ultrafine mode (e.g., Fitzgerald et al. 1991), accumulation mode (e.g., Willeke and Whitby, 1975; Meng and Seinfeld, 1994), and coarse mode (e.g., Seinfeld, 1986). The term of these three modes do not have a universally agreed definition but is widely accepted as describing particles of less than 0.05 μm in diameter, 0.1 μm, 0.1-1μm, and 2.5-100 μm, respectively. Nucleation, ultrafine and accumulation ranges constitute the “fine” particle size fraction (Harrison, 2004).

The “nucleation” range (Whitby, 1978; Fitzgerald et al. 1991; Oberdörster et al. 1995), consists of particles with diameters less than ~0.05 μm. Nucleation particles are typically fresh hydrocarbons or sulfate that are emitted directly from combustion

sources (Puxbaum and Wopenka, 1984) or that condense on primary particles from cooled gases soon after emission (Kittelson, 1998), or that freshly nucleate resulting from atmospheric reactions (Fitzgerald et al. 1991). The nucleation range is detected only when fresh emissions are close to a measurement site or when new particles have been recently formed in the atmosphere (Willeke and Whitby, 1975) since they will rapidly coagulate with larger particles or serve as nuclei for cloud or fog droplets (Rodhe et al. 1999; Facchini et al. 1999) in 1-2 hours after emission.

The “ultrafine” particles consist of particles with diameters less than 0.1 μm. Nucleation particles are the main proportion in ultrafine size range. Ultrafine particles typically dominate the particle number count, and make a significant contribution to surface area, but very little to mass (Fitzgerald et al. 1991). Due to their high number concentration, especially near their source, these small particles coagulate rapidly with each other and with particles in the accumulation mode. Similar to nuclei particles, ultrafine particles have relatively short lifetimes in the atmosphere and end up in the accumulation mode. The mode in the number distribution of ultrafine mode particles is typically ca. 20-30 nm in diameter (Harrison et al. 2000). Generally, direct emissions from vehicles and stationary fuel combustion sources have been considered the main sources of ultrafine particles in the urban atmosphere (Case et al. 2000). Few data are

available on the chemical composition of ultrafine particles due to the fact that the chemical characterization of submicron aerosol particles is made difficult by the requirement to fractionate and collect sufficient aerosol mass for subsequent chemical analysis. An earlier investigation was conducted near a street with heavy traffic in Vienna by Puxbaum and Wopenka (1984), showing a clear dominated peak in the nucleation mode size fraction for total carbon, Pb, and Br^-. More detailed measurements (Cass et al. 2000) for chemical composition of ultrafine particles in seven Southern California cities show that ultrafine particle concentrations in the size range of 0.056-0.1 μm average 0.55-1.16 μg m^{-3}. The chemical composition of these ultrafine particle samples averages 50% organic compounds, 14% trace metal oxides, 8.7% elemental carbon, 8.2% sulphate, 6.8% nitrate, 3.7% ammonium ion (excluding one outlier), 0.6% sodium and 0.5% chloride. The most abundant catalytic metal measured in the ultrafine particles is Fe. A source emissions inventory constructed for the South Coast Air Basin that surrounds Los Angeles shows a primary ultrafine particle emissions rate of 13 tonnes per day.

The “accumulation” range consists of particles with diameters between 0.1 and l μm (Willeke and Whitby, 1975; Meng and Seinfeld, 1994). These particles originate from the coagulation of smaller particles emitted from: (i) combustion sources, (ii)

gas-to-particle conversion, (iii) condensation of volatile species, and (iv) finely ground dust particles. Accumulation mode particles are subject to rather inefficient loss from the atmosphere by wet and dry deposition processes and are of primary importance for potential toxicity of species present in urban aerosols due to the surface adsorption or condensation that promotes toxicity (Natusch and Wallace, 1974). Particles in this mode are not subject to significant further growth through coagulation because of low coagulation rates. They have an atmospheric lifetime of several days and can therefore travel over very long distances within the atmosphere. Particles can be removed by rainout or washout. The size range of the accumulation mode includes the wavelengths of visible light, and these particles account for most of the visibility effects of atmospheric aerosols. John et al. (1990) observed two modes in accumulation size ranges for nitrate, ammonium ion and sulfate size distributions measured in the Southern California air quality study. He interpreted the peak centered at ~0.2 μm as a "condensation" mode containing gas-phase reaction products, and the ~0.7 μm peak as a "droplet" mode resulting from growth by nucleation of particles in the smaller size ranges and by reactions that take place in water droplets. The terms of "condensation" and "droplet" were widely used afterwards. Recently, the bimodal character of the accumulation mode for mass, number concentration, and chemical-specific size

distributions was reported by several studies (Kerminen and Wexler, 1995; Hering et al. 1997). Meng and Seinfeld (1994) examined the mechanisms of formation of the droplet mode. They found that coagulation, secondary formation by condensation growth, or growth due to water accretion cannot explain the formation of the droplet mode particles, although activation of condensation mode particles to form fog or cloud drops followed by aqueous-phase chemistry and fog evaporation was shown to be a plausible mechanism for formation of the droplet mode (Blando and Turpin, 2000).

The coarse mode, corresponding to particles above 2 or 2.5 μm in diameter, is formed through mechanical attrition and disintegration processes such as the formation of sea spray from bubble bursting in the ocean and the wind-blown suspension of land surface dusts, soil, trash, pollen and spore and abrasion of leaves, tyres, brake linings. Because of their large size, the coarse particles readily settle out or impact on surfaces, thus their lifetime is rather short. There is comparatively little mass exchange between the fine mode and coarse mode. In the urban atmosphere, there is an inverse correlation between mass concentrations in the two modes. Low wind velocity reduces the concentration of windblown soil particles and high wind velocity does the opposite.

2.1.3 Particle number

The size distributions of particle number are quite different compared to mass distribution because of the cube dependence of volume and mass on diameter. Harrison, et al. (2000) showed that 10^9 particles of 10 nm diameter have the same mass as 1000 particles of 1 μm diameter or one particle of 10 μm diameter. Therefore quite a large number of particles in nuclei mode may represent only a small proportion of total particle mass, while several particles in coarse mode may occupy the majority of mass.

The typical average number concentration (3-500 nm) is 22000 cm^{-3} with an average mode size of 40 nm in a Pittsburgh urban area (Stainer et al. 2004). Rural number concentrations are a factor of 2-3 lower (on average) than the urban values. The patterns in number concentrations are influenced by the sources of particles (atmospheric nucleation, traffic, and other combustion sources). New particle formation from homogeneous nucleation is significant at a site far away from emitters.

The number concentration of particles, per log-diameter interval of the size distribution ($dN\ dlogDp^{-1}$), are shown on the y-axis; N is the particle number and Dp is the particle diameter. When data are plotted in this way, the area under the curve gives the number concentration of particles in that size range, given that the y-axis is

on a linear scale and the x-axis is on a log scale.

2.1.4 Major chemical composition and sources

The chemical components in particulate matter have been intensively investigated throughout the world. Most of the particulate mass in urban and non-urban areas can be explained by a combination of the five major chemical components (Solomon et al. 1989), including: carbonaceous material, sulfate, nitrate, ammonium soil-related material. Carbonaceous material comprises elemental carbon and organic matter. The organic matter is estimated by multiplying the measured concentration of organic carbon by a factor of 1.2-2.1, which varies with location, season, and time of day as the mix of organic compounds in the aerosols (Turpin and Lim, 2001). Sulfate, nitrate, and ammonium are the most common inorganic components that can be analyzed by ion chromatography. The thermodynamic equilibrium among atmospheric ammonium, sulfate, and nitrate has been an important problem since early 1980's. Soil-related material is the sum of soil-related oxides from elemental analyses by X-ray fluorescence. Sea salt was the most abundant aerosols in the marine atmosphere. Sometimes, it was found near coastal areas. Furthermore, a portion of the liquid water is generally present in the samples despite sample equilibration at round 40-50% relative humidity prior to weighing (Solomon et al. 1989). It is rarely measured but is

sometimes estimated.

Organic carbon (OC) and elemental carbon (EC) are the most abundant species in motor vehicle related emissions (e.g., tailpipe exhausts, brake and tire wear, and oil drips), accounting for ~80% of the total mass in real-world on-road measurements (Gilles et al. 2001). Particulate organic carbon is a component of particles emitted from incomplete combustion of organic materials, the degradation of carbon containing products such as vehicle tyres (Rogge et al. 1993a) and of vegetation (Rogge et al. 1993b), but it also can consist of secondary organic aerosol (SOA) formed through the condensation or sorption onto other particles of organic carbon gases (gas-phase degradation routes) in the atmosphere (Stern et al. 1987; Jones and Harrison, 2005). Sources of organic carbon gases may arise from the combustion of organic material, the evaporation of fuels, or the natural emission of volatile organic compounds from vegetation (Jones and Harrison, 2005). Both primary and secondary OC consist of hundreds of separate compounds that contain more than 20 carbon atoms (>C20), oxygen, and hydrogen, many of which are known to be toxic (i.e. PAHs, nitro-PAHs, etc.) (Schauer et al. 1996; Reisen and Arey, 2005). Therefore OC volatilizes and decomposes upon heating in an oxygen-free environment. While most of the primary organic carbons and all of secondary organic carbons are in particles

with diameter of less than accumulation size range (Pandis et al. 1993), degradation of any material is likely to give rise to particles with larger sizes than those resulting from combustion (Jones and Harrison, 2005). Certain fractions of particulate organic matter, especially those containing polycyclic aromatic hydrocarbons (PAHs), have a potential effect on human health since organic carbon aerosols have been shown to be mutagenic and carcinogenic in a number of bioassays and animal studies (Klingenberg and Winneke, 1990).

EC is black, often called “soot.” EC contains pure, graphitic carbon, but it also contains high molecular weight, dark-colored, non-volatile organic materials such as tar, biogenics, and coke, as a surface coating. EC is emitted from incomplete combustion, occurring in sources such as diesel engines (Hamilton and Mansfield, 1991; Hansen and Rosen, 1990; Gray and Cass, 1998; Heintzenberg and Winkler, 1984), biomass burning (Cachier et al. 1989; Kirchstetter et al. 2003), and the pyrolysis of biological material during combustion (Jones and Harrison, 2005). EC only combusts in the presence of oxygen and it comprises all visible-light absorbing carbon. Most elemental carbon exists in the accumulation mode. The lifetimes of elemental carbon range from 40 hours in rainy climates to well over 1 week in clean, dry regions (Ogren and Charlson, 1983). Although wet scavenging is likely to be the

dominant removal mechanism for EC (Ogren and Charlson, 1983), the effect is believed to depend on the extent to which the EC is coated with hygroscopic substances (Ogren et al. 1984). In other words, it depends on whether EC is an internal mixture or external mixture. An internal mixture is one where EC is physically in contact with other, perhaps more abundant, hygroscopic aerosol constituents (e.g., sulfates), with the other compounds dominating the physical and chemical properties of the EC-containing particles. External mixture defines EC physically isolated from other constituents, so that the properties of the EC-containing particles with respect to water are determined by EC alone (Ogren and Charlson, 1983).

Sulfate (SO_4^{2-}) is the most abundant inorganic component of the atmospheric aerosol. Primary emissions of sulfate arise from industries, production, vehicle exhausts, and use of sulfate minerals such as gypsum. In general, however, these represent only a small proportion of atmospheric sulfate, by far the major proportion arising from the oxidation of sulfur dioxide in the atmosphere (secondary aerosol) (Claes et al. 1998). The concentrations of sulfate in the atmosphere are strongly influenced by ambient temperature. Ammonium sulfate ($(NH_4)_2SO_4$), ammonium bisulfate (NH_4HSO_4), and sulfuric acid (H_2SO_4) are the most common forms of sulfate found in atmospheric particles, resulting from conversion of gases to particles. The conversion of gases to

particles fall into two groupings, either homogeneous reactions taking place in the gas phase, or heterogeneous processes in cloud, fog water or aerosol droplets phase with subsequent liquid phase oxidation (Claes et al. 1998). Sulfate, being essentially non-volatile, have a size distribution controlled by gas-phase diffusion, therefore it almost exclusively tends to accumulate in the smaller particles less than 2 μm in diameter (Bassett and Seinfeld, 1984). Bimodal distributions were found for sulfate in the accumulation mode by Hering and Friedlander (1982). The 0.17-0.25 um mode was ascribed to homogeneous gas phase reactions and the larger mode to the reaction of sulfur dioxide with pre-existing accumulation mode particles in liquid droplets (Hering and Friedlander, 1982). Sodium sulfate (Na_2SO_4) may be found in coastal areas where sulfuric acid has been neutralized by sodium chloride (NaCl) in sea salt.

Typically, nitrate (NO_3^-) is the second most abundant secondary aerosol component in polluted atmospheres. There is little primary particulate nitrate in the atmosphere other than close to industrial sources such as ammonium nitrate fertilizer works which can provide appreciable point sources. Generally, atmospheric nitrate arises from the oxidation of nitrogen dioxide to nitric acid which may either react reversibly with ammonia forming ammonium nitrate, or irreversibly with sodium chloride to form sodium nitrate (Claes et al. 1998). Ammonium nitrate (NH_4NO_3) is the most abundant

nitrate compound, occurring when ammonia or HNO_3 is introduced into an air parcel in amounts above that needed for the necessary concentration product of HNO_3 times NH_3 to equal the equilibrium dissociation constant for NH_4NO_3 (Russell et al. 1983). Bimodal distributions were found for NH_4NO_3 in the accumulation mode by Wall et al. (1988). Gas phase reaction of nitric acid with ammonia formed the 0.1-0.3 μm mode and reaction of nitric acid with pre-existing fine particles to form the 0.5-0.7 μm mode. Being more volatile than sulfate, in practice, it seems most unlikely that sufficient super-saturation is achieved to cause homogeneous nucleation for ammonium nitrate, and most probably these compounds condense onto existing particles (Claes et al. 1998). Ammonium nitrate centered at 0.5-0.7 μm tends to evaporate from the smaller particles and deposit on larger particles (Bassett and Seinfeld, 1984) because submicron ammonium nitrate particles are subject to a significant Kelvin effect which destabilizes them if compared with larger particles (Claes et al. 1998). Large sodium nitrate ($NaNO_3$) particles may be formed in marine-influenced terrestrial atmospheres with low ammonia concentrations (Wall et al. 1988; Claes et al. 1998). While sodium nitrate ($NaNO_3$) exists only in the surface layers of 1-4 μm coastal aerosol (Bruynseels and Van Grieken, 1985), and the reaction rate is dependent on the NaCl surface area presented to the nitric acid as well as on the mass of sodium chloride available to react

(Wall et al. 1988). The non-volatile sodium nitrate serves as a permanent removal mechanism for nitric acid (Wall et al. 1988).

Geological material or suspended dust consists mainly of oxides of aluminum, silicon, calcium, titanium, iron, and other metal oxides. The precise combinations of these minerals depend on the geology of the area and other human activities, such as industrial processes and constructions. Geological material is mostly in the coarse particle fraction (Patterson and Gillette, 1977).

2.1.5 Urban particle and its impacts on climate and health

In the current debate on global change, the effect of tropospheric aerosols on the global radiative balance and climate has resulted in more investigations. Particles play an important role in radiative transfer and climate directly and indirectly, the former by scattering and absorbing radiation (Langner and Rodhe, 1991; Taylor and Penner, 1994; Haywood and Shine, 1995; Schult et al., 1997; Charlson et al. 1992; Penner et al. 1992; Jacobson, 2001) and the latter by influencing the droplet size distribution and albedo of planetary layer clouds (Charlson et al. 1987). Fine particles emitted at the tropical and sub-tropical surface, in a geographical location like Hong Kong, might be transported into the stratosphere rather than particles emitted at northern mid-latitudes because the main physical process, deep convection that is responsible for the vertical

transport of gases and particles, is most intensive in the tropics and sub-tropical zones in respect of cloud top height and number of events (Köhler et al. 2001).

More recently, anthropogenic aerosol in particular was found to impose a major perturbation to this forcing, for example cooling effect resulting from sulfate (Charlson et al. 1992) and warming effect as a result of soot (Jacobson, 2001). Soot is large and dark particles tending to absorb light, thus warming Earth's atmosphere. In contrast, very small particles such as sulfate and organic material, regardless of color and composition, tend to scatter light, thus increasing the albedo of the atmosphere. The light-scattering effect seems to prevail at most latitudes, but at high latitude, where snow and ice covered surfaces are highly reflective, absorption effects can dominate (Harvey, 1988). Whether carbonaceous particles principally warm or cool the atmosphere depends on the aerosol single scattering albedo, which is the ratio of incident radiation that is scattered to the incident radiation that is absorbed. It follows that the aerosol SSA depends on the relative amounts of absorbing EC and scattering OC, represented by OC/EC ratios (Novakov et al. 2005).

Particles also exert an indirect effect in their role as a major source of cloud condensation nuclei (Novakov and Penner, 1993). They increase the concentration of cloud droplets with the increased concentration of condensation nuclei, like sulfate

and organic aerosols, resulting in an increase in the scattering surface of clouds. Also, rain may be inhibited, since the mean droplet size decreases with increasing numbers of droplets, leading to a further increase in the cloud cover. On the other hand, clouds also absorb solar and terrestrial radiation (Rodhe, 1999); heat gained from this absorption will counter the heat lost by the scattering effect of clouds. Although the relative strengths of these two processes are not known with precision, evidence accumulated thus far indicates that the scattering effect dominates, with sulfates and cloud formation resulting in a net cooling of the planet.

Evidence from epidemiology and toxicology (Dockery et al. 1993; Schwartz et al. 1996; Katsouyanni et al. 2001; Horak et al. 2001) has suggested statistically significant association between morbidity and ambient particle concentrations. Coarse inhalable particles may be deposited in the upper respiratory tract whereas fine particles travel deeper into the lungs. An influential study, conducted by Dockery et al. (1993), of six US cities monitored a cohort of 8111 adult subjects for 14-16 years from the mid-1970s and found that increased fine particle concentrations were correlated with increased mortality (26% increase over an 18.6 μg m^{-3} range of particle concentrations) from all causes, but especially from cardiopulmonary disease. More previous studies have found a linkage between morbidity with PM_{10} (Dockery et al.

1992; Seaton et al. 1995). The evidence showed that coarse particles contribute to increased risk of hospitalization for heart and lung disease (Zanobetti et al. 2003), increased respiratory symptoms (Mar et al. 2004), and decreased lung function (Gauderman et al. 2000). During the last decade, $PM_{2.5}$ has been increasingly emphasized. Various toxicological and physiological considerations suggest that fine particles may play an important role in affecting human health. For example, they may be more toxic because they include sulfates, nitrates, acids, metals, and carbon on their surface. Currently, ultrafine particles ($PM_{0.1}$) are considered to be another important fraction because they serve as a primary source of fine particle exposure and because poorly soluble ultrafine particles may be more likely than larger particles to translocate from the lung to the blood and other parts of the body (Hughes et al. 1998, Oberdörster et al. 2005). Several studies (Ferin et al. 1992; Donaldson, 1998; Oberdörster, 2001; Li et al. 2003) have demonstrated the increased toxicity or interstitialisation of ultrafine articles compared to fine particles of the same material.

Toxic response of particulate matter is dependent less upon the mass of the particles than the number, size and composition. Particles in accumulation mode (0.1-1 μm) have the greatest health impact because they penetrate most deeply into the lung (Natusch, 1974). Carbonaceous aerosols (organic compounds and elemental carbon),

especially those found in diesel exhausts, have been demonstrated to induce disease in human or animals (Klingenberg and Winneke, 1990; Mar et al. 2000; Metzger et al. 2004). Sulfuric acid has been shown to impair lung clearance (Schlesinger, 1990). In addition, several trace metals, such as iron, nickel, and zinc, are found to suppress the human immune system (Goyer, 1986; Burnett et al. 2000). The well-established toxic effects of lead resulted in specific US NAAQS for this metal and the phase-out of leaded fuels over the past two decades.

Although much has been learned upon the health effects of PM, there are important gaps in our knowledge, such as what kind of PM or which part of PM is most at risk and what specific air pollutants, combination of pollutants, and sources of pollutants are most responsible for the observed health effects (Pope III and Dockery, 2006). These questions can be answered partly because there is some unknown knowledge on PM by far. Unresolved scientific issue dealing with the health effects of PM air pollution motivates further study on PM in atmosphere.

2.2 Tunnel studies

The on-road transport related emissions may be estimated from tunnel studies. Engine-related particulate emissions are composed primarily of lead halides, sulfates, and carbonaceous matter and are mostly smaller than 1 μm in diameter. About 40% of

particles from tire wear are less than 10 μm (about 20% less than 1.0 μm) and are primarily carbon. Particles from brake linings are less than 1 μm and are composed of asbestos and carbon mainly. Fugitive dust emissions are mostly large particles that usually settle a short distance from the source, therefore resulting in a limited impact on the environment.

Particulate emitted from vehicles are by-products of the fuel and lube oil combustion process (exhausts) and from evaporation of the fuel itself. The nature and rates of vehicle emissions are controlled by many factors such as fuel composition (Mulawa et al. 1997; Wang et al. 2000; Alander et al. 2004), engine condition and efficiency (Cadle et al. 1997; Norbeck et al. 1998; Shah et al. 2004), vehicle loading (Morawska et al. 1998) and road surface situations. In order to obtain an accurate characterization of vehicle emissions, tunnel studies (Moeckli et al. 1996; Pierson et al. 1996; Weingartner et al. 1997; Fraser et al., 1998; Allen et al. 2001; Gillies et al. 2001; Schmid et al. 2001; Gertler et al. 2002; Jamriska et al. 2004; Lough et al. 2005) are commonly conducted, by measuring the pollutant concentrations simultaneously at the entrance and exit of a tunnel as well as monitoring aspects such as traffic counts, vehicle speed, temperature, wind speed and pressure in the tunnel. This method is believed to result in representative emission factors for the on-road vehicles and is

lower in cost and complexity than the traditional dynamometer method (Jamriska et al. 2004).

Several tunnel studies (Allen et al. 2001; Gillies et al. 2001; Gertler et al. 2002; Jamriska et al. 2004; Lough et al. 2005) have measured emission factors for $PM_{2.5}$ that represent the particle fraction emitted mainly from vehicle exhausts. Gillies et al. (2001) reported the average $PM_{2.5}$ emission factor for the mixed light-duty (97.4%) and heavy-duty vehicles (2.6%) as 0.052±0.027 g $veh^{-1}km^{-1}$ in the Sepulveda Tunnel, Los Angeles, California during 1996. In a 1997 study conducted in the Caldecott Tunnel, San Francisco Bay, Allen et al. (2001) measured fine particle (diameter less than 1.9 μm) mass emission rates of 0.430±0.079 g veh^{-1} km^{-1} and 0.006±0.000 g veh^{-1} km^{-1} from heavy- and light-duty vehicles. In the Tuscarora Mountain Tunnel of Pennsylvania, Gertler et al. (2002) reported the average $PM_{2.5}$ emission factors for heavy- and light-fleets during 1999 as 0.135±0.018 and 0.014±0.013 g $veh^{-1}km^{-1}$ respectively. Carbonaceous aerosols were generally major components in fine particle emissions reported by above studies. A more recent study used continuous monitoring instruments, TEOM (the Tapered Element Oscillating Microbalance) and DustTrak (TSI Inc.), in the Woolloonngabba Tunnel of Brisbane, Australia (Jamriska et al. 2004). The mean $PM_{2.5}$ emission factor of diesel buses using TEOM was 0.267±0.207 g

$veh^{-1}km^{-1}$, which was thought to be possibly 20-30% lower than the true value, while a higher emission factor of 0.583±0.451 g $veh^{-1}km^{-1}$ was obtained using DustTrak.

2.3 Modeling

2.3.1 The Positive Matrix Factorization (PMF) receptor model

Positive matrix factorization (PMF) receptor model has been developed by Dr. Paatero at the University of Helsinki in Finland in the mid 1990's. It has provided a flexible modeling approach that can effectively use the information content in the data. PMF uses a least squares approach to solve the factor analysis problem by integrating non-negativity constraints into the optimization process and utilizing the error estimates for each data value as point-by-point weights. PMF has been successfully applied to a number of data sets (Polissar et al. 1998; Xie et al. 1999; Chueinta et al. 2000; Willis, 2000; Song et al. 2001). Lee et al. (1999) used PMF to identify the sources of RSP in Hong Kong. The species analyzed in the study were Al, Ca, Mg, Pb, Na^+, V, Cl^-, NH_4^+, SO_4^{2-}, Br^-, Mn, Fe, Ni, Zn, Cd, K^+, Ba, Cu, and As. Unlike the conventional receptor modeling algorithm, factor analysis PMF only generates non-negative source profiles. More recently, Yuan et al. (2006) reanalyzed the PM_{10} data in Hong Kong with more accurate carbon data and they concluded secondary

sulfate and local vehicle emissions were responsible for the largest contribution to PM_{10} in HK (25% each), followed by secondary nitrate (12%).

2.3.2 The Chemical Mass Balance (CMB) receptor model

The CMB receptor model (Watson et al. 1990, 2004) is one of the several receptor models that have been applied to air resources management. It has become a popular tool for determining the contribution of particulate matter to ambient levels in the past decade (e.g., SCAQMD, 1996). The CMB receptor model consists of a solution to linear equations that express each receptor's chemical concentration as a linear sum of products of source profile abundances and source contributions (Watson et al. 2004). The source profile abundances (i.e., the mass fraction of a chemical or other property in the emissions from each source type) and the receptor concentrations, with appropriate uncertainty estimates, serve as input data to CMB. In order to distinguish between source type contributions, the measured chemical and physical characteristics must be such that they are present in different proportions in different source emissions and changes in these proportions between source and receptor are negligible or can be approximated. The CMB model calculates values for the contributions from each source and the uncertainties of those values.

CMB model assumptions (Watson et al. 2004) are: 1) compositions of source

emissions are constant over the period of ambient and source sampling; 2) chemical species do not react with each other (i.e., they add linearly); 3) all sources with a potential for contributing to the receptor have been identified and have had their emissions characterized; 4) the number of sources or source categories is less than or equal to the number of species; 5) the source profiles are linearly independent of each other; and 6) measurement uncertainties are random, uncorrelated, and normally distributed. The six assumptions are fairly restrictive and they will never be totally complied with in practice. Fortunately, the CMB model can tolerate reasonable deviations from these assumptions, though these deviations increase the stated uncertainties of the source contribution estimates (Watson et al. 2004).

The formalized protocol for CMB model application and validation is applicable to the apportionment of gaseous organic compounds and particles. The seven-step protocol are: 1) determine model applicability, 2) select a variety of profiles to represent identified contributors, 3) evaluate model outputs and performance measures, 4) identify and evaluate deviations from model assumptions, 5) identify and correct input data deficiencies, 6) verify consistency and stability of source contribution estimates, and 7) evaluate CMB results with respect to other data analysis and source assessment methods. Particulate matter elements, ions, and carbon have been used in the CMB to

distinguish sources.

2.3.3 The Potential Source Contribution Function (PSCF) receptor model

From a receptor point of view, pollutants can be roughly categorized into two source types: source known and source unknown. When significant knowledge about the source profile exists, the CMB receptor models can be used to estimate the contribution of each of the various source categories to the concentration measured at the receptor. For sources that have known tracers but do not have complete emission profiles, factor analysis tools, like Principal Component Analysis (PCA), UNMIX, PMF, can be used to identify source tracers. For pollutant sources that are unknown, hybrid models that incorporate wind trajectories, like PSCF, can be used to resolve source locations.

PSCF analysis has been employed in a number of prior studies to develop a conditional probability function that can be used to identify the possible locations of the sources of pollution that is being detected at a given location (Gao et al. 1994; 1996; Cheng et al. 1993; Hopke et al. 1995). The PSCF function is the conditional probability that an air parcel with a level of pollutant concentration above a criterion value arrives at a receptor site after having passed through a specific geographical area. By using the chemical concentrations and wind trajectories to give a model of the

locations where pollutants are emitted, the PSCF model combines chemical along with meteorological data (Gao et al. 1996).

2.4 Previous studies on aerosols in Hong Kong

HKEPD has monitored the air quality in Hong Kong since 1984 with a monitoring network of about 10 stations. Three roadside stations and one ambient station were established later. The measurements for particulate matter include OC/EC, ion, and elements in TSP and RSP. The data provided by HKEPD (Qin et al. 1997) showed that the concentration of atmospheric aerosols was low in Hong Kong compared to some large cities located in East Asia. RSP and most of the chemical species show seasonal variations which reflect the weather conditions: low concentrations in the rainy season of summer and high concentrations for the rest of the year. The higher temperatures in summer months induce larger mixing heights, which favors the dispersion of pollutants. The rains in summer help to wash out pollutants more frequently. The south-westerly prevailing wind in the summer also helps to replenish the region with cleaner oceanic air. Carbonaceous aerosols accounted for approximately half of the mass and dominated the seasonal and spatial variations of RSP concentrations. Sulfate, ammonium and nitrate accounted for a quarter of RSP mass. Chemically speciated $PM_{2.5}$ and PM_{10} data from a 1998-99 pilot at TW, Hong Kong, showed that: 1) ~70%

of PM_{10} is in the $PM_{2.5}$ fraction, 2) carbonaceous aerosol and secondary ammonium sulfate constituted a major portion of $PM_{2.5}$, 3) $PM_{2.5}$ concentrations and compositions varied over twofold between the warm and cold seasons, and 4) elevated levels of OC were the main contributor to elevated $PM_{2.5}$ concentrations during winter. Recently, HKEPD conducted a 12-month study of $PM_{2.5}$ mass concentration levels at strategic locations in Hong Kong to represent urban ambient (TW), roadside (MK) and rural (HT) environment from November 2000 to October 2001 (Louie et al. 2002). The main focus of the study is on chemical speciation of $PM_{2.5}$ particulate with special focus on organic speciation. Carbonaceous aerosol concentrations at MK are 1-2 times higher than those at TW, and the values at TW are more than 2 times higher than those at HT. Chemical characterization of the water-soluble organic compounds (WSOC) was performed as part of the 12-month $PM_{2.5}$ study. The WSOC accounts for a significant portion of the total organic carbon mass, ranging from 14% to 64%. The highest WSOC contribution occurs in the fall composite at HT, and the lowest in the summer composite at MK. The WSOC concentrations are comparable in their concentration levels at the three sites. This is similar to the spatial distribution of secondary inorganic aerosols in Hong Kong (i.e., sulfate and nitrate). These observations seem to suggest that the WSOC fraction is mainly of secondary origin.

The WSOC/OC ratio shows a clear spatial pattern, highest at Hok Tsui and lowest at Mong Kok. The OC/EC ratio also exhibits the same spatial pattern. Both observations indicate that the contribution of secondary organic aerosol is more prominent at the rural site. Several past studies in PM_{10} (Yu et al. 2004b; Qin et al. 1997) and $PM_{2.5}$ (Cao et al. 2003; Ho et al. 2003; Pathak et al. 2003; Louie et al. 2005) have been conducted in Hong Kong including the investigation of aerosol characterization and source apportionment. Characteristics of particulates and its major chemical components in Hong Kong ambient atmosphere is the combined effects of emissions from local and regional sources. In ambient atmosphere, carbonaceous materials, i.e., sum of EC and organic mass, take up 37% of PM_{10} mass, being the most abundant component of the Hong Kong PM_{10} mass (Yu et al. 2004b). OC has dominant sources of local vehicle exhausts while it is also influenced by polluted air mass that transport from Asian continent. The wintertime OC is two times higher than the summertime OC at the ambient monitoring stations in Hong Kong (Ho et al. 2003; Yu et al. 2004b; Louie et al. 2005) because of the OC transported from northern China in winter (Yu et al. 2004b; Louie et al. 2005). To the contrary, the seasonality of EC is much weaker and variable among the monitoring sites. EC seasonality is found to depend on the distance from and relative location of the nearby road (Louie et al. 2005) and the city's

container port (Yu et al. 2004b). Sulfate and ammonium were the secondary important species in particles. In total, about 40% of the sulfate and ammonium of $PM_{2.5}$ in Hong Kong measured in Pathak's study (Pathak et al. 2003) was from continental air masses and most of them occurred in autumn, winter, and spring.

Ho et al. (2003) conducted a study for PM_{10} and $PM_{2.5}$ aerosol samples that were collected in wintertime from November 2000 to February 2001 at three different sampling locations in Hong Kong. PM_{10} and $PM_{2.5}$ were collected by high-volume samplers and the concentrations of major elements, ions, organic and elemental carbons were quantified. The ratios of $PM_{2.5}/PM_{10}$ were 0.61 and 0.78 at the PolyU campus and Kwun Tong (KT), respectively. The concentrations of anthropogenic species (e.g. Pb and Cu) in PM_{10} and $PM_{2.5}$ measured at urban areas were generally higher than at an urban background site of Hok Tsui (HT). The major fractions of sulfate at three monitoring sites are non-sea-salt sulfates. Fung and Wang (1995) applied receptor modeling with SAS statistical software and regression analysis to apportion the sources of aerosols at five stations in the New Territories of Hong Kong with trace elements as markers. Six sources were identified including sea aerosol, coal-fired power plants, oil combustion, wind-blown dust, construction work, and automobile/incineration.

With a MOUDI cascade impactor (Micro-Orifice Uniform Deposit Impactor) at Hong Kong University of Science and Technology (HKUST) station, the size distributions of particulate sulfate, nitrate, and ammonium in Hong Kong were measured (Zhuang et al. 1999a). They were tri-modally distributed in the size range of 0.052-10 μm in diameter. Sulfate and ammonium were particularly abundant in fine particles with a condensation mode (0.2 μm in diameter) and a droplet mode (0.57 μm in diameter) while nitrate was mainly associated with coarse mode. Yu et al. (2004a) investigated the size distributions of water soluble organic carbon in HKUST. Regardless of air mass origins being mainly marine or continental, WSOC exhibited bimodal size distributions with a dominant fine mode and a minor coarse mode in the size range of >0.43 μm. The two modes had a mass mean aerodynamic diameter (MMAD) of 0.77 and 4.07 μm, respectively. The fine WSOC accounted for the major proportion of the total WSOC, ranging from 66% to 80%.

Chapter 3 Methodology

In this chapter the methodology of the study will be organized by first describing the choice of sampling locations and then discussing sampling details. The summary tables (Table 3.1, 3.2, and 3.3) show all sampling information. This will be followed by reviewing principles of models that were used in this study. The chapter ends with a brief section on quality assurance and quality control for sampling and experiments.

3.1 Sampling locations

3.1.1 The PU Supersite

This PU air quality monitoring Supersite (22.30° N, 114.17° E, Figure 3.1 and Appendix B-Photo 3.1) has been established by the Hong Kong Polytechnic University, located in a street canyon in a residential and commercial area near Victoria Harbor. PU Supersite is about 1 meter away from the curb of Hong Chong Road (Photo 3.2). The Hong Chong Road is approximately 30 m in width with four lanes for both directions, leading to the busiest cross-harbour tunnel in Hong Kong. The sampling site is about 400 m away from the tunnel entrance. Vehicle numbers, speeds and types were counted by the toll gate of the cross-harbour tunnel. Besides restaurant/household cooking, industries or other anthropogenic sources were not

found in the vicinity.

The traffic numbers are extremely high on the Road. Traffic density changes in both directions nearly simultaneously. The maximum and minimum daily average of traffic number in 2005 is 125853 in November and 120426 in February (the annual traffic census, 2005). The traffic data were obtained in terms of the number of cars running in both directions per day. The average speed of traffic in the lane close to the sampling location is slow mainly due to periodic slowing down of the traffic by the traffic lights before passing the sampling site. But all vehicle engines are warmed up.

There are two traffic rush hours with one in the morning (8:00-10:00) and the other in the evening (17:00-19:00). The diurnal variations of vehicle fractions (the annual traffic census, 2004) are quite similar over days on this road with higher traffic number in daytime and lower values at nighttime. During daytime, over 6000 vehicles per hour pass the sampling site, of which about 30% are diesel-fueled vehicles, 60% are gasoline-fueled vehicles, and 10% are Taxis (liquefied petroleum gas fueled). Most of diesel-fueled vehicles are light goods vehicles (about 90%). Only 10 % are medium and heavy goods vehicles. The average hourly gasoline-fueled vehicles ranged from 35% at 11:00-12:00 to 60% at 19:00-20:00 and diesel-fueled vehicles varied from 10% at 22:00-23:00 to 50% at 11:00-12:00. Similar traffic conditions were found in 2003

and 2004.

3.1.2 The Shing Mun Tunnel

The Shing Mun Tunnel is an urban two-bore tunnel (Figure 3.1) with two lanes of traffic per bore (without walkways), and is currently used on average by 53300 vehicles per day (the annual traffic census, 2004). The tunnel has a length of 2.6 km and is separated into two sections, including the east side and the west side. Two sampling stations were located in the south bore of the west side (Figure 3.2), which carries the vehicle flow from Shatin to Tsuen Wan. The length of the west side of the tunnel is approximately 1.6 km and there is an upgrade of 1.054% towards the exit from the entrance. The cross sectional area of the tunnel is 70.0 m^2. The vehicle speed limit is 80 km h^{-1}. The ventilation mode is longitudinal, and is achieved from the piston effect of the vehicles traversing it. There are 80 jet fans and 4 exhaust air fans positioned along the ceiling throughout the tunnel. They are only activated occasionally during morning rush hours periods (8:00-10:00). Therefore, the emissions measured during morning rush hours might be underestimated in this study. The average wind speed in the tunnel is obtained from the two sensors near the sampling stations installed on the inside top roof of the tunnel. The distance between the sensors and tunnel roof top was approximately 1.2 meters. The measured air velocities were

assumed to represent average air velocities at the cross section of the tunnel.

3.1.3 The rural sampling site (Hok Tsui)

A background observation station (Figure 3.1 and Appendix B-Photo 3.3), Hok Tsui (HT), was selected to carry out measurements in order to trace the sources of long-range transported air masses from the Asian continent. HT background station (22.22° N, 114.25° E, Figure 1) has been established by the Hong Kong Polytechnic University, ~10 km to the southeastern of PU Supersite. It is surrounded by a coastal setting (60 m above sea level) with 240° of ocean view from northeast to southwest. Air masses arriving at HT from the northeast or east regions normally do not pass the urban areas in Hong Kong. No other anthropogenic sources were found in the vicinity of sampling site. Therefore, during winter, the particle characteristics at this study site are expected to be largely determined by the transport of air masses from South China or PRD region. Occasionally, air masses from the island of Taiwan and passing ships can reach the sampling site. The pollutants originating from the inland of Hong Kong have little impact on marine aerosols. In summer, it is influenced by clean marine air.

3.2 Measurements at sampling locations

3.2.1 Sample collection at PU Supersite

The detailed sampling program at PU Supersite is shown in Table 3.1. Photos for parts

of instruments used at PU Supersite are displayed in Appendix B.

3.2.1.1 Integrated $PM_{1.0}$/ $PM_{2.5}$/ PM_{10} and speciation sampling

PM_1, $PM_{2.5}$, and PM_{10} were collected simultaneously with a URG sampler (URG-3000ABC, Chapel Hill, USA, Photo 3.4) on 47 mm quartz fiber (# 1851047, QMA, Whatman International Ltd., Maidstone, England) and Teflon filters (# 42254, Teflo^{TM}, Pall Corporation. Life Science, Michigan, USA) for each size fraction in order to better understand the characteristics and relationships of PM_1, $PM_{2.5}$, PM_{10}, and $PM_{coarse.}$ URG-3000ABC particulate sampler is made by Air Sampling Instrumentation, Chapel Hill, USA, which is designed for specific sampling needs. The eight channels of URG-3000ABC, 4 channels for PM_{10}, 2 channels for $PM_{2.5}$, and 2 channels for $PM_{1.0}$, can be operated at 8.3 l min^{-1} at the same time with one pump to provide a comparable data set for different size fractions. The detailed information related to the sampling at PU Supersite is shown in Table 3.1.

Daily $PM_{1.0}$ and $PM_{2.5}$ samples were acquired at PU Supersite with two-collocated Partisol Plus Model 2025 Sequential Air Sampler (RP2025, Rupprecht and Patashnick Co. Inc., Albany, NY, Photo 3.5) operated at 16.7 l min^{-1}, for gravimetric and OC/EC analyses. The collection membrane was 47 mm quartz fiber filter (# 1851047, QMA, Whatman International Ltd., Maidstone, England). The Plus Model 2025 Sequential

Air Sampler (Rupprecht and Patashnick Co. Inc., Albany, NY) is a multi-filter sampler (up to 16 filters) that performs automatic exchanges according to a user-defined sampling schedule. The sampling is stopped if 5% bias of flow rate is detected. The sampler stores records of input data every 30 minutes by default. These include the averages over the data storage interval of meteorological inputs and sampling information. The sampling took place from January to May 2004 to characterize the PM during winter episode days. Two- or three-hr sampling was also taken using the RP2025 sequential sampler in order to obtain the diurnal patterns of $PM_{2.5}$ and chemical species during summer episode days.

3.2.1.2 Sampling for ultrafine particles

The Micro-Orifice Uniform Deposit Impactor (MOUDI) was used for size distribution measurements in this study. The ten-stage MOUDI 110 (MSP Corp. USA, Photo 3.6), operated at 30 l min^{-1}, and three-stage Nano-MOUDI 115 (Photo 3.7), operated at 10 l min^{-1} were used at PU Supersite. Particles were classified by the MOUDI in the following aerodynamic particle diameter ranges: 0.010-0.018, 0.018-0.032, 0.032-0.056, 0.056-0.10, 0.10-0.18, 0.18-0.32, 0.32-0.56, 0.56-1.0, 1.0-1.8, and 1.8-2.5 μm. One backup filter was used in this study and an artificially lower “cut size” of 0.001 μm was used. Teflon membranes (# 42254, Teflo^{TM}, Pall Corporation.

Life Science, Michigan, USA) or aluminum foils (MSP Corp. USA) in diameters of 47 mm were used to collect particles in all stages. The MOUDI was operated on a 48- or 70-hr schedule in order to collect enough particles on individual stages for chemical analyses. OC and EC analyses on aluminum foils were done by thermal/optical reflectance (TOR) following the Interagency Monitoring of Protected Visual Environments (IMPROVE) protocol (Chow et al. 1993), however, the pyrolysis correction could not be done directly for samples collected on aluminum foils because of the uneven distribution of particles on sampling substrates. The OC concentrations were not used in this study because there was lubricant in the MOUDI system, easily leading to contaminant for OC under high ambient temperature. However, organic matter concentrations can be roughly estimated by subtracting the sum of the rest other species from the total mass concentrations in this study. This estimation may overestimate the concentrations of organic matters since the water content was not considered. Half of aluminum foils was extracted to conduct water-soluble ion analyses using IC (Ion Chromatography). The mass and elemental concentrations were determined from the Teflon membranes. Forty elements on Teflon filters were determined at the Desert Research Institute, USA, with X-ray fluorescence (EDXRF) method (Watson et al, 1999), including Na, Mg, Al, Si, P, S, Cl, K, Ca, Ti, V, Cr, Mn,

Fe, Co, Ni, Cu, Zn, Ga, As, Se, Br, Rb, Sr, Y, Zr, Mo, Pd, Ag, Cd, In, Sn, Sb, Ba, La, Au, Hg, Tl, Pb, and U. During the sampling periods in this study, the effects of particle bounce were neglected since the relative humidity was high (60% to 80%) enough to prevent particle bounce.

3.2.1.3 Continuous monitoring for $PM_{2.5}$, PM_{coarse}, and BC

A model SPM-613D dichotomous beta gauge monitor (Photo 3.8), manufactured by Kimoto Electric Co., LTD., Japan, was used to take the real time data for $PM_{2.5}$, PM_{coarse} ($PM_{2.5-10}$), and OBC (optical black carbon). The concept of a beta gauge is to determine the mass collected on a filter by measuring the relative change in the β-particle intensity passing through the filter when clean and then loaded with the collected particle mass (Chueinta and Hopke, 2001). The SPM-613D aspirates the ambient aerosol through a standard 16.7 l min^{-1} inlet and introduces the fractionated PM_{10} aerosol into a custom designed virtual impactor. The particles are then separated by the virtual impactor into two channels, namely $PM_{2.5}$ and PM_{coarse}. The $PM_{2.5}$ deposited on Teflon filter was quantified by beta gauge method. A heater (30 °C) is located downstream of the sampler's inlet to maintain the relative humidity of the aspirated air stream because beta rays are attenuated by condensed water, resulting in an overestimation of the particle mass (Chang et al. 2001).

Black carbon on the Teflon filters is estimated by measuring the reflection of LED light by the samples (I) and reference (I_0). BC concentrations (*C*) can be calculated based on the following formula:

$$C = -A \times \ln(I / I_0) \qquad 3.1$$

where A is the static span coefficient. The previous span calibrations performed by users, the theoretical relationship between reflection of LED light and collected BC mass are used to estimate the mass of BC on Teflon filter.

3.2.1.4 Measurements of particle numbers in fine and ultrafine size ranges

Due to the different physical characteristics of particulates in different size ranges, different methods have to be applied for measurements of size spectra of small particles and large particles (Morawska et al. 1998). In the present study, particles of diameter 7-217 nm were measured using a TSI Scanning Mobility Particle Sizer (SMPS3936, TSI Inc., US, Photo 3.9). The SMPS system comprises a Model 3081 Electrostatic Classifier (EC) and a Model 3022A Condensation Particle Counter (CPC). Particles are first drawn into the EC and classified into 64 channels in a range of 7-217 nm in diameter using an electrical mobility detection technique, and then counted by the CPC. The flow rate of aerosols is 1.5 l min^{-1}. A PMS (Particle Measuring Sytem,

US, Photo 3.10) Optical Particle Counter (OPC) Model 1003 measured the particle sizes from 100 to 2000 nm in eight channels. Sampled air is drawn through the laser beam by a small vacuum pump operated at 0.028 l min^{-1}. As entrained particles in the air pass through the laser beam, the laser light interacts with the particles and is scattered. The burst of light energy from each particle is converted into a pulse of electrical energy to determine the size and quantity of particle. Both the SMPS system and PMS OPC 1003 used in the present study are brand-new instruments, which were pre-calibrated by the manufacturer.

To avoid the rainy days, intermitted sampling was conducted on weekdays during January 5-31, 2005 and July 8-27, 2005. Once sampling was started, the SMPS and the OPC were operating simultaneously. The sampling interval is 30-minutes. The instruments were placed on a bench in a shelter with an air conditioner. The inlet was connected with a 2.5-meter sampling line with a silicagel drier installed in the middle. Although the drier possibly results in ~20% losses of particles (Aalto et al. 2005), it is essential to add it because the penetration of water into the sampling lines would lead to unstable flow of the CPC. The PMS OPC 1003 was also placed in the shelter with a 1-meter sampling line outside.

3.2.2 Measurements in the Shing Mun Tunnel

The $PM_{2.5}$ was measured at the entrance and exit of the Shing Mun Tunnel to obtain the emission factors for vehicles. The sampling was made during varying times that encompassed different traffic fractions of diesel-fueled vehicles. The sampling duration, environmental conditions, and traffic counts for each run are given in Table 3.2. The average temperature during the sampling periods was 24.0 °C, and the average pressure was 761.1 mmHg. A total of 27310 vehicles traversed the tunnel during the study with the number per hour ranging from 786 to 2842 vehicles. Diesel-fueled vehicles represented the highest proportion (more than 60%) during 11:00-13:00 and 14:00-16:00, whereas the lowest (~30%) was found during 8:00-10:00 (morning rush hours), 17:00-19:00 (evening rush hours) and 21:00-23:00 (evening). The traffic speed for every run did not vary significantly, with most speeds recorded within the range of 60 to 70 km h^{-1}. The average wind speed recorded in the tunnel during the sampling periods was 4.7 m s^{-1}.

For the filter-based $PM_{2.5}$ samples, the sampling schedule consisted of 16 sampling periods (Run 1-16), including 4 runs in summer and 12 runs in winter of 2003 (Table 3.2). The sampling interval was 2 hours in the summer, changing to 1 hour in the winter to avoid possible risk of saturating the filters. The sampling time was chosen to

cover a wide range of diesel-fueled vehicle proportions at different time periods. Two samples were collected simultaneously at the tunnel entrance and exit during each sampling run, using two DRI (Desert Research Institute, US) particulate samplers (Watson et al. 1994a). The inlet sampling station was located 686 m inside the entrance of the Shing Mun Tunnel south bore and the outlet sampling station was located 350 m upwind of the exit (Figure 1). The sampling system (Photo 3.12) included a fine-particle size-selective inlet (Bendix/Sensidyne 240 cyclone for $PM_{2.5}$); an inverted U-shaped copper tube (~1.2 cm diameter); an homogenizing chamber (~4 cm diameter by 50 cm); a flow splitter (~5 cm diameter); two 47-mm filter holders; two flow control valves; and a Gast 1023 ¾ HP carbon-vane vacuum pump. A total of 113 l min^{-1} was drawn through the inlet and then was divided into two equal air streams leading to the different sampling substrates (47 mm quartz and 47 mm Teflon filter). $PM_{2.5}$ samples were simultaneously collected on Teflon-membrane and quartz-fiber filter substrates using this sampling system. The sampler was fixed at ground level, ~1.2 m away from the tunnel wall, with an inlet at a height of ~1.5 m. The flow rates were checked in the field before and after each run using a calibrated flow meter. All loaded samples were stored inside a cooler chilled with blue ice during delivery of samples to the laboratory. They were then stored in a refrigerator before

being sent to DRI (packed in blue ice) for chemical analyses. Teflon membrane filters were pre- and post- weighed at least twice (the difference between two weights deviating less than 10%) on a Mettler Toledo MT5 Microbalance in DRI, with a sensitivity of ±1 μg, to determine mass concentrations. Before weighing, the filters were equilibrated in a desiccator at 20-30ºC with a relative humidity of 30-40% for 24 hours.

Two DustTrak air monitors (Model 8520, TSI Inc., US, Photo 3.13) were operated to monitor $PM_{2.5}$ concentrations alongside the DRI particulate samplers at the tunnel's entrance and exit for 9 of the 16 runs (Table 3.2). One-minute means of $PM_{2.5}$ was collected during each sampling run from which 15-minute, 1-hour or 2-hour means were calculated. DustTrak is a simple instrument, which gives a direct reading of mass concentration based on the scattering of laser light by aerosols. The particulate concentrations for diesel exhausts derived from DustTrak were found to correlate well with the data measured gravimetrically (R=0.93 to 0.99), but the slope of the correlation varied between 0.55 and 1.3 (Moosmuller et al. 2001). Therefore, in this study, to obtain more precise values, a calibration test was conducted to convert the results given by the DustTrak into corresponding concentrations, using gravimetric methods. The two DustTrak air monitors used in tunnel measurements were calibrated

separately against the DRI particulate samplers for the entrance and exit. $PM_{2.5}$ measurements using DustTrak were firstly averaged for the same sampling periods with the DRI sampler. The correlation coefficient (R) was 0.78 and 0.86 for the entrance and exit, respectively. DustTrak measurements were ~1.7 times the gravimetrically obtained values at the tunnel entrance and ~1.4 times those at the exit.

Traffic composition and volume were determined by manual counts at the entrance of the tunnel tube at 15-minute intervals during the sampling periods. Video-recording was also taken for data validation and review purposes. The vehicle types were classified into three major categories, namely gasoline-fueled vehicles (motor cycle and private car), LPG-fueled taxis and diesel-fueled vehicles (big bus, heavy goods vehicle, light goods vehicle and minibus). The manual traffic counts were compared to the records of Toll Plaza, approximately 200 m away from the tunnel entrance. The data obtained from the manual counts and toll plazas were in reasonable agreement with a deviation of less than 10%. Traffic speed surveys were periodically conducted at Shing Mun Tunnel using the car chasing method. The “chasing” vehicle was equipped with a Darwin microwave speed sensor, the tachometer recording vehicle speed on a second-by-second basis.

3.2.3 Measurements at Hok Tsui

3.2.3.1 BC monitoring

A model AE-42 Aethalometer (Magee Scientific Inc. Berkeley CA, Photo 3.11) was used to measure aerosol BC in real time at HT background station from June 2004 to May 2005 (Table 3.3). The Model AE-42 is a portable unit that embodies all of the standard Aethalometer features. It measures optical absorption at 880 nm for particles deposited on the 1.6 cm^2 quartz-fiber filter (PALL Corp., NY). The Aethalometer was placed at 1.5 m above ground and operated at 5 l min^{-1}. The principle is to measure the attenuation of a beam of the light transmitted through a fibrous quartz filter at successive regular intervals of a time-base period, while the filter is continuously collecting an aerosol sample. The increase in optical attenuation from one period to the next is due to the increment of aerosol BC collected from the air stream during the period. Dividing this increment by the volume of air sample during that time, the mean BC concentration in the sampled air stream during the period is calculated by the optical attenuation method. The measurement is assumed to be continuous as the time-base is short compared to the time scale of other variations in the air mass under study. Conventionally a specific attenuation cross section (σ_{aeth}) of 16.6 m^2 g^{-1}, recommended by the manufacturer and based on the study of Gundel et al. (1984), has

been applied to calculate BC (or EC) concentrations.

The Aethalometer measures the attenuation of a beam of light ($ATN_{(\lambda)}$) transmitted through a filter, as particles are collected on the filter. The instrument has two photo-detectors. One, *RB* (reference beam), measures the intensity of light that crosses a 'clean' spot of quartz filter; the other, *SB* (sensing beam), measures the intensity of the same light that crosses the sample spot where the aerosol is continuously accumulating. The Aethalometer also measures the signals at the sensors when the light source is turned off (*RZ* for the reference beam and *SZ* for the sensing beam). These values are subtracted from the sensors' levels when the light source is turned on in order to correct the measurements from the dark currents. The attenuation is defined as:

$$ATN_{(\lambda)} = -100 \times \ln((SB - SZ)/(RB - RZ)) \qquad 3.2$$

Where the factor of 100 is introduced for numerical convenience. By using the appropriate value of the specific attenuation cross-section ($\sigma_{(1/\lambda)}$), the black carbon content of the aerosol deposit can be determined at each time-base cycle, as follows:

$$BC = \frac{ATN(T) - ATN(0)}{\sigma_{(1/\lambda)}} \times \frac{A}{V} \qquad 3.3$$

Where *ATN(0)* and *ATN(T)* are the initial and the final attenuations due to the aerosol deposit on the filter during each timebase cycle; *A* (m^2) is the area of the exposed spot on the filter; and *V* (m^3) is the volume of air drawn through the filter. The BC minimum detection limit (MDL) is below 10 ng m^{-3} for the Aethalometer AE-42 used in this study. This is the standard deviation in small fluctuations determined by sampling filtered air in a cleaning room with the Aethalometer for eight hours. All data measured at HT have higher concentrations than the MDL. The 5-m BC data were subsequently averaged to a time resolution of one hour in order to be aligned with meteorological data and other studies.

3.2.3.2 EC measurements in parallel

For comparison, time-integrated $PM_{2.5}$ samples were collected, in parallel with the Aethalometer, at 24-hr interval on quartz-fiber filters (QMA, Whatman International Ltd., Maidstone, England, 47mm in diameter) with a Plus Model 2025 Sequential Air Sampler (Rupprecht and Patashnick Co. Inc., Albany, NY) at HT (Table 3.3). The details of RP2025 sequential sampler has been described previously. The carbonaceous content was determined using a DRI Model 2001 Thermal/Optical Carbon Analyzer (AtmAA Inc, Calabasas, CA, US) with the IMPROVE TOR protocol

(Chow et al. 1993; 2004).

The comparison between the collocated Aethalometer BC data and the TOR EC data from June 2004 to May 2005 were performed, as shown in Figure 3.3. Five-minute Aethalometer BC data were averaged into 24-hr values temporally matching the 249 EC data derived from in-parallel, filter-based samples. A good relationship is found between the Aethalometer and TOR measurements, with a high correlation coefficient of 0.88 (R), indicating that they respond similarly. The BC concentrations derived from the Aethalometer were ~20% lower than TOR measurements. These results provide the information needed to adjust the BC concentrations determined by the Aethalometer, so that BC determined by Aethalometer agrees with BC determined from the TOR technique.

3.2.4 Hourly $PM_{2.5}$ data collection by HKEPD

To compare with our data, the real time $PM_{2.5}$ data from two HKEPD stations, Tusen Wan (TW) and Tung Chung (TC), was used in this study. Figure 3.1 shows the locations of two HKEPD stations that measured hourly $PM_{2.5}$ mass with the Tapered Element Oscillating Microbalance 1400a $PM_{2.5}$ Monitor (TEOM, Rupprecht & Patashnick Co., Inc., Albany, NY, US). The TEOM is a true “gravimetric” instrument that draws ambient air through a filter at 16.7 l min^{-1} (a 3 l min^{-1} air stream is for the

instrument's mass transducer and a 13.7 l min^{-1} air stream is bypassed), continuously weighing the Teflon-coated glass filter and calculating near real-time $PM_{2.5}$ mass concentrations. The sample stream is preheated to 50 °C before entering the mass transducer to eliminate the necessity of humidity equilibration for the hydrophobic filter. The data are saved to a microcomputer, which can interface with external data collection systems.

3.3 Chemical analysis

3.3.1 Gravimetric analysis

To determine particle mass by gravimetric analysis, all filters used in this study were pre- and post- weighed at least twice (more times can be done if the difference between two weights deviated more than ±10%), and the net weights were obtained by subtracting the initial weights from the final weights. The net weights are divided by the total sampling volume with consideration of the temperature and pressure during sampling periods, thus the mass concentrations were obtained.

Before weighing, filters are exposed for a minimum of 24 hours at the equilibration temperature of 20-23 °C and relative humidity of 30-40%. The filters were weighted twice before and after sampling using a Microbalance (Model MC5, Sartorius AG, Goettingen, Germany) with the sensitivity of ±1 μg in the 0-250 mg range. The Model

MC5 Sartorius Microbalance contains separated weighing cell and evaluation unit, which ensures maximum precision-disturbing thermal influences are practically eliminated. The weighing cell and evaluation unit are interfaced together and also interfaced with a power supply unit. Automatic door functions on the glass draft shield facilitated operation and prevented vibrations. The Model MC5 Sartorius Microbalance contains a fully automatic, temperature-controlled internal calibration and linearization feature, which automatically calibrates the balance when necessary. In operation, a filter is placed on the weighing pan and the door of the glass draft shield is automatically closed. After approximately 20 to 30 seconds, the filter weight is registered on the digital display of the evaluation unit.

3.3.2 Carbonaceous analysis

The methods currently being applied for the determination of organic and elemental carbon in particulate filters are operationally defined and it is currently a popular subject of investigation owing to the important roles carbon play in atmospheric chemistry and policy formulation. A major uncertainty in determining total carbon using thermal evolution methods results from differences in volatilization of certain organic compounds during sampling and storage (Fitz, 1990; Chow et al. 1996a; Watson et al. 2001a; Watson et al. 1994b; Watson and Chow, 2002a; Watson and

Chow, 2002b). The split of organic and elemental carbon in thermal analysis is even more ambiguous because it depends on temperature setpoints and a number of operating parameters, and these parameters are only empirically defined. To overcome this problem, a laser is used to monitor changes in filter darkness during the thermal evolution process by reflectance or transmittance method.

In this study, samples were analyzed for OC and EC using DRI Model 2001 Thermal/Optical Carbon Analyzer (AtmAA Inc, Calabasas, CA, US) with the IMPROVE TOR protocol (Chow et al. 1993) that has been demonstrated to be much suitable for Hong Kong aerosol samples rather than transmittance protocol (Chow et al. 2005). The DRI Model 2001 carbon analyzer (Chow et al. 2004) is based on the preferential oxidation of OC and EC compounds at different temperatures. It relies on the fact that OC is volatilized from the sample deposit in a helium (He) atmosphere at low temperatures, while EC is not consumed. The TOR protocol heats the sample (0.526 cm^2 per punch) stepwise at temperatures of 120 °C (OC1), 250 °C (OC2), 450 °C (OC3) and 550 °C (OC4) in a non-oxidizing He atmosphere, and 550 °C (EC1), 700 °C (EC2) and 800 °C (EC3) in an oxidizing atmosphere with 2% oxygen (O_2) in He. The carbon evolved was oxidized to carbon oxide (CO_2) and then reduced to methane (CH_4) for quantification with a flame ionization detector (FID). The pyrolysis

of OC was continuously monitored by a helium-neon (He-Ne) laser at a wavelength of 632.8 nm. OC is defined as the portion of carbon that evolved before the temperature at which the filter reflectance resumes the initial level, whereas the carbon evolved beyond this temperature is defined as EC. The MDL of carbon combustion methods is 0.82 μg cm^{-2} for OC, 0.19 μg cm^{-2} for EC, and 0.93 μg cm^{-2} for total carbon (sum of OC and EC). All of the samples in this study have concentrations higher than MDL. Replicated analyses were performed for ~10% of all samples.

3.3.3 Ion analysis

Ion analysis was performed on the quartz fiber filters. Half of the quartz filter was extracted with 10 ml of distilled-deionized water and the extracted materials were analyzed for chloride, nitrate, sulfate, sodium, ammonium and potassium ions by IC (Chow and Watson, 1999). Ion Chromatography is a liquid chromatographic technique based on an ion exchange mechanism and suppressed conductivity detection for the separation and determination of anions. Each ion's affinity for the exchange site, known as its selectivity quotients, is largely determined by its radius and its valence. Ions are identified by its retention time within the ion exchange column and ionic concentrations are quantitatively determined from conductivity peak area. The detection limits of chloride, nitrate, sulfate, sodium, ammonium and potassium were

0.5, 15, 20, 15, 15 and 15 μg l^{-1}, respectively. Blank and replicate analyses were performed for 10 % of all samples according to standard operating procedures.

3.3.4 Elemental Analysis

All elemental analyses for the samples in this study were conducted in DRI using the energy dispersive X-ray fluorescence (XRF) method. The XRF analytical method (Watson et al. 1999) was applied to determine the concentrations of about 40 different elements in particles on Teflon filters without destroying the sample, including Na, Mg, Al, Si, P, S, Cl, K, Ca, Ti, V, Cr, Mn, Fe, Co, Ni, Cu, Zn, Ga, As, Se, Br, Rb, Sr, Y, Zr, Mo, Pd, Ag, Cd, In, Sn, Sb, Ba, La, Au, Hg, Tl, Pb, and U. XRF spectroscopy is based on the measurement of X-ray energy produced by the ejection of an inner shell electron from an atom in the sample. The X-ray is specific for different atoms and the intensity of the X-ray is proportional to the number of atoms in the sample. Therefore the concentrations of elements can be quantitatively determined through a comparison with known standards. A few blank Teflon filters were also analyzed to minimize the contamination during transportation. For the detection limits of each element, readers should refer to the study of Louie et al. (2005).

3.4 Calculations and modeling

3.4.1 Estimation of emission factors during the tunnel study

The calculation of the emission factor follows the method of Pierson (Pierson et al. 1983, 1996). The vehicle emission factor is the mass of specific pollutants produced in a unit kilometer. It can be determined from:

$$EF_{veh} = \frac{(C_{out} - C_{in})AUt}{NL} \qquad 3.4$$

where EF_{veh} is the average vehicle emission factor in mg vehicle^{-1} km^{-1} traveled. C_{out} and C_{in} represent the mass concentration of specific pollutants in mg m^{-3}, at the tunnel exit and entrance. A is the tunnel cross-section area in m^2, U is the wind speed in m s^{-1}, and t is the sampling duration. N is the total traffic number during the sampling period. L is the distance in km between the two monitoring stations.

The emissions of the diesel-fueled vehicles (DV) and non-diesel-fueled vehicles (NDV, the combination of gasoline- and LPG-fueled vehicles) can be differentiated, according to the method described by Pierson et al. (1996). For the nth sampling period, EF can be written as:

$$EF = xEF_{DV} + (1-x)EF_{NDV} = (EF_{DV} - EF_{NDV})x + EF_{NDV} \qquad 3.5$$

where x is the DV fraction; 1-x is the NDV fraction; and EF is the emission factor

for mixed vehicles during each run. The plot of a series of EF during each run versus x gives a straight line with EFDV at x=1. By choosing varying times of day and night for performing the experimental measurements, a wide range in the fraction of diesel-fueled vehicles can be sampled, thus minimizing extrapolation errors (Gertler et al. 2002).

3.4.2 PMF receptor model

EPA PMF 1.1 solves the general receptor modeling problem using constrained, weighted, least-squares. The general model assumes there are p sources, source types or source regions (termed factors) impacting a receptor, and linear combinations of the impacts from the *p* factors give rise to the observed concentrations of the various species. Mathematically stated as:

$$x_{ij} = \sum_{k=1}^{p} g_{ik} f_{kj} + e_{ij} \qquad 3.6$$

where x_{ij} is the concentration at a receptor for the j^{th} species on the i^{th} day, g_{ik} is the contribution of the k^{th} factor to the receptor on the i^{th} day, f_{kj} is the fraction of the k^{th} factor that is species j, and e_{ij} is the residual for the j^{th} species on the i^{th} day. In EPA PMF, it is assumed that only the x_{ij}'s are known and that the goal is to estimate the

contributions (g_{ik}) and the fractions (or profiles) (f_{kj}).

The task of EPA PMF is to minimize the sum of squares:

$$Q = \sum_{i=1}^{n} \sum_{j=1}^{m} \left[\frac{x_{ij} - \sum_{k=1}^{p} g_{ik} f_{ki}}{u_{ij}} \right] \qquad 3.7$$

where u_{ij} is the uncertainty in the j^{th} species for day i. EPA PMF 1.1 operates in a robust mode, meaning that "outliers" are not allowed to overly influence the fitting of the contributions and profiles.

If the model is appropriate for the data and if the uncertainties specified are truly reflective of the uncertainties in the data, then Q should be approximately equal to the number of data points in the concentration data set. The application of PMF depends on the estimated uncertainties for each of the data values. The uncertainty estimation provides a useful tool to decrease the weight of missing and below detection limit data in the solution as well as account for the variability in the source profiles.

3.4.3 CMB receptor model

The CMB model quantifies contributions from chemically distinct source types by using a variance weighted least squares solution to the following equation to solve for

the mass contribution of each source (S_j).

$$C_i = \sum_{j=1}^{p} \sum a_{ij} S_j, i = 1, n \qquad 3.8$$

where C_i is the concentration of species i measured at the receptor, and a_{ij} is the fraction of species *i* in the emissions from source j, *S* is the total mass concentration contributed by source *j*, and *p* is the number of sources, and n is the number of species, with $n \geq p$. The C_i and a_{ij} are known and the S_j are found by a least squares solution of the over-determined system of equations. The CMB model is a simple, linear mixing model which requires conservation of composition between source and receptor but makes no assumptions about transport or removal processes and it requires an accurate knowledge of all significant source emissions compositions (Chow et al. 1996b). The model cannot separate emissions of particular emitters with the same source profiles.

3.4.4 PSCF receptor model

PSCF is a statistical method that evaluates the source contribution of air pollution at a receptor site by counting each trajectory segment endpoint that terminates within each cell (Ashbaugh, 1983, Malm et al. 1985). The probability of an event at the receptor site is related to that cell. The PSCF value can be interpreted as the conditional

probability that concentrations larger than a given criterion value are related to the passage of air parcels through the cell during transport to the receptor site. The PSCF value for a single grid cell is a normalized value that can be calculated as follows:

$$PSCF_{ij} = \frac{n_{ij}}{m_{ij}} \qquad 3.9$$

where m_{ij} is the number of endpoints for ij^{th} cell recording times of arrival at the sampling site corresponding to pollutant concentrations higher than a given criterion value. n_{ij} means the number of all endpoints that fall in the same cell. Cells with high PSCF values indicate that the regions are high potential contributions to the pollution at the receptor site.

3.5 Quality assurance and quality control

3.5.1 Filter handling, sampling, experiments

Before sampling, quartz fiber filters were preheated in an electric furnace at 900 °C for at least 3 hours in order to remove carbonaceous contaminants, while the temperature is 550 °C for aluminum foil to prevent melting of membranes. The filters such as quartz, aluminum, Teflon filters were equilibrated in a desiccator with temperature of 20-30 °C and relative humidity of 30%-40% for 24 hours before

pre-sampling weighing. At the end of each sampling interval, filters were placed into plastic petri dishes, and then all petri dishes were put into a sealed plastic bag before quick transportation to a desiccator, followed by post-sampling weighing. The filters were handled only with tweezers cleaned by dry KimWipes (Kimberly-Clark Corporation, US) to reduce the possibility of contamination. After weighing, samples were stored in a refrigerator at about 4 °C before chemical analysis to prevent the evaporation of volatile components.

3.5.2 Calibration and flow check

- For RP2025 and URG Sampler, the flow rates were checked before and at the end of each sampling campaign to assure a constant flow rate through the size separator. Routine cleaning of the samplers and their components were conducted to make sure that all the parts functioned well and contamination could be minimized.
- For size segregated samplers, such as: MOUDI 110 and Nano MOUDI 115, the flow rates were checked before and at the end of the study to assure a constant flow rate. Routine cleaning of the samplers and their components were conducted. The multi-orifice in stages, which were used to collect very fine particles, was further cleaned by compressed air.

- For Kimoto monitor, the Teflon tape (GS-25K, Kimoto Electric Co., LTD., Japan) was changed and the calibration was routinely made every month.
- The SMPS3936 is a brand new instrument and it was calibrated in the factory. During the study, a schedule of maintenance activities was adhered to, including daily, weekly, and monthly equipment inspections focusing on maintenance of dry butanol in condensation particle counters, leak checks, and flow calibration. In addition, the impactor was cleaned with dry KimWipes and a think layer of Dow Corning High Vacuum Grease (TSI Incorporated, US) was put on it before sampling.
- Although the self-maintained Aethalometer doesn't need any more special action, it was deemed necessary to compare the BC data, obtained from Aethalometer, Kimoto PMS-316D, to that of filter-based EC to confirm the reliability of the measurements.

3.5.3 Chemical analysis

Field blanks, which accompanied samples to the sampling sites, were used to determine any background contamination. They were analyzed by the same approach for chemical analysis with samples.

For the DRI Model 2001 OC/EC analyzer, regular operation for the analyzer involves

cleaning the punching tool and tweezers between each sample with dry Kimwipes (Kimberly-Clark Corporation). It was noted that with usage, the quartz rods will lose transparency due to deposition of material from the samples and a white deposit forms on quartz when it is heated at high temperature, which may influence the output signals. Cleaning or replacement of the quartz rods was carried out to restore the performance. It was also ensured that calibration was done after any repairs. Four standards are used in calibrating the carbon analyzers: 5% nominal CH_4 in He, 5% nominal CO_2 in He, KHP, and sucrose. Analyzer calibration was routinely performed every six months with one of the four calibration standards. The calibration was done by injection of known volumes of the standard to yield a calibration curve of peak area ratio of injected carbon: CH_4 (internal standard) versus μg of carbon injected (Internal Standard Calibration Method). There is also a CH_4 in He that is injected at the end of each analysis to serve as an internal standard. System blank and standard samples (samples that were conducted by inter-laboratory comparisons) were run on a weekly basis. Replication from a prior sample was run with each set of 10 samples. When a standard sample differed from others by more than ±10% or when a replicate concentration differed from the original value by more than ±10%, the samples are re-analyzed. Other else, inter-laboratory comparisons and spiked sample analysis (a

filter on which known carbon concentrations were deposited) were conducted.

It was noted that for the XRF analysis, the samples on the filters should not be too heavy because the ideal conditions are designed specifically for thin films. Otherwise the internal absorption of both incident and emitted X-rays within the samples will influence the determined concentrations of elements. Optimum filter loading was approximately 150 μg m^{-3} (1 mg per filter for 37 mm filters, and 2 mg per filter for 47 mm filter) to comply with these assumptions. Three types of XRF standards were used for calibration, performance testing, and auditing: vacuum-deposited thin-film elements and compounds (Micromatter), polymer films, and NIST standards. A separate Micromatter thin-film standard was used to calibrate the system for each element. The vacuum deposits cover the largest number of elements and are used as calibration standards. The polymer film and NIST standards were employed as quality control (QC) standards. NIST standards are the definitive standard reference material, such as SRM, 1832 (species Al, Ca, Co, Cu, Mn) and SRM, 1833 (Si and Fe, Pb, K, Si, Ti and Zn). A QC standard and a replicate from a previous batch were analyzed with each set of 10 samples. When a QC value differed from specifications by more than ±5% or when a replicate concentration differs from the original value by more than ±10%, the samples are re-analyzed. In order to allow the blank spectra to be developed

and the subsequent calculations to proceed, analysis was done for the lab blanks in the first run for any batch.

The plastic-tube and glassware used during the pretreatment of ion analysis by IC were first washed with detergent and soaked in a detergent bath overnight, then rinsed thoroughly with tap water. After they were soaked in a 10% concentrated nitric acid bath for twenty-four hours, all the plastic-tube and glassware were then washed thoroughly with double-distilled deionized water. They were ready to use after air-drying in a clean cabinet with luminar flow. The ion standards (DIONEX) were used to prepare working standards on a monthly basis. Calibration standards were prepared from the working standards weekly or biweekly in routine operations. For ion analysis with IC, calibration standard for each ion spanned the entire range of sample concentrations, and separate calibration curves were required for samples with low and high concentrations. During instrument calibration, if any calibration point varied by more than ±5% of the specified value, a new calibration standard was prepared to assure the accuracy of the analysis. Replicates from a prior sample were run with each set of 10 samples. Inter-comparisons amongst different laboratories and spiked sample analysis (a filter on which known ionic concentrations were deposited) were conducted.

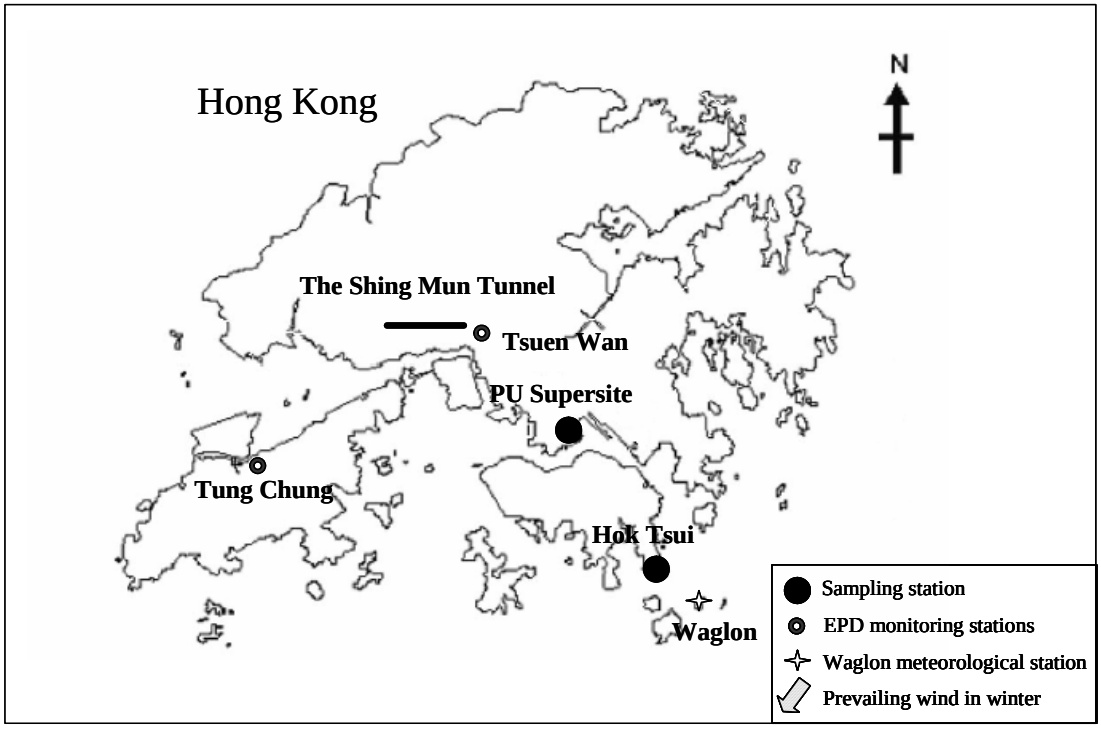

Figure 3.1 Hong Kong map, locations of major cities in the PRD region, and locations of sampling sites in this study.

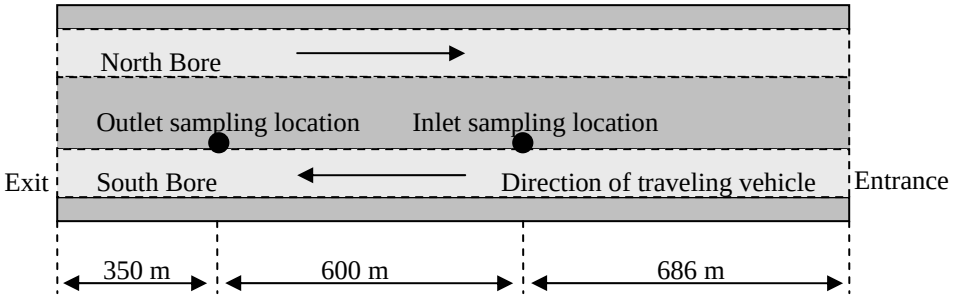

Figure 3.2 The schematic diagram of the west side of the Shing Mun Tunnel.

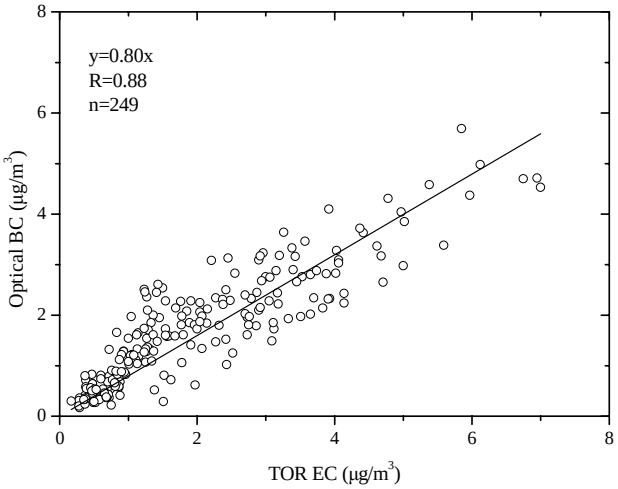

Figure 3.3 Comparison of 24-hour average BC mass concentrations between the Aethalometer and TOR method; n is the number of sampling days.

Table 3.1 Sampling program at PU Supersite.

Observation and Method	Period	Sampling Interval	Frequency	Filter	Chapter
Continuous Particle Mass and Chemistry					
Kimoto SPM-613D for $PM_{2.5}$, PM_{coarse}, BC mass	01/15/2005-12/9/2005	1-hr	Continuous		Chapter 4
Bulk Aerosol (Mass and Chemistry)					
$PM_{1.0}$, $PM_{2.5}$, PM_{10} mass, ions, carbon, Elements (URG sampler with Quartz/Teflon filters)	10/01/2004-09/30/2005	24-hr	3 or 4 sample sets per month	60 T (47mm) 60 Q (47mm)	Chapter 4
$PM_{2.5}$ mass and carbon (RP2025 / Quartz filters)	01/21/2004-05/31/2004	24-hr	Daily	193 Q (47mm)	Chapter 5
$PM_{1.0}$ mass and carbon (RP2025 / Quartz filters)	01/21/2004-05/31/2004	24-hr	Daily	193 Q (47mm)	Chapter 5
Diurnal variation of $PM_{2.5}$, ions, carbon (RP2025 / Quartz filters)	07/20-22/2005 07/26-28/2005	2-hr	Intensive	65 Q (47mm)	Chapter 5
Size Segrated Aerosol (Mass and Chemistry)					
Mass, ion and elemental size distribution (MOUDI 0.010-2.5 μm in 11 fraction with Teflon & Aluminum foils)	06/03/2005-07/28/2005 11/15/2005-01/13/2006	48-hr to 72-hr	3 sets on Aluminum foils and 2 sets on Teflon substrats for each season	36 T (47mm and 37 mm) 72 Q (47mm and 37 mm)	Chapter 6
Particle Counts					
Particle numbers in size range of 0.007-0.217 μm (TSI SMPS 3936)	Jan-Feb 05 Jul-05	30-min	Continuous monitor in days without rainfall		Chapter 6
Particle numbers in size range of 0.1-2 μm (OPC 1003)	The same as the SMPS	30-min	Continuous		Chapter 6

Table 3.2 Sampling program in the Shing Mun Tunnel study.

Run No.	Date	Duration	Sampling items		Traffic number			WS[c]	VS[d]	Temp[e]	Pres[f]
		Hour			Non-diesel[a]	Diesel[b]	Total	m s^{-1}	km h^{-1}	°C	mmHg
Run 1	Aug/13/03	1700-1900	DRI sampler	DustTrak	1526	1656	3182	5.0	60.5	31.0	747.5
Run 2	Aug/16/03	1700-1900	DRI sampler	DustTrak	1372	646	2018	4.6		28.9	748.2
Run 3	Aug/17/03	0800-1000	DRI sampler	DustTrak	1000	692	1692	3.9	68.3	31.1	748.1
Run 4	Aug/31/03	0800-1000	DRI sampler	DustTrak	1072	676	1748	3.9		30.6	749.1
Run 5	Jan/12/04	1700-1800	DRI sampler	DustTrak	904	1040	1944	5.2	62.2	23.0	766.8
Run 6	Jan/13/04	1400-1500	DRI sampler		516	824	1340	5.1	62.7	22.3	767.0
Run 7	Jan/14/04	2200-2300	DRI sampler		626	356	982	4.0	64.3	21.0	765.9
Run 8	Feb/1/04	0800-0900	DRI sampler		464	322	786	3.5	67.4	20.9	760.5
Run 9	Feb/9/04	0900-1000	DRI sampler	DustTrak	1384	1108	2492	4.9		16.3	768.8
Run 10	Feb/10/04	0800-0900	DRI sampler		1736	1106	2842	4.8		18.7	769.0
Run 11	Feb/11/04	1400-1500	DRI sampler	DustTrak	516	824	1340	5.3		23.3	767.4
Run 12	Feb/11/04	1500-1600	DRI sampler	DustTrak	534	906	1440	5.3		21.8	767.4
Run 13	Feb/14/04	2100-2200	DRI sampler		624	294	918	3.8		21.1	763.2
Run 14	Feb/23/04	1700-1800	DRI sampler		688	892	1580	5.4		23.7	763.5
Run 15	Feb/23/04	1800-1900	DRI sampler		896	752	1648	4.8		23.7	763.5
Run 16	Feb/25/04	1100-1200	DRI sampler	DustTrak	484	874	1358	5.3		26.1	761.9
Average					896	811	1707	4.7	64.2	24.0	761.1

[a] number of gasoline-fueled vehicles and LPG-fueled taxis; [b] number of diesel-fueled vehicles; [c] wind speed; [d] vehicle speed; [e] temperature; [f] pressure.

Table 3.3 Sampling program at HT rural station.

Observation and Method	Period	Sampling Interval	Frequency	Filter	Chapter
Continuous Particle Mass and Chemistry					
Aethalometer (AE-42) for BC	06/2004-05/2005	5-min	Continuous		Chapter 5
Bulk Aerosol (Mass and Chemistry)					
$PM_{2.5}$ mass and carbon (RP2025 / Quartz filters)	06/2004-05/2005	24-hr	Daily	249 Q (47mm)	Chapter 5

Chapter 4 Comparisons of Chemical Characteristics of Fine and Coarse Particles

4.1 Introduction

Particle emissions from on-road vehicles have a wide range of particle sizes from ultrafine particulate matter (vehicle exhausts, brake-wear emissions), to fine particulate matter (most of vehicle exhausts by mass), to coarse particulate matter (tire wear emissions, resuspension from moving vehicles). To correctly characterize the particulates at the roadside environment, these different size fractions must be considered. On January 17, 2006, the USEPA Administrator proposed to introduce a 24-hour PM_{coarse} standard of 70 μg m^{-3} and eliminate the PM_{10} NAAQS. However, investigations on the new standards are still quite limited throughout the world so far, thus the advantage of the proposed new standards is not clear. Moreover, there is a suspicion that the PM_{coarse} can be represented by the current air quality standard of PM_{10}. In this Chapter, the comparison of chemical characteristics of fine ($PM_{2.5}$) and coarse (PM_{coarse}) particles was conducted to identify the commonality and difference among them at PU Supersite, which may provide valuable information for toxicological study. The question of whether PM_{10} can reflect PM_{coarse} has been

answered in this chapter. The ultrafine fraction will be examined in Chapter 6.

Besides the chemical properties of aerosols, a new technique capable of measuring new PM_{coarse} standard was tested in this chapter. Multi-site evaluations of candidate methodologies for determining coarse particulate matter (PM_{coarse}) concentrations have been already conducted by USEPA (Vanderpool et al. 2004). The Kimoto System (SPM-613D) was tested to make comparison for $PM_{2.5}$, PM_{10}, and PM_{coarse} with FRM samplers in the Vanderpool et al. (2004) study and satisfactory success was achieved. In the present study, the SPM-613D sampler was employed at PU Supersite as a semi-continuous monitor for measuring $PM_{2.5}$, PM_{coarse}, as well as BC, and the results were compared with collocated filter-based URG sampler and Aethalometer. The diurnal, weekly, and seasonal variations of fine and coarse particles were examined and the influencing factors on fine and coarse particulate concentrations were also determined. These details are presented in this chapter.

4.2 Results and discussion

4.2.1 The comparison of chemical characteristics of 24-hr integrated $PM_{1.0}$, $PM_{2.5}$, PM_{10}, and PM_{coarse}

4.2.1.1 Measurement validation

The 24-hr integrated $PM_{1.0}$, $PM_{2.5}$, PM_{10} and PM_{coarse} data reported in this section were

derived from the URG sampler, which took samples on the collocated Teflon filter membranes and quartz fiber filter, simultaneously, from October 2003 to September 2004, with about three or four sets of samples for each month. The Teflon filter membrane collected particles for mass determination by gravimetry in Air laboratory of HK PolyU and for 40 elements (Na to U) by XRF (Watson et al. 1999) in DRI. The quartz fiber filter was analyzed for mass by gravimetry and for OC and EC by DRI model 2001 OC/EC analyzer and for ion species (i.e., Cl^-, NO_3^-, SO_4^{2-}, NH_4^+, K^+) by IC in Air laboratory of HK PolyU. Major mass constituents, including OC, EC, SO_4^{2-}, NO_3^-, NH_4^+, and elements (e.g., Mg, Al, Si, Ca, Fe, and Zn) were detected in almost every sample. Of the 40 elements, 28 were found to have higher concentrations than three times the minimum detection limit for fine particles, including Na, Mg, Al, Si, P, S, Cl, K, Ca, Ti, V, Cr, Mn, Fe, Ni, Cu, Zn, Ga, As, Se, Br, Rb, Sr, Zr, Sn, Sb, Au, Pb; and 25 elements exceeding three times of the minimum detection limit for coarse particles, including Na, Mg, Al, Si, P, S, Cl, K, Ca, Ti, V, Cr, Mn, Fe, Ni, Cu, Zn, Ga, As, Se, Br, Rb, Sr, Y, and Zr.

It is often necessary to conduct consistency tests based on known physical relationships between variables to the assembled data because particles were sampled on multiple substrates when chemical characterization is desired and chemical

analyses were performed with several instruments at different laboratories. The consistency tests include a number of measures as shown in previous studies (Chow et al. 2002; Louie et al. 2005). (1) comparisons between mass concentrations and the weighted sum of chemical species; (2) comparisons between concentrations of the same species measured by different analysis methods (e.g., sulfate by IC versus total sulfur by XRF; soluble potassium by IC versus total potassium by XRF; and chloride by IC versus chlorine by XRF); (3) charge balances between anions and cations; and (4) comparisons between mass and chemical concentrations in different size fractions (e.g., $PM_{2.5}$ concentrations must always be less than or equal to PM_{10} concentrations).

Figure 4.1 shows the comparison between gravimetric mass measurements from the collocated Teflon filter membranes and quartz fiber filter membranes. The data displayed in the figure includes $PM_{1.0}$, $PM_{2.5}$, and PM_{10}, with 40 samples for each fraction. Good agreements (slope and ratio close to 1) and high correlation (R=0.97) indicates consistent sampling and gravimetrical analysis results from the Teflon- and quartz-fiber filter membranes in the present study. A similar phenomenon was found from the observations of Engelbrecht et al. (2001) in US and of Louie et al. (2005a) in Hong Kong. Since quartz filters are known to have positive sampling artifacts by absorbing gaseous organic compounds and water (Turpin et al. 1994; Kirchstetter et al.

2001; Arhami et al. 2006) and tend to shred and loose part of material after heating (Chow and Watson, 1998), the following discussion refers to Teflon-membrane filter mass unless otherwise specified.

The relationship between gravimetrical mass and the sum of species in this study is shown in Figure 4.2 for $PM_{1.0}$, $PM_{2.5}$, and PM_{10}, respectively. Total sulfur (S), soluble chloride (Cl^-), and soluble potassium (K^+) are excluded from the sum to avoid double counting since sulfate (SO_4^{2-}), chlorine (Cl), and total potassium (K) are included in the sum. On average, the $PM_{1.0}$ and $PM_{2.5}$ sum agree well with the corresponding measured mass (y/x ratio and R close to 1), although there is slight fluctuation around the one to one line. The sum of individual chemical species measured in $PM_{1.0}$ and $PM_{2.5}$ explains almost all fine particulate mass. Theoretically, the gravimetrically measured particulate mass should be equal to or higher than the sum of the individual chemical species concentrations because the measurements do not account for metal oxides in crustal material, unmeasured cations, or hydrogen and oxygen associated with organic carbon. The sum of individual species exceeded the $PM_{1.0}$ and $PM_{2.5}$ mass concentrations for samples with low mass concentrations, which is perhaps due to the greater uncertainty of chemical analyses on low loading samples. The sum of individual species for PM_{10} only accounted for ~91% of the total mass concentrations

in the present study. It is not surprising because PM_{10} were expected to consist of more crustal material than fine particles; as a consequence, more unmeasured metal and oxides, hydrogen, and oxygen should exist in PM_{10}, leading to significantly decreased mass from the sum of the individual species.

The composition of chemical species concentrations measured by different chemical analysis methods was examined. As seen from Figure 4.3, the water-soluble ions determined by IC from the quartz fiber membranes, namely sulfate, potassium, and chloride, show good correlations with the total elemental concentrations by XRF from the Teflon filter membrane, with the correlation coefficients (R) ranging from 0.95 to 0.97. The ratio of sulfate to total sulfur was close to three with small intercept less than 1 in this study, indicating that more than 90% of sulfur was present as soluble sulfate in the atmosphere and that both XRF and IC measurements are valid. The scattering plot of soluble and elemental potassium also gave a small intercept close to zero, which means the slope is nearly close to the ratio of y-axis and x-axis, meaning near 90% of potassium element present as soluble potassium in the atmosphere. This probably indicates the major sources of potassium are vegetative burning or cooking aerosols rather than of geological origins. The correlation coefficient between chloride and chlorine was a bit lower than the others. This is because the uncertainties of

chloride and chlorine measurements were higher: the chloride's elution peak in ion chromatographic analysis is close to the distilled water dip which, in turn, shifts the baseline of the chromatogram (Chow and Watson, 1999).

Ammonium sulfate, ammonium bisulfate and ammonium nitrate are the dominant forms of ammonium in aerosols. Ammonium can be calculated based on the stoichiometric ratios of the different compounds. Ammonium is calculated from nitrate and sulfate, assuming that all nitrate was in the form of ammonium nitrate and all sulfate was in the form of either ammonium sulfate (i.e., calculated ammonium = [0.38×sulfate] + [0.29×nitrate]) or ammonium bisulfate (i.e., ammonium = [0.192×sulfate] + [0.29×nitrate]). Figure 4.3 shows the correlations between calculated and measured ammonium, which were good for both cases. The slope is 1.87 when ammonium sulfate is assumed and close to one when ammonium bisulfate is assumed. This result seems to support the premise that majority of ammonium is in the form of ammonium bisulfate during the study period because the calculated ammonium can be explained completely by actual ammonium in the atmosphere in this case. PM_{10} showed higher slope (1.90) than $PM_{1.0}$ and $PM_{2.5}$ when ammonium sulfate is assumed. This is perhaps because of the presence of sulfate and/or nitrate salts that might be associated with water-soluble calcium (Ca^{2+}) or sodium (Na^{+}) ions.

The anion and cation balance in Figure 4.4 also shows the correlations were high (R=0.97) for all determined size fractions. A deficiency in cations that is not accounted for by measured anions was found, especially for high loading samples, which maybe because there are other cations in atmosphere that were not measured in this study concerning the marine view of Hong Kong. The data shown in Figure 4.4 was calculated from Cl^-, NO_3^-, SO_4^{2-} for anions, and from Na^+, K^+, NH_4^+ for cations.

Most of the particulate mass in urban and non-urban areas can be explained by a combination of the five major chemical components (Solomon et al. 1989), including: carbonaceous material, sulfate, nitrate, ammonium, and mineral material and minor elements. In the present study, sea salt was added since Hong Kong is located in a coastal area in South Asia. To correct for unmeasured oxygen, hydrogen, sulfur, and nitrogen from the organic matter, OC concentrations were multiplied by 1.4 (Grosjean and Friedlander, 1975; Gray et al. 1986). The geological material was equal to 1.89×Al + 2.14×Si + 1.40×Ca + 1.43×Fe (Solomon et al. 1989). Non-crustal minor elements are the sum of other-than-geological minor elements. Figure 4.2 displays the scattering plot of the reconstructed particle mass and gravimetrical mass. The reconstructed particle mass was almost equal to the gravimetric mass with some fluctuations along the 1:1 line. On average, the ratio of reconstructed and gravimetric

mass in this study was 1.07±0.13 for $PM_{1.0}$, 1.04±0.21 for $PM_{2.5}$, and 0.91±0.19 for PM_{10}. The reconstructed PM_{10} mass concentrations were much lower than gravimetrical mass due to unmeasured abundant mineral materials in it.

The comparisons between particulate mass can be performed in different size fractions to check the internal consistency of the data obtained in this study. Figure 4.5 illustrates the scatter plots of $PM_{2.5}$ against other particulate fractions, such as $PM_{1.0}$, $PM_{1.0\text{-}2.5}$, PM_{coarse}, and PM_{10}. With three exceptions during the study period, Figure 4.5 shows all $PM_{2.5}$ mass concentrations are higher than $PM_{1.0}$ ($PM_{1.0}/PM_{2.5}$=0.81±0.18) and all PM_{10} mass concentrations are higher than $PM_{2.5}$ ($PM_{2.5}/PM_{10}$=0.69±0.09). The correlation coefficient (R=0.97) was higher between $PM_{1.0}$ and $PM_{2.5}$ than that (R=0.88) between $PM_{1\text{-}2.5}$ and $PM_{2.5}$, indicating the sources of $PM_{2.5}$ are more similar to $PM_{1.0}$. While the relationship was poor between $PM_{2.5}$ and PM_{coarse} (R=0.66), showing they are different aerosols in nature, the correlation between PM_{10} and $PM_{2.5}$ was good (R=0.95).

4.2.1.2 Annual average mass concentrations

Annual mean and standard deviations of $PM_{1.0}$, $PM_{2.5}$, PM_{10}, and PM_{coarse} species concentrations are presented in Table 4.1, 4.2, 4.3, 4.4. The particulate mass concentrations fluctuated significantly during the study period, ranging from 14.3 to

93.6 μg m^{-3} for $PM_{1.0}$, from 14.4 to 118.1 μg m^{-3} for $PM_{2.5}$, from 28.0 to 172.8 μg m^{-3} for PM_{10}, and from 5.8 to 60.6 μg m^{-3} for PM_{coarse}. The annual mean was 44.5±19.5 μg m^{-3}, 55.4±25.5 μg m^{-3}, 81.3±37.7 μg m^{-3}, and 25.9±15.5 μg m^{-3} for $PM_{1.0}$, $PM_{2.5}$, PM_{10}, and PM_{coarse}, respectively. On average, $PM_{1.0}$ accounted for ~80% of $PM_{2.5}$ and $PM_{2.5}$ contributed ~70% to PM_{10}. As a result, PM_{coarse} only occupied nearly 30% of PM_{10}. The annual average of $PM_{2.5}$ at PU Supersite was similar with that measured during 2000/2001 at MK (a typical roadside in Hong Kong) (Louie et al. 2005a), but much higher than the HT background site of Hong Kong (Louie et al. 2005a) by a factor of 2.3 and higher than the US EPA's annual $PM_{2.5}$ NAAQS of 15 μg m^{-3} by a factor of 3.7. The annual mean of PM_{10} at PU Supersite was 1.2 times the 2005 annual mean of 68.6 μg m^{-3} at MK by HKEPD, which is reasonable because the instruments used by HKEPD is TEOM were supposed to underestimate the true values due to loss of semi-volatile compounds, like ammonium nitrate (Charron et al. 2004). Approximately one-third of the $PM_{2.5}$ acquired at PU Supersite exceeded 65 μg m^{-3} (short-term 24-hr average standard in US) and was less than five percent of the PM_{10} exceed 180 μg m^{-3} (short-term 24-hr average standard in HK).

The majority of aerosol mass for individual species exist in different size fractions. The details are shown in Figure 4.6. In addition to abundant species such as OC, EC,

and sulfate, some other species also mainly exist in fine particle fractions (more than 60%), like ammonium, K, P, V, Ni, and Zn, although the concentrations were low. On the contrary, some elements have the majority of mass in coarse mode (more than 60%), like soluble chloride, Al, Si, Ca, Ti, Fe and Cl.

4.2.1.3 Chemical mass closure

Figure 4.7 shows the chemical mass closure charts for $PM_{1.0}$, $PM_{2.5}$, PM_{10}, and PM_{coarse} data acquired at PU Supersite. Overall, EC, organic matter (OM), and sulfate comprised the majority of $PM_{1.0}$ and $PM_{2.5,}$ accounting for ~81% of total $PM_{1.0}$ mass and ~78% of the total $PM_{2.5}$ mass. The total amount of nitrate, ammonium, sea salt, and geological material and minor elements only contributed about ~18% and ~20% to $PM_{1.0}$ and $PM_{2.5}$, respectively. OM, EC, and sulfate were still the major constituents in PM_{10}, while the total percentage decreased to ~62% as the increase of the total percentage of the remained constituents. PM_{coarse} showed difference in chemical composition with other size fractions, with the geological material and minor elements being the most abundant components (~32%) followed by unidentified material (~17%). The unidentified material mainly represents unmeasured metal and oxides, hydrogen, and oxygen that related to geological materials, organics, and water. The third abundant component was OM that has been found to be partly present in coarse

fractions (Yu et al. 2004). The percentage of sea salt and nitrate in PM_{coarse} was much higher than that in $PM_{1.0}$, $PM_{2.5}$, and PM_{10}. This is consistent with the expectation and previous studies on sea salts (Yao et al. 2001) and nitrate (Zhuang et al. 1999a). EC and sulfate, the major components in fine particles, accounted only ~7% of PM_{coarse} for each.

4.2.1.4 Seasonal patterns of aerosols

The seasonal average mass concentrations of particulate matter (including $PM_{1.0,}$ $PM_{2.5}$, PM_{10}, and PM_{coarse}) indicate identical seasonal patterns (Figure 4.8), with high value during cold seasons (e.g., winter, spring, and autumn) and low value in warm season (e.g., summer). As shown in Table 4.1, 4.2, 4.3, 4.4, the seasonal variability of $PM_{1.0}$ was lowest, with about 1.4-fold difference between wintertime and summertime $PM_{1.0}$. The average wintertime PM_{coarse} mass was ~2.3 times of the summertime PM_{coarse}, which is the highest seasonal difference, followed by PM_{10}, $PM_{2.5}$.

The highest OC concentrations were found in winter for $PM_{1.0,}$ $PM_{2.5}$, and $PM_{10,}$ approximately 1.5 times of those OC in the other three seasons. This seasonal pattern is similar with particulate mass, reflecting the fact that changes in the fine OC aerosols are generally proportional to the particulate matter loadings. Regional or long range transport of continental aerosols was believed to be the dominating factor leading to

higher OC levels during winter because Hong Kong is a downwind receptor for continental air masses that contain higher carbonaceous aerosol loading during the wintertime (Pathak et al. 2003; Wang et al. 2003; Yu et al. 2004; Louie et al. 2005b). Local vehicles emissions would not have significant day-to-day variations due to the consistent traffic flow each day (The Annual Traffic Census, 2004). Several pollutants in the Hong Kong atmosphere have been affected by long-range transport of continental aerosols, which lead to higher pollution levels in cold seasons than warm season (Pathak et al. 2003; Louie et al. 2005b; Yu et al. 2004). Most of these pollutants are secondary aerosols, such as OC (Louie et al. 2005b; Yu et al. 2004), and sulfate and ammonium (Pathak et al. 2003), that were thought to be produced by gas-to-particle conversion, or chemical reaction, during the long-range transport. OC was also an important species in PM_{coarse}. The fluctuations in PM_{coarse} OC concentrations were not found to be significant in different seasons, as shown in Figure 4.8, indicating that there are stable sources for coarse mode OC. Most coarse OC in atmosphere is of biologic origin based on the observation in the US (Mamane et al. 1990; Graham et al. 2003). The water-soluble organic carbon (WSOC) has been studied in Hong Kong by Yu et al. (2004) and it was found that the coarse mode WSOC, centered at 4.0±0.3 μm, was largely made of the polar compound group with

low molecular weight. Tire dust is another potentially stable source for coarse OC (Rogge et al. 1993). The instant OC concentrations throughout the entire year indicate that coarse OC is unlike the fine OC that is mainly formed from local vehicle emission and is influenced by the winter monsoon.

The average wintertime EC in the four fractions was lower than the summertime EC, which is consistent with prior investigations on $PM_{2.5}$ EC (Yu et al. 2004; Louie et al. 2005b; Lee et al. 2006). EC originates from relatively simple sources and does not form in atmosphere due to its nearly inert property (Ogren and Charlson, 1983). It mainly originates from incomplete combustion of carbon-containing material (Ogren and Charlson, 1983). The prior studies concluded that the EC spatiality and seasonality in urban area of Hong Kong depends on whether the location is near a road (Louie et al. 2005b) and/or at the downwind area of a container terminal (Yu et al. 2004) because both primary emissions from on-road vehicle and ship are the dominant sources for EC. Situated at the south tip of Kowloon Peninsula, the PU roadside site is within 1 km away from the Victoria Harbour, one of the finest deep-water ports in the world. Several container ports stretch for miles along the south coast of Kowloon Peninsula. Therefore, we concluded that the major reason of increased EC loading in summer is that the site's location becomes downwind of Victoria Harbour under the

prevailing winds. A report released recently by the Institute for the Environment at the Hong Kong University of Science and Technology and Civic Exchange (http://civic-exchange.org/) also reports elevated pollution levels around Victoria Harbour due to the influences of local vehicle and marine under southerly prevailing wind conditions.

Sulfate and ammonium had similar seasonal variations and the patterns of seasonal variations were similar for the four fractions. The average concentration of sulfate was at the same level during cold seasons, which is about 2-3 times of that in summer (Table 4.1, 4.2, 4.3, 4.4, Figure 4.8). Previous study on ions in Hong Kong, performed by Pathak et al. (2003), showed that the concentrations of sulfate and ammonium can be elevated to about 40% by long-range transported continental air massed during autumn, spring, and winter. The trend of increase is supported by the data acquired in this study. Nitrate showed higher concentrations in spring and winter than that in summer and autumn for each fraction by factors of ~3. In the study done by Pathak et al. (2003), continental long-range transport of aerosols contributes a little to nitrate.

There were different seasonal patterns of chloride between fine ($PM_{1.0}$ and $PM_{2.5}$) and coarse particles (PM_{coarse} and PM_{10}). Only less than 30% of total chloride was in fine particles, with the highest average concentration in winter and lowest in the summer. On the contrary, the majority of chloride was in PM_{coarse}, with the highest

concentrations in summer and the lowest in autumn. The coarse mode chloride was generally associated with marine aerosols in Hong Kong (Zhuang et al. 1999a; Yao et al. 2001). It is reasonable to obtain the highest chloride concentration in summer because southerly wind prevails in summer, bringing marine aerosols into Hong Kong. Chloride depletion of sea salt by both nitrate and sulfate formation was observed when Hong Kong was under prevailing easterly wind accompanied with high relative humidity (Zhuang et al. 1999a; Yao et al. 2001).

Silicon is a representative element related to geological material, which mainly presents in PM_{coarse}. In the present study, the average concentration of silicon in coarse particles was high during cold seasons. The summertime silicon was the low. The elevated concentrations during cold seasons are probably associated with the combined effects of dry road surface and high wind speed, while the low concentrations in summer are maybe due to the frequent rainfall that results in wet road surface. Regional transportation is less important for coarse particles due to the large sizes. Resuspension of roadway dust was previously reported to depend on weather, road surface conditions, traffic volumes, and fractions of heavy trucks (Lough et al. 2005).

Elements associated with tailpipe emissions and brake and tire wear, including coarse

mode Cu, Zn, Ba, Pb, and S (Lough et al. 2005), did not show significant seasonal variations, which is consistent with the stable traffic flow and composition from day to day.

4.2.1.5 Sources and transformation of aerosols

Through above investigation in this study, it is found that substantial differences exist in chemical characteristics and seasonal variations between fine and coarse aerosols. In this section, the sources and formation of major chemical constituents will be further identified for fine and coarse aerosols using enrichment factor (EF), OC/EC ratio and linear regression method.

It is very useful to use enrichment factor to examine the origin of elements. Based upon the assumption that all detected Al in each size range originate from resuspended soil material, the earth crust is considered the dominant source of the elements that show EF values close to one using Al as a reference element ($EF_{crust} = (X/Al)_{air}/(X/Al)_{crust}$). Elements with EF_{crust} value larger than five are called enriched elements and have some sources other than crustal weathering, which may be anthropogenic. Based on the results of EF analyses (Table 4.5), five elements (Al, Si, Ca, Ti, and Fe) at PU Supersite station closely resembled material from the earth crust (Taylor and McLennand, 1995), regardless of size ranges. Coarse Na, Mg, K, and Mn were also

related to crustal elements, while the fine mode part possibly combined with those in origin of non-crustal sources, showing slightly higher EF. Several trace elements in coarse particles, including Se, Sr, and Zr, were also mainly from upper crust. For the remaining species, anthropogenic sources dominate their emissions.

The ratio of OC to EC concentrations has been used to study emission and transformation characteristics of carbonaceous aerosols. The underlying hypothesis is EC is from primary anthropogenic sources and is not formed by reactions involving gaseous hydrocarbon precursors in the atmosphere, while OC may be emitted directly from sources as primary particles, but secondary organic aerosols can also be formed in the atmosphere from the low vapor pressure products by atmospheric chemical reactions. At a source-dominated site, like roadside, the OC/EC ratios should reflect the properties of primary source. Numerous studies on vehicle emissions (e.g., Norbeck et al. 1998; Gillies et al. 2001; Laschober et al. 2004) indicated low primary OC/EC ratios of around or less than 1. In this study, the average OC/EC ratios at PU Supersite were less than 1 for $PM_{1.0}$ (0.7±0.3), $PM_{2.5}$ (0.7±0.3), and PM_{10} (0.8±0.3), showing the characteristics of local primary vehicle emissions. Moreover, the time series of OC and EC in fine particles follow each other through years (Figure 4.9), indicating OC and EC have the same origin. However the average OC/EC ratio for

PM_{coarse} (7.8±14.2) was much higher than that for fine particles and the trends of coarse OC and EC were different, as shown in Figure 4.9. These indicate that OC and EC have different sources. Coarse organic aerosols are perhaps secondary or formed from other sources. Since the concentrations of coarse OC aerosols are stable through years, the biologic aerosols and tire dust are expected to be potential sources. Coarse EC showed similar trend to fine EC in summer, suggesting soot macro-aggregates from ships are main sources.

Fine sulfate and nitrate were mainly associated with ammonium in this study, which is supported by the similar temporal variations and high inter-species correlation coefficients, as shown in Figure 4.10 and Table 4.6-4.7, respectively. Ammonium sulfate (or ammonium bisulfate) and ammonium nitrate are formed from conversion of gases to particles. Significant increase was found in concentrations of ammonium, sulfate and nitrate when the air mass was from upwind areas in this study, indicating they are mainly regional inputs. Based on previous studies, sulfate is a representative species for regional inputs in Hong Kong, and ~40% of fine mode sulfate has been found to arise from the Mainland China (Pathak et al. 2003). Coarse sulfate and nitrate had better relationship with Na, rather than ammonium, as shown in Figure 4.10 and Table 4.8. Since the coarse sulfate and nitrate did not accurately follow the

fluctuations of fine sulfate and nitrate (R=0.39), it is concluded that regional inputs have less contributions to coarse sulfate and nitrate. However, it is clear that coarse sulfate and nitrate were influenced by seasonal variation because the concentrations were higher in cold seasons than in warm season. The underlying reasons for the sources of coarse sulfate and nitrate may need further study.

Inter-species correlations of fine particles also give information on elements (Table 4.6 and 4.7). Both K^+ (K) and Pb also had good relationships with Br and Rb, which is supported by a previous study by Louie et al. (2005a). Both K^+ and Pb associate with material burning, like field burning (biomass burning) and lead fueled burning, suggesting these four elements were from material burning process. In addition, good relationships were found between As and Au, as well as Cr and Ni, which is most likely to be related to some emissions that transported from upwind region since there are no industries in the Hong Kong Territory. The crustal-elements correlated moderately (R>0.70) for each other, e.g., Al, Si, Ca, Ti, and Fe.

As can be seen from Table 4.8, the typical crustal elements, such as Mg, Al, Si, K Ca, Ti, Fe, and Mn, mainly presented in coarse mode, showed good correlations with each other. These elements were most likely to have originated from the resuspended road dust. Previous studies have reported a strong contribution of resuspended road dust to

the coarse particles (e.g., Manoli et al. 2002; Lin et al. 2005). Elements K and Rb were probably also from burning process, the same as fine particles. Coarse Cl and Na correlated moderately to each other, which is consistent with the expectation since both elements in coarse fraction are representative for marine aerosols (Fitzgerald, 1991).

Correlations among different size fractions were conducted and the results were shown in Table 4.9. It can be seen that the species were split into two groups. Nearly half of the species showed good correlations among $PM_{1.0}$, $PM_{2.5}$, and PM_{10}, while these species had poor relationships with PM_{coarse}. Overall, both $PM_{1.0}$ and $PM_{2.5}$ indicate totally different properties, compared with PM_{coarse}. Moreover, PM_{10} have properties of fine particles, rather than PM_{coarse}.

4.2.2 Semi-continuous measurements of $PM_{2.5}$, PM_{coarse}, and BC

4.2.2.1 Evaluation of the Kimoto system (SPM-613D) as a semi-continuous monitor for measuring $PM_{2.5}$, PM_{coarse}, and BC

Measurement methods developed by different organizations may give different results when sampling the same atmosphere even though the techniques appear to be similar (e.g., Hitzenberger et al. 2004). Therefore, inter-comparison of samplers is very important in determining how well various samplers agree and how various design

choices influence what is actually measured. Continuous monitors can not only capture the prosperities of particles in better resolution but also prove more economical to operate by reducing sampling site visits and eliminating the need for laboratory facilities and analysis costs. It is currently impractical to perform better time resolution samples using traditional time-integrated particulate samplers, like Partisol RP2025 and URG sampler, for a long-term scale, thus developing continuous monitors is extremely important.

At present, a steadily increasing literature describing the development and evaluation of continuous PM monitors with β-gauge method at minimum cost has emerged over the past decade (Chang et al. 2001; Chueinta and Hopke, 2001). The previous studies found that the β-gauge system provides satisfactory precision when the deliquescent point is not exceeded. One of the major targets at PU Supersite program is to evaluate the new techniques, a semi-continuous automated dichotomous monitor SPM-613D (Kimoto electric co. LTD., Japan) for hourly $PM_{2.5}$, PM_{10}, and BC, by making comparison with traditional filter-based samplers. Twenty four hour average concentrations were calculated from the semi-continuous measurements to temporally match the time-integrated quartz filter samples in the following discussion.

The $PM_{2.5}$ mass concentrations derived from TEOM and URG sampler were used to

make comparison with the SPM-613D β-gauge monitor. Figure 4.11 shows the scattering plot of hourly $PM_{2.5}$ mass concentrations determined by SPM-613D against those measured by TEOM. The data in Figure 4.11 was a result of nearly 5-month measurements, from 15 January to 8 June 2005. The comparison revealed a good correlation of the $PM_{2.5}$ concentrations measured by two methods (R=0.85). However, on average, the SPM-613D overestimated the TEOM $PM_{2.5}$ by a factor of 1.3±0.4. This is partly due to the higher setting temperature (50 °C) at the drying tank of the TEOM than that (30 °C) of SPM-613D. The temperature is an important factor influencing the particle mass determined since the presence of volatile and semi-volatile organic materials in aerosols. Both of TEOM and SPM 613D need preheating the air stream before particles are deposited on filters due to the limitation of detect techniques. The TEOM is operated at 50 °C in order to eliminate the effect of condensation or evaporation of particle-bound water. However, at 50 °C most semi-volatile material is also evaporated. Therefore, the TEOM, operated at 50 °C, may be considered to measure the mass of non-volatile PM, leading to lower readings than filter-based methods (e.g., Allen et al. 1997; Ayers et al. 1999; Salter et al. 1999; Soutar et al. 1999). The SPM-613D β-gauge mass monitor heats the inlet at 30 °C, but does not otherwise control the temperature at the filter. This heating theoretically

causes evaporation of a fraction of the particle-bound water and an unknown fraction of the semi-volatile PM if the heating is effective. Thus, the β-gauge may be considered to measure the non-volatile PM plus a small fraction of the particle-bound water and an unknown fraction of the semi-volatile PM.

The hourly data derived from the semi-continuous instruments (SPM-613D and TEOM) was taken average at 24-hr interval in order to align with the time-integrated samplers. The daily $PM_{2.5}$ mass concentrations showed less fluctuation than the hourly $PM_{2.5}$ mass concentrations for both SPM-613D and TEOM, leading to a much higher correlation coefficient of 0.93, as shown in Figure 4.12. The daily $PM_{2.5}$ were also collected by one collocated URG sampler that took about three sets of samples each month on quartz and Teflon membranes simultaneously from January to December 2005. In Figure 4.13, we can find the comparison between the semi-continuous method (SPM-613D and TEOM) and the bulk aerosol concentrations obtained from URG sampler. The results showed good correlations (R=0.73 and 0.89) between the semi-continuous methods and the gravimetric method on Teflon filters. The $PM_{2.5}$ mass concentrations by URG sampler were slightly lower than those by SPM-613D. The higher PM concentrations obtained by SPM-613D might be associated with the high relative humidity in Hong Kong that ranges from 64% to 86% reported as

monthly average in 2005. When the particle-bound water can not be removed efficiently at 30 °C because of high passing air volume, water absorption by the inorganics of aerosols leads to higher PM concentrations of the β-gauge compared to those of the manual sampler (Chang et al. 2001). The ratio of the URG sampler to TEOM was 1.32±0.46, which is reasonable because gravimetrical method by Teflon filter samples avoid loosing labile particle-bound water and volatile materials resulting from preheating of sampling air stream for TEOM.

Figure 4.14 presents the comparison between 24-hr coarse particle mass concentrations measured by the Kimoto SPM-613D and URG sampler. A good correlation was found between the instruments (R=0.86). The average PM_{coarse} ratio of the URG (Teflon) to SPM-613D was 0.83±0.25. The mass difference is perhaps due to the same reason as the overestimation of fine particles by the SPM-613D measurements. A previous study by USEPA concluded that the SPM-613D sampler prove precise, highly correlated results for PM_{coarse} measurements, with the PM_{coarse} measurements within ±10% of that of the collocated FRM samplers (Vanderpool et al. 2004).

Two methods for measuring aerosol EC were compared (Figure 4.15). One sample set in Figure 4.15 wass from the semi-continuous monitoring of SPM-613D by optical

method, the other was from the $PM_{2.5}$ samples taken by URG sampler, which then were analyzed for EC using TOR protocol. The BC and EC concentrations were highly correlated over the study period (R=0.84). The regression equation is BC=1.38×EC-4.82. Meanwhile, the mean BC (19.4±6.1 μg m^{-3}) and EC (18.7±7.8 μg m^{-3}) concentrations were quite similar and the range was from 9.8 to 32.3 μg m^{-3} and from 7.6 to 36.0 μg m^{-3}, respectively.

4.2.2.2 Basic statistics of $PM_{2.5}$, PM_{coarse}, and BC

As shown in Figure 4.16, hourly concentrations of $PM_{2.5}$, PM_{10}, and PM_{coarse} measured by SPM-613D in 2005 fairly followed normal distributions. The annual mean was 54.7±25.6 μg m^{-3} for hourly $PM_{2.5}$, 75.6±32.3 μg m^{-3} for hourly PM_{10}, 20.9±11.7 μg m^{-3} for hourly PM_{coarse}, and 18.2±14.6 μg m^{-3} for hourly BC. $PM_{2.5}$ accounted for more than 70% of PM_{10}, while PM_{coarse} only accounted for less than 30%. All of these data are comparable with those of filter-based data. The hourly PM concentrations vary significantly, ranging from 10.0 to 192.9 μg m^{-3} for $PM_{2.5}$, 13.1 to 251.7 μg m^{-3} for PM_{10}, 0.0 to 109.3 μg m^{-3} for PM_{coarse}, and 1.0 to 95.3 μg m^{-3} for BC. Nearly 25% of daily $PM_{2.5}$ concentrations were above 65 μg m^{-3} (the short term air quality standard for $PM_{2.5}$ in US) and no data for PM_{10} were above 180 μg m^{-3} (the short term air quality standard for PM_{10} in HK).

4.2.2.3 Temporal variations of $PM_{2.5}$ and PM_{coarse}

As shown in Figure 4.17, daily $PM_{2.5}$ and PM_{10} concentrations followed the same trends, with low concentrations in summer and high concentrations during cold seasons. The scattering plots also support the close relationships between $PM_{2.5}$ and PM_{10}, as shown in Figure 4.18. Previous studies on 24-hr $PM_{2.5}$ (Ho et al. 2003; Louie et al. 2005b) and PM_{10} (Qin et al. 1997) reported the same seasonal patterns and the continental air masses carried by winter monsoons was found to be the dominant reasons for the elevated fine particulate concentrations in winter. However, 24-hr average PM_{coarse} concentrations did not follow the trend of $PM_{2.5}$ (R=0.46, Figure 4.18), especially in cold seasons, as shown in Figure 4.17. In addition, the seasonal variation of PM_{coarse} was less important than that of fine particles. This is not surprising because coarse particles can not be transported for a long distance by wind due to the large size and gravimetry. The major removing processes from atmosphere for coarse particles are dry deposition by gravimetry, which differ from the wet scavenging for fine particles ($PM_{2.5}$) by precipitation. Moreover, the wind speeds are unusually low when the pollution episodes that are related to the continental air masses occur (Louie et al. 2005b; Cheng et al. 2006). As a consequence, the

contributions from continental air masses should be less important for PM_{coarse}. PM_{coarse} at a traffic-impacted urban site has been found to be mainly from the resuspended materials by the nearby on-road vehicle generated turbulence (Manoli et al. 2002). The wet road surface due to rainfall in summer may be the reason for the decreased PM_{coarse} concentrations during that period.

4.2.2.4 Influencing factors on the fine and coarse particulate mass concentrations

The weekly cycles of $PM_{2.5}$ and PM_{10} suggest that both PM fractions are related to the traffic volume (Figure 4.19). The diurnal patterns were similar for each day, but the concentrations were lower on Sunday when compared with other days. This is because the decreased traffic flows on Sunday (Public holiday), especially for the diesel-fueled vehicles. It should be noted that Saturday is a work day in Hong Kong. Two major peaks for $PM_{2.5}$ and PM_{10} occurred at 10:00-11:00 and 17:00-18:00, respectively, during daytime. The period between 10:00 to 11:00 was recorded as the maximum level of diesel-fueled vehicle proportion in a day, accounting for more than 50% of total on-road traffic counts during that period. The period of 17:00-18:00 was the evening rush hours. The lowest concentrations were measured during early morning (2:00-5:00) when all the categories of vehicles were at a minimum level in a day. Hourly PM_{coarse} data generally followed the trends of total traffic volume, with high

concentrations in daytime and low concentrations in nighttime.

The relationship between PM concentrations and traffic counts were examined by calculating the correlation coefficients (R) from the hourly data sets, as shown in Table 4.10. All size fractions, including $PM_{2.5}$, PM_{10} and PM_{coarse}, were related to the total traffic volume, which is supported by high correlation coefficients between PM and total vehicle numbers. Better correlations were found for PM with diesel- and gasoline-fueled vehicles than with the LPG-fueled taxis. Out of the six categories of diesel-fueled vehicles, double decker bus and goods vehicles (<=5.5 ton) appear more related to $PM_{2.5}$ and PM_{10} mass. The exhausts from Taxis contribute very little to PM (Cheng et al. 2006), thus poor relationship were observed. As the most abundant species in fine particles, BC was associated with diesel-fueled vehicles, like double decker bus and goods vehicles (<=5.5 ton and 5.5-24 ton). PM_{coarse} had closer relationship with private cars, compared to other vehicle categories.

PM_{coarse} mass concentrations were also found to depend upon wind speeds when wind speeds varied from 0 to 5.6 m s^{-1}, while $PM_{2.5}$ was not. The hours with wind speeds higher than 5.6 m s^{-1} were found to be temporal events that can not last for more than 3 hours and only occupied 1.6% of total number of hourly wind speeds (Figure 4.20). Figure 4.21 displays the median concentrations of $PM_{2.5}$, PM_{10}, and PM_{coarse} measured

for each 0.4 m s^{-1} wind speed bin. Median concentrations were used here to represent the concentrations with the largest frequency. The calculation of these medians soothes the variability of concentrations due to the other influencing factors. The median $PM_{2.5}$ concentrations showed poor correlations with wind speeds (R=0.51), which is to be expected because fine particles were mainly emitted from diesel-fueled vehicles. The effects of dilution and dispersion of wind seem less important for fine particles at this street canyon. However, PM_{10} and PM_{coarse} showed obvious increase as the elevation of wind speeds with statistical significance (R=0.89 for PM_{10} and R=0.98 for PM_{coarse}). The median PM_{10} concentrations increase from about 54 to 70 μg m^{-3}, and from 13 to 24 μg m^{-3} for PM_{coarse}, as wind speeds strengthen from 0 m s^{-1} to stronger winds of 5.6 m s^{-1}. This clearly indicates the wind-suspended mechanism have an effect on coarse particles. Harrison et al. (2001) considered the coarse particle fraction as comprising two components, a nonwind-suspended component that corresponds to particles emitted from the anthropogenic sources, like industrial, construction activities, traffic-generated resuspension, and biological particles, as well as a wind-suspended component that arose mainly from natural sources such as sea spray and surface soils, or dusts on paved areas. In this study, apparently the coarse particles are also mainly from two components, traffic-generated and wind suspended resupension.

4.3 Summary

PM_{coarse} showed distinguished differences in chemical characteristics when compared with other particulate fractions, e.g., $PM_{1.0,}$ $PM_{2.5}$, and PM_{10}. The annual mean particulate mass concentration was 44.5±19.5 μg m^{-3} for $PM_{1.0}$, 55.4±25.5 μg m^{-3} for $PM_{2.5}$, 81.3±37.7 μg m^{-3} for PM_{10}, and 25.9±15.5 μg m^{-3} for PM_{coarse}. $PM_{1.0}$ and $PM_{2.5}$ are main contributors of PM_{10}, accounting for ~54% and ~70% of PM_{10}, respectively; while PM_{coarse} occupies only ~30% of PM_{10}. The three most abundant species for $PM_{1.0}$ and $PM_{2.5}$ in descending rank are EC, sulfate, and OC. Low OC/EC ratios (less than 1) in $PM_{1.0}$ and $PM_{2.5}$ were found at PU Supersite, indicating that fresh vehicle exhaust is the main source. On the other hand, PM_{coarse} comprise of multi-components, with several abundant species of OC, nitrate, sulfate, Si, Fe, Cl, ammonium, and Na. The OC/EC ratios in PM_{coarse} were much higher than 1, averaging 7.8±14.2, suggesting that coarse carbonaceous aerosols have other sources rather than fresh vehicular exhaust.

The diurnal variations of fine particles are closely associated with the daily cycle of vehicle numbers, especially the double decker buses, with high concentrations in daytime and low concentrations in the early morning. By analyzing the seasonal

variations of particles, it is found that the aerosol mass and chemical components of $PM_{1.0}$, $PM_{2.5}$ and PM_{10} are also influenced by large-scale weather system, namely the East Asia monsoon, showing increased loadings due to the transported continental pollution during cold seasons. For PM_{coarse}, the hourly mass concentrations have positive relationships with both traffic volume and wind speeds. Meanwhile the seasonal variations are less important for PM_{coarse} compared to fine particles, since the effect of continental pollution transported from Asia on PM_{coarse} mass concentrations was insignificant.

Like most of other semi-continuous monitors, there are sampling artifacts for SPM-613D. However, the comparison of aerosol mass indicated close concentrations and identical trends between the SPM-613D and those already widely-used methods.

Based on the analyses of chemical characteristics in each particle fraction, the conclusion can be drawn that PM_{coarse} has different sources from $PM_{1.0}$ and $PM_{2.5}$, and PM_{10} cannot reflect the properties of PM_{coarse}, thus being a poor indicator for coarse particulate pollution.

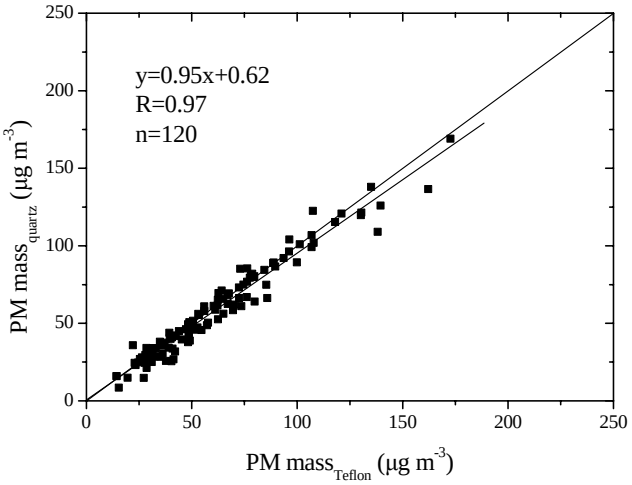

Figure 4.1 Particulate gravimetric mass acquired from Teflon-membrane and quartz fiber filters at PU Supersite during the 12-month study.

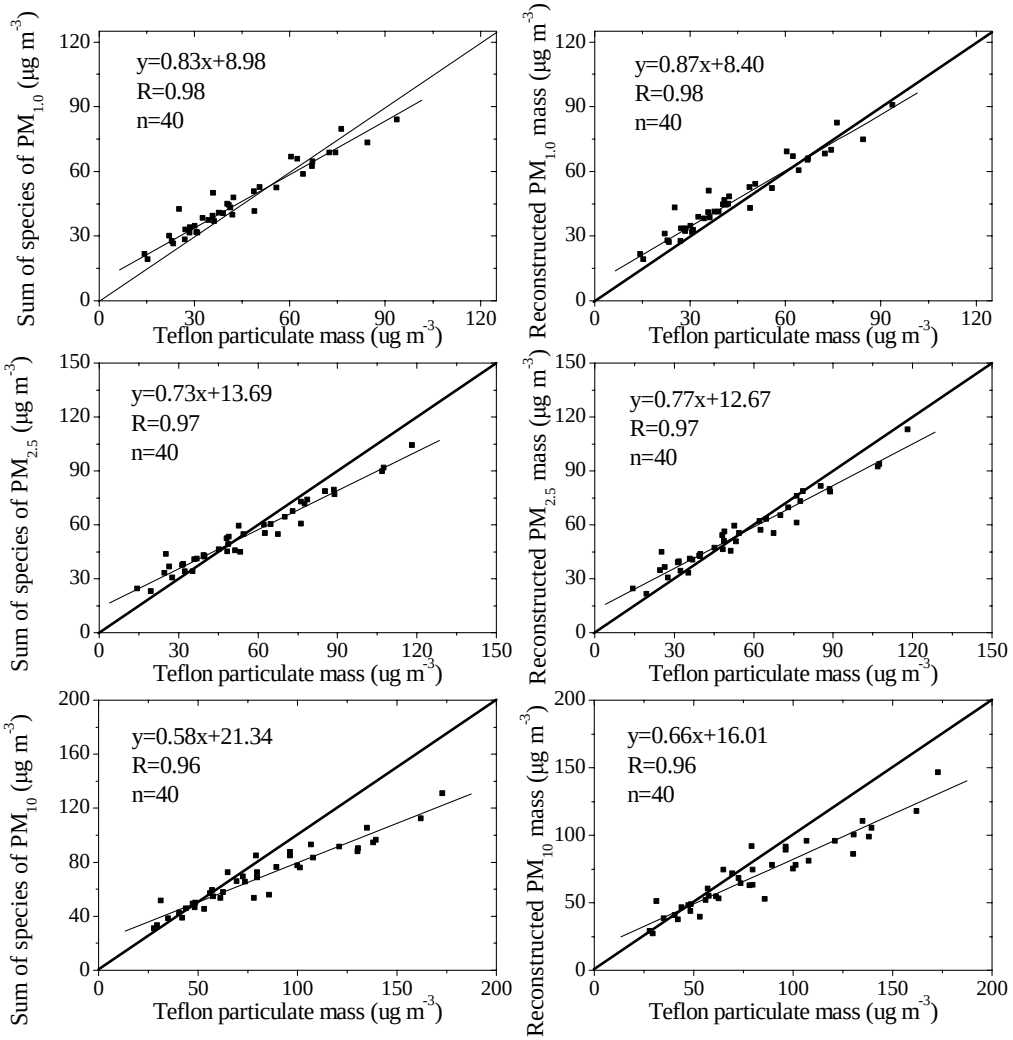

Figure 4.2 The scatter plots of Teflon particulate mass concentrations against the sum of individual chemical species in $PM_{1.0}$, $PM_{2.5}$, and PM_{10}, respectively.

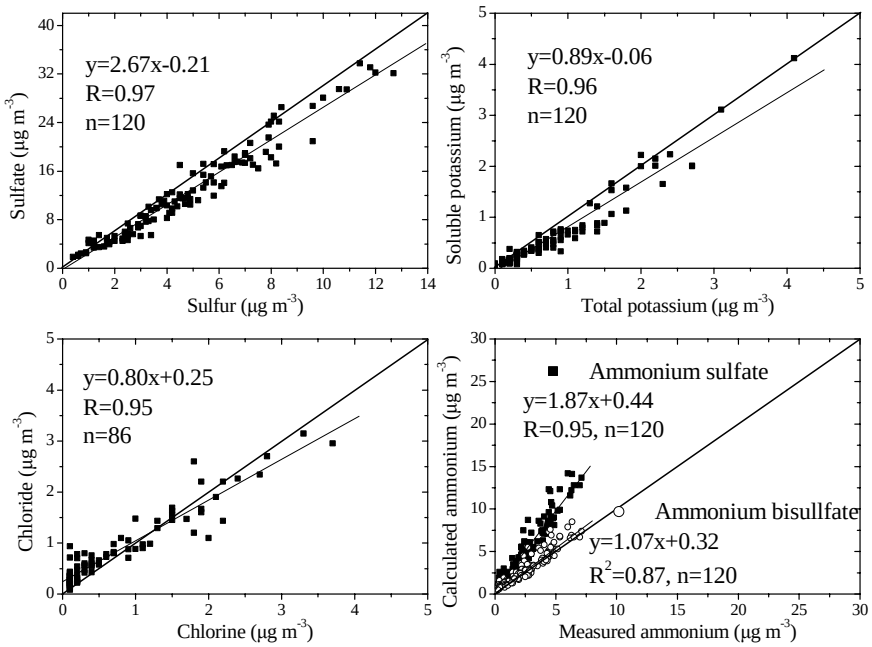

Figure 4.3 The physical consistency test with $PM_{1.0}$, $PM_{2.5}$, and PM_{10} in one plot.

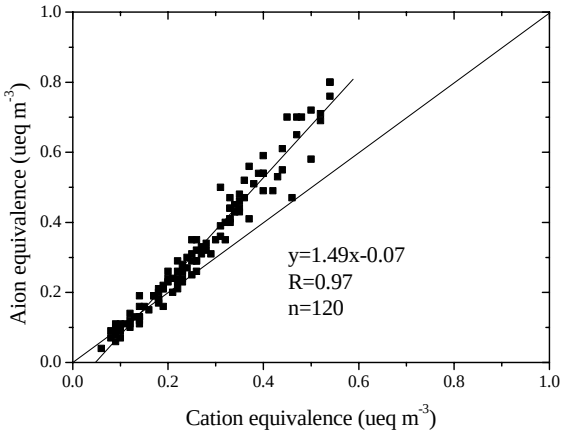

Figure 4.4 Scatter plots of cation versus anion measurements from $PM_{1.0}$, $PM_{2.5}$, and PM_{10} data.

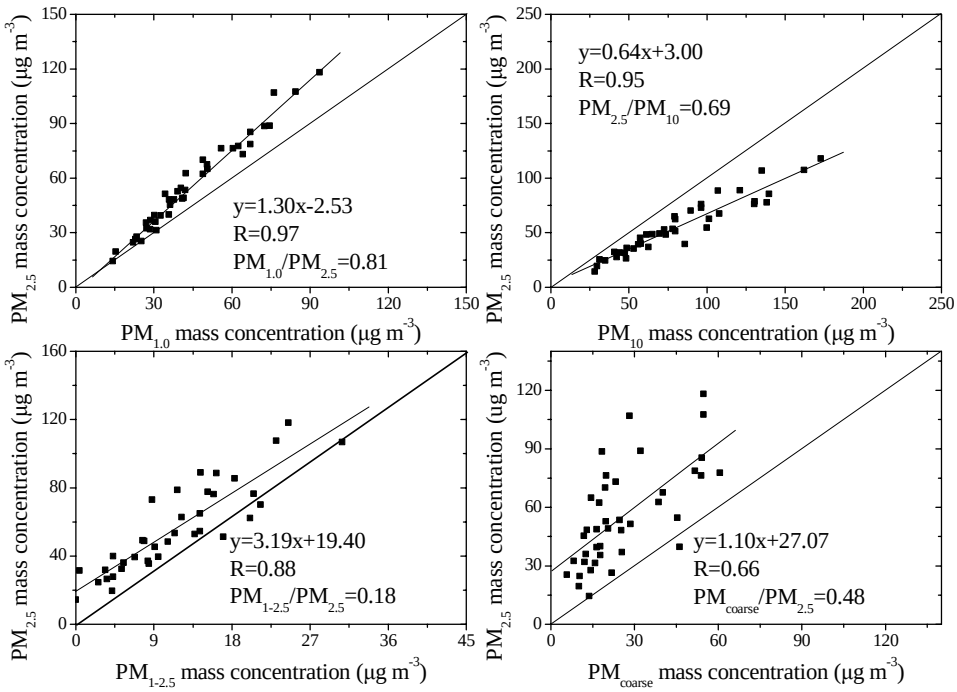

Figure 4.5 The comparisons of particulate mass in different size fractions.

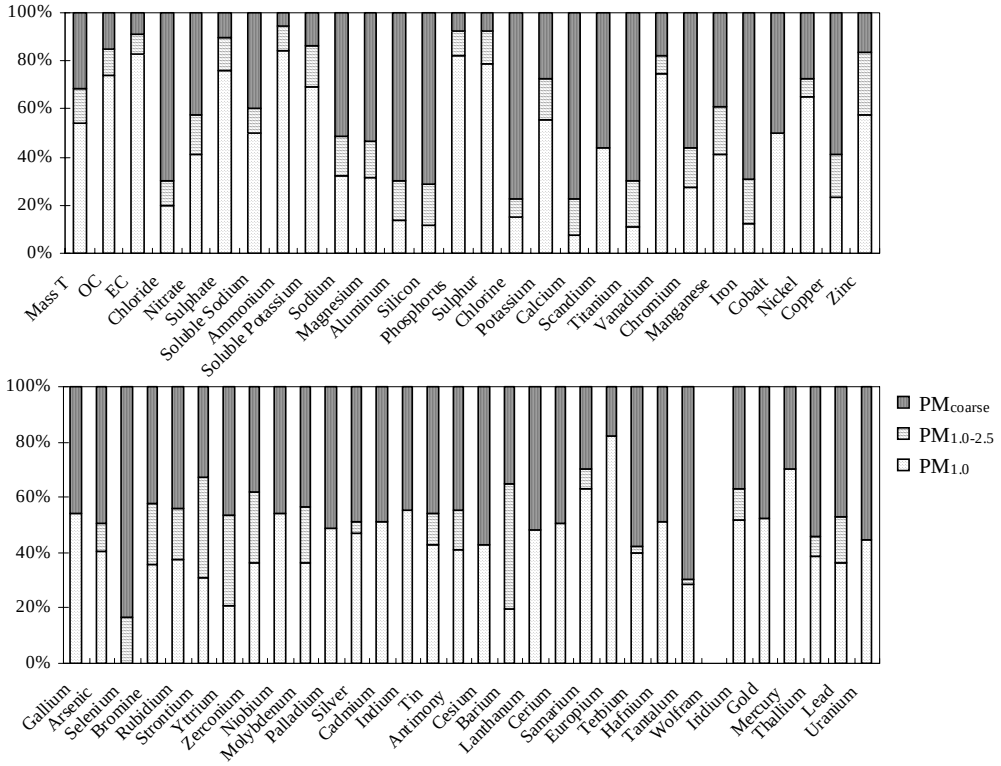

Figure 4.6 The average $PM_{1.0}$, $PM_{1.0\text{-}2.5}$, and PM_{coarse} percentages of the total PM_{10}.

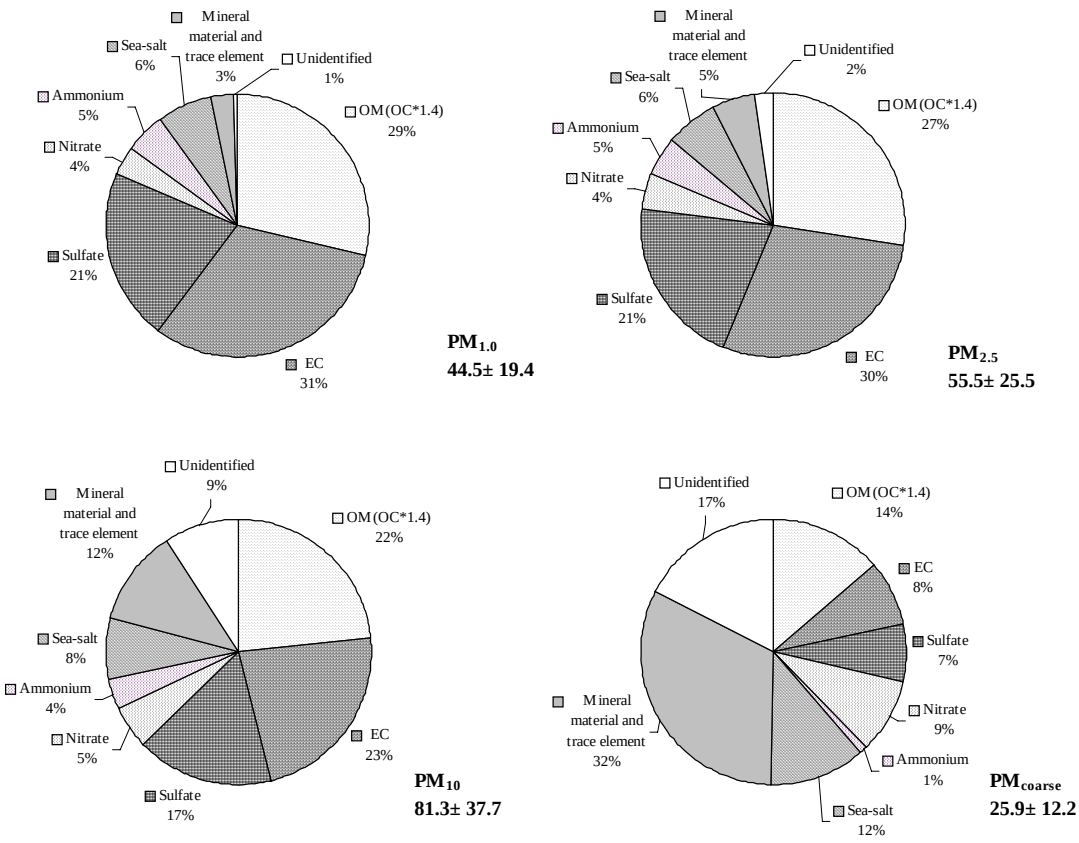

Figure 4.7 Mass closure charts for $PM_{1.0}$, $PM_{2.5}$, PM_{10}, and PM_{coarse} data acquired at PU Supersite.

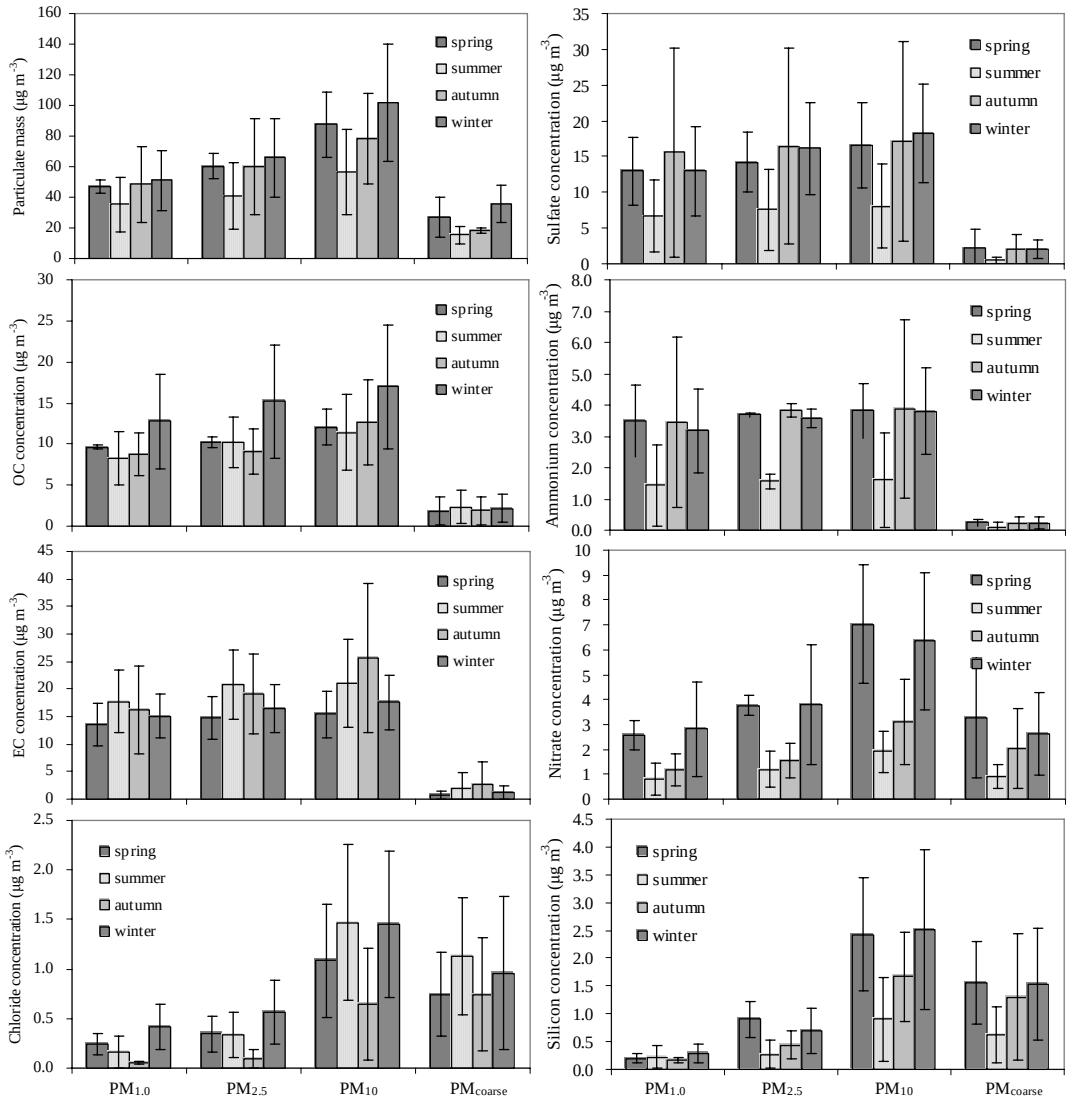

Figure 4.8 Seasonal patterns of PM and the major species acquired at PU Supersite.

(24-hour samples taken from midnight to midnight, n=40 in total).

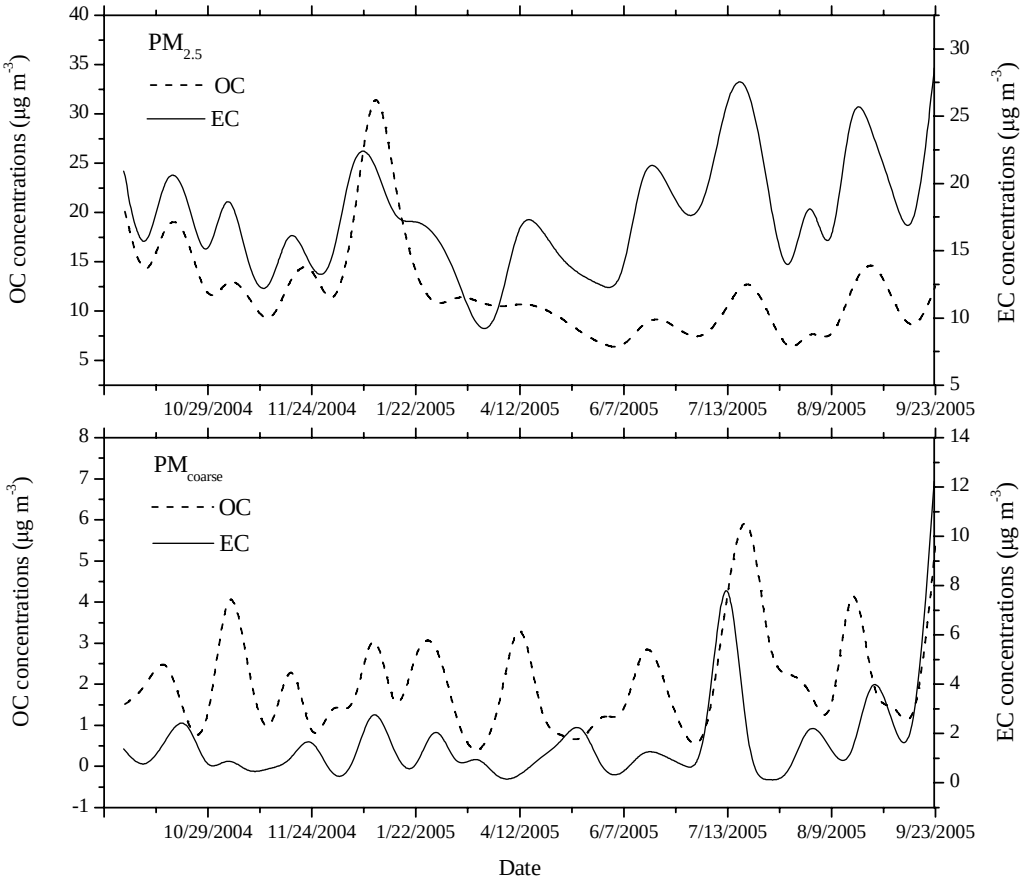

Figure 4.9 Time series of carbonaceous aerosol in fine and coarse particles.

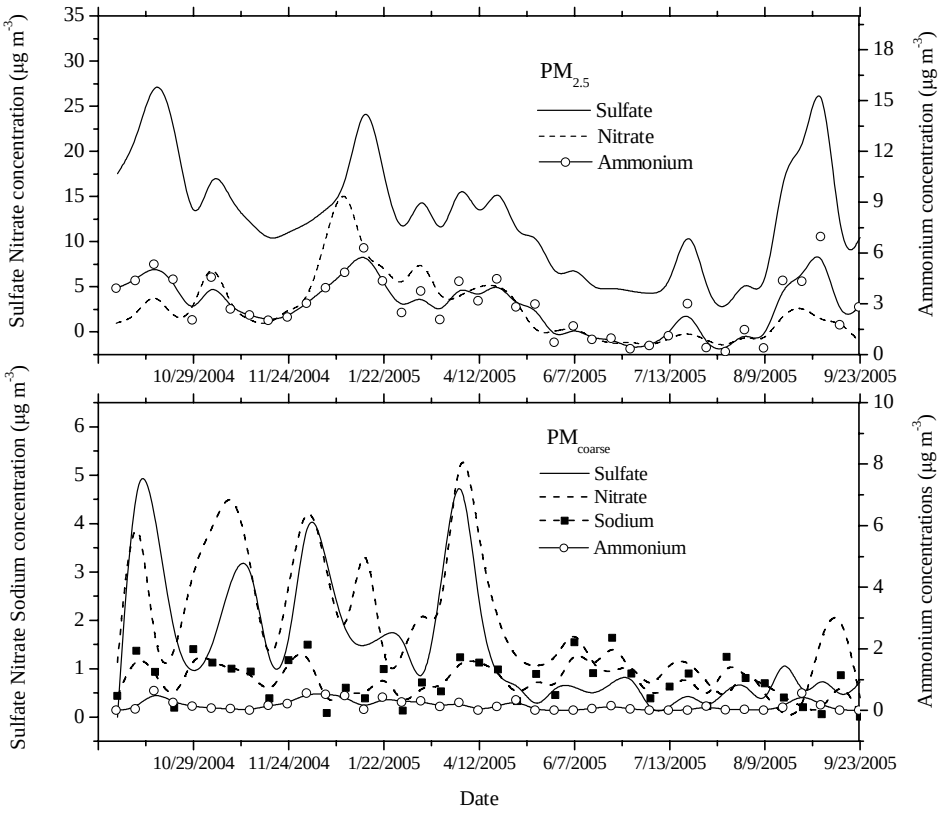

Figure 4.10 Time series of ions in fine and coarse particles.

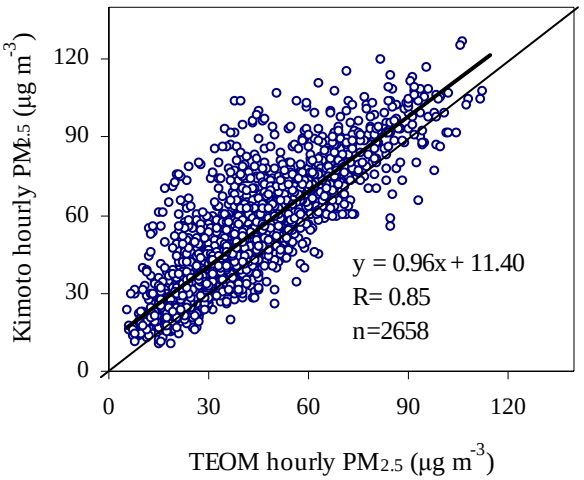

Figure 4.11 Scattering plot of hourly $PM_{2.5}$ from Kimoto SPM-613D against TEOM.

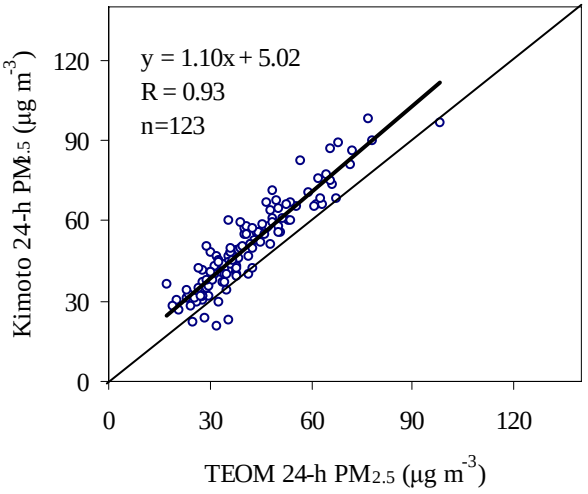

Figure 4.12 Scattering plot of daily $PM_{2.5}$ from Kimoto SPM-613D against TEOM.

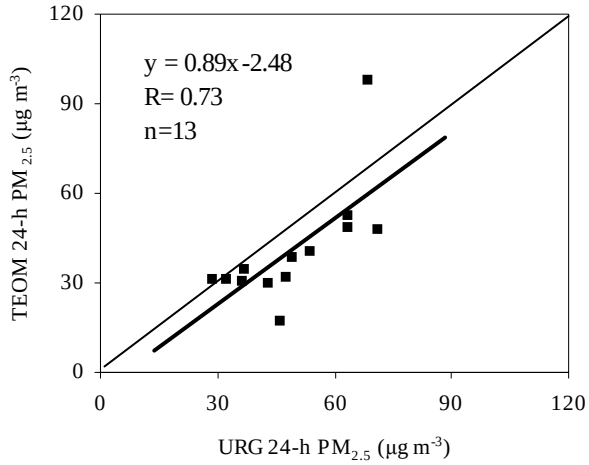

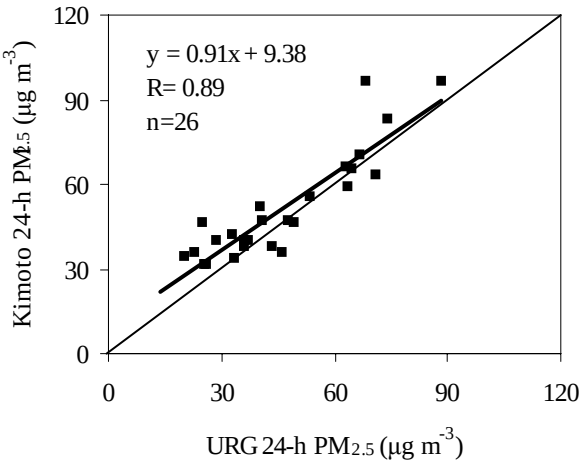

Figure 4.13 The comparisons of daily $PM_{2.5}$ mass concentrations among Kimoto SPM-613D, TEOM and URG sampler.

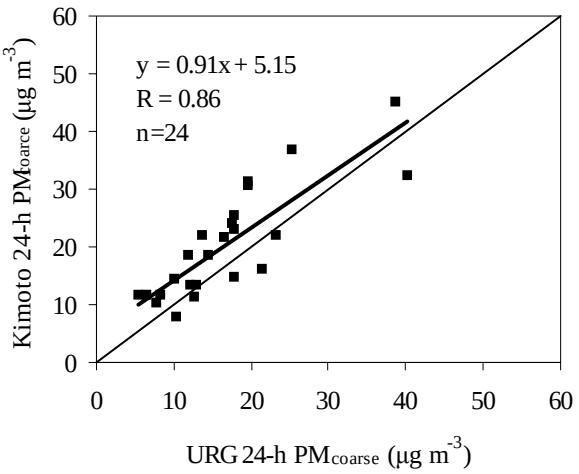

Figure 4.14 The 24-hour PM_{coarse} mass acquired from Kimoto SPM-613D and URG sampler.

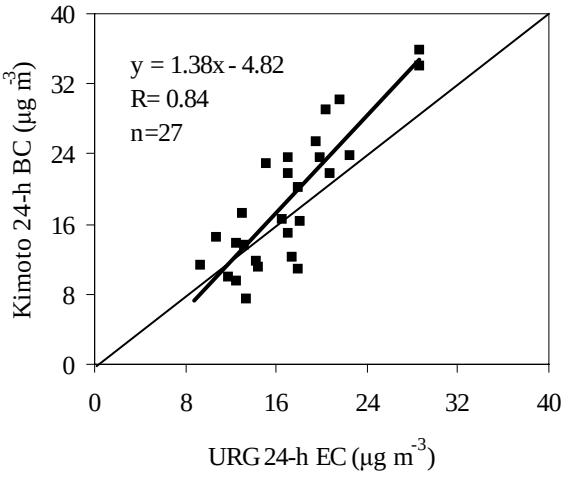

Figure 4.15 The comparison of 24-hour EC between Kimoto SPM-613D and URG sampler.

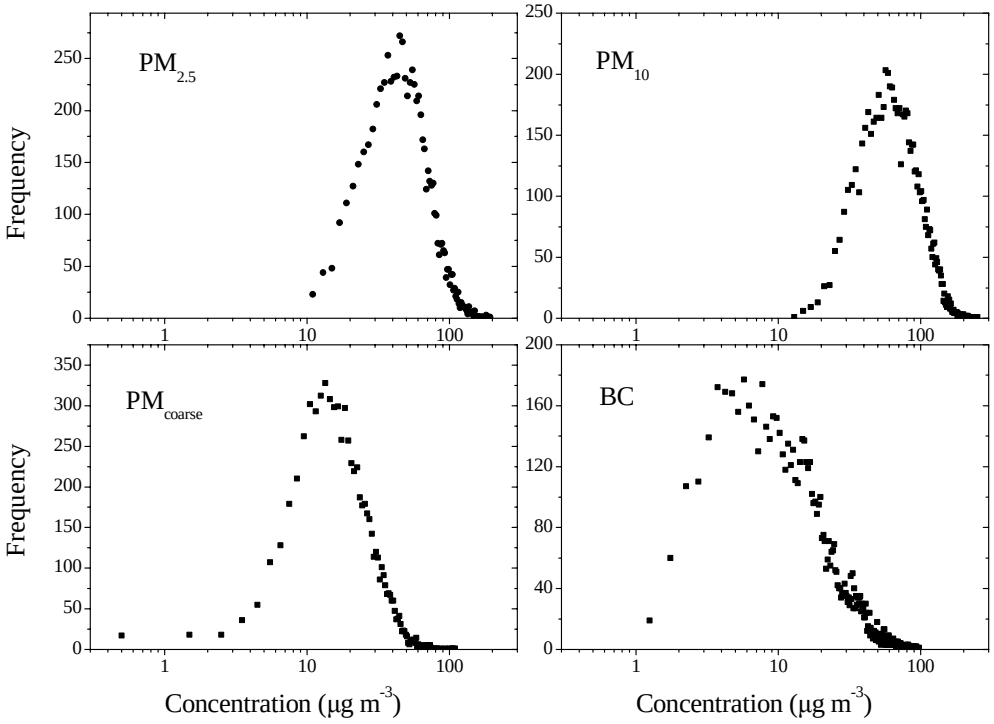

Figure 4.16 Frequency counts for $PM_{2.5}$, PM_{10}, PM_{coarse}, and BC concentrations measured at PU roadside. Hourly data from January to December 2005 (n=7132).

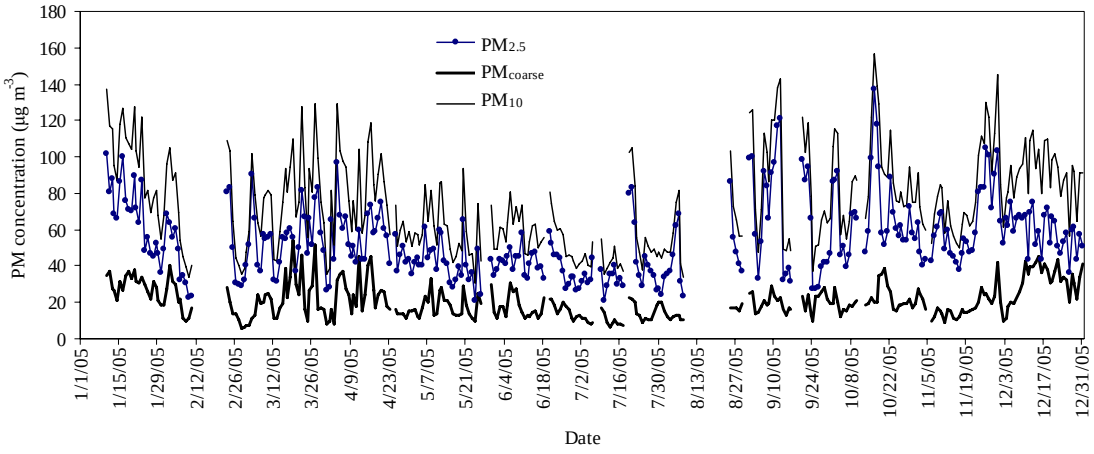

Figure 4.17 Daily average concentrations for $PM_{2.5}$, PM_{10}, and PM_{coarse} at PU roadside site.

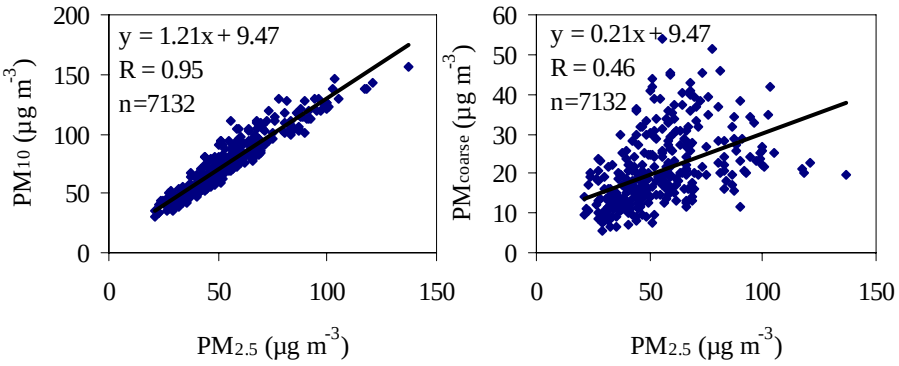

Figure 4.18 Scatter plots for daily $PM_{2.5}$ and PM_{10}, $PM_{2.5}$ and PM_{coarse} at PU roadside site.

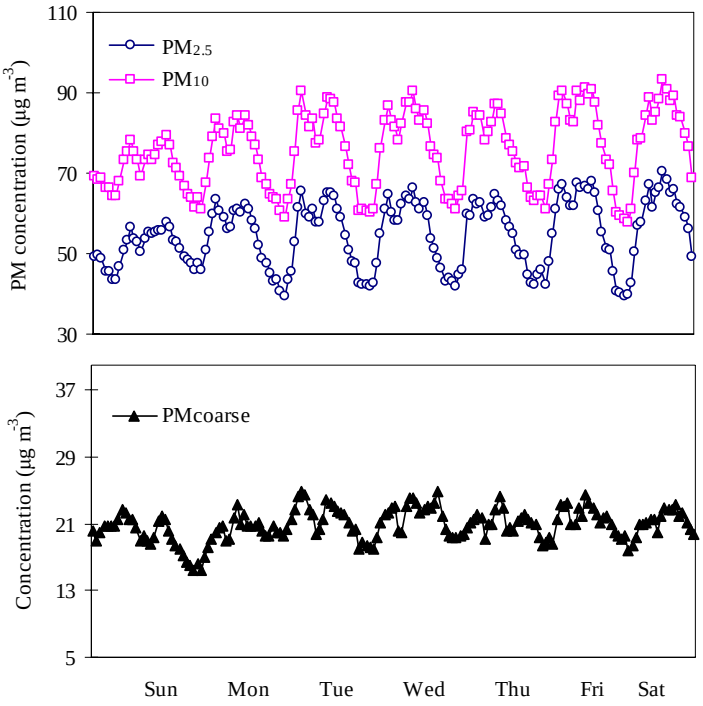

Figure 4.19 Weekly cycles of $PM_{2.5}$, PM_{10}, and PM_{coarse} concentrations at PU roadside site.

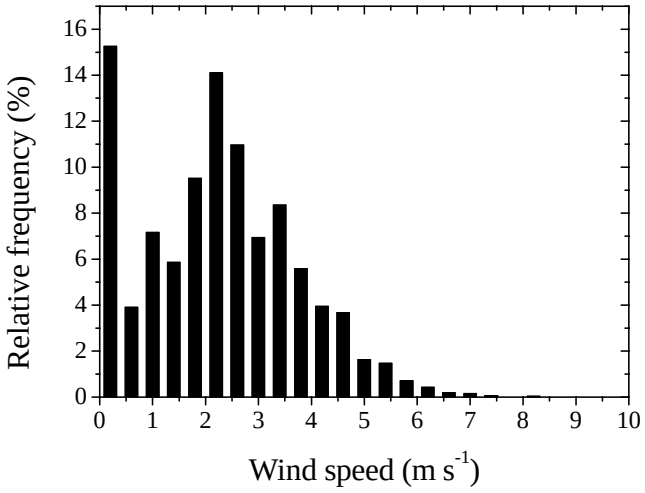

Figure 4.20 Relative frequency of wind speed when each size bin is 0.4 m s^{-1}. Hourly data from Jan to Aug 2005.

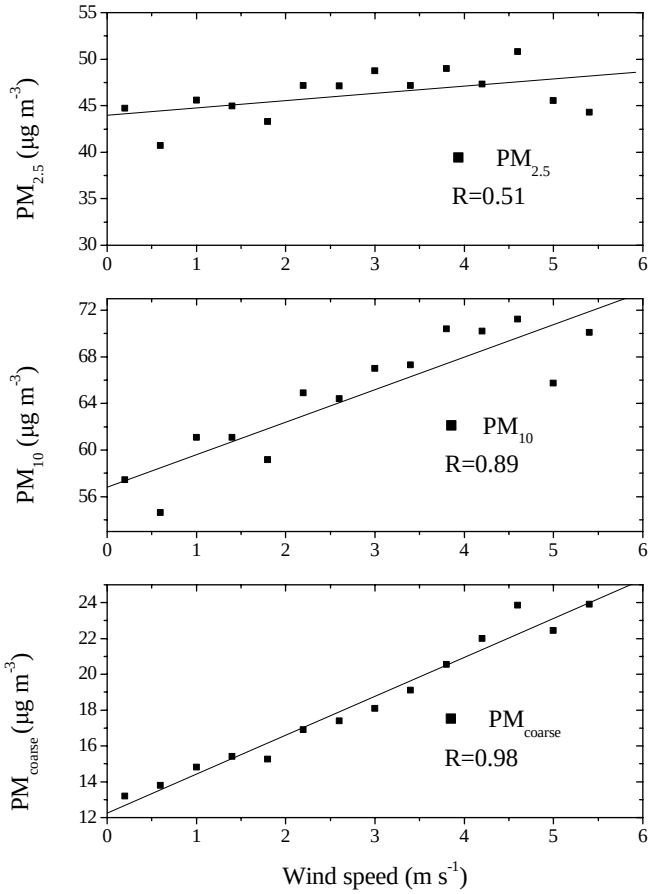

Figure 4.21 Median concentrations of $PM_{2.5}$, PM_{10}, and PM_{coarse} at PU roadside versus the wind speeds.

Table 4.1 Statistical summary of $PM_{1.0}$ measurements at PU Supersite from Oct 2004 to Sep 2005 (24-hour samples taken from midnight to midnight, n=40).

$PM_{1.0}$	Spring		Summer		Autumn		Winter		Total	
$\mu g\ m^{-3}$	Mean	SD	Mean	SD	Mean	SD	Mean	SD	Mean	SD
Mass (Teflon)	44.3650	6.6892	34.7893	17.9196	56.3238	21.0964	47.0662	19.1087	44.0438	19.4390
OC	9.6295	0.2771	8.2196	3.2591	11.2981	4.1395	12.7988	6.3811	10.4859	4.8976
EC	13.5285	3.7935	17.7812	5.7607	16.4216	5.2127	14.4830	3.9981	16.0758	5.0587
Chloride (Cl^-)	0.2380	0.1078	0.1634	0.1637	0.1704	0.0996	0.4919	0.2272	0.2745	0.2253
Nitrate (NO_3^-)	2.5634	0.5757	0.8190	0.6505	1.4880	0.5160	3.2933	2.1017	1.8789	1.6483
Sulphate (SO_4^{2-})	12.9806	4.7515	6.7441	5.0444	16.5034	8.9384	11.2301	5.7976	10.7077	7.0778
Soluble Sodium (Na^+)	1.2386	0.1065	1.2598	0.1999	1.1731	0.1516	1.3723	0.1975	1.2754	0.1928
Ammonium (NH_4^+)	3.4808	1.1507	1.4286	1.3080	3.6184	1.7312	2.9400	1.3675	2.5289	1.6485
Soluble Potassium (K^+)	0.4201	0.2680	0.1845	0.1729	0.8243	0.5993	0.6154	0.5635	0.4738	0.4947
Sodium (Na)	0.5181	0.1658	0.3901	0.3601	0.6075	0.2682	0.4820	0.2354	0.4752	0.2944
Magnesium (Mg)	0.1309	0.0573	0.1053	0.0690	0.1869	0.0619	0.1300	0.0374	0.1322	0.0631
Aluminum (Al)	0.1450	0.0610	0.1168	0.1079	0.1304	0.0489	0.1468	0.0875	0.1317	0.0868
Silicon (Si)	0.2211	0.0810	0.1401	0.1749	0.2484	0.1049	0.2790	0.1949	0.2148	0.1717
Phosphorus (P)	0.2303	0.0772	0.1230	0.1028	0.2805	0.1388	0.1709	0.0573	0.1795	0.1115
Sulphur (S)	5.4466	2.0059	2.6924	2.3622	6.2716	3.1257	4.2734	1.7939	4.1654	2.6472
Chlorine (Cl)	0.0638	0.0096	0.0984	0.0264	0.0775	0.0045	0.3378	0.3259	0.2096	0.2600
Potassium (K)	0.5099	0.3584	0.1956	0.2090	0.8849	0.5811	0.7242	0.5462	0.5373	0.5126
Calcium (Ca)	0.0671	0.0144	0.0775	0.1113	0.0787	0.0258	0.0700	0.0507	0.0745	0.0743
Scandium (Sc)	0.0000	0.0000	0.0004	0.0007	0.0002	0.0006	0.0001	0.0002	0.0002	0.0006
Titanium (Ti)	0.0046	0.0036	0.0095	0.0131	0.0068	0.0016	0.0084	0.0076	0.0082	0.0091
Vanadium (V)	0.0222	0.0073	0.0166	0.0186	0.0090	0.0059	0.0183	0.0195	0.0162	0.0166
Chromium (Cr)	0.0025	0.0015	0.0022	0.0020	0.0026	0.0011	0.0026	0.0013	0.0025	0.0015
Manganese (Mn)	0.0206	0.0048	0.0152	0.0129	0.0227	0.0089	0.0272	0.0233	0.0212	0.0166
Iron (Fe)	0.1639	0.0359	0.2482	0.3829	0.2128	0.0831	0.2202	0.1868	0.2251	0.2587
Nickel (Ni)	0.0066	0.0036	0.0054	0.0051	0.0025	0.0017	0.0063	0.0065	0.0052	0.0051
Copper (Cu)	0.0112	0.0009	0.0117	0.0128	0.0148	0.0035	0.0149	0.0087	0.0134	0.0095
Zinc (Zn)	0.1422	0.0626	0.1763	0.2091	0.2490	0.0888	0.2365	0.2048	0.2087	0.1800
Gallium (Ga)	0.0001	0.0000	0.0080	0.0057	0.0085	0.0080	0.0093	0.0050	0.0081	0.0060
Arsenic (As)	0.0104	0.0000	0.0050	0.0042	0.0128	0.0064	0.0144	0.0112	0.0127	0.0093
Selenium (Se)	0.0000	0.0000	0.0000	0.0000	0.0000	0.0000	0.0000	0.0000	0.0000	0.0000
Bromine (Br)	0.0125	0.0058	0.0071	0.0052	0.0114	0.0060	0.0164	0.0151	0.0116	0.0104
Rubidium (Rb)	0.0044	0.0040	0.0017	0.0009	0.0063	0.0039	0.0053	0.0054	0.0045	0.0041
Strontium (Sr)	0.0050	0.0060	0.0041	0.0022	0.0039	0.0012	0.0051	0.0035	0.0045	0.0027
Yttrium (Y)	0.0000	0.0000	0.0007	0.0007	0.0010	0.0015	0.0009	0.0012	0.0008	0.0009
Zerconium (Zr)	0.0085	0.0012	0.0082	0.0049	0.0090	0.0042	0.0050	0.0032	0.0074	0.0043
Niobium (Nb)	0.0014	0.0015	0.0012	0.0017	0.0005	0.0011	0.0012	0.0017	0.0011	0.0016
Palladium (Pd)	0.0120	0.0014	0.0112	0.0080	0.0112	0.0059	0.0098	0.0036	0.0108	0.0060
Silver (Ag)	0.0054	0.0043	0.0065	0.0042	0.0071	0.0057	0.0084	0.0060	0.0073	0.0051
Cadmium (Cd)	0.0047	0.0027	0.0080	0.0058	0.0119	0.0069	0.0071	0.0055	0.0082	0.0059
Indium (In)	0.0117	0.0050	0.0131	0.0050	0.0100	0.0063	0.0111	0.0050	0.0117	0.0052
Tin (Sn)	0.0286	0.0168	0.0154	0.0083	0.0276	0.0123	0.0398	0.0243	0.0274	0.0192
Antimony (Sb)	0.0280	0.0116	0.0380	0.0065	0.0397	0.0085	0.0374	0.0079	0.0374	0.0080
Cesium (Ce)	0.0145	0.0000	0.0086	0.0027	0.0071	0.0026	0.0047	0.0045	0.0078	0.0038
Barium (Ba)	0.0128	0.0007	0.0252	0.0234	0.0323	0.0203	0.0295	0.0140	0.0271	0.0191
Gold (Au)	0.0000	0.0000	0.0080	0.0062	0.0002	0.0000	0.0106	0.0069	0.0077	0.0063
Mercury (Hg)	0.0011	0.0000	0.0000	0.0000	0.0002	0.0000	0.0001	0.0000	0.0005	0.0006
Thallium (Tl)	0.0024	0.0027	0.0024	0.0019	0.0005	0.0000	0.0030	0.0021	0.0022	0.0019
Lead (Pb)	0.0426	0.0298	0.0171	0.0220	0.0736	0.0408	0.0648	0.0508	0.0473	0.0444
Uranium (U)	0.0018	0.0019	0.0016	0.0022	0.0005	0.0010	0.0029	0.0028	0.0018	0.0023

Table 4.2 Statistical summary of $PM_{2.5}$ measurements at PU Supersite from Oct 2004 to Sep 2005 (24-hour samples taken from midnight to midnight, n=40).

$PM_{2.5}$	Spring		Summer		Autumn		Winter		Total	
$\mu g\ m^{-3}$	Mean	SD	Mean	SD	Mean	SD	Mean	SD	Mean	SD
Mass (Teflon)	60.2375	8.2906	40.9273	21.8575	70.9538	26.5744	61.2285	25.7896	55.4615	25.5361
OC	10.2408	0.6756	9.1090	3.1107	13.7864	5.0666	14.9287	7.6522	12.0491	5.7599
EC	14.7030	3.9079	19.1165	6.2547	18.7572	5.4690	15.9840	4.4859	17.5852	5.4469
Chloride (Cl^-)	0.3430	0.1845	0.3393	0.2295	0.2833	0.2192	0.6362	0.3510	0.4196	0.2975
Nitrate (NO_3^-)	3.7664	0.4107	1.1820	0.7229	2.1095	0.8796	4.3796	2.6293	2.6212	2.0825
Sulphate (SO_4^{2-})	14.2187	4.2240	7.5927	5.7159	18.8025	9.4207	14.4781	5.4629	12.6903	7.6033
Soluble Sodium (Na^+)	1.5513	0.0685	1.4988	0.2213	1.4950	0.3661	1.6363	0.2798	1.5457	0.2641
Ammonium (NH_4^+)	3.6911	0.8277	1.5539	1.4292	3.9527	1.7434	3.3839	1.3711	2.8282	1.7303
Soluble Potassium (K^+)	0.4540	0.2604	0.1983	0.1713	1.0030	0.7607	0.8799	0.9200	0.5919	0.6935
Sodium (Na)	0.7421	0.2816	0.5755	0.2151	0.8319	0.2321	0.8119	0.3431	0.7203	0.2865
Magnesium (Mg)	0.2671	0.1027	0.1459	0.0544	0.2314	0.0799	0.2128	0.0692	0.1968	0.0796
Aluminum (Al)	0.4571	0.1384	0.1833	0.1509	0.3970	0.1932	0.3121	0.1896	0.2953	0.1927
Silicon (Si)	0.8953	0.2799	0.2740	0.2502	0.7427	0.3012	0.6051	0.4348	0.5375	0.3911
Phosphorus (P)	0.2397	0.0654	0.1292	0.1032	0.3143	0.1531	0.2051	0.0707	0.2019	0.1211
Sulphur (S)	5.9995	1.7410	2.9776	2.4070	7.3781	3.5537	5.2001	1.7636	4.8822	2.8933
Chlorine (Cl)	0.2069	0.0854	0.2871	0.2855	0.1213	0.0396	0.4556	0.4123	0.3125	0.3230
Potassium (K)	0.6374	0.3927	0.2521	0.2663	1.1684	0.7914	0.9660	0.7796	0.7059	0.6949
Calcium (Ca)	0.2868	0.1024	0.1582	0.0685	0.3130	0.1213	0.2223	0.1379	0.2229	0.1212
Scandium (Sc)	0.0002	0.0004	0.0003	0.0007	0.0001	0.0003	0.0001	0.0004	0.0002	0.0005
Titanium (Ti)	0.0314	0.0104	0.0175	0.0136	0.0281	0.0131	0.0232	0.0165	0.0229	0.0146
Vanadium (V)	0.0233	0.0138	0.0185	0.0212	0.0093	0.0075	0.0204	0.0200	0.0180	0.0183
Chromium (Cr)	0.0051	0.0014	0.0023	0.0015	0.0052	0.0020	0.0048	0.0021	0.0040	0.0022
Manganese (Mn)	0.0302	0.0097	0.0211	0.0154	0.0377	0.0179	0.0399	0.0324	0.0314	0.0234
Iron (Fe)	0.6272	0.1785	0.4786	0.1990	0.6822	0.2623	0.5792	0.3308	0.5669	0.2623
Nickel (Ni)	0.0064	0.0036	0.0057	0.0054	0.0041	0.0018	0.0068	0.0053	0.0058	0.0046
Copper (Cu)	0.0210	0.0031	0.0196	0.0081	0.0278	0.0075	0.0274	0.0127	0.0239	0.0100
Zinc (Zn)	0.2425	0.0769	0.2282	0.2636	0.3915	0.1464	0.3586	0.3050	0.3047	0.2510
Gallium (Ga)	0.0102	0.0101	0.0069	0.0103	0.0077	0.0065	0.0058	0.0062	0.0069	0.0077
Arsenic (As)	0.0180	0.0092	0.0058	0.0052	0.0166	0.0101	0.0209	0.0139	0.0155	0.0116
Selenium (Se)	0.0000	0.0000	0.0000	0.0000	0.0096	0.0000	0.0000	0.0000	0.0096	0.0000
Bromine (Br)	0.0157	0.0080	0.0076	0.0038	0.0132	0.0051	0.0209	0.0190	0.0139	0.0126
Rubidium (Rb)	0.0021	0.0012	0.0022	0.0014	0.0082	0.0044	0.0059	0.0042	0.0052	0.0042
Strontium (Sr)	0.0071	0.0031	0.0034	0.0018	0.0054	0.0042	0.0054	0.0030	0.0048	0.0030
Yttrium (Y)	0.0005	0.0006	0.0023	0.0028	0.0022	0.0016	0.0021	0.0013	0.0018	0.0015
Zerconium (Zr)	0.0037	0.0021	0.0074	0.0044	0.0101	0.0053	0.0080	0.0033	0.0077	0.0043
Niobium (Nb)	0.0018	0.0021	0.0006	0.0014	0.0012	0.0014	0.0009	0.0010	0.0009	0.0014
Palladium (Pd)	0.0065	0.0020	0.0099	0.0056	0.0123	0.0047	0.0138	0.0055	0.0113	0.0055
Silver (Ag)	0.0042	0.0047	0.0068	0.0034	0.0121	0.0107	0.0068	0.0041	0.0075	0.0059
Cadmium (Cd)	0.0055	0.0033	0.0059	0.0049	0.0125	0.0050	0.0075	0.0071	0.0079	0.0060
Indium (In)	0.0079	0.0107	0.0089	0.0056	0.0135	0.0080	0.0080	0.0063	0.0094	0.0068
Tin (Sn)	0.0340	0.0052	0.0183	0.0091	0.0337	0.0168	0.0378	0.0248	0.0293	0.0187
Antimony (Sb)	0.0439	0.0139	0.0403	0.0108	0.0396	0.0151	0.0414	0.0088	0.0409	0.0111
Cesium (Ce)	0.0112	0.0021	0.0091	0.0069	0.0104	0.0006	0.0105	0.0037	0.0103	0.0032
Barium (Ba)	0.0328	0.0148	0.0537	0.0131	0.0512	0.0133	0.0454	0.0192	0.0484	0.0162
Gold (Au)	0.0000	0.0000	0.0078	0.0056	0.0000	0.0000	0.0052	0.0020	0.0070	0.0048
Mercury (Hg)	0.0000	0.0000	0.0002	0.0000	0.0000	0.0000	0.0000	0.0000	0.0002	0.0000
Thallium (Tl)	0.0019	0.0007	0.0039	0.0023	0.0025	0.0028	0.0029	0.0026	0.0031	0.0022
Lead (Pb)	0.0502	0.0208	0.0198	0.0249	0.0982	0.0550	0.0862	0.0709	0.0611	0.0594
Uranium (U)	0.0014	0.0022	0.0030	0.0026	0.0018	0.0025	0.0017	0.0024	0.0022	0.0025

Table 4.3 Statistical summary of PM_{10} measurements at PU Supersite from Oct 2004 to Sep 2005 (24-hour samples taken from midnight to midnight, n=40).

PM_{10}	Spring		Summer		Autumn		Winter		Total	
$\mu g\ m^{-3}$	Mean	SD	Mean	SD	Mean	SD	Mean	SD	Mean	SD
Mass (Teflon)	87.4925	21.2322	56.2967	27.6935	110.3325	37.3561	90.4800	36.7502	81.3330	37.7013
OC	12.0664	2.2479	11.4166	4.6356	15.6753	5.6518	16.7576	8.3968	14.0691	6.4487
EC	15.3983	4.1697	21.0259	7.9190	21.4546	9.0859	17.0260	4.9316	19.2489	7.1784
Chloride (Cl^-)	1.0865	0.5692	1.4661	0.7857	0.9262	0.5901	1.5972	0.7743	1.3568	0.7486
Nitrate (NO_3^-)	7.0289	2.3571	1.9180	0.8242	4.1332	1.8803	6.9986	2.8370	4.4599	2.9955
Sulphate (SO_4^{2-})	16.5339	5.9489	8.0939	5.8745	20.5803	10.5160	16.4610	5.2503	14.0953	8.3260
Soluble Sodium (Na^+)	2.7618	1.0509	2.4369	0.5798	2.2700	1.0570	2.6470	1.0013	2.5006	0.8566
Ammonium (NH_4^+)	3.8251	0.8722	1.6031	1.4976	4.0992	1.8626	3.6110	1.4017	2.9608	1.8185
Soluble Potassium (K^+)	0.5205	0.3662	0.2318	0.1824	1.0591	0.7500	1.0748	1.1330	0.6804	0.7990
Sodium (Na)	1.6559	0.6391	1.3041	0.5516	1.4859	0.6960	1.5444	0.6724	1.4538	0.6184
Magnesium (Mg)	0.6326	0.2305	0.3028	0.1324	0.5081	0.1629	0.4171	0.1336	0.4140	0.1792
Aluminum (Al)	1.2150	0.5511	0.4782	0.4303	1.4915	0.7794	1.1173	0.7506	0.9623	0.7310
Silicon (Si)	2.4525	1.0280	0.8450	0.7600	2.7930	1.4137	2.1428	1.3619	1.8171	1.3615
Phosphorus (P)	0.2413	0.0673	0.1348	0.0982	0.2973	0.1368	0.2013	0.0726	0.1996	0.1120
Sulphur (S)	6.3339	1.5281	3.2061	2.2585	7.4643	3.3194	5.6946	1.8953	5.1793	2.8084
Chlorine (Cl)	1.2700	0.9214	1.3939	1.0279	0.8137	0.8411	1.5709	0.7876	1.3230	0.9156
Potassium (K)	0.9180	0.5047	0.3872	0.3373	1.5319	0.9526	1.2974	1.0022	0.9650	0.8739
Calcium (Ca)	1.0759	0.4058	0.5847	0.2958	1.4281	0.5124	1.0988	0.6695	0.9696	0.5796
Scandium (Sc)	0.0002	0.0004	0.0005	0.0006	0.0004	0.0006	0.0001	0.0003	0.0003	0.0005
Titanium (Ti)	0.0910	0.0405	0.0508	0.0347	0.0997	0.0519	0.0825	0.0543	0.0749	0.0484
Vanadium (V)	0.0241	0.0116	0.0204	0.0236	0.0108	0.0068	0.0218	0.0224	0.0193	0.0198
Chromium (Cr)	0.0105	0.0042	0.0065	0.0039	0.0110	0.0031	0.0088	0.0036	0.0086	0.0040
Manganese (Mn)	0.0525	0.0142	0.0315	0.0192	0.0659	0.0286	0.0615	0.0360	0.0502	0.0304
Iron (Fe)	1.9199	0.5385	1.3755	0.6405	2.2320	0.8323	1.9253	0.8130	1.7799	0.7818
Nickel (Ni)	0.0076	0.0030	0.0063	0.0053	0.0046	0.0029	0.0078	0.0064	0.0066	0.0052
Copper (Cu)	0.0521	0.0088	0.0463	0.0231	0.0714	0.0267	0.0609	0.0253	0.0566	0.0248
Zinc (Zn)	0.2832	0.0810	0.2595	0.2833	0.4593	0.1673	0.4197	0.3042	0.3539	0.2654
Gallium (Ga)	0.0115	0.0099	0.0084	0.0065	0.0079	0.0068	0.0065	0.0053	0.0080	0.0063
Arsenic (As)	0.0079	0.0072	0.0109	0.0097	0.0197	0.0124	0.0193	0.0196	0.0159	0.0147
Selenium (Se)	0.0000	0.0000	0.0020	0.0000	0.0029	0.0000	0.0009	0.0000	0.0019	0.0010
Bromine (Br)	0.0206	0.0101	0.0107	0.0056	0.0192	0.0088	0.0276	0.0212	0.0189	0.0149
Rubidium (Rb)	0.0028	0.0021	0.0028	0.0022	0.0096	0.0056	0.0080	0.0097	0.0066	0.0073
Strontium (Sr)	0.0143	0.0066	0.0060	0.0028	0.0116	0.0060	0.0114	0.0067	0.0098	0.0060
Yttrium (Y)	0.0037	0.0022	0.0018	0.0013	0.0007	0.0007	0.0019	0.0012	0.0021	0.0016
Zerconium (Zr)	0.0144	0.0066	0.0084	0.0050	0.0141	0.0035	0.0155	0.0037	0.0125	0.0054
Niobium (Nb)	0.0000	0.0000	0.0015	0.0017	0.0000	0.0001	0.0015	0.0016	0.0011	0.0015
Palladium (Pd)	0.0091	0.0016	0.0078	0.0038	0.0131	0.0080	0.0121	0.0072	0.0104	0.0062
Silver (Ag)	0.0095	0.0073	0.0081	0.0052	0.0071	0.0046	0.0075	0.0050	0.0079	0.0051
Cadmium (Cd)	0.0051	0.0068	0.0055	0.0052	0.0092	0.0042	0.0106	0.0057	0.0080	0.0056
Indium (In)	0.0111	0.0013	0.0114	0.0085	0.0129	0.0090	0.0098	0.0047	0.0112	0.0070
Tin (Sn)	0.0383	0.0076	0.0151	0.0069	0.0417	0.0163	0.0510	0.0311	0.0344	0.0248
Antimony (Sb)	0.0444	0.0108	0.0478	0.0097	0.0517	0.0079	0.0545	0.0092	0.0504	0.0096
Cesium (Ce)	0.0118	0.0000	0.0065	0.0060	0.0061	0.0061	0.0076	0.0034	0.0072	0.0048
Barium (Ba)	0.0971	0.0089	0.0858	0.0539	0.0899	0.0396	0.0919	0.0407	0.0897	0.0431
Gold (Au)	0.0001	0.0000	0.0021	0.0000	0.0011	0.0000	0.0021	0.0000	0.0015	0.0009
Mercury (Hg)	0.0000	0.0000	0.0000	0.0000	0.0000	0.0000	0.0000	0.0000	0.0000	0.0000
Thallium (Tl)	0.0000	0.0000	0.0032	0.0040	0.0005	0.0000	0.0023	0.0018	0.0026	0.0031
Lead (Pb)	0.0635	0.0363	0.0229	0.0286	0.1056	0.0659	0.1022	0.0775	0.0693	0.0670
Uranium (U)	0.0024	0.0027	0.0012	0.0018	0.0016	0.0029	0.0005	0.0012	0.0012	0.0020

Table 4.4 Statistical summary of PM_{coarse} measurements at PU Supersite from Oct 2004 to Sep 2005 (24-hour samples taken from midnight to midnight, n=40).

PM_{coarse}	Spring		Summer		Autumn		Winter		Total	
$\mu g\ m^{-3}$	Mean	SD	Mean	SD	Mean	SD	Mean	SD	Mean	SD
Mass (Teflon)	27.2550	14.1269	15.3693	6.5487	39.3788	17.8834	29.6300	15.5513	25.9013	15.7189
OC	1.8256	1.7291	2.3075	2.0546	1.8889	1.6568	2.1508	1.7168	2.1240	1.7845
EC	0.6953	0.7094	1.9093	3.0336	2.6974	3.9889	1.2510	1.1798	1.7439	2.6756
Chloride (Cl^-)	0.7434	0.4201	1.1268	0.5914	0.7433	0.5682	0.9610	0.7774	0.9634	0.6355
Nitrate (NO_3^-)	3.2626	2.4164	0.8968	0.4775	2.0238	1.5977	2.6190	1.6663	1.9269	1.6167
Sulphate (SO_4^{2-})	2.3152	2.4695	0.5011	0.4086	2.0364	2.1285	1.9829	1.3022	1.4428	1.5490
Soluble Sodium (Na^+)	1.2105	0.9975	0.9382	0.4784	0.8859	0.8890	1.1050	0.9366	1.0073	0.7481
Ammonium (NH_4^+)	0.2380	0.1122	0.0862	0.1486	0.2105	0.2274	0.2270	0.1874	0.1712	0.1816
Soluble Potassium (K^+)	0.0915	0.1164	0.0335	0.0417	0.0643	0.0852	0.1949	0.2781	0.0937	0.1725
Sodium (Na)	0.9138	0.4069	0.7822	0.4519	0.6539	0.5635	0.7325	0.4278	0.7528	0.4522
Magnesium (Mg)	0.3656	0.1350	0.1727	0.1009	0.2767	0.1432	0.2044	0.1144	0.2244	0.1289
Aluminum (Al)	0.7579	0.4165	0.3219	0.2838	1.0945	0.5958	0.8052	0.5920	0.6862	0.5538
Silicon (Si)	1.5572	0.7492	0.6232	0.5050	2.0503	1.1353	1.5377	1.0108	1.3166	1.0024
Phosphorus (P)	0.0192	0.0203	0.0147	0.0138	0.0180	0.0024	0.0192	0.0122	0.0168	0.0124
Sulphur (S)	0.3344	0.2258	0.3388	0.2273	0.2822	0.2044	0.4945	0.3179	0.3864	0.2656
Chlorine (Cl)	1.1149	0.8454	1.2026	0.7918	0.7227	0.8135	1.1504	0.6410	1.0809	0.7476
Potassium (K)	0.2807	0.1306	0.1469	0.0769	0.3636	0.1736	0.3315	0.2547	0.2666	0.1953
Calcium (Ca)	0.7891	0.3065	0.4629	0.2045	1.1151	0.3935	0.8765	0.5538	0.7680	0.4592
Scandium (Sc)	0.0002	0.0004	0.0004	0.0005	0.0004	0.0006	0.0001	0.0003	0.0003	0.0005
Titanium (Ti)	0.0596	0.0302	0.0360	0.0234	0.0716	0.0403	0.0593	0.0418	0.0535	0.0362
Vanadium (V)	0.0029	0.0001	0.0045	0.0027	0.0040	0.0021	0.0031	0.0030	0.0038	0.0025
Chromium (Cr)	0.0055	0.0032	0.0054	0.0031	0.0058	0.0027	0.0040	0.0027	0.0050	0.0029
Manganese (Mn)	0.0224	0.0059	0.0119	0.0057	0.0282	0.0127	0.0238	0.0154	0.0202	0.0126
Iron (Fe)	1.2927	0.3613	0.9870	0.3738	1.5498	0.5782	1.3461	0.5941	1.2535	0.5281
Nickel (Ni)	0.0024	0.0020	0.0017	0.0010	0.0022	0.0005	0.0028	0.0015	0.0022	0.0012
Copper (Cu)	0.0312	0.0070	0.0296	0.0129	0.0436	0.0243	0.0335	0.0157	0.0339	0.0166
Zinc (Zn)	0.0407	0.0127	0.0407	0.0408	0.0678	0.0299	0.0813	0.0737	0.0597	0.0524
Gallium (Ga)	0.0153	0.0037	0.0074	0.0069	0.0127	0.0000	0.0076	0.0059	0.0089	0.0063
Arsenic (As)	0.0024	0.0020	0.0093	0.0103	0.0074	0.0054	0.0081	0.0067	0.0077	0.0070
Selenium (Se)	0.0000	0.0000	0.0020	0.0000	0.0029	0.0000	0.0009	0.0000	0.0019	0.0010
Bromine (Br)	0.0079	0.0055	0.0037	0.0028	0.0069	0.0037	0.0093	0.0043	0.0065	0.0043
Rubidium (Rb)	0.0024	0.0007	0.0046	0.0028	0.0027	0.0016	0.0065	0.0066	0.0047	0.0048
Strontium (Sr)	0.0071	0.0038	0.0042	0.0028	0.0083	0.0044	0.0094	0.0068	0.0071	0.0051
Yttrium (Y)	0.0049	0.0001	0.0018	0.0013	0.0000	0.0000	0.0024	0.0009	0.0026	0.0015
Zerconium (Zr)	0.0107	0.0073	0.0066	0.0042	0.0078	0.0036	0.0082	0.0036	0.0081	0.0043
Niobium (Nb)	0.0000	0.0000	0.0013	0.0017	0.0000	0.0001	0.0011	0.0015	0.0008	0.0014
Palladium (Pd)	0.0035	0.0015	0.0086	0.0032	0.0097	0.0031	0.0073	0.0047	0.0075	0.0039
Silver (Ag)	0.0101	0.0072	0.0057	0.0034	0.0054	0.0033	0.0040	0.0026	0.0057	0.0040
Cadmium (Cd)	0.0048	0.0000	0.0075	0.0055	0.0086	0.0000	0.0086	0.0041	0.0080	0.0044
Indium (In)	0.0088	0.0016	0.0082	0.0069	0.0112	0.0105	0.0071	0.0043	0.0083	0.0063
Tin (Sn)	0.0072	0.0054	0.0061	0.0025	0.0138	0.0088	0.0178	0.0129	0.0129	0.0106
Antimony (Sb)	0.0077	0.0075	0.0087	0.0094	0.0140	0.0124	0.0147	0.0096	0.0116	0.0101
Cesium (Ce)	0.0000	0.0000	0.0065	0.0060	0.0074	0.0063	0.0055	0.0029	0.0064	0.0046
Barium (Ba)	0.0643	0.0105	0.0648	0.0495	0.0471	0.0327	0.0577	0.0292	0.0582	0.0348
Gold (Au)	0.0001	0.0000	0.0000	0.0000	0.0011	0.0000	0.0021	0.0000	0.0011	0.0010
Mercury (Hg)	0.0000	0.0000	0.0000	0.0000	0.0000	0.0000	0.0000	0.0000	0.0000	0.0000
Thallium (Tl)	0.0000	0.0000	0.0044	0.0052	0.0000	0.0000	0.0021	0.0018	0.0033	0.0037
Lead (Pb)	0.0202	0.0163	0.0101	0.0050	0.0171	0.0109	0.0196	0.0244	0.0162	0.0169
Uranium (U)	0.0012	0.0024	0.0006	0.0016	0.0016	0.0029	0.0003	0.0010	0.0008	0.0018

Table 4.5 Enrichments factors for elements in $PM_{1.0}$, $PM_{2.5}$, and PM_{coarse}.

Enrichment Factors	$PM_{1.0}$	$PM_{2.5}$	PM_{coarse}
Sodium (Na)	10.0	6.8	**3.1**
Magnesium (Mg)	6.1	**4.0**	**2.0**
Aluminum (Al)	**1.0**	**1.0**	**1.0**
Silicon (Si)	**0.4**	**0.5**	**0.5**
Phosphorus (P)	156.5	78.6	**2.8**
Potassium (K)	11.7	6.9	**1.1**
Calcium (Ca)	**1.5**	**2.0**	**3.0**
Titanium (Ti)	**1.7**	**2.1**	**2.1**
Vanadium (V)	165.0	81.7	7.4
Chromium (Cr)	42.9	30.8	16.8
Manganese (Mn)	21.5	14.3	**3.9**
Iron (Fe)	**3.9**	**4.4**	**4.2**
Nickel (Ni)	159.1	79.1	12.9
Copper (Cu)	326.2	260.2	159.1
Zinc (Zn)	1793.7	1168.6	98.6
Gallium (Ga)	292.5	110.3	61.3
Arsenic (Ar)	5160.0	2817.5	598.4
Selenium (Se)		52.3	**4.5**
Rubidium (Rb)	24.4	12.7	**4.9**
Strontium (Sr)	7.8	**3.7**	**2.4**
Yttrium (Y)	22.7	22.3	14.0
Zerconium (Zr)	23.7	11.1	**5.0**
Palladium (Pd)	13200727.7	6155586.5	1764880.8
Silver (Ag)	88702.0	40928.9	13346.8
Cadmium (Cd)	50906.3	21856.2	9505.2
Tin (Sn)	3034.9	1450.8	275.8
Antimony (Sb)	113968.6	55639.6	6791.5
Barium (Ba)	30.1	24.0	12.4
Lead (Pb)	1444.2	832.4	94.9
Uranium (U)	390.1	213.7	32.0

Table 4.6 Correlation coefficients of inter-species in $PM_{1.0}$.

$PM_{1.0}$	Mass	OC	EC	Cl^-	NO_3^-	SO_4^{2-}	Na^+	NH_4^+	K^+	Na	Mg	Al	Si	P	S	Cl	K	Ca	Ti	V	Cr	Mn	Fe	Ni	Cu	Zn	Ga	As	Br	Rb	Sr	Y	Zr	Sn	Sb	Au	Pb
Mass	1.00																																				
OC	**0.84**	1.00																																			
EC	0.46	0.45	1.00																																		
Cl^-	0.11	0.29	-0.32	1.00																																	
NO_3^-	0.64	0.77	0.03	0.55	1.00																																
SO_4^{2-}	**0.82**	0.52	0.10	0.03	0.44	1.00																															
Na^+	0.24	0.26	-0.07	0.49	0.38	0.32	1.00																														
NH_4^+	**0.87**	0.64	0.12	0.16	0.64	**0.96**	0.32	1.00																													
K^+	**0.84**	**0.86**	0.19	0.24	0.61	0.65	0.22	0.69	1.00																												
Na	0.50	0.31	0.24	-0.13	0.27	0.57	-0.01	0.58	0.34	1.00																											
Mg	0.59	0.38	0.22	0.00	0.29	0.66	0.13	0.65	0.47	0.72	1.00																										
Al	0.46	0.34	0.31	-0.08	0.40	0.44	0.14	0.50	0.33	0.78	0.67	1.00																									
Si	0.59	0.54	0.33	0.08	0.52	0.51	0.17	0.57	0.55	0.77	0.65	**0.88**	1.00																								
P	0.78	0.39	0.15	-0.06	0.36	**0.94**	0.20	**0.91**	0.52	0.65	0.70	0.51	0.50	1.00																							
S	**0.80**	0.44	0.11	0.01	0.44	**0.97**	0.26	**0.96**	0.56	0.64	0.68	0.53	0.54	**0.98**	1.00																						
Cl	0.09	0.29	-0.08	**0.89**	0.53	-0.18	0.22	0.07	0.07	-0.20	-0.11	-0.17	-0.07	-0.24	-0.14	1.00																					
K	**0.83**	**0.83**	0.17	0.26	0.63	0.66	0.21	0.71	**0.98**	0.41	0.50	0.41	0.65	0.54	0.60	0.06	1.00																				
Ca	0.16	0.12	0.29	-0.14	0.12	0.16	0.00	0.19	0.13	0.71	0.59	**0.83**	0.77	0.23	0.23	-0.17	0.20	1.00																			
Ti	0.04	0.04	0.29	-0.14	0.08	0.02	-0.06	0.04	0.00	0.57	0.39	0.75	0.67	0.08	0.08	-0.18	0.07	**0.84**	1.00																		
V	0.53	0.50	0.46	-0.01	0.58	0.29	0.27	0.41	0.23	0.32	0.26	0.52	0.42	0.39	0.38	0.16	0.23	0.18	0.21	1.00																	
Cr	0.21	0.17	0.13	0.07	0.18	0.24	0.14	0.25	0.21	0.54	0.46	0.58	0.65	0.25	0.27	0.01	0.28	0.71	0.54	0.09	1.00																
Mn	0.40	0.37	0.18	0.10	0.27	0.34	0.08	0.34	0.41	0.61	0.26	0.42	0.66	0.28	0.34	-0.03	0.51	0.30	0.32	0.12	0.39	1.00															
Fe	0.10	0.08	0.26	-0.11	0.07	0.09	-0.04	0.11	0.07	0.78	0.49	0.75	0.73	0.15	0.16	-0.17	0.16	**0.92**	**0.82**	0.12	0.68	0.52	1.00														
Ni	0.52	0.54	0.43	0.00	0.62	0.26	0.22	0.38	0.27	0.32	0.20	0.52	0.47	0.33	0.33	0.18	0.26	0.21	0.24	**0.97**	0.12	0.20	0.17	1.00													
Cu	0.48	0.51	0.39	0.03	0.45	0.35	0.05	0.43	0.42	**0.80**	0.66	**0.84**	**0.86**	0.38	0.40	0.03	0.47	**0.85**	0.71	0.46	0.70	0.44	**0.82**	0.49	1.00												
Zn	0.54	0.44	0.32	-0.08	0.30	0.47	0.08	0.46	0.41	0.65	0.30	0.47	0.59	0.46	0.50	-0.11	0.46	0.22	0.26	0.45	0.21	0.83	0.42	0.50	0.48	1.00											
Ga	0.09	-0.04	-0.06	-0.13	0.01	0.28	0.21	0.24	-0.07	0.39	0.19	0.20	0.14	0.32	0.31	-0.26	-0.06	0.18	0.26	0.30	0.04	0.02	0.27	0.31	0.33	0.29	1.00										
As	0.47	0.52	-0.01	0.14	0.56	0.39	0.30	0.47	0.52	0.29	0.16	0.18	0.54	0.09	0.26	0.05	0.59	0.22	0.22	0.07	0.55	0.55	0.43	0.15	0.38	0.47	-0.13	1.00									
Br	0.66	**0.80**	0.12	0.36	**0.81**	0.37	0.35	0.51	0.72	0.28	0.29	0.36	0.51	0.29	0.34	0.29	0.73	0.13	0.08	0.55	0.11	0.30	0.08	0.57	0.49	0.34	-0.20	0.37	1.00								
Rb	0.74	0.73	0.14	0.38	0.52	0.47	0.03	0.51	**0.88**	0.40	0.49	0.27	0.49	0.34	0.37	0.57	**0.85**	0.19	0.02	0.22	0.15	0.30	0.13	0.22	0.56	0.29	-0.51	0.25	0.76	1.00							
Sr	-0.15	-0.20	-0.17	0.05	-0.10	-0.02	-0.01	-0.07	-0.13	0.27	0.08	0.15	0.13	-0.03	-0.01	-0.26	-0.08	0.12	0.32	-0.18	0.05	0.34	0.29	-0.15	0.04	0.28	0.41	0.25	-0.20	-0.19	1.00						
Y	-0.16	-0.15	0.04	-0.34	0.18	-0.17	-0.48	-0.08	-0.18	0.32	0.26	0.33	0.41	-0.10	-0.07	0.69	-0.06	0.46	0.45	0.04	0.08	0.25	0.45	0.07	0.42	0.05	0.33	0.58	0.09	-0.27	0.16	1.00					
Zr	-0.20	-0.35	-0.12	-0.37	-0.36	-0.16	-0.28	-0.22	-0.11	-0.16	-0.25	-0.18	-0.23	-0.09	-0.12	-0.42	-0.11	-0.20	-0.13	-0.25	-0.19	-0.01	-0.19	-0.24	-0.37	-0.07	-0.20	-0.14	-0.22	-0.09	-0.11	-0.16	1.00				
Sn	0.52	0.51	0.20	0.35	0.63	0.46	0.32	0.53	0.43	0.26	0.34	0.40	0.51	0.36	0.44	0.12	0.49	0.19	0.10	0.31	0.03	0.24	0.12	0.31	0.30	0.26	-0.06	0.33	0.44	0.32	0.16	0.20	-0.25	1.00			
Sb	0.35	0.15	0.19	-0.01	0.05	0.36	0.07	0.30	0.20	0.29	0.13	0.10	0.23	0.33	0.35	0.02	0.21	0.03	0.06	0.14	0.05	0.32	0.13	0.09	0.13	0.38	0.34	0.35	0.14	0.34	0.23	0.11	-0.21	0.19	1.00		
Au	0.11	0.02	-0.16	0.17	0.35	0.38	0.27	0.28	0.27	0.02	-0.28	-0.09	0.16	0.26	0.32	**1.00**	0.16	0.12	0.34	-0.38	0.91	-0.02	-0.09	-0.50	0.15	-0.01	0.30	**0.88**	0.02	0.01	0.36	-0.49	-0.02	0.31	0.64	1.00	
Pb	**0.85**	**0.86**	0.25	0.25	0.69	0.68	0.23	0.74	**0.93**	0.37	0.50	0.45	0.68	0.56	0.62	0.10	**0.95**	0.20	0.17	0.39	0.25	0.45	0.12	0.42	0.51	0.49	0.06	0.56	0.73	0.76	-0.16	-0.04	-0.22	0.56	0.22	0.09	1.00

Table 4.7 Correlation coefficients of inter-species in $PM_{2.5}$.

$PM_{2.5}$	Mass	OC	EC	Cl^-	NO_3^-	SO_4^{2-}	Na^+	NH_4^+	K^+	Na	Mg	Al	Si	P	S	Cl	K	Ca	Ti	V	Cr	Mn	Fe	Ni	Cu	Zn	Ga	As	Br	Rb	Sr	Y	Zr	Sn	Sb	Au	Pb
Mass	1.00																																				
OC	**0.81**	1.00																																			
EC	0.45	0.41	1.00																																		
Cl^-	0.18	0.33	-0.25	1.00																																	
NO_3^-	0.63	0.72	0.01	0.58	1.00																																
SO_4^{2-}	**0.86**	0.54	0.18	0.10	0.48	1.00																															
Na^+	0.21	0.12	-0.21	0.34	0.29	0.27	1.00																														
NH_4^+	**0.89**	0.60	0.20	0.13	0.61	**0.96**	0.22	1.00																													
K^+	**0.82**	**0.91**	0.19	0.32	0.64	0.65	0.15	0.66	1.00																												
Na	0.46	0.25	-0.16	0.24	0.30	0.49	0.31	0.48	0.35	1.00																											
Mg	0.51	0.30	-0.14	0.11	0.33	0.55	0.12	0.57	0.40	0.67	1.00																										
Al	**0.80**	0.67	0.21	0.14	0.49	0.70	0.09	0.72	0.72	0.57	0.71	1.00																									
Si	0.77	0.66	0.16	0.13	0.49	0.65	0.14	0.67	0.70	0.61	0.75	**0.97**	1.00																								
P	**0.83**	0.42	0.24	-0.07	0.34	**0.96**	0.17	**0.93**	0.53	0.51	0.55	0.65	0.62	1.00																							
S	**0.85**	0.47	0.20	-0.01	0.40	**0.97**	0.21	**0.95**	0.59	0.55	0.60	0.70	0.67	**0.99**	1.00																						
Cl	0.12	0.21	-0.12	**0.87**	0.52	0.05	0.08	0.14	0.15	0.06	0.03	0.06	0.01	-0.11	-0.06	1.00																					
K	**0.83**	**0.88**	0.19	0.27	0.58	0.68	0.12	0.67	**0.98**	0.40	0.50	0.78	0.78	0.58	0.64	0.10	1.00																				
Ca	0.73	0.67	0.23	0.06	0.35	0.60	-0.01	0.59	0.73	0.54	0.72	**0.93**	**0.94**	0.59	0.63	-0.05	**0.82**	1.00																			
Ti	0.71	0.63	0.30	0.11	0.38	0.55	0.12	0.57	0.61	0.57	0.66	**0.92**	**0.90**	0.54	0.58	-0.01	0.68	**0.89**	1.00																		
V	0.51	0.46	0.49	0.01	0.54	0.28	0.09	0.40	0.22	0.17	0.10	0.39	0.33	0.29	0.29	0.11	0.20	0.23	0.49	1.00																	
Cr	0.61	0.55	0.00	0.11	0.48	0.58	0.09	0.60	0.62	0.50	0.69	0.73	0.75	0.54	0.59	-0.02	0.66	0.75	0.72	0.26	1.00																
Mn	0.56	0.49	0.11	0.24	0.28	0.50	0.12	0.46	0.56	0.62	0.54	0.71	0.77	0.44	0.49	0.12	0.65	0.73	0.69	0.07	0.55	1.00															
Fe	0.63	0.61	0.39	0.10	0.22	0.47	-0.01	0.46	0.59	0.50	0.49	0.78	**0.81**	0.46	0.49	-0.05	0.67	**0.84**	**0.85**	0.22	0.57	0.84	1.00														
Ni	0.53	0.50	0.38	0.03	0.57	0.31	0.09	0.43	0.30	0.25	0.17	0.41	0.35	0.31	0.32	0.11	0.27	0.26	0.47	**0.95**	0.30	0.09	0.20	1.00													
Cu	0.77	**0.89**	0.51	0.14	0.53	0.56	-0.02	0.62	**0.80**	0.35	0.38	0.73	0.71	0.51	0.53	0.05	0.79	0.76	0.76	0.49	0.61	0.55	0.76	0.51	1.00												
Zn	0.66	0.64	0.29	0.23	0.37	0.51	0.20	0.50	0.61	0.59	0.34	0.71	0.72	0.46	0.49	0.15	0.64	0.67	0.77	0.39	0.51	0.83	**0.82**	0.38	0.70	1.00											
Ga	0.41	0.31	0.10	0.00	0.26	0.38	0.25	0.40	0.24	0.21	0.28	0.37	0.31	0.35	0.36	-0.02	0.16	0.26	0.37	0.43	0.26	0.02	0.20	0.55	0.33	0.22	1.00										
As	0.66	**0.81**	0.13	0.24	0.69	0.35	0.09	0.47	**0.86**	0.05	0.25	0.50	0.53	0.21	0.27	0.11	**0.82**	0.51	0.30	0.17	0.43	0.17	0.25	0.30	0.56	0.20	0.06	1.00									
Br	0.61	**0.80**	0.07	0.50	**0.81**	0.34	0.22	0.45	0.74	0.46	0.40	0.61	0.64	0.24	0.31	0.39	0.72	0.58	0.58	0.48	0.51	0.43	0.45	0.50	0.67	0.54	0.15	0.66	1.00								
Rb	0.67	0.70	0.17	0.15	0.37	0.58	0.08	0.52	**0.87**	0.32	0.18	0.49	0.48	0.51	0.53	-0.09	**0.85**	0.58	0.44	0.05	0.56	0.36	0.41	0.12	0.63	0.43	0.03	0.64	0.54	1.00							
Sr	0.05	0.11	-0.25	0.02	0.08	0.16	-0.19	0.17	0.15	0.10	0.50	0.25	0.28	0.15	0.17	-0.10	0.23	0.27	0.13	-0.18	0.29	0.09	0.15	-0.09	0.13	-0.05	0.28	0.17	0.03	0.04	1.00						
Y	0.64	0.40	0.45	0.02	0.12	0.67	-0.41	0.65	0.31	0.31	0.09	0.17	0.00	0.63	0.61	0.27	0.22	0.12	0.30	0.46	0.48	0.47	0.27	0.49	0.64	0.63	0.12	-0.69	-0.15	0.37	-0.26	1.00					
Zr	0.29	0.27	0.15	0.16	0.17	0.27	-0.05	0.22	0.33	0.14	0.17	0.22	0.18	0.25	0.23	0.19	0.30	0.23	0.27	0.21	0.30	0.15	0.14	0.23	0.33	0.21	0.03	0.26	0.24	0.42	-0.10	0.39	1.00				
Sn	0.42	0.38	0.05	0.16	0.42	0.38	0.13	0.42	0.53	0.18	0.30	0.36	0.38	0.29	0.34	0.01	0.44	0.37	0.25	0.12	0.49	0.33	0.22	0.20	0.31	0.24	0.04	0.48	0.30	0.16	0.04	0.31	-0.12	1.00			
Sb	0.22	0.27	0.22	0.17	0.10	0.14	0.09	0.12	0.23	0.13	0.22	0.40	0.40	0.08	0.11	-0.13	0.27	0.39	0.46	0.25	0.20	0.34	0.45	0.21	0.31	0.27	0.12	0.10	0.23	0.01	0.11	-0.03	0.04	0.28	1.00		
Au	-0.13	-0.34	-0.10	-0.11	-0.10	-0.45	0.17	-0.56	-0.44	0.10	0.02	-0.04	-0.03	-0.67	-0.61	0.00	-0.40	0.09	0.16	0.11	0.34	-0.23	-0.13	0.73	-0.31	-0.06	**0.99**	**1.00**	-0.18	**-1.00**	-0.28	.	0.13	-0.29	-0.61	1.00	
Pb	**0.84**	**0.87**	0.18	0.23	0.57	0.71	0.18	0.72	**0.95**	0.43	0.50	**0.80**	**0.80**	0.61	0.66	0.11	**0.96**	**0.80**	0.70	0.24	0.73	0.65	0.66	0.31	**0.82**	0.68	0.23	0.77	0.70	**0.83**	0.15	0.42	0.33	0.42	0.23	-0.42	1.00

Table 4.8 Correlation coefficients of inter-species in PM_{coarse}.

PM_c	Mass	OC	EC	Cl^-	NO_3^-	SO_4^{2-}	Na^+	NH_4^+	K^+	Na	Mg	Al	Si	P	S	Cl	K	Ca	Ti	V	Cr	Mn	Fe	Ni	Cu	Zn	Ga	As	Br	Rb	Sr	Y	Zr	Sn	Sb	Pb
Mass	1.00																																			
OC	0.20	1.00																																		
EC	-0.14	0.33	1.00																																	
Cl^-	-0.14	-0.28	-0.19	1.00																																
NO_3^-	0.50	-0.11	-0.34	0.27	1.00																															
SO_4^{2-}	0.55	-0.03	-0.22	0.25	0.70	1.00																														
Na^+	0.23	-0.22	-0.32	0.66	0.73	0.63	1.00																													
NH_4^+	0.30	0.15	0.11	-0.20	-0.06	0.31	0.00	1.00																												
K^+	0.49	0.18	-0.02	-0.08	0.23	0.35	0.08	0.41	1.00																											
Na	0.22	-0.04	-0.38	0.70	0.47	0.35	0.58	-0.03	0.12	1.00																										
Mg	0.75	0.19	-0.15	0.08	0.41	0.52	0.36	0.34	0.39	0.39	1.00																									
Al	**0.84**	0.24	0.05	-0.40	0.25	0.40	-0.04	0.40	0.59	-0.12	0.63	1.00																								
Si	**0.84**	0.25	0.05	-0.43	0.26	0.40	-0.05	0.39	0.55	-0.13	0.64	**0.99**	1.00																							
P	-0.07	-0.14	0.08	0.30	-0.17	0.17	0.15	0.17	-0.02	0.36	0.23	-0.09	-0.10	1.00																						
S	0.23	0.07	-0.04	-0.07	0.01	-0.12	-0.14	0.21	0.29	0.20	0.21	0.14	0.15	0.32	1.00																					
Cl	-0.08	-0.22	-0.30	**0.88**	0.39	0.29	0.65	-0.17	0.13	0.78	0.09	-0.35	-0.38	0.24	0.06	1.00																				
K	**0.81**	0.25	0.07	-0.35	0.23	0.34	-0.02	0.43	0.73	-0.02	0.61	**0.94**	**0.93**	-0.01	0.32	-0.24	1.00																			
Ca	0.78	0.25	0.07	-0.42	0.21	0.36	-0.09	0.37	0.63	-0.13	0.55	**0.96**	**0.96**	-0.10	0.09	-0.36	**0.90**	1.00																		
Ti	0.78	0.28	0.08	-0.43	0.20	0.32	-0.06	0.42	0.59	-0.10	0.66	**0.94**	**0.94**	-0.12	0.30	-0.36	**0.91**	**0.91**	1.00																	
V	0.29	0.08	0.02	-0.14	-0.18	-0.10	0.08	0.19	0.37	-0.18	0.15	0.37	0.34	-0.03	0.13	-0.18	0.43	0.32	0.35	1.00																
Cr	0.25	0.35	0.00	-0.54	-0.31	-0.20	-0.34	0.09	0.05	-0.34	0.28	0.43	0.42	-0.20	0.00	-0.60	0.35	0.40	0.49	0.40	1.00															
Mn	0.73	0.17	0.12	-0.46	0.17	0.37	-0.15	0.43	0.57	-0.19	0.48	**0.90**	**0.88**	-0.08	0.15	-0.45	**0.86**	**0.88**	**0.83**	0.40	0.37	1.00														
Fe	0.74	0.40	0.22	-0.55	0.06	0.24	-0.21	0.42	0.48	-0.28	0.57	**0.91**	**0.92**	-0.02	0.15	-0.53	**0.84**	**0.90**	**0.92**	0.36	0.57	0.84	1.00													
Ni	0.25	-0.10	-0.14	-0.15	0.21	0.25	0.00	0.24	0.61	-0.12	0.17	0.47	0.42	0.03	0.10	-0.07	0.46	0.51	0.50	0.33	0.19	0.53	0.43	1.00											
Cu	0.55	0.35	0.17	-0.38	0.13	0.35	0.03	0.20	0.35	-0.15	0.37	0.60	0.61	0.00	-0.05	-0.37	0.53	0.62	0.59	0.46	0.32	0.53	0.67	0.35	1.00										
Zn	0.67	0.39	0.00	-0.46	0.24	0.14	-0.08	0.16	0.37	-0.09	0.35	0.65	0.67	0.07	0.56	-0.43	0.69	0.62	0.68	0.43	0.38	0.66	0.68	0.21	0.60	1.00									
Ga	0.56	0.07	0.05	-0.16	0.52	0.41	0.04	0.17	0.36	0.05	0.31	0.36	0.38	-0.38	-0.32	-0.06	0.34	0.24	0.21	0.10	-0.20	0.46	0.19	-0.16	0.07	0.29	1.00								
As	0.04	0.37	0.02	-0.37	0.00	-0.09	-0.34	-0.20	0.02	-0.35	-0.20	0.19	0.19	**-0.83**	0.35	-0.33	0.09	0.15	0.23	0.12	0.38	0.26	0.27	-0.14	0.04	0.53	0.26	1.00							
Br	0.55	0.07	-0.35	0.00	0.70	0.47	0.38	0.05	0.34	0.27	0.33	0.41	0.40	0.07	0.35	0.20	0.45	0.33	0.35	0.04	-0.05	0.35	0.23	0.38	0.22	0.49	0.01	0.14	1.00						
Rb	0.35	0.38	0.04	-0.37	-0.27	-0.28	-0.40	0.38	**0.87**	-0.10	0.10	0.62	0.57	-0.14	0.55	-0.20	0.73	0.69	0.63	0.68	0.29	0.72	0.63	0.64	0.24	0.71	0.33	0.16	0.04	1.00					
Sr	0.63	0.14	-0.10	0.03	0.38	0.45	0.31	0.39	0.78	0.12	0.44	0.64	0.60	-0.15	0.10	0.10	0.67	0.66	0.62	0.55	0.10	0.59	0.50	0.54	0.38	0.42	0.28	-0.15	0.33	0.71	1.00				
Y	0.22	0.22	0.02	0.03	0.26	0.61	0.20	0.42	-0.11	-0.02	0.51	0.12	0.18	-0.39	0.10	0.09	0.05	0.07	0.06	0.15	0.04	0.18	0.14	-0.18	0.10	0.04	**0.80**	-0.03	-0.16	**-0.89**	-0.02	1.00			
Zr	0.14	0.10	-0.20	0.00	0.14	0.06	0.04	-0.12	-0.33	0.19	0.30	-0.04	0.03	0.03	0.02	0.09	-0.07	-0.03	0.06	-0.48	0.04	-0.16	0.06	-0.07	-0.10	-0.08	-0.48	-0.10	0.09	-0.38	-0.22	0.42	1.00		
Sn	0.31	0.39	0.11	-0.22	0.22	0.16	-0.10	0.16	0.21	0.09	0.01	0.27	0.29	0.70	0.52	-0.22	0.40	0.23	0.29	-0.09	-0.05	0.34	0.23	0.11	0.16	0.68	0.28	0.33	0.56	0.22	0.05	-0.50	-0.20	1.00	
Sb	0.00	0.03	0.31	-0.32	0.02	0.03	-0.19	-0.03	0.08	-0.34	-0.23	0.03	0.05	0.19	0.30	-0.33	0.07	0.08	0.06	0.02	-0.05	0.13	0.13	0.42	0.37	0.31	-0.07	-0.09	0.29	0.05	-0.01	-0.11	-0.31	0.42	1.00
Pb	0.55	0.40	0.11	-0.32	0.27	0.20	-0.07	0.08	0.27	0.12	0.30	0.40	0.42	0.19	0.41	-0.24	0.53	0.37	0.45	0.15	0.07	0.45	0.44	0.15	0.32	0.73	0.38	0.04	0.46	0.37	0.27	-0.20	0.14	0.79	0.35

Table 4.9 Correlations among different size factions.

R	$PM_{1.0}$&$PM_{2.5}$	$PM_{2.5}$&PM_{10}	$PM_{1.0}$&PM_{10}	PM_{10}&PM_c	$PM_{1.0}$&PM_c	$PM_{2.5}$&PM_c
Mass	**0.99**	**0.95**	**0.93**	**0.86**	0.64	0.67
OC	**0.98**	**0.96**	**0.96**	0.51	0.31	0.25
EC	**0.96**	**0.95**	**0.92**	0.76	0.51	0.51
Cl^-	0.76	0.51	0.34	**0.92**	0.04	0.14
NO_3^-	**0.97**	**0.84**	**0.83**	0.74	0.28	0.26
SO_4^{2-}	**0.96**	**0.99**	**0.95**	0.54	0.38	0.39
Na^+	0.53	0.49	0.22	**0.96**	0.09	0.23
NH_4^+	**0.98**	**0.99**	**0.98**	0.51	0.41	0.42
K^+	**0.98**	**0.98**	**0.96**	0.69	0.52	0.55
Na	0.42	0.71	0.06	**0.86**	-0.03	0.30
Mg	0.46	0.71	0.31	**0.91**	0.17	0.34
Al	0.39	**0.92**	0.38	**0.99**	0.38	**0.85**
Si	0.58	**0.91**	0.62	**0.99**	0.62	**0.84**
P	**0.96**	**0.98**	**0.95**	-0.12	-0.17	-0.26
S	**0.97**	**0.99**	**0.96**	0.01	-0.11	-0.11
Cl	**0.82**	0.59	0.22	**0.95**	-0.08	0.26
K	**0.99**	**0.99**	**0.99**	**0.92**	**0.89**	**0.88**
Ca	0.09	**0.90**	0.04	**0.99**	0.05	**0.86**
Sc	-0.16	0.03	0.05	**0.85**	0.09	-0.23
Ti	-0.01	**0.85**	0.03	**0.98**	0.05	0.72
V	**0.98**	**0.99**	**0.99**	0.59	0.55	0.47
Cr	0.32	0.62	0.21	**0.84**	0.07	0.09
Mn	**0.91**	**0.90**	0.76	0.71	0.22	0.33
Fe	0.24	**0.84**	-0.01	**0.97**	-0.05	0.69
Ni	0.11	-0.13	**0.94**	**1.00**	0.27	0.08
Cu	**0.93**	**0.94**	0.30	0.39	0.21	0.56
Zn	0.52	0.79	**0.90**	**0.94**	0.42	0.38
Ga	**0.93**	**0.97**	-0.17	0.58	-0.22	-0.25
As	0.74	0.75	0.69	0.75	0.35	0.24
Br	**0.91**	**0.95**	**0.92**	0.61	0.46	0.33
Rb	**0.86**	0.79	**0.89**	**0.90**	**0.88**	0.61
Sr	0.03	0.26	0.08	**0.88**	0.04	-0.19
Sn	0.70	**0.82**	**0.84**	0.65	0.59	0.15
Sb	-0.18	0.15	0.20	0.57	0.12	-0.64
Pb	**0.93**	**0.97**	**0.97**	0.42	0.47	0.18

Table 4.10 Correlation coefficients between hourly particle concentrations and vehicle numbers. (hourly samples for one week, n=168).

R	$PM_{2.5}$	PM_{10}	BC	PM_{coarse}
Private cars	**0.85**	**0.85**	0.74	**0.80**
Motocycles	0.77	0.78	0.73	0.74
Light Buses	-0.58	-0.55	-0.73	-0.34
Single deck bus	0.74	0.73	0.75	0.58
Double deck bus	**0.90**	**0.89**	**0.94**	0.75
Goods vehicles (<=5.5 ton)	**0.80**	0.77	**0.93**	0.57
Goods vehicles (5.5-24 ton)	0.66	0.63	**0.84**	0.42
Goods vehicles (>24 ton)	0.31	0.33	0.26	0.41
Taxis	-0.30	-0.27	-0.42	-0.06
Gasoline-fueled vehicles	**0.85**	**0.86**	0.75	**0.80**
Diesel-fueled vehicles	**0.85**	**0.83**	**0.96**	0.64
Total vehicle numbers	**0.90**	**0.90**	**0.86**	**0.83**

Chapter 5 Case Study on Fine Particulate Episode in Cold and Warm Seasons

5.1 Introduction

As reported in previous studies, the air pollution in Hong Kong has close relations to synoptic systems, especially frequently continental high pressure emerged in cold seasons (Pathak et al. 2003; Wang et al. 1997; 2003; Louie et al. 2005b) and occasionally tropical storms in the warm seasons (Cheng et al. 2006; Wang et al. 2006). Under suitable synoptic systems, the pollution originating from upwind areas (normally the Asian continent) can be carried to Hong Kong territory, forming fine particulate episodes in atmosphere.

Most previous studies on pollution episodes have focused on the cold seasons (Pathak et al. 2003; Wang et al. 1997; 2003; Louie et al. 2005a), but only a few attentions have been paid to the warm seasons like Tanner's studies (Tanner, 1999; Tanner and Law, 2002). Meanwhile, the knowledge of the air mass transport pathways and the source areas for the long-range-transported pollution have remained largely unexplored. In this chapter, the results of two case studies are presented in order to characterize the PM during pollution episodes at PU Supersite in both cold and warm seasons.

Carbonaceous aerosols, e.g. OC and EC, were the main study objectives in cold seasons, for the previous studies have demonstrated the existence of a significant impact of regional pollution on secondary aerosols (e.g., sulfate, nitrate, and ammonium). On the other hand, both carbonaceous aerosols and water-soluble ions were investigated in the summer case study. Another aim of this chapter is to identify the source areas of continental pollution by using the PSCF receptor model (Ashbaugh, 1983). This work is valuable because it is the first step in the process of devising effective strategies to control pollutants through the co-operation of Hong Kong and Mainland. Once the previously unknown sources are identified, advanced characterization can then be implemented (e.g., stack sampling, upwind sampling) to obtain the characterization of the source's emission, followed by the development of a control strategy including the possibility of revised or new regulations.

5.2 Results and discussion

5.2.1 Case study in cold seasons

$PM_{1.0}$ and $PM_{2.5}$ were collected daily by one RP2025 sequential sampler at PU Supersite from January to May 2004. An integrated data set, including aerosol mass (by gravimetrical method) and concentrations of carbonaceous aerosols (by IMPROVE TOR) associated with pollution episode and non-episode days, has been

obtained from the quartz filters. The HKEPD $PM_{2.5}$ data monitored by TEOM at ambient stations, e.g., TW and TC, were used to make comparison with the roadside $PM_{2.5}$ concentrations. The information obtained and presented below is especially important for us to improve the current understanding of the fine particle pollution.

5.2.1.1 Meteorological parameters during sampling period

Throughout the sampling period from January to May 2004, the mean air pressure, temperature, and relative humidity did not vary significantly. During wintertime, the prevailing surface wind direction was northeasterly with ~82% of hourly winds from the resultant vector of 38º, as shown in Figure 5.1 a. This means that nearly all winter winds traveled over China's continental land mass before reaching Hong Kong. During springtime, however, the mean directions of hourly surface winds varied in all vectors. The resultant vector is 77º, as shown in Figure 5.1 b, accounting for ~48% of wind distribution. Wind from the south (90º-270º) was ~38% of distribution. Wind-rose analysis suggests that the air masses arriving at Hong Kong in spring were not only from the continent, but also sometimes from the South China Sea. The above weather parameters were measured at Waglan Meteorological Station (22.18º N, 114.30º E) of Hong Kong Observation, which is located on Waglan Island in an open landscape.

5.2.1.2 Pollution episodes in winter

As shown in Figure 5.2, time series of $PM_{1.0}$ and $PM_{2.5}$ at PU Supersite exhibited seven episode days, January 30, February 14-15, February 23, February 26, April 19-20, respectively, during which $PM_{2.5}$ exceeded the average concentration by a factor of two. It was found that the PM occurring during episode days differed statistically from non-episode days (*p*-values <0.05, *t*-test). Concurrent peaks for $PM_{2.5}$ were also found at two urban ambient monitoring stations (TC and TW). For instance, the average $PM_{2.5}$ loading during the episodes at TW exceeded the average level throughout the study period by a factor of 2.4.

Five-day back trajectories were conducted for those episode days using a HYSPLIT model (Draxler and Hess, 1997). All of the air masses during episode days originated from north China, traveling across southeastern China along the coastline before reaching Hong Kong and bringing aged, polluted aerosols. Similar pollution episodes have been found in prior studies (Yu et al. 2004; Louie et al. 2005b).

Regression analysis in Figure 5.3 a shows that $PM_{2.5}$ collected at TW and TC generally had good relationship with a correlation coefficient (R) equal to 0.86 in non-episode days, and 0.90 during episode days. This indicates that they are controlled by similar urban- and regional-scale sources, including remote sources. The particulate

spatial distribution tended to be more even in the ambient atmosphere, due to the effects of remote sources. As seen in Figure 5.3 b, PU roadside $PM_{2.5}$ moderately correlated with $PM_{2.5}$ at TW in non-episode days (R=0.75), implying that vehicular emissions, as an urban plume, had contributed to urban ambient $PM_{2.5}$ during non-episode days. Poor relationship (R=0.28) was found during episode days, which suggests that particles at PU roadside comprised sources that do not contribute much to urban atmosphere. Most likely, nearby vehicular emissions were those sources.

Occurrence of episodes in Hong Kong during winter was found to be associated with a mesoscale subsiding airstream with a moderate to stagnant easterly transport (Louie et al. 2005b). In this study, the average mixing height during episode days was 666 m, which was much lower than average mixing height during the non-episode days (936 m). This indicated poor dispersion conditions when the episodes occurred. Thus, the elevated concentrations of pollutants observed at PU during episode days were attributed to the combination of stagnant vehicular emissions from the nearby road, and subsiding continental aerosols from long-range transport.

Table 5.1 shows concentrations of mass and carbonaceous aerosols for each episode day. Carbonaceous aerosols on 14 February were found to be much higher than on other episode days (Table 5.1), making up of ~67.4% of $PM_{1.0}$ and ~54.3% of $PM_{2.5}$. It

is suspected that the PM high concentrations were attributed to some unknown local event. Therefore, the calculation of average values for episode days excludes the data on 14 February.

On episode days, the average OC concentration in $PM_{1.0}$ and $PM_{2.5}$ increased ~70% and ~100%, respectively, compared to average values. EC showed only a 20-30% increase. Regional or long-range transport of continental aerosols was believed to be the dominant factor leading to higher OC levels in Hong Kong during winter, because vehicles emissions would not have significant day-to-day variations due to the consistent traffic flow on each day (source: 2004 Annual Traffic Census). As mentioned before, several pollutants in the Hong Kong atmosphere have been affected by long-range transport of continental aerosols, which leads to higher pollution levels in winter; when compared with other seasons (Pathak et al. 2003; Louie et al. 2005; Yu et al. 2004). Most of these pollutants are secondary aerosols, such as OC (Louie et al. 2005; Yu et al. 2004) and sulfate and ammonium (Pathak et al. 2003), that were thought to be produced by gas-to-particle conversion or chemical reaction during transport. In a study done by Pathak et al. (2003), continental long-range transport of aerosols was found to increase sulfate and ammonium concentrations in Hong Kong's air by 49% to 383%, and 33% to 302%, in 2000-2001. On the contrary, EC originates

from relatively simple sources and does not form in the atmosphere due to its nearly inert property (Ogren and Charlson, 1983). It mainly originates from incomplete combustion of carbon-containing material (Ogren and Charlson, 1983). In addition, the air masses reaching Hong Kong did not travel over the main source regions for EC in mainland China as mentioned in the study of Streets et al. (2001). Therefore, EC observed in this case study is controlled by local sources, such as vehicular exhausts that continuously emit EC into the atmosphere.

During episode days, total carbonaceous aerosols accounted for ~33% and ~37% of $PM_{1.0}$ and $PM_{2.5}$, respectively (Table 5.1), which were lower than average contributions in sampling period, ~47% and ~46% of TC in $PM_{1.0}$ and $PM_{2.5}$, respectively. Moreover, the average OC/EC ratio increased from 0.9 during non-episode days to 1.5 during episode days. This indicates that particles at PU roadside were influenced by remote sources that had different sources for carbonaceous aerosols with higher OC/EC ratios.

5.2.2 Case study in warm seasons

In this summer case study, one RP2025 sampler was deployed to collect sufficient mass for chemical analyses at two- or three-hour intervals on 20-22 and 26-28 July 2005. The mass concentrations of $PM_{2.5}$ (by gravimetrical method), organic and

elemental carbon (by IMPROVE TOR), sulfate, nitrate, and ammonium (by IC) were determined from the integrated samples on quartz filters.

5.2.2.1 Classification of air masses

Figure 5.4 shows the 48-hour isentropic back trajectories reaching the sampling location at 500 m height. The back trajectories were calculated at six-hour interval over each day (20, 21, 22, 26, 27, and 28 July 2005), using the HYSPLIT model. Three categories of back trajectories were identified. The first was from south China on 20 July 2005. The air pathways illustrated that the air parcels traveled anti-clockwise over south China before reaching Hong Kong, starting from the North Pacific, which was due to the influence of Typhoon Haitang over the western North Pacific (http://www.hko.gov.hk/informtc/tc2005/tc0507.htm). The second pathway was from the west regions to Hong Kong, passing some countries in South Asia (on 21 and 22 July 2005). The third was from South China Sea, which brought clean marine aerosols into Hong Kong (on 26-28 July 2005). To make it simple, we named the three conditions as Case I, II, and III. Case I and III represented the air masses experiencing long-range transport over continental areas and air masses dominantly originating from local sources, respectively, and Case II was the transit period.

5.2.2.2 Pollution episodes in summer

The temporal variations of the $PM_{2.5}$, elemental carbon, organic carbon, sulfate, nitrate, and ammonium are shown in Figure 5.5. It can be seen that there is significant increase in mass concentrations of particles and chemical species during Case I compared to those during Case III and the increase was not from vehicle emissions. Meanwhile, high ozone levels, with a maximum of 138 ppbv, were observed in ambient atmosphere of Hong Kong on 20 July (http://www.epd.gov.hk). Previous studies (Wang, 2003; Wang et al. 2006) have shown that the stagnation caused by the descending air mass at the outskirt of a low-pressure system is the dominant synoptic cause of photochemical pollution in summer in the atmosphere of Hong Kong.

In this study, fine particle pollution was observed also due to the influence of Typhoon Haitang, which was originally generated over the western North Pacific on 14 July (http://www.hko.gov.hk/informtc/tc2005/tc0507.htm). On 20 July, the reduced visibility to less than 1000 m was recorded in Hong Kong. There were intense isolation active thunderstorms over Guangdong on 20 July, and then it drifted into Hong Kong at around 22:00 on 20 July under the northwesterly winds, leading to a total amount of 20.4 mm rainfall during two-hour period over Hong Kong. Sulfate concentrations reached the minimum level in a day during the rainfall period. This is

believed to be the effect of wet scavenging of rainfall (Figure 5.5).

The air mass arriving at Hong Kong on 20 July carried a number of anthropogenic pollutants, for it had experienced long-range transportation over south China (PRD region) before reaching Hong Kong. The average concentrations of particles and chemical components in $PM_{2.5}$ during the three Cases are shown in Table 5.2. Out of the three Cases, the average $PM_{2.5}$ mass concentration was the highest during Case I (103.9±35.6 μg m^{-3}) and the lowest during Case III (37.9±10.8 μg m^{-3}). Assuming that Case III represents the locally generated emission in Hong Kong, continental transportation of aerosols was found to increase the $PM_{2.5}$ mass concentrations by ~174%. The OC, EC, sulfate, nitrate, and ammonium increased by ~125%, ~100%, ~120%, ~150%, and ~200%, respectively.

During Case I, total carbonaceous aerosols accounted for ~38% of the total $PM_{2.5}$ mass, which were lower than Case III (~51% of the $PM_{2.5}$ mass). However, the average OC/EC ratio of 0.9 during Case I was at the same level of the average OC/EC ratio (0.9) during Case III. This is because the increase in EC concentrations is also significant during Case I in this summer case study, which differs from the episode days observed in the winter case study. The different magnitude of increase in EC

concentrations between winter and summer may imply the air masses had traveled over different areas over Mainland China before reaching Hong Kong.

5.2.2.3 Evolution of OC/EC ratios

EC is a sensitive indicator for primary emissions and there is a representative ratio of OC/EC for each primary aerosol (Novakov, 1984; Gray et al., 1986; Turpin and Huntzicker, 1991). The ratio of OC and EC changes with the changes of sources, even at a source-dominated site. In this summer case study, the ratios of OC/EC were low to 0.4 during daytime and high to 2.8 during nighttime, as shown in Figure 5.5. These differences are because aerosol is a superposition of source emissions with perceptible contributions at multiple scales, such as micro (~10 m), middle (~100-1000m), neighborhood (~1-5 km), urban (~5-50 km), regional (~50-1000 km), continental (~1000-5000 km) and global (>5000 km) spatial scales (Watson and Chow, 2001b). During daytime, the low OC/EC ratios (from 0.4 to 1.1) showed characteristics of vehicle emissions at micro scale, sometimes combined with anthropogenic pollutants from an upwind area at continental scale. The anthropogenic pollutants from the upwind areas maybe have similar OC/EC ratios with the PU Supersite, as previously mentioned. During nighttime, on the other hand, the high OC/EC ratios (from1.0 to

2.8) showed characteristics of regional background aerosols due to lack of nearby sources at micro scale. The 24-hr OC/EC ratios measured at the regional background site (HT) of Hong Kong ranged from 2.0-8.0 in July 2004 (unpublished data). The nighttime OC/EC ratios were much lower during Case I and Case II than Case III because of the influence of continental pollution. Figure 5.6 shows the scatter plots of OC against EC in the summer case study, which clearly indicates the different relationship of OC and EC between daytime (8:00-20:00) and nighttime (20:00-24:00 and 24:00-8:00).

5.2.2.4 Diurnal variations of aerosols

As the compliance metric of air quality standards for particulate matter, 24-hr integrated measurements of particulate mass was used throughout the world so far. However, the key influencing factors to ambient particle concentration and size distribution, such as the emission strengths of particle sources, temperature, RH, wind direction and speed as well as mixing height, fluctuate in time scales that are substantially shorter than 12-24 hours (Shen et al. 2002). Individual human activity also varies in time period considerably shorter than 24 hours. Therefore, the 24-hr particulate mass is a rough indication of particles exposures to which the population is

subjected (Tanner et al. 2005). The value of semi-continuous/continuous measurements, not only for fine particles but also for individual chemical species, has been recognized in recent years and a number of studies (Turpin and Huntzicker, 1995; Hogrefe et al. 2004; Tanner et al. 2005) have disseminated information on the formation and nature of airborne particles in practice by investigating the diurnal variations of species.

As seen from Figure 5.5, $PM_{2.5}$ had obvious diurnal patterns with high concentrations in daytime and low concentrations at night, which is similar to the daily cycle of total traffic flows. We take Case III as an example in the following description, because it had less impact from continental pollutants. During Case III, the average $PM_{2.5}$ mass concentrations were 50.1±10.7 μg m^{-3} at rush hours (8:00-10:00), 43.5±12.0 μg m^{-3} at midday (14:00-16:00) and 18.4±14.6 μg m^{-3} at midnight (1:00-4:00), respectively. The highest traffic density normally occurs at rush hours, suggesting that the emissions observed over this period are more representative for primary vehicle emissions. At rush hours, EC was the most abundant chemical components (~38% of $PM_{2.5}$), followed by OC (~22% of $PM_{2.5}$). Sulfate was the third species, contributing to ~14% of $PM_{2.5}$. The lowest $PM_{2.5}$ concentration was found at midnight due to lack of emission sources, like vehicles. OC was the most abundant chemical component,

amounting to ~32% of $PM_{2.5}$, followed by EC (~23% of $PM_{2.5}$) and sulfate (~22% of $PM_{2.5}$).

Sulfate was the most important species among the water-soluble inorganic ions. It correlated well with ammonium (R=0.88), with a minimum in the early morning hours before dawn and a maximum in the afternoon (Figure 5.5). In the atmosphere of Hong Kong, sulfate and ammonium were mainly in droplet mode (0.57 μm) (Zhuang et al. 1999a; 1999b). The formation of the droplet mode cannot be explained by primary emission, gas-phase nucleation or condensation (Meng and Seinfeld, 1994). The possible formation mechanism of this mode has been explained by SO_2 oxidation in cloud and fog droplets, most likely by H_2O_2 (Zhuang et al. 1999a). Here this explanation is consistent with the presence of the major sulfate peak in the afternoon, because oxidants have their maximum value at the same time. After being oxidized, sulfate is initially in the form of sulfuric acid, and then it is neutralized by ammonia in the atmosphere, which inevitably progresses as a consequence (Claes et al. 1998). This could explain the good correlations between sulfate and ammonium. Given the high humidity of air and near combustion sources, the catalytic formation of sulfate on the surface of soot particles (Novakov et al. 1974) might occur at the roadside.

The concentrations of nitrate in $PM_{2.5}$ were always low and showed relatively weak fluctuations when compared to sulfate and ammonium (Figure 5.5). In a previous study (Zhuang et al. 1999b), nitrate in the atmosphere of Hong Kong has predominantly been found in coarse-mode sea-salt or soil aerosols centered at 3.95±0.69 μm, while little fine mode nitrate was found, which is consistent with the results of low nitrate levels in $PM_{2.5}$ during this measurement. Fine mode nitrate observed in Hong Kong is mainly formed by the homogeneous gas-phase transformation of NO_x to HNO_3, which later reacts with pre-existing fine particles to form the droplet mode nitrate (Zhuang et al. 1999a). Ammonium nitrate centered in the droplet mode tends to evaporate from the smaller particles and deposit on larger particles (Bassett and Seinfeld, 1984), which is because submicron ammonium nitrate particles are subject to a significant Kelvin effect which destabilizes them relative to larger particles (Claes et al. 1998).

5.2.3 Identification of remote source areas using BC as an indicator

5.2.3.1 Site selection

Hok Tsui rural station is located a downwind of eastern Asia and China, as described in Chapter 3. There the southward outflow of continental pollution prevails in the lower atmosphere during cold seasons, e.g., winter, spring, and autumn. A number of

past studies (Ho et al. 2003a; Wang et al. 1997; 2001; 2003; Cohen et al. 2004; Louie et al. 2005b) have investigated the influence of regional and long-range transport of aerosols in the atmosphere of HT. Therefore, BC was monitored at this rural site as an indicator of anthropogenic inflow from upwind area.

5.2.3.2 Pollution rose of BC

The yearly means for this study were evaluated from hourly average BC data collected by Aethalometer. Measured from June 2004 to May 2005, annual average BC concentration at Hok Tsui was 2.4±1.8 μg m^{-3} (Table 5.3). This is comparable to the previous studies conducted by Cohen et al. (2004), with a mean of 2.3±1.7 μg m^{-3}, and Louie et al. (2005a), with a mean of 2.0±0.9 μg m^{-3}. Cohen et al. (2004) estimated $PM_{2.5}$ BC by measuring the transmission of (He/Ne) laser light (wavelength 0.633 nm) through Teflon filters before and after exposure, while Louie et al. (2005a) determined $PM_{2.5}$ EC concentrations on quartz filters using the IMPROVE TOR protocol. Throughout the sampling period, the lowest one-hour BC value was 63.0 ng m^{-3} in summer, which is quite similar with the EC concentrations (68-71 ng m^{-3}) observed in the central North Pacific Ocean measured by the thermal/combustion technique (Kaneyasu and Murayama, 2000).

Figure 5.7 displays the temporal patterns of hourly BC from June 2004 to May 2005.

The diurnal patterns were found to be variable during the study period. Morning peaks usually observed during traffic rush hours at PU Supersite, but were not found at HT. This proves our previous assumption that contributions from the local major source in Hong Kong, namely vehicle exhausts, were less important at this sampling location. Moreover, the seasonal pattern of BC observed at HT also reflects the influence of regional- or remote-scale pollution, with the highest monthly average in January (4.1±2.3 μg m^{-3}) and the lowest in July (1.0±1.3 μg m^{-3}) (Figure 5.8). This seasonal patten of BC was opposite to that observed at PU Supersite (see Chapter 4).

The contribution of BC from different wind directions is illustrated by the pollution roses in Figure 5.9. As can be seen, BC loadings during the sampling period increased when surface winds were from the north/northeast/east (0-105 degree). Hourly BC concentrations from this sector were in the 2-7 μg m^{-3} range, much higher than the 1-2 μg m^{-3} from the southwest. Since mainland China lies north of Hong Kong, high BC levels are most likely due to the influence of continental aerosols that transported from the mainland by the northeast monsoon, which is generated by the cooling and heating of the great Asian land mass. During the sampling period, more than ~70% of surface winds were from the northeast with average wind speeds exceeding 6 m s^{-1}. As Figure 5.9 shows, northerly/northeasterly winds usually prevailed in fall, winter and spring,

corresponding with the relatively high BC concentrations during these seasons. In contrast, during the summer only ~28% of the surface winds came from the northeast. Southerly and northwesterly winds occurred for ~60% and ~12% of summer season, respectively. BC concentrations were 1-2 μg m^{-3} when southerly winds dominated, indicating that the air masses bring relatively clean marine aerosols to HT. High BC concentrations (3-10 μg m^{-3}), averaging 3.3±2.7 μg m^{-3}, were observed in the winds from the northwest, PRD region, although only ~12% of winds came from this sector. The hourly wind speed and wind direction was measured at Waglon meteorological Station (22.18°C, 114.30°C) of Hong Kong Observation, which is close to the HT station and located on Waglon Island in an open landscape.

5.2.3.3 Source areas identified by PSCF receptor model

In order to evaluate the potential source contribution to air pollution in the atmosphere of Hok Tsui, the PSCF values were calculated based on a total of three hundred and sixty two 7-day back trajectories (Draxler and Hess, 1998) arriving at HT at 12:00 (local time) of each day from 4 June 2004 to 31 May 2005. The 24-hr average BC concentration measured at HT in each day was used as an indicator showing whether there are the anthropogenic pollution transported from Asian continent to Hong Kong. The annual mean concentration of BC data (2.4 μg m^{-3}) was the given criteria value in

calculating the PSCF values.

According to the results of the PSCF analysis shown in Figure 5.10, four potential source areas were identified as having important contributions to anthropogenic pollution in Hong Kong. Source area I was coastal portion of southeastern China, including the Yangtze River Delta region, and Jiangxi, Zhejiang, and Fujian Province. Source area II was the region between Hebei and Shandong Province. Source area III was on the border between Shangdong and Henan Province. The PRD region constituted source area IV.

Streets et al. (2003) developed a BC emission inventory for China in 2000, which included all major anthropogenic sources and biomass burning. As reported by Streets et al. (2001; 2003), BC emissions in China were dominated by the residential sector (~74%) and were concentrated in a west-to-east swath curving across the agricultural heartland of China from Sichuan Province to Hebei Province (Streets et al. 2001, see Figure 1). Most air masses arriving at HT do not travel over the major documented BC emission source areas in China. Although source areas II and III, identified in the present study, are located in the boundary zone of the important BC emission areas, few of the polluted air mass trajectories directly pass through these regions. BC emissions in source areas I and IV have more effectively influence on the BC in Hong

Kong than source areas II and III, because most polluted air parcels arriving at HT travel over source area I in cold seasons, and travel over source area IV in warm seasons. This can be seen from the polluted air mass back trajectories in four seasons, shown in Figure 5.11.

Rapid industrialization in southeastern China (source area I) recently implies its significance as a long-range transport source in the future. Energy consumption in southeastern China is expected to increase dramatically and BC emissions are predicted to increase from 1996 to 2050, particularly due to the transportation sector (Streets et al. 2004). Hong Kong, as a receptor, experiences higher BC levels from long-range transport sources in winter, spring, and fall if effective control strategies are not implemented.

The PRD region (source area IV) is an important regional source area for pollutants observed at Hong Kong in the summer. Residential coal and biofuel combustion were the dominant BC emitters in 1995 (Streets et al. 2001), accounting for ~65% of total emitted BC in PRD region. Agricultural burning and other activities made up ~5% and ~30%, respectively. ‘‘Other activities’’ include motor vehicles, industrial emissions, and power plants (available at http://www.epd.gov.hk/epd). In the Hong Kong area, high BC emissions are associated with the traffic emissions at roadside sites (Louie et

al. 2005b) and marine ship emissions near the port (Yu et al. 2004). BC arriving at Hong Kong in summer is a mixture from residential and agricultural combustion, industry, power plants, motor vehicles, and ship emissions from the PRD region (including Hong Kong).

5.3 Summary

Occurrence of episodes during the winter case study was found to be associated with a mesoscale subsiding airstream with a moderate to stagnant easterly transport and a low mixing height. During the seven fine-particle episodes, $PM_{1.0}$ and $PM_{2.5}$ responded in similar ways; i.e., with elevated mass and OC concentrations. Moreover, the average OC/EC ratio increased from 0.9 for non-episodes to 1.5 for episode days. Combining the present and previous findings, the conclusion can be drawn that secondary aerosols (e.g., organic materials, sulfate, and ammonium) formed during long-range transport, significantly contributing to the air quality of Hong Kong in winter.

Occurrence of episodes during the summer case study was shown to be associated with a tropical storm and a low mixing height. During the episode days, concentrations of $PM_{2.5}$ mass and major chemical species (e.g., OC, EC, sulfate, nitrate, and ammonium) significantly increased. Moreover, the average OC/EC ratio (0.9) during

episode days was at the same level to that (0.9) of non-episode days. This means that the continental pollution contributes significantly to both primary and secondary aerosols under this tropical storm system.

To better understand anthropogenic pollution originating in Asia and its transport into Hong Kong, BC emissions, as an indicator of anthropogenic pollutants, were measured continuously from June 2004 to May 2005 at HT, a rural location with less local sources. On an Aethalometer, the BC concentrations exhibited a clear seasonal pattern, with high levels in cold seasons and low levels in warm seasons. During the cold seasons, high BC concentrations frequently occurred due to the southward long-range transport of polluted air masses in the boundary layer over the southeast China. Therefore, coastal areas of southeastern China were identified as the major potential source areas. During the warm seasons, the anthropogenic pollutants transported from the PRD region were found to be an important cause of particulate episodes in Hong Kong. The pollution sources in the PRD region include residential and agricultural combustion, industry, power plants, motor vehicles, and ships.

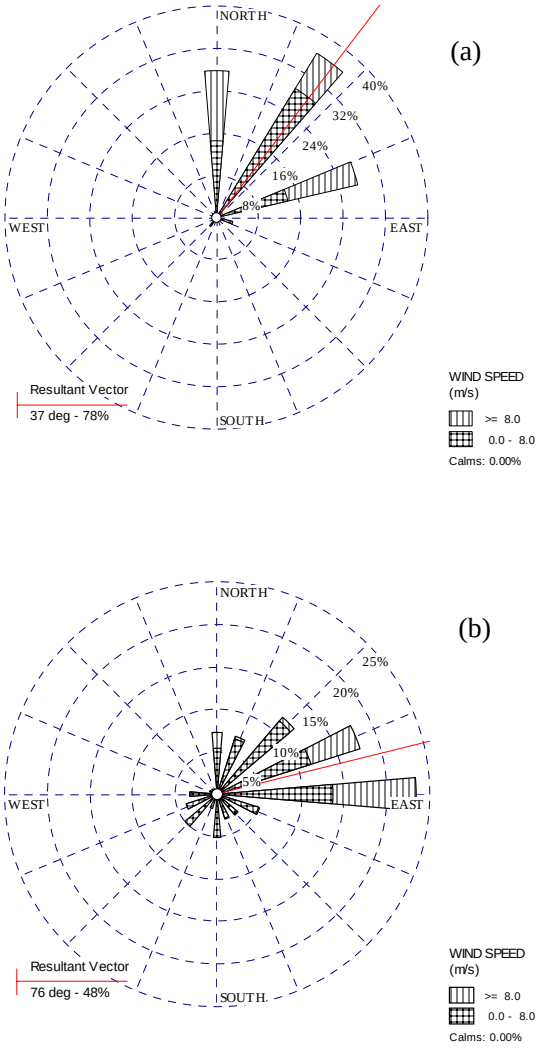

Figure 5.1 Frequency distribution of surface wind in winter (a) and in spring (b).

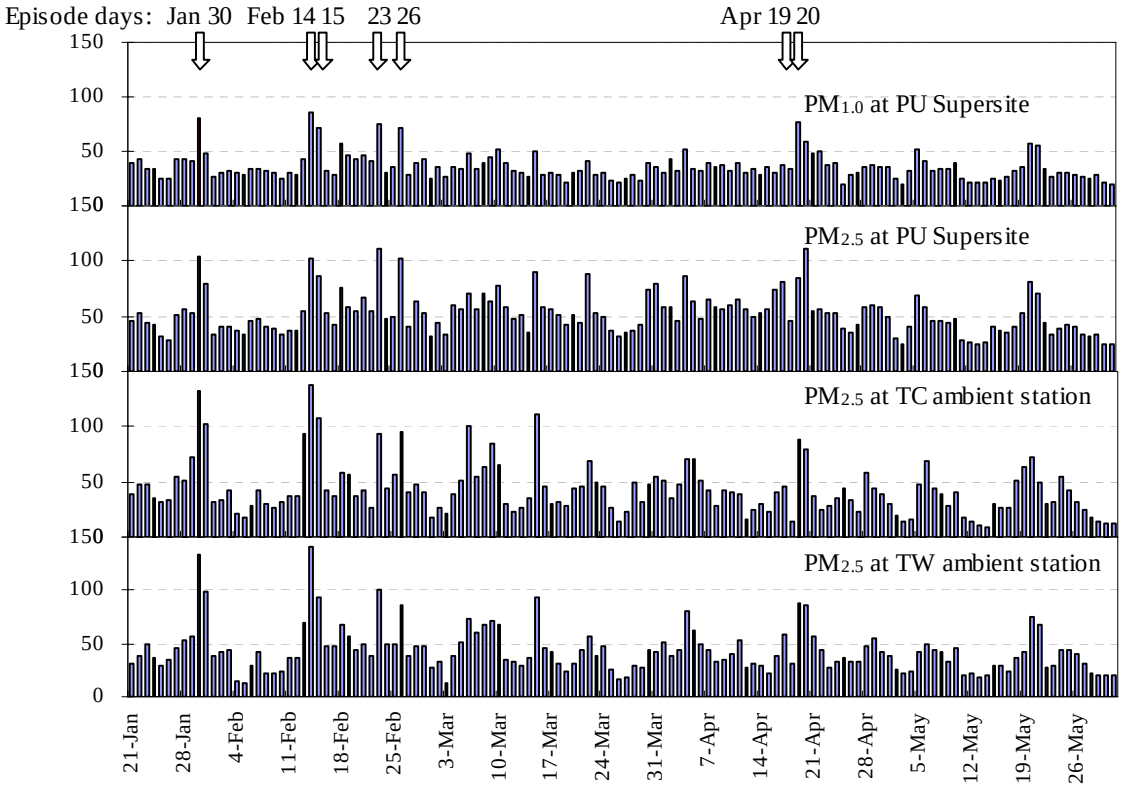

Figure 5.2 Time series of daily $PM_{1.0}$ and $PM_{2.5}$ concentrations at PU Supersite and daily $PM_{2.5}$ at TC and TW ambient station from January to May 2004.

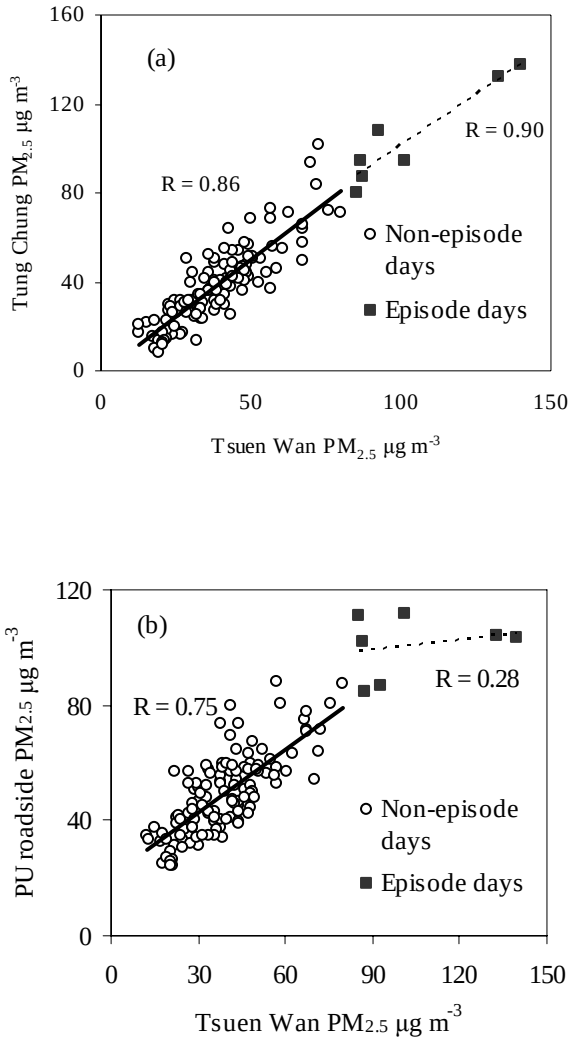

Figure 5.3 Correlations of $PM_{2.5}$ mass between Tsuen Wan and Tung Chung (a) as well as Tsuen Wan and PU Roadside Station (b) during January to May 2004.

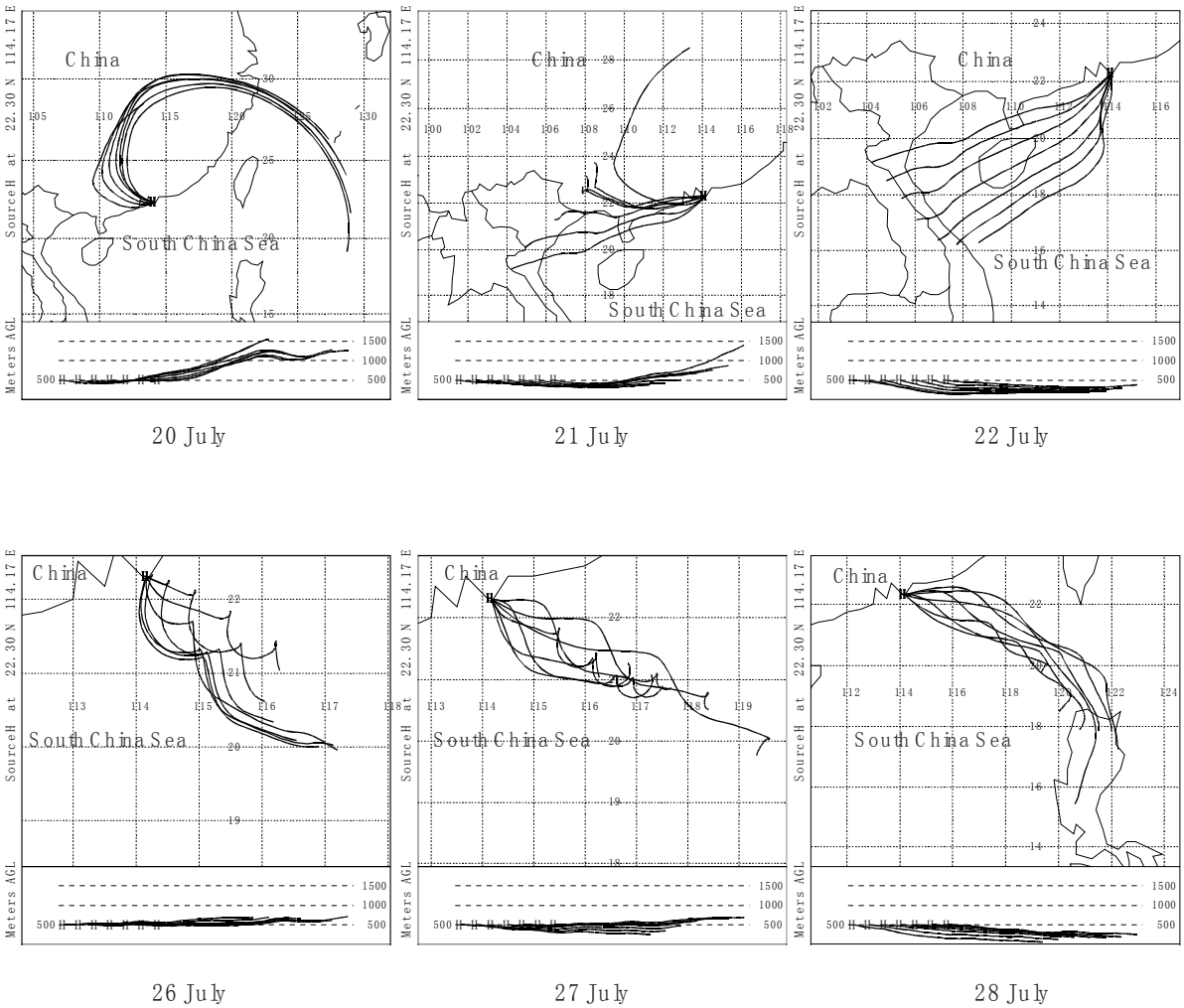

Figure 5.4 The 48-hour back trajectories every sixth hour during each sampling day of the case study.

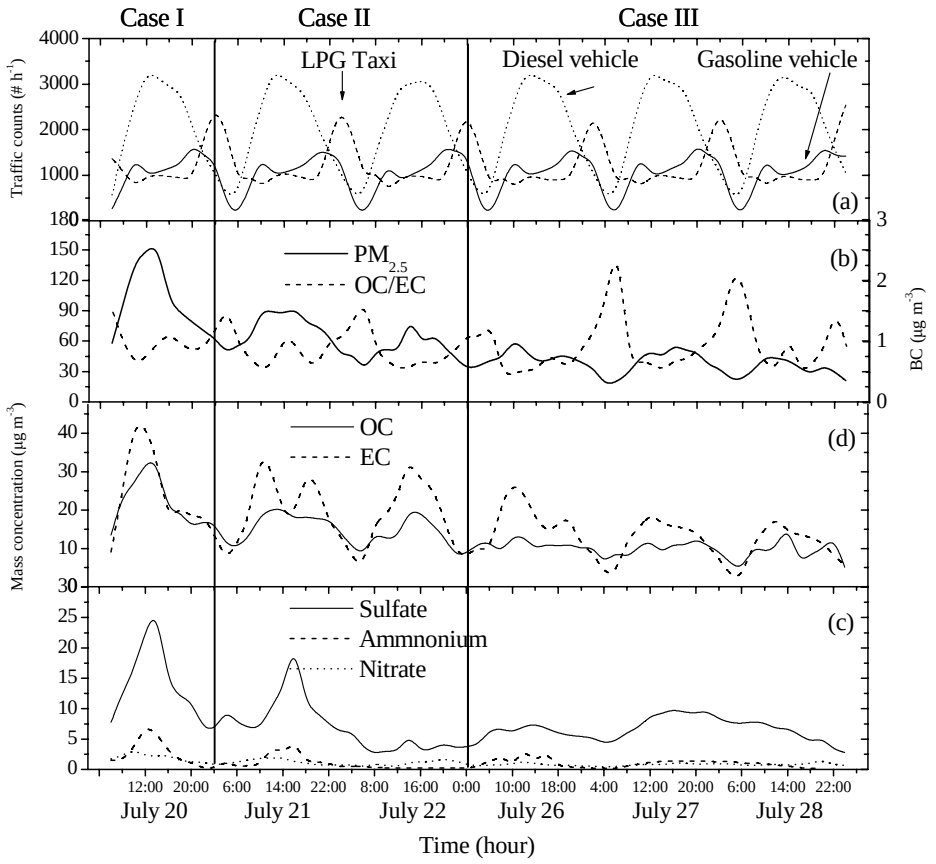

Figure 5.5 Time series of the mass concentrations of $PM_{2.5}$ and individual chemical species, as well as traffic counts.

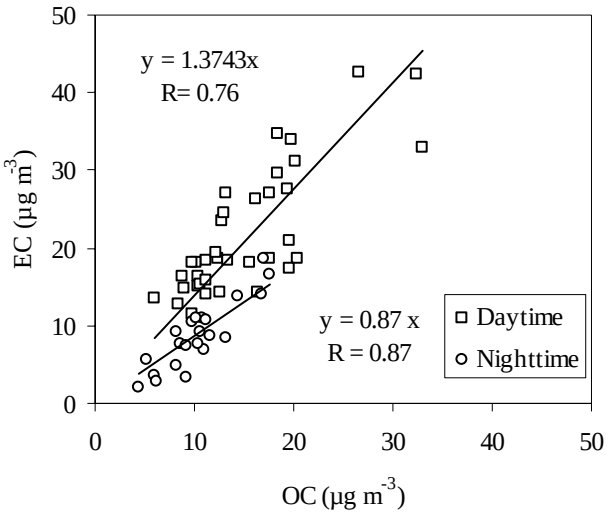

Figure 5.6 Scattering plots of OC against EC during the summer case study.

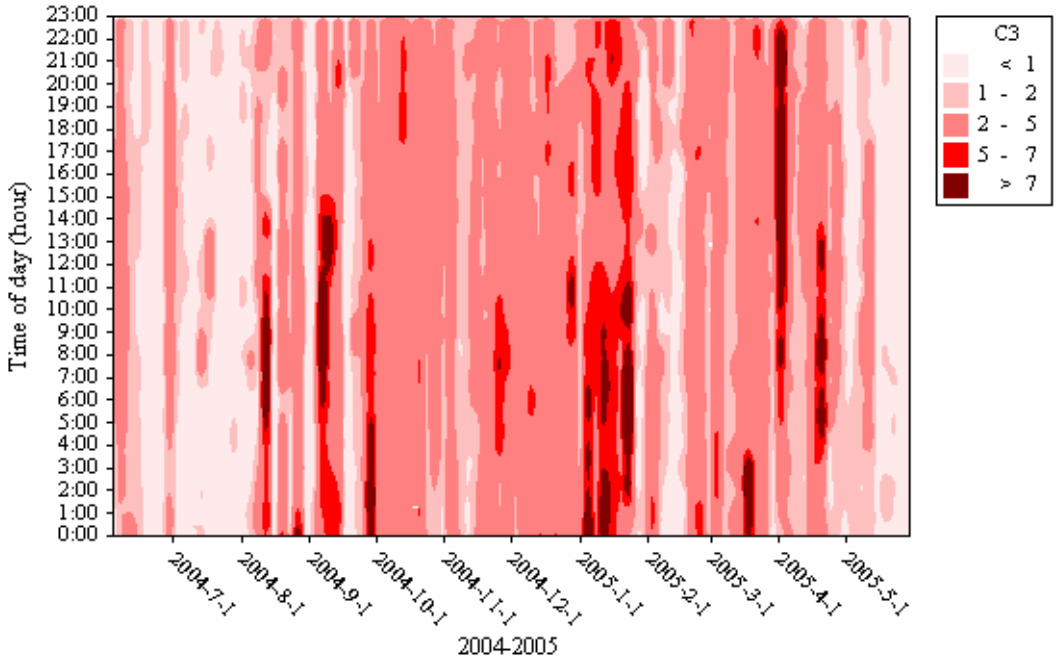

Figure 5.7 Detailed temporal patterns of black carbon during June 2004 to May 2005.

C3 represents the BC concentrations in µg m^{-3}.

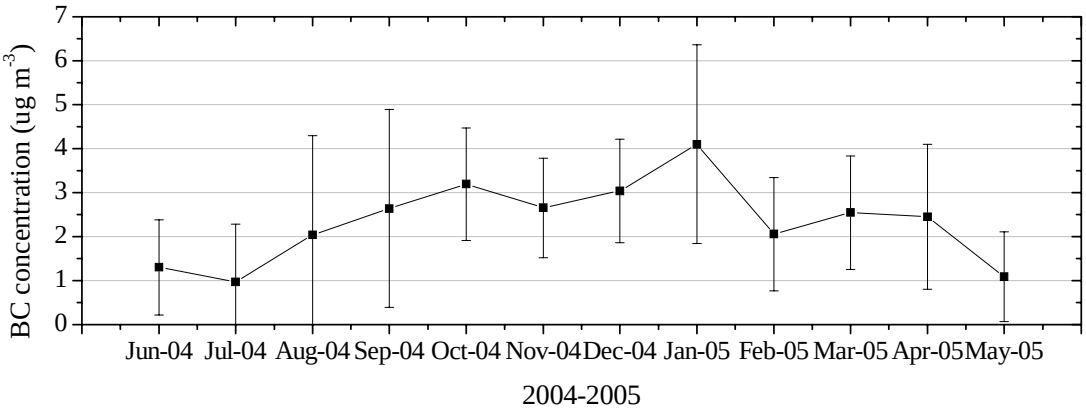

Figure 5.8 Monthly average BC concentrations; the bar represents one standard deviation of hourly averages.

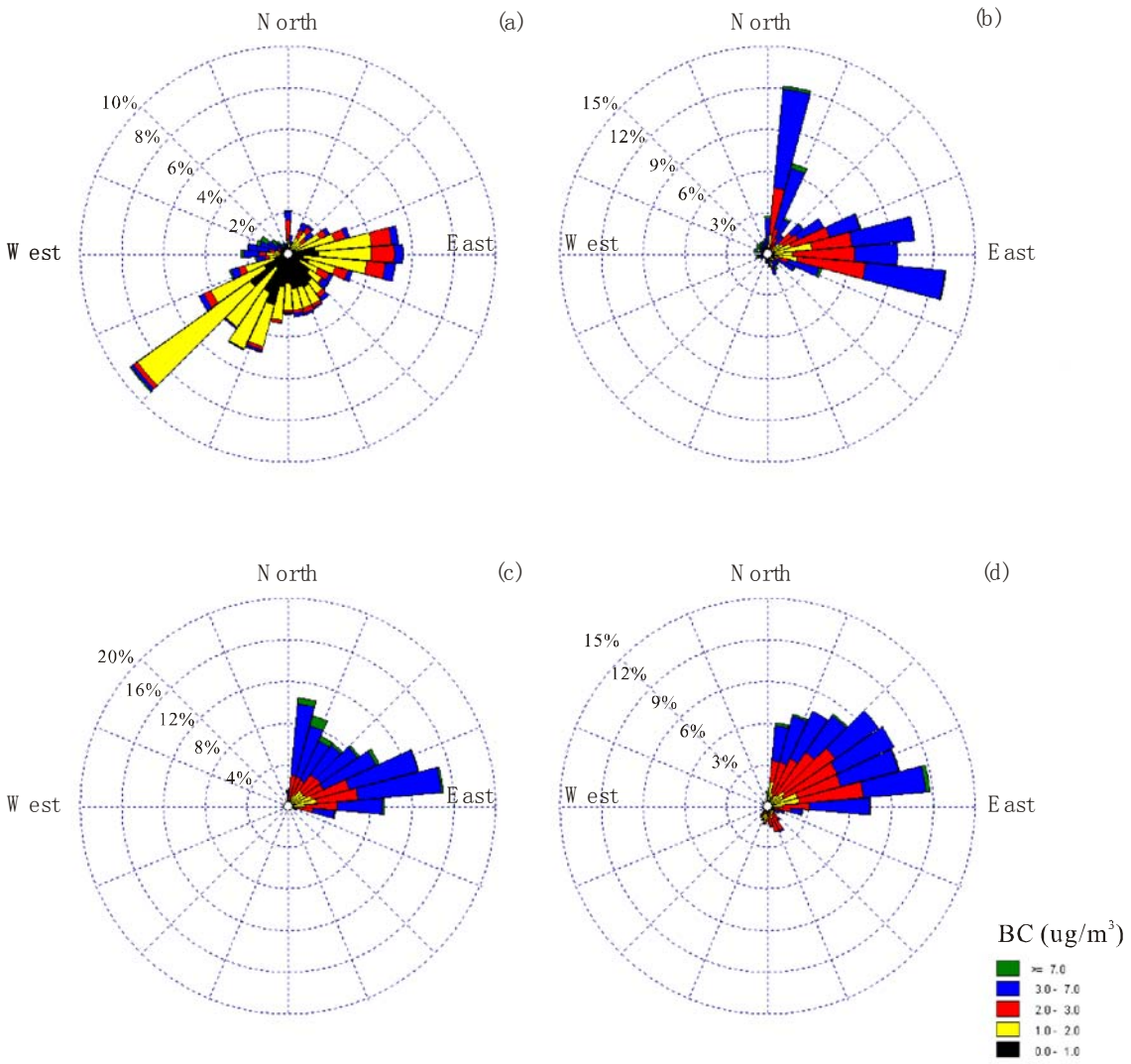

Figure 5.9 Pollution roses of hourly average BC in summer (a), fall (b), winter (c), and spring (d).

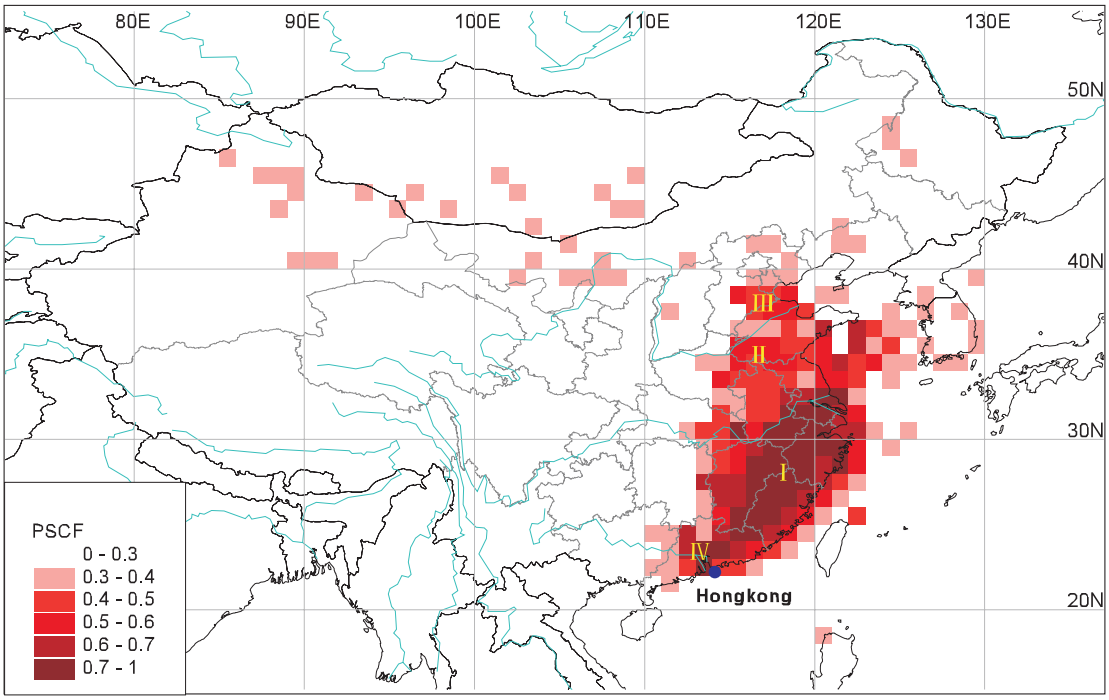

Figure 5.10 PSCF map for southward outflow of anthropogenic aerosols in 2004-2005.

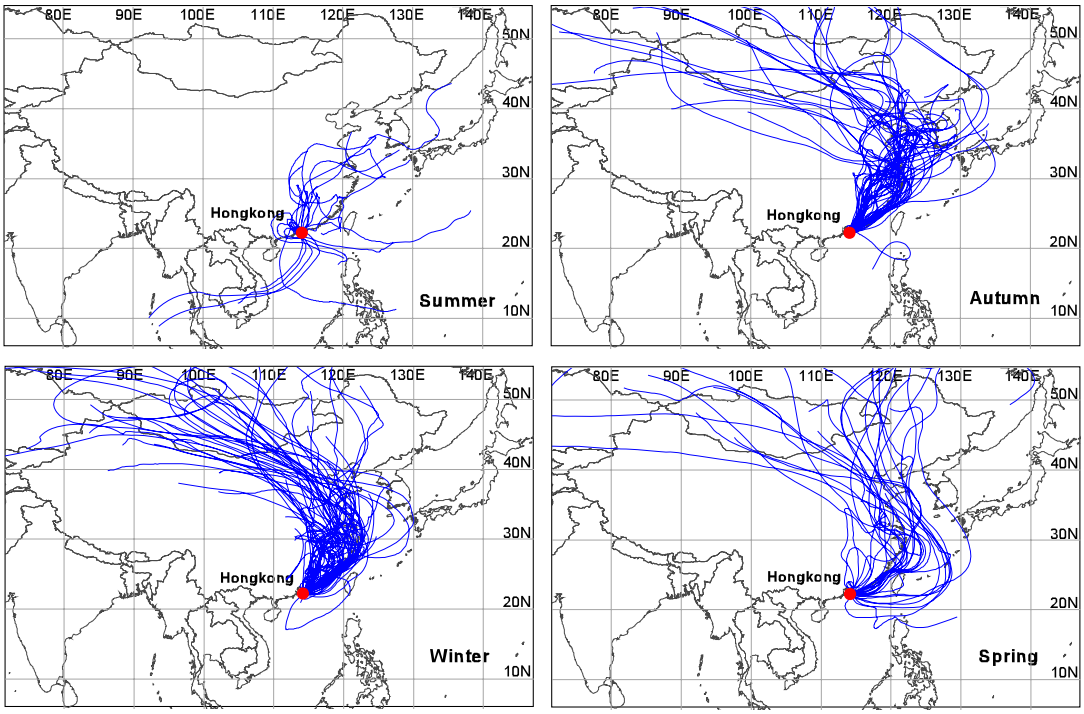

Figure 5.11 Seven-day air mass back trajectories during those days with BC concentrations exceeding the mean value in summer, fall, winter and spring.

Table 5.1 Summary statistics for the concentrations of PM, carbonaceous aerosols, and ratios during winter episode days in 2004.

Date			Episode days						
			30 Jan	14 Feb[a]	15 Feb	23 Feb	26 Feb	19 Apr	20 Apr
$PM_{1.0}$	$PM_{1.0}$	$\mu g\ m^{-3}$	80.6	85.0	71.0	74.6	70.9	77.3	59.0
	OC	$\mu g\ C\ m^{-3}$	13.5	23.3	15.4	9.5	13.4	9.4	9.6
	EC	$\mu g\ C\ m^{-3}$	11.5	22.9	9.2	10.8	15.1	14.8	11.6
	OC/EC		1.2	1.0	1.7	0.9	0.9	0.6	0.8
	$OC/PM_{1.0}$	%	16.7	27.4	21.7	12.7	18.9	12.2	16.3
	$EC/PM_{1.0}$	%	14.3	26.9	13.0	14.5	21.3	19.1	19.7
$PM_{2.5}$	$PM_{2.5}$	$\mu g\ m^{-3}$	103.7	103.1	86.5	111.4	102.3	84.8	110.8
	OC	$\mu g\ C\ m^{-3}$	23.2	35.8	21.1	21.9	30.6	13.9	22.4
	EC	$\mu g\ C\ m^{-3}$	13.9	28.6	11.5	10.9	18.7	15.0	20.3
	OC/EC		1.7	1.3	1.8	2.0	1.6	0.9	1.1
	$OC/PM_{2.5}$	%	22.4	34.7	24.4	19.7	30.0	16.3	20.2
	$EC/PM_{2.5}$	%	13.4	27.8	13.3	9.7	18.3	17.6	18.3

[a] the sample might be contaminated.

Table 5.2 Statistical summaries of 24-hr $PM_{2.5}$ and species during summer episode days (Case I) and non-episode days (Case III).

Case		$PM_{2.5}$	OC	EC	Sulfate	Nitrate	Ammonium
		ug m^{-3}					
Case I	Mean	103.9	22.3	25.2	14.5	2.0	2.9
	SD	35.6	7.1	11.7	6.5	0.7	2.4
Case II	Mean	62.8	15.0	19.4	7.0	1.1	1.3
	SD	17.9	3.9	8.8	4.4	0.5	1.3
Case III	Mean	37.9	9.9	12.8	6.5	0.8	1.0
	SD	10.8	2.5	5.9	1.9	0.2	0.8

Table 5.3 Statistical summary from hourly average BC mass concentrations from June 2004 to May 2005.

Season	n[a]	Mean	Standard Deviation	Minimum	Maximum
		(µg m^{-3})	(µg m^{-3})	(µg m^{-3})	(µg m^{-3})
Summer	2812	1.4	1.6	0.1	13.4
Fall	1464	2.9	1.8	0.1	12.1
Winter	2849	3.0	1.7	0.4	17.5
Spring	1464	2.5	1.5	0.3	13.3
Total	8589	2.4	1.8	0.1	17.5

[a] Number of hours

Chapter 6 Physical and Chemical Characteristics of Atmospheric Ultrafine Particles

6.1 Introduction

Experimental evidences in epidemiological studies (Ferin et al. 1992; Oberdörster et al. 1995; Donaldson et al. 1998; Oberdörster et al. 2001) have shown that exposures to ultrafine particles have stronger effects on health than fine and coarse particulates at equivalent masses. Several current hypotheses about the possible mechanisms for damage to the respiratory system due to ultrafine particles, as summarized in the study of Hughes et al. (1998), have been found to depend largely upon the chemical composition and size of particles. However, most of current findings and hypotheses are based on the laboratory-generated ultrafine particles, like MnO_2 and Teflon, because of the lack of details regarding the accurate compositions of ultrafine particles in the atmosphere. As a result, it is necessary to investigate the chemical composition and number concentrations of actual atmospheric ultrafine particles, in order to construct future experiments that represent ambient atmospheric ultrafine particles as accurately as possible.

Ultrafine particles are emitted from certain sources, particularly combustion sources (Hildemann et al. 1991a; Eldering and Cass, 1996), thus a typical urban roadside like the PU Supersite is an ideal location for studying ultrafine particles. New technologies, like Nano-MOUDI and SMPS, have been developed in the past decade, which makes chemical composition and number distribution of atmospheric ultrafine particles possible. The aim of this chapter is to describe a measurement program designed to measure both the chemical composition and number distribution of ultrafine particles present in polluted urban air. The chemical composition of the ultrafine particles were determined on Teflon substrates and aluminum foils that collected using combined Nano-MOUDI 115 (0.010-0.056 μm) and MOUDI 110 (0.056-2.5 μm) and the number distribution of the ultrafine particles were derived from SMPS3936 (7-217 nm) and OPC 1003 (0.1-2 μm).

6.2 Results and Discussion

6.2.1 Ultrafine particle mass concentrations and chemical constituents in summer and winter

6.2.1.1 Concentrations and composition of ultrafine particles

Table 6.1 summarizes the detailed information for each sample set collected using combined MOUDI units, including sample ID, sampling date and interval, and the

chemical analysis applied. The mean concentrations of the nano, ultrafine, and fine particles on Teflon filters were 1.3±0.8, 6.5±1.8, and 99.0±4.7 μg m^{-3} in summer and 0.7±0.1, 6.2±0.8, and 109.8± 8.2 μg m^{-3} in winter, respectively. The mass concentrations of ultrafine particles measured at PU Supersite were generally higher than that measured in other roadside and urban sites (e.g., Hughes et al. 1998; Keywood et al. 1999; Kim et al. 2002; Pakkanen et al. 2001). For example, the 4.12 μg m^{-3} for ultrafine particle measured at Downey, LA (Kim et al. 2002); the 0.5 μg m^{-3} for ultrafine particle obtained at a height of 3.5 m, at 14 m away from a road in Vallila, Helsinki (Pakkanen et al. 2001); the 1.6 μg m^{-3} on a rooftop in Pasadena, CA (Hughes et al. 1998); and the $PM_{0.15}$ concentrations of 1-4 μg m^{-3} obtained at six cities in Australia (Keywood et al. 1999).

OC and EC were the most abundant constituents in ultrafine particles among the chemical species determined in this study, with the average concentrations of 2.4±0.6 and 2.7±0.5 μg m^{-3} in summer and 2.8±0.2 μg m^{-3} and 2.7±0.5 μg m^{-3} in winter, respectively. The percentage of OC and EC in ultrafine particulate mass was ~38% and ~44% in summer and ~45% and 43% in winter. The average concentrations of sulfate and ammonium (on quartz fiber filter) were low, 0.6±0.1 and 0.4±0.1 in summer and 0.4±0.1, and 0.2±0.0 μg m^{-3} in winter. According to the concentrations,

the elements in ultrafine particles were divided into three groups: major elements, e.g., Mg, Al, Si, K, Ca, Fe; sub-major elements, e.g., Zn, Sn, Sb, Pd; and minor elements, e.g., Ti, Cu, Br, Sr, Zr, Pb. Major elements were mainly composed by crustal elements, while sub-major and minor elements were anthropogenic. About 60% of the measured particulate elements were crustal elements, followed by sub-major elements (more than 30%) and minor elements (less than 10%). The concentrations of transition metals in atmospheric aerosols are of particular interest to toxicologists because of their catalytic function on oxidative reactions. Fe was the most abundant transition metal in this study, followed by Cu and Zn, but all toxic metals measured at PU Supersite had lower concentrations than the corresponding air quality limits set by the World Health Organization (WHO, 2000).

6.2.1.2 Size-resolved aerosols and chemical composition

The size distributions of fine particle mass are shown in Figure 6.1. Two modes were found, peaking at around 0.4 μm and 1 μm, respectively. The first mode was slightly larger than the second one. The size distributions of particle mass were similar in winter and summer possibly because the stable sources of vehicle-related emissions near the sampling location over years. The size distributions of aerosol mass measured

at Pittsburgh supersite has been reported to change with the different aerosol sources (Cabada et al. 2004).

The size distributions of major components are generally similar between summer (Figure 6.2) and winter (Figure 6.3), except that the peaks are broader in winter. Most of EC mass was in accumulation mode in summer, peaking at around 0.3 μm. In addition, another minor EC peak was found in ultrafine particle size range. This small portion of EC in ultrafine size range is also observed at Downey where the sampling site is impacted primarily by relatively fresh PM emissions (Geller et al. 2002). EC in ultrafine size range often occurred as a left tail of the major peak in the accumulation mode in most studies, as shown in the results of winter in this study (Figure 6.3) and in the Caldecott Tunnel by Allen et al. (2001).

Sulfate showed a bi-modal distribution with a major peak around 0.5-0.7 μm (droplet mode) and a minor peak around 0.2 μm (condensation mode). The two modes were generally overlapping and the condensation mode appears as a ‘shoulder’ in the raw measurements in Figure 6.2 and 6.3. Measurements in suburban Hong Kong during winter of 1996 (Zhuang et al. 1999a) reported similar major peak and ‘shoulder’ with this study; meanwhile, the high concentrations of droplet mode sulfate were believed to be associated with high relative humidity and low-cloud weather conditions in

Hong Kong. Several authors (Hering and Friedlander, 1982; Wall et al. 1988; John et al. 1990; McMurry and Wilson, 1983) have reported the existence of these two modes in the size distribution of sulfate and ammonium from ambient samples. The sulfate condensation mode, peaking at ~0.2 μm, is associated with the gas phase oxidation of SO_2 and the droplet mode, peaking at ~0.7 μm, is the product of heterogeneous reactions mainly in clouds and the accumulation of material from the lower mode (Meng and Seinfeld, 1994). The similar size distributions of sulfate at roadside and suburban Hong Kong indicate the similar sources of sulfate over Hong Kong.

Ammonium size distributions were similar to those of sulfate, indicating two modes peaking at ~0.2 μm and ~0.7 μm, respectively, which is reasonable because ammonium always co-exists with sulfate in atmosphere by heterogeneous reactions as described in Chapter 5. Fine particulate ammonium originates from ammonia vapor, which reacts or condenses on an acidic particle surface and accumulates in the droplet mode. Alternatively, ammonia directly reacts with acidic gases such as sulfuric acid, forming ammonium sulfate in the condensation mode. Ammonia prefers to react with sulfuric acid or sulfate rather than nitrate and chloride in atmosphere because ammonium sulfate are most stable than other products, e.g., ammonium nitrate and ammonium chloride.

Nitrate had most of its mass in the coarse mode, while a small fraction was in the fine mode. Fine mode nitrate is formed by the homogeneous gas-phase transformation of NO_x to HNO_3, which later reacts with ammonia gas to form ammonium nitrate, or reacts with pre-existing fine particles (Seinfeld, 1986). The concentration of fine mode nitrate was low because of the high volatility of ammonium nitrate.

The size distributions of major elements are shown in Figure 6.4 and 6.5 for summer and winter measurements. It was noticed that the winter measurements seemed more representative than the summer measurements because some elements determined in summer were close to the detection limits. According to the characteristics of the size distributions, they were divided into several groups. The representative elements for each group were shown in the figures. The crustal elements and sea salts mainly present in coarse mode such as Mg, Al, Si, K, Ca, Fe, Na, and Cl. Element V and Ni had one single mode peaking at ~1.8 μm, implying they may be from the same sources, like the residual oil combustion. In a previous study conducted by Yu et al. (2004), element V and Ni were found to mainly originate from ship emissions (oil combustion) and the levels of V and Ni depended on the distance from (or relative location to) the city's container port (Yu et al. 2004a). Element Zn in the roadside atmosphere is about two times higher than in the suburban atmosphere. It is known that zinc oxide is added

as a vulcanization agent in the tire tread. The diameter of particulate ZnO was reported to be about 1 μm (Adachi and Tainosho, 2004), which agrees well with the size distribution of Zn observed in this study. This further suggests that the tire dust is the dominant source for Zn observed in this study. The size distributions of Cu and Ba are similar. They were found to mainly originate from brake dust (Adachi and Tainosho, 2004).

6.2.2 Ultrafine particle number concentrations in summer and winter

6.2.2.1 Particle number concentrations

The particle number concentrations are summarized in Table 6.2 for various size ranges, including nanoparticles (7-50 nm), ultrafine particles (7-100 nm), particles in SMPS size range (7-217 nm), and in OPC size range (100-2000 nm, accumulation mode). The values were integrated from the individually measured value for each channel. Throughout the sampling periods, the average particle number concentration was 33036±21932 cm^{-3} for nanoparticles, 39498±24846 cm^{-3} for ultrafine particles, 47150±27861 cm^{-3} for particles in SMPS sizes and 3822±2042 cm^{-3} for particles in OPC size range. Particle numbers in the ultrafine size range significantly contribute to the total particle number concentrations in the roadside environment, accounting for ~85% of total particle counts in SMPS sizes (7 nm-217 nm), while the particles in

OPC size range (accumulation mode) were less important, showing about an order of magnitude lower concentrations than ultrafine particles. The number concentrations of ultrafine particles in this study were much higher than at other roadside measurements in the urban atmosphere in U.S. (e.g., Kim et al. 2002) and Europe (e.g., Harrison et al. 1999). The high ultrafine particle number concentrations are an important potential risk for health because it is possible that the sheer number of such particles can overwhelm the alveolar macrophages, whose job it is to clear the lungs of inhaled substances.

Obviously a seasonal pattern was seen for the particle concentrations in every size range, with high concentrations in winter and low concentrations in summer (Table 6.2). The particle number concentrations in winter were about 1-2 times higher than those in the summer for nanoparticles, ultrafine particles, and particles in SMPS size range, and 2-2.5 times for particles in OPC size range. The same seasonal trend for particle number concentrations had also been reported in European cities (8-400 nm, Hussein et al. 2003; Aalto et al. 2005) and US cities (3-2000 nm, Watson et al. 2006). Moreover, Hussein et al. (2003) observed a clear annual periodic behavior of particles, which was inversely related to behavior of the temperature, through investigating the temporal variations of total particle number concentration (8-400 nm) during 1997-

2001. This indicates the dependence of particle number concentrations on meteorological parameters in the urban atmosphere, especially on ambient temperature (Bukowiecki et al. 2003; Kittelson et al. 2004).

6.2.2.2 Size distributions of particle number

Figure 6.6 presents the average size distribution of particle number in the roadside environment in winter (Figure 6.6 a) and summer (Figure 6.6 b). The results of measurement conducted independently by the SMPS and OPC instruments were presented on the same figure. The first OPC channel (100-200 nm), overlapping with the SMPS, showed good correlation with the SMPS (R=0.87 in winter and R=0.77 in summer). The absolute values of the first OPC channel in number concentration were almost the same with the SMPS in winter, while they were slightly lower than that from SMPS in summer. The low efficiency of capturing particle counts by OPC may be caused by some water-soluble inorganic species, like sulfate, which shift to a larger size under high-humidity conditions.

The overall size distributions of particle number were similar in winter and summer. The characteristics of particle size distribution can be generalized within two or three modes, which maybe present either simultaneously or not. In winter the particle number size distribution was characterized by one major peak in ultrafine mode and

one minor peak in accumulation mode, centering at 10-50 nm and 100-200 nm, respectively (Figure 6.6 a). In summer particles also had two such similar modes, but a shoulder at ~80 nm occurred in 'soot' mode (Figure 6.6 b). Among three modes, the peak area of ultrafine mode contained approximately 90% of the total particle number distribution, which indicates the ultrafine mode is a typical size range in terms of particle number for measurements at roadside sites (Kittelson, 1998; Molnár et al. 2002; Charron and Harrison, 2003; Kittelson et al. 2004).

Figure 6.7 compares size distributions of hourly averaged particle number at different time periods in a day, during which the number and proportion of diesel-fueled vehicles differ. The particle size distributions were stable over time of day in winter season, regardless of changes of diesel vehicle numbers, with one dominant peak in the ultrafine mode (Figure 6.7 a). Similar characteristics were observed in summer, but the dominant peak in ultrafine mode was broader than that in winter, especially in the early morning and late evening (Figure 6.7 b). This might be associated with the low temperature and high relative humidity during the periods, leading to part of particles increasing in radius.

6.2.2.3 The relationship among particle number, mass, volume, and surface

The size distributions for mass, volume, and surface can be calculated from the recorded number size distribution by assuming that particles are in a spherical shape with the density of 1.8 g cm^{-3}, which is a typical density for soot (Park et al. 2004). We used the density of soot because most particles in this case are in ultrafine size ranges and soot is the major species in this fraction. Figure 6.8 illustrates the overall size distributions of number, mass, volume and surface. The Gaussian fit was used to fit their distributions. It can be seen that particle mass showed substantially different distributions with particle numbers in size ranges of 7-2000 nm. Particles in the accumulation mode dominated the aerosol mass, while particles in the ultrafine mode contributed the main part of particle numbers. The size distributions of volume and surface area were similar with mass in this study. Previous investigations in an urban atmosphere (Harrison et al. 1999; Harrison et al. 2000; Kittelson et al. 2004; Stanier et al. 2004) reported similar size distributions with those in this study, either for particle number, mass, volume or surface area.

The current air quality standards for particles are expressed in terms of particle mass concentrations, either for $PM_{2.5}$ or PM_{10}. As the increasing evidences from epidemiological studies (Ferin et al. 1992; Oberdörster et al. 1995; Donaldson et al.

1998; Oberdörster et al. 2001) revealed strong relationship between ultrafine particles and health effects, it is suspected that whether the current particulate standard of $PM_{2.5}$ is able to reflect the level of particle numbers. If it is, the number concentrations of ultrafine particles also can be reduced as the eliminations of the current particulate standard. In the present study, the hourly ultrafine particle numbers by SMPS were compared to hourly $PM_{2.5}$ and PM_{10} mass concentrations by co-collocated SPM-613D using the linear regression method (Figure 6.9). It can be seen that the correlation was poor between ultrafine particle number concentrations and PM mass concentrations ($R=0.52$ for $PM_{2.5}$ and $R=0.51$ for PM_{10}) (Figure 6.9), implying no obvious effect on ultrafine particle number concentrations when $PM_{2.5}$ or PM_{10} mass concentrations are reduced. This finding was supported by several previous studies in other cities (Molnár et al. 2002; Fine et al. 2004).

Molnár et al. (2002) had reported a good correlation between accumulation mode particles (100-368 nm) and $PM_{2.5}$. Here this study has found that the correlation between accumulation mode particles (100-1000 nm) and $PM_{2.5}$, PM_{10} are also good, with the correlation coefficients of 0.86 for $PM_{2.5}$ and 0.73 for PM_{10} (Figure 6.9). Overall, the results from linear regression suggested that $PM_{2.5}$ and PM_{10} mass concentrations are dominated by particles in the accumulation mode and do not

represent the changes of ultrafine particle number concentrations. Therefore, particle mass can not be a surrogate measurement of particle number in the roadside environment.

6.2.2.4 Diurnal variations

Figure 6.7 also reveals that the particle number concentrations observed at PU Supersite are impacted significantly by the changes of traffic numbers. For example, the number concentrations of ultrafine particle were lowest during early morning (2:00) in both winter and summer (Figure 6.7), due to decreased total traffic volume in each category compared to day time. The traffic composition is another important influencing factor on particle number concentrations. It can be seen from the comparison of particle number concentrations at 11:00 and 22:00 in Figure 6.7. Although the total traffic flows were almost the same, 6000 vehicles per hour, the concentrations of ultrafine particles were much lower at 22:00 than at 11:00. This can only be explained by the differences of traffic compositions. Diesel-fueled vehicles accounted for ~48% of total traffic numbers at 11:00, while it was only ~16% at 22:00. This further enforced the previous findings (Harris and Maricq, 2001, Mathis et al. 2005) that diesel-fueled vehicles emit much more particles than other-fueled vehicles.

The average diurnal patterns of ultrafine particle numbers are examined, as shown in Figure 6.10. The variations of ultrafine particles in a day showed a close relationship with traffic density, as indicated by the elevated ultrafine particle number concentrations (>50000 cm^{-3}) in daytime. The total number of ultrafine particles normally showed about 3-5 peaks during daytime, which almost coincided with the fluctuations in BC concentrations. The evening peaks were occasionally observed due to the late traffic in the evening. The lowest particle number concentration (<30000 cm^{-3}) was observed during the early morning time (2:00-5:00) when the traffic activities were lowest, which can be considered as the background at PU Supersite.

For entire sampling periods, good correlations were obtained between hourly ultrafine particles and BC concentrations (Figure 6.11), with high correlation coefficient (R) of 0.84 in winter and 0.87 in summer. This is consistent with our previous finding from Nano-MOUDI measurements that EC is an important component in ultrafine particles. Moreover, the good agreements of ultrafine particles and BC suggested that ultrafine particles come from the same primary source with BC, namely the nearby diesel-fueled vehicle emissions on road, since BC has been demonstrated to be coming mainly from diesel-fueled vehicle exhausts in Hong Kong (HKEPD, 2005) and in other cities (Norbeck et al. 1998; Gertler et al. 2002).

The relationship of diurnal patterns of aerosol number concentrations in different size ranges also have been examined in this study, and the size ranges include particles less than 10 nm in diameter, nanoparticles, ultrafine particles, SMPS sizes (7-217 nm) and OPC 1003 sizes (100-2000 nm), and total aerosol number (7-2000 nm). Diurnal patterns of nanoparticles, ultrafine particles, SMPS sizes, and total particles were almost identical, with the highest correlation coefficients among them ($R>0.95$) during the entire sampling period. Particles of less than 10 nm in diameter also showed good correlations with nanoparticles, ultrafine particles, SMPS sizes, and total particles, with all correlation coefficients larger than 0.81. Accumulation mode particles (OPC size ranges) had the poorest relationship with other size range particles, with the correlation coefficients lower than 0.77, which is not surprising because accumulation mode particles have been previously demonstrated to relate more to particulate mass, rather than particle number.

6.2.2.5 Influencing factors on ultrafine particle number concentrations

In a roadside microenvironment, the level of pollutants in the atmosphere depends on various factors, such as the emission characteristics of sources, the changes of meteorological parameters, and traffic conditions. Multiple Linear Regression, which is a statistical method taking more than one variable into account, is often used to

model the concentrations of pollutants in the atmosphere (Van der Wal and Janssen, 2000; Cheng and Tsai, 2000). In order to identify the impact factors for ultrafine particle concentrations, the measured hourly meteorological data and vehicle counts were initially examined using stepwise multiple linear regression method, which involves modelling the ultrafine particle concentrations (y) that contains the fewest number of variables (x), while accounting for the greatest variation in the dependent variable. The initial variables included hourly traffic number of gasoline- and diesel-fueled vehicles, and hourly data of temperature, relative humidity, mixing height, wind speed, and solar radiation. Considering other minor sources that were not included in the model, the constant was configured to be larger than zero. The estimated regression coefficients shown in Table 6.3 were examined by the *t*-test. The results showed that all of *P* values were less than 0.05 at a 95% significant level. The comparison between simulated and observed particle number revealed that correlation coefficient (R) was 0.70 in winter and 0.74 in summer.

The results (Table 6.3) from the model indicated that the number of diesel-fueled vehicles was the dominant factor to the ultrafine particle concentrations in both winter and summer. This interpretation is consistent with the prior findings reported in this study and other studies (Harris and Maricq, 2001, Mathis et al. 2005). Meteorological

parameters had little impact on the ultrafine particles in winter, while mixing height was an important factor in summer, ranking second to the diesel-fueled vehicles. Moreover, the standardised regression coefficient showed that relationship between mixing height and particle number was negative. It also can be seen from Figure 6.10 that in addition to the traffic density and composition, the changing of mixing height influenced the particle number concentrations in summer. In the morning, the primary emissions from vehicle exhausts, including ultrafine particles and BC, begin to accumulate continuously in the atmosphere due to the combination of the increasing traffic flow and low mixing height (<500 m in most cases). Thus the morning peak of ultrafine particles and BC just occurred before the mixing height starts to increase rapidly. When the mixing height exceeded ~1000 m, the concentrations of ultrafine particles and BC dropped gradually due to strengthened vertical dispersion with a larger air volume. The mixing heights were usually in range of 1000-2000 m at midday and the maximum occurred at round 14:00-15:00. The absence of afternoon rush hour peak in summer might be the result of the high mixing height (~1000 m) and wind speed (>2.0 m s^{-1}), diluting the emissions.

Based on the above analysis, dilution is found to be the main process affecting particle concentrations after they are emitted in a street canyon in the present study, whereas

rate of coagulation and deposition is too slow to alter the size distribution and total particle number concentrations during this period. The same finding has been reported by previous studies (Vignati et al. 1999; Ketzel and Berkowicz, 2004; Zhang and Wexler, 2004). Zhang and Wexler (2004) claimed that exhausts near roadways usually experienced two distinct dilution stages after being emitted, namely 'tailpipe-to-road' and 'road-to-ambient'. The first stage dilution is induced by traffic-generated turbulence and the second stage dilution is mainly dependent on atmospheric turbulence. In this study, the traffic pattern was almost consistent for both winter and summer (Figure 6.10), with around 6000 vehicles per hour in daytime (7:00-22:00) and around 2000 vehicles per hour in early morning (2:00-5:00). This means the traffic-generated turbulence is probably quite similar for each day. Therefore, atmospheric turbulence, such as the changes of mixing height in a day, dominated the changes of the primary ultrafine particles.

Besides vehicular emissions, new particle growth by the nucleation process in the atmosphere is another important source of ultrafine particles in urban and rural atmospheres. A number of recent studies at both rural and urban sites around the world have reported the occurrence of nucleation events and two key features were present in those reported nucleation events (Harrison et al. 1999; Shi et al. 2001; Alam et al.

2003; Stanier et al. 2004; Zhang et al. 2005; Watson et al. 2006). Firstly it was the midday peak in nuclei mode (<10 nm) particles accompanied by the peak of solar radiation, and the other was the continuous growth of particle sizes from several nanometers to around 100 nm. In order to confirm the findings from multi-linear regression method, the evolution of particle size distributions on a typical summer day (14^{th} July) was further examined in Figure 6.12. On 14^{th} July, particles in diameter less than 100 nm had two peaks at 9:30 and 11:00, respectively (Figure 6.12). The first peak of ultrafine particle obviously formed due to the increased vehicles during morning rush hour because the solar radiation is quite low at this moment. This means they are fresh particles that were emitted directly from combustion sources or that had condensed on primary particles from cooled gases soon after emission, instead of nucleation processes in atmospheric reactions. It seemed that the nanoparticle number concentrations reached a high level at 11:00 and accompanied by the occurrence of high solar radiation value (Figure 6.10), probably indicated new particle growth by nucleation process in atmosphere. However, it is not easy to conclude whether there is new particle growth in atmosphere in this case, because the evolution of particle size distributions did not exhibit continuous growth of particle sizes, as did particle sizes in other studies (Alam et al. 2003; Stanier et al. 2004; Zhang et al. 2005), as shown in

Figure 6.12. Moreover, based on the results of multi-linear regression shown in Table 6.3, solar radiation is not important impactor on ultrafine particles. This at least demonstrated that no obvious nucleation process occurred in the atmosphere of the roadside microenvironment, or the nucleation process was too poor to be detectable. This result agreed with our expectation because the sampling location was a source-dominated site. A considerable number of fresh particles are continuously emitted into atmosphere from 7:00 to 22:00 for each day. New particle growths are less favourable in polluted urban atmospheres by nucleation, in comparison to the condensation of vapours of low volatility onto existing particles due to the high pre-existing particle surface area (Alam et al. 2003; Charron and Harrison, 2003).

6.3 Summary

The mass concentrations of ultrafine particle measured at PU Supersite were generally higher than those roadside and urban measurements in other cities. The average mass concentration of ultrafine particles was 6.5±1.8 μg cm^{-3} in summer and 6.2±0.8 μg cm^{-3} in winter. OC and EC are the largest contributors to the ultrafine particle mass. A small amount of sulfate and ammonium is also presented in these particles. Crustal elements are the most prominent metals found in the ultrafine particles, including Mg,

Al, Si, K, Ca, and Fe. These data may assist the health effects research community in constructing realistic animal or human exposure studies involving ultrafine particles.

Although the particulate mass concentrations contributed by ultrafine particles are small by comparison to the air quality standards like $PM_{2.5}$ and PM_{10}, ultrafine particle number concentrations are very large. During the entire sampling period, ultrafine particles were found to be the dominant proportion in the roadside environment, accounting for ~85% of the total particle counts (7-217 nm) and about one order of magnitude higher than particles in accumulation mode (0.1-2.0 μm). Moreover, the number concentration of ultrafine particles measured at PU Supersite was much higher than those roadside and urban measurements in other cities. Current air quality standards are based on the PM mass concentrations, which can not be a surrogate measurement of particle number because the mass concentration of PM_{10}, even $PM_{2.5}$, is dominated by accumulation mode particles rather than ultrafine particles.

Ultrafine particles mainly originate from vehicle exhausts, especially diesel-fueled vehicles, which is supported by good correlations between hourly ultrafine particle number concentrations and BC concentrations (R=0.84 in winter and R=0.87 in summer) and the typical size distributions of ultrafine particles from combustion sources. Both ultrafine particles and BC showed the same diurnal patterns, with high

loading when the traffic density is high and low loading when the traffic density is low. Mixing height is another influencing factor on untrafine particle number concentrations, especially in summer, showing inverse relationship with particle number concentrations. The possibility worth considering is that new ultrafine particle formed by nucleation process in the atmosphere can be ignored at PU Supersite site.

The particle numbers had one dominant peak in the ultrafine mode, which represents the typical size distribution of combustion. The aerosols and most of the chemical components showed similar size distributions in winter and summer, which is possibly because the sampling location is quite close to the primary source of vehicle emissions. The size distribution of particulate mass showed two modes peaked at around 0.4 μm and 1 μm, respectively. Most of EC mass concentrations were in the accumulation mode, which is a typical size range for particles formed from combustion processes. Sulfate and ammonium showed a bi-modal distribution with a major peak around 0.7 μm (droplet mode) and a minor peak around 0.2 μm (condensation mode). Coarse mode nitrate was the dominant species, while fine mode nitrate was low in concentrations due to its characteristics of volatilization. The crustal elements and sea salts mainly present in coarse mode such as Mg, Al, Si, K, Ca, Fe, Na, and Cl. V and Ni had one single mode peaking at ~1.8 μm, implying they are from the same source

of ship emissions. The size distributions of Cu, Ba, and Zn are similar. They originate from break and tire dust. Since most chemical species present in size range larger than 0.1 μm, the mass of ultrafine particles seemed less important than larger particles.

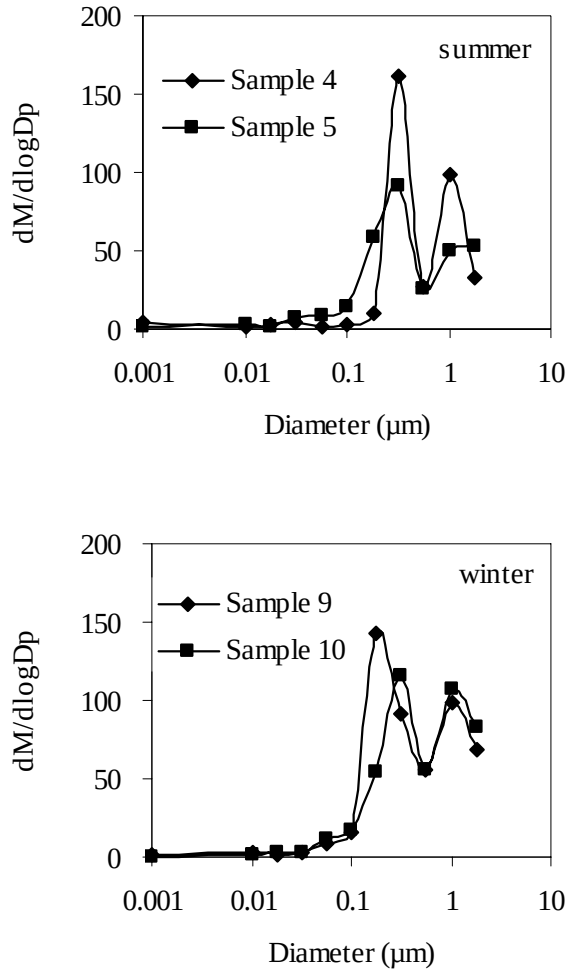

Figure 6.1 Size distribution of particulate mass (Teflon) in summer (Sample 4 and 5) and winter (Sample 9 and 10).

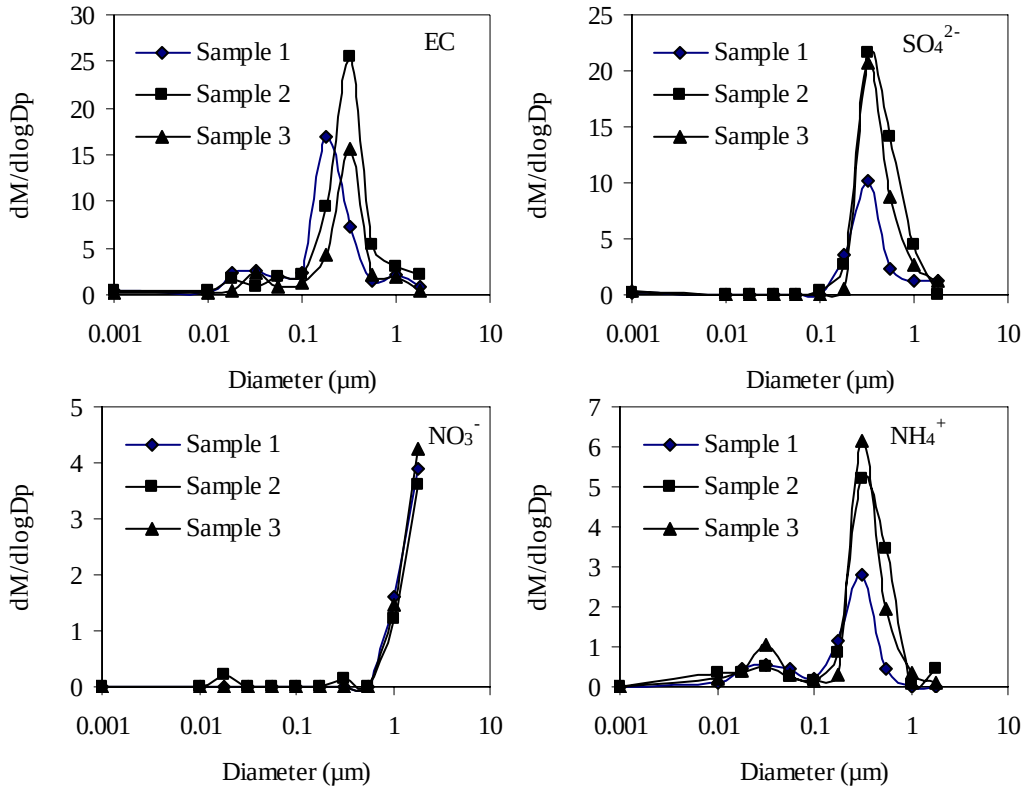

Figure 6.2 Size distributions of major chemical species, from the aluminum filters, in summer.

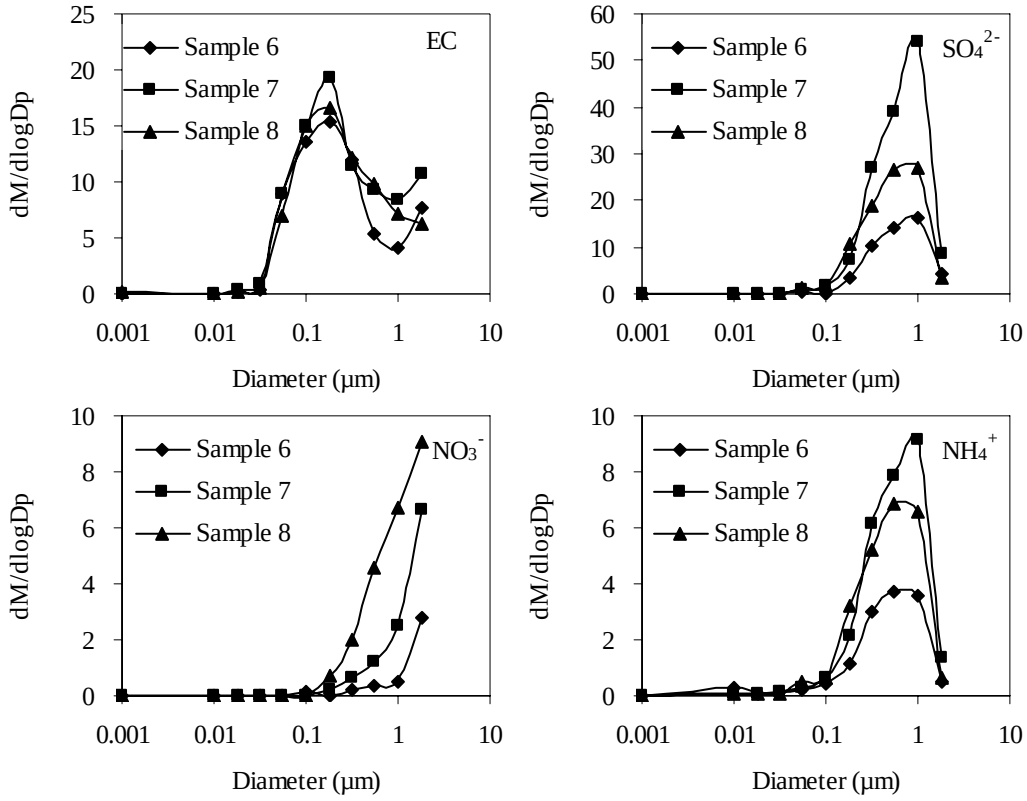

Figure 6.3 Size distributions of major chemical species, from the aluminum filters, in winter.

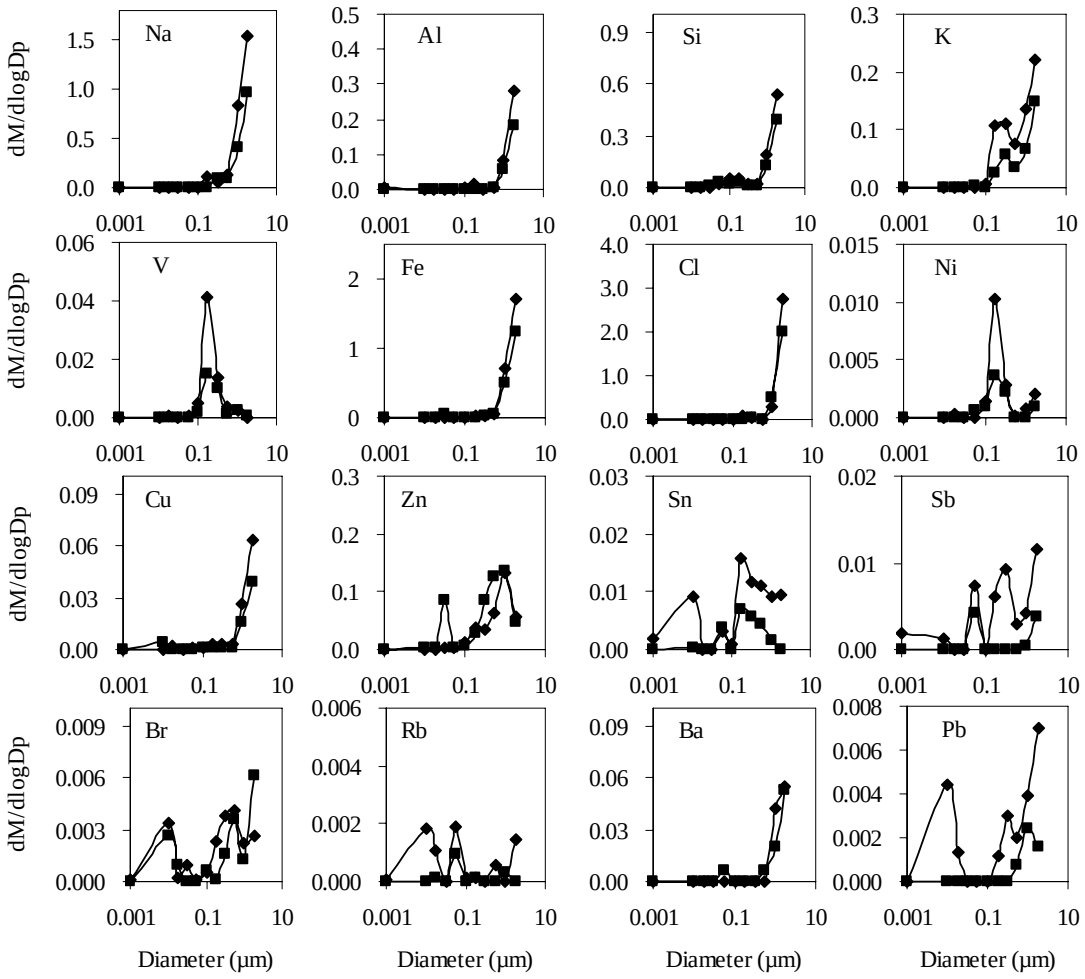

Figure 6.4 Size distributions of metals, from the Teflon substrates, in summer (Sample 4 and 5).

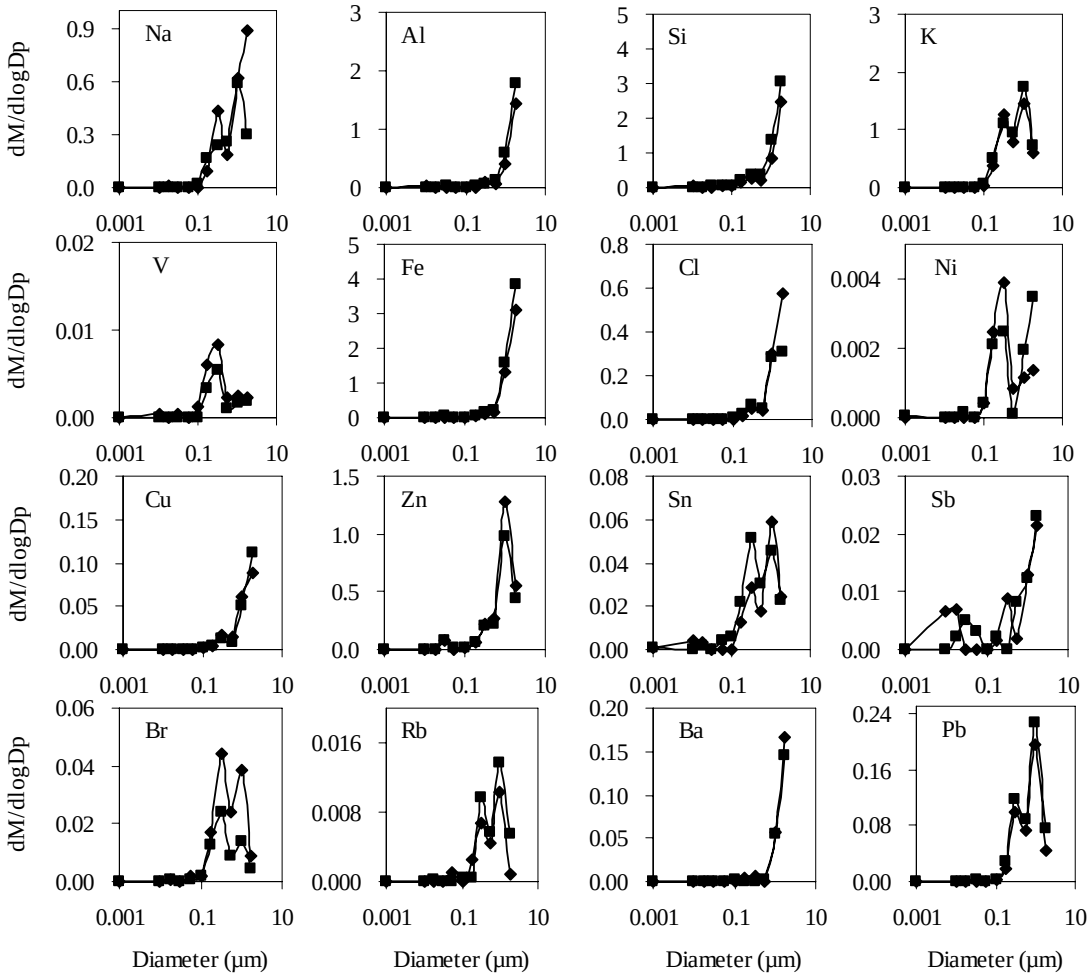

Figure 6.5 Size distributions of metals, from the Teflon substrates, in winter (Sample 9 and 10).

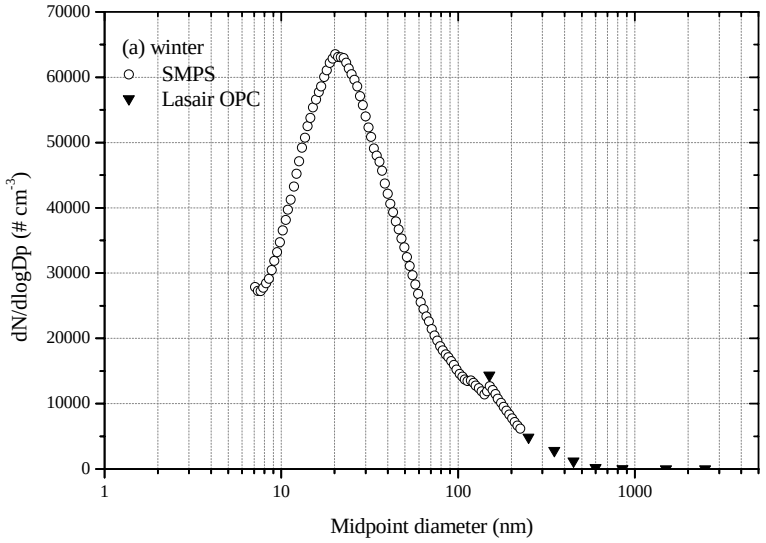

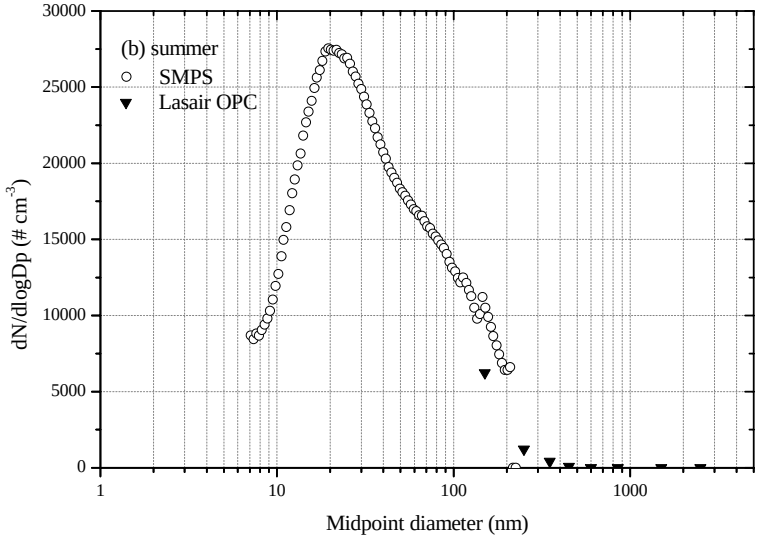

Figure 6.6 The typical size distributions of particle number (7-2000 nm) at roadside in winter (a) and in summer (b).

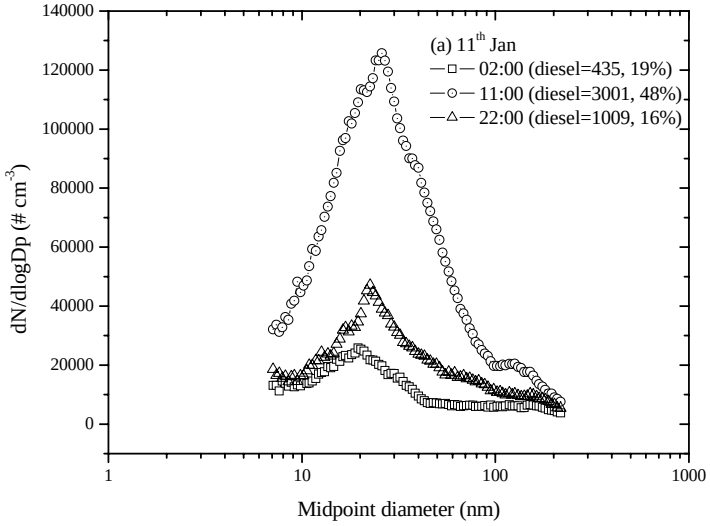

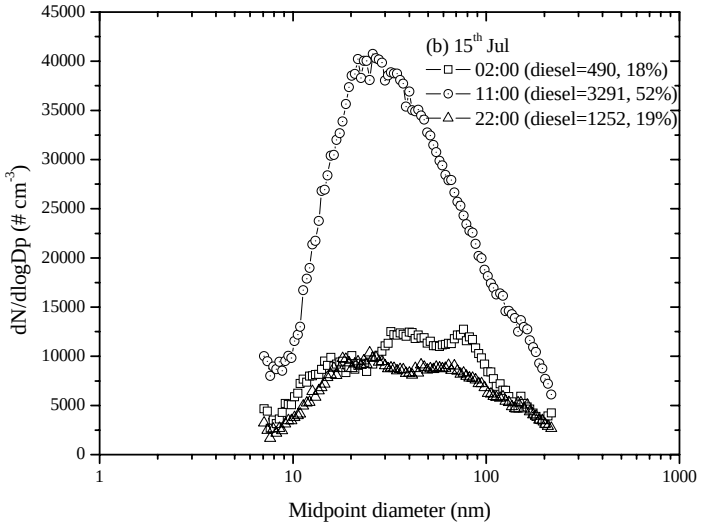

Figure 6.7 The size distributions of fine particles during different time period on 11th Jan and 15th Jul.

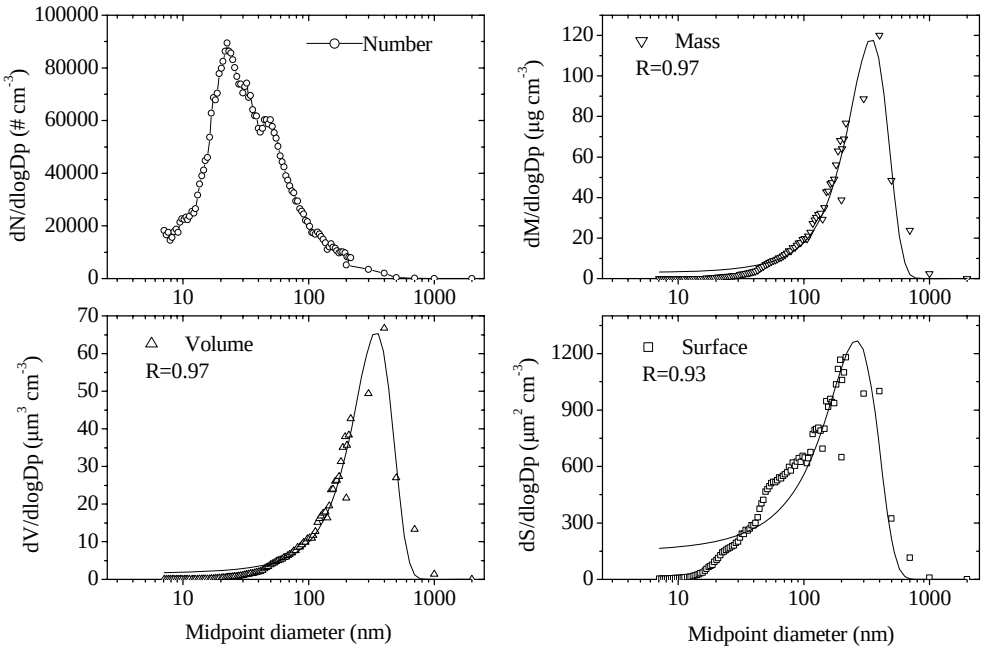

Figure 6.8 The typical size distributions for particle number, mass, volume and surface in roadside environment (16:00 on 20th Jan 2005). A Gaussian fit was used to fit the size distribution of mass, volume, and surface.

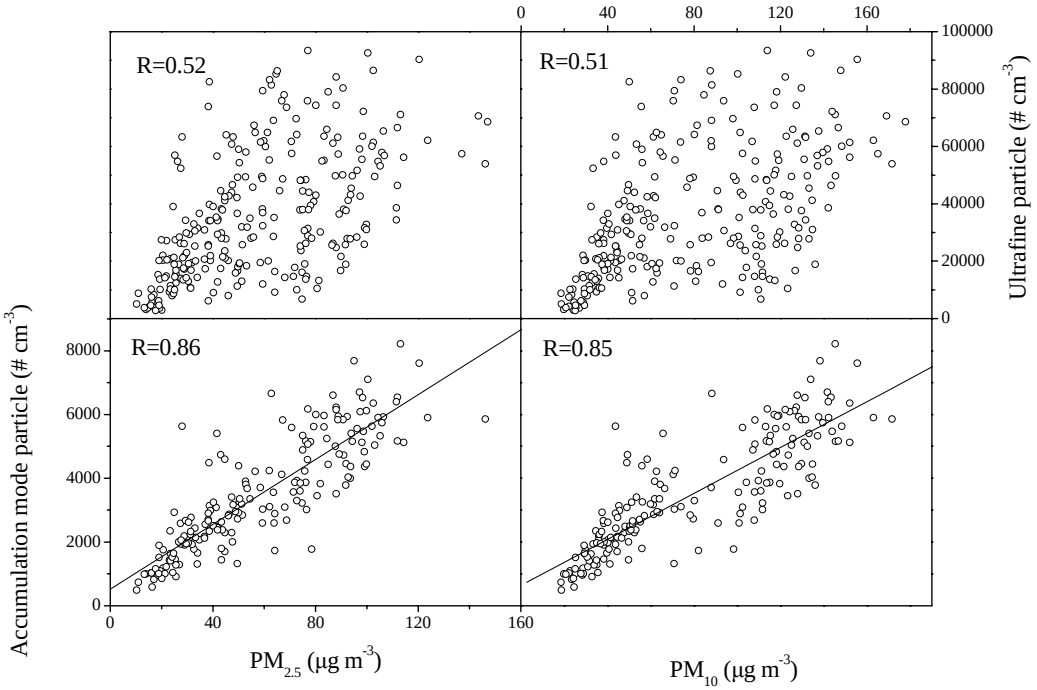

Figure 6.9 The relationship between ultrafine particle number concentrations and $PM_{2.5}$&PM_{10}, as well as the relationship between accumulation mode particle number concentrations and $PM_{2.5}$&PM_{10}.

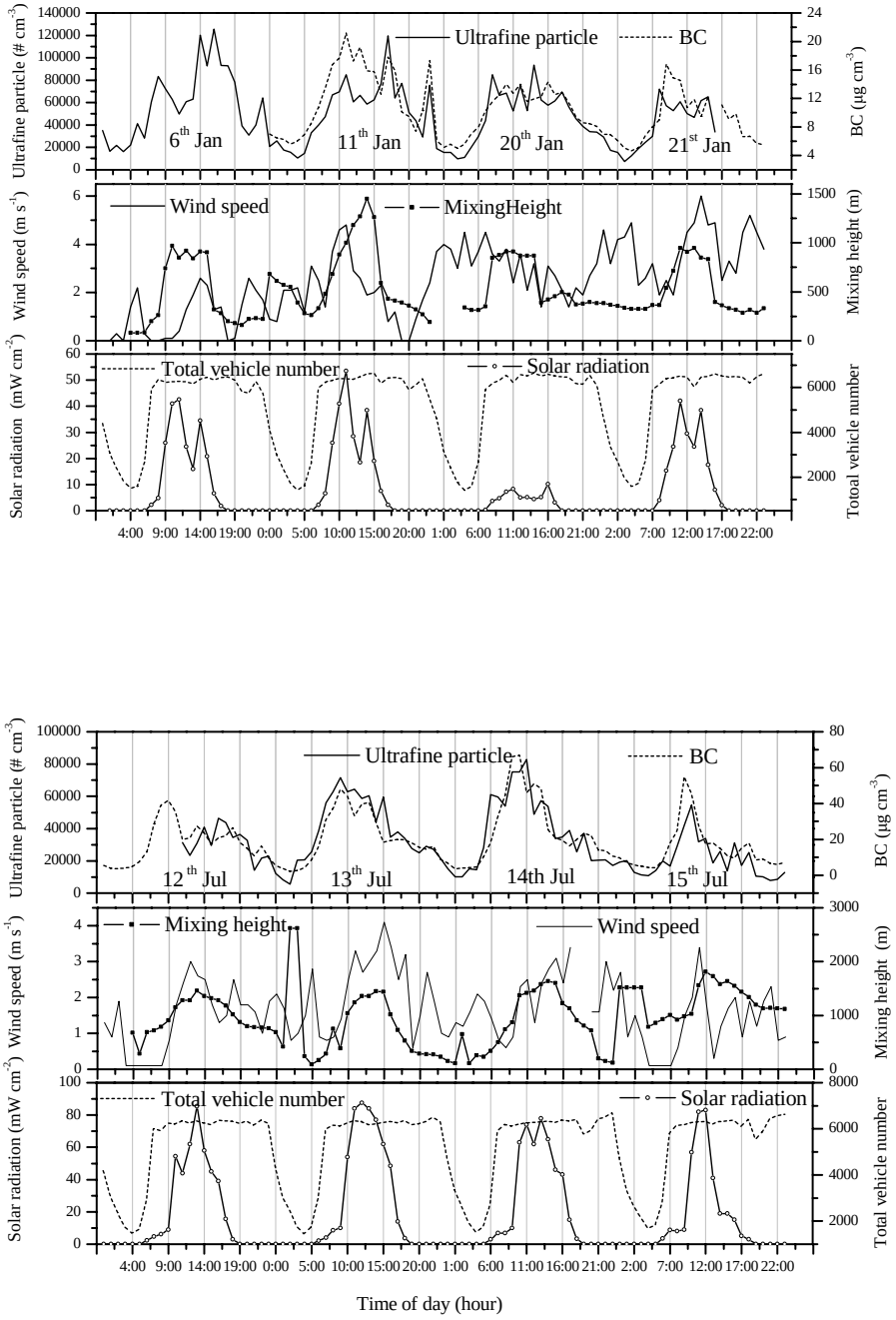

Figure 6.10 The diurnal patterns of ultrafine particle, BC, total traffic number and meteorological parameters.

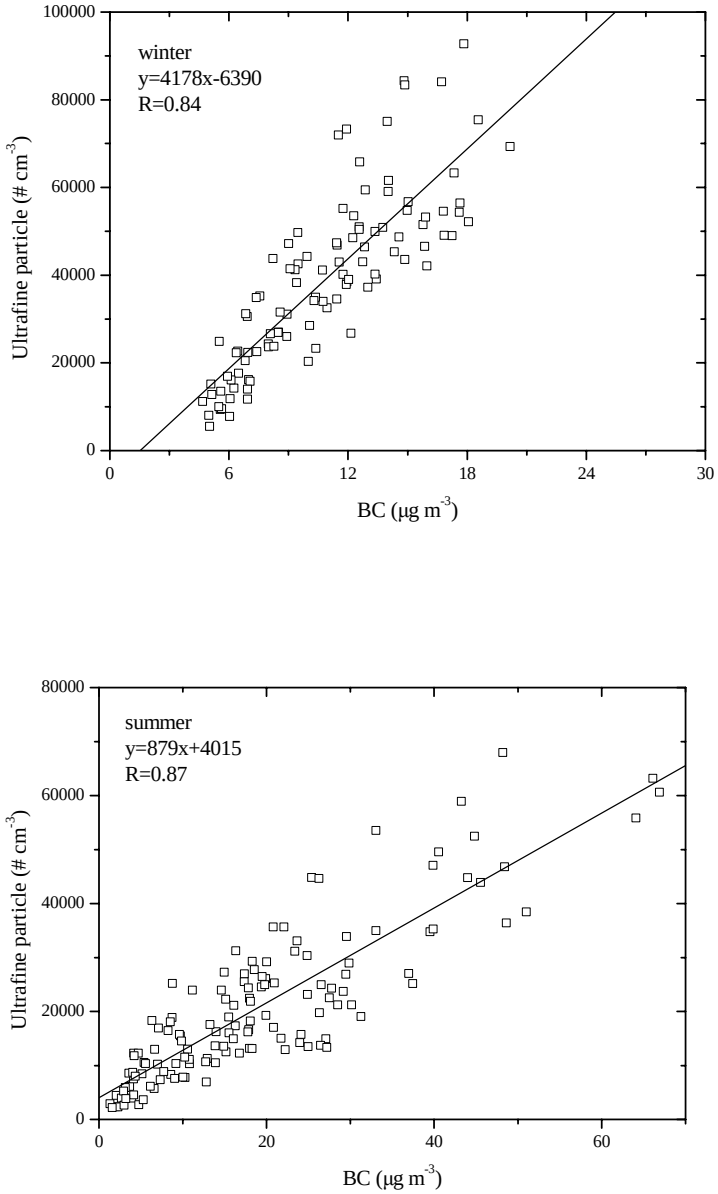

Figure 6.11 Relationships between ultrafine particles and BC in winter and summer.

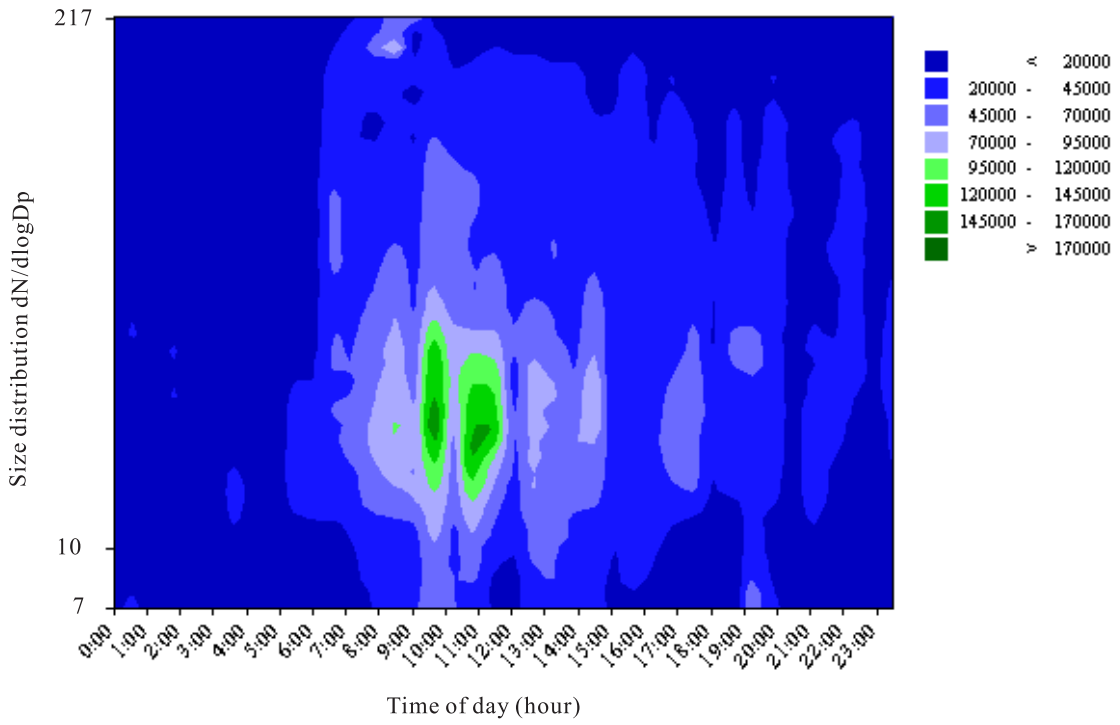

Figure 6.12 Evolution of ultrafine particle size distribution in a typical day.

Table 6.1 Sampling information for particulate mass size distribution.

Sample ID	Starting data	Starting time	Sampling interval (hr)	Filter	Analyses
Sample 1	14-Jul-05	10:00	72	quartz fiber	EC, Ions
Sample 2	20-Jul-05	10:00	72	quartz fiber	EC, Ions
Sample 3	26-Jul-05	10:00	72	quartz fiber	EC, Ions
Sample 4	3-Jun-05	10:00	72	Teflon	Mass, elements
Sample 5	29-Jun-05	10:00	72	Teflon	Mass, elements
Sample 6	15-Nov-05	10:00	72	quartz fiber	EC, Ions
Sample 7	21-Nov-05	10:00	72	quartz fiber	EC, Ions
Sample 8	11-Jan-06	10:00	72	quartz fiber	EC, Ions
Sample 9	7-Dec-05	10:00	72	Teflon	Mass, elements
Sample 10	14-Dec-05	10:00	72	Teflon	Mass, elements

Table 6.2 Statistical summary for particle number concentrations in various size ranges.

Season	Size range		Particle concentration (# cm^{-3})			
			Average	Standard deviation	Minima	Maxima
winter	Nanoparticles	(7-50 nm)	40 426	23 192	2806	118 668
	Ultrafine particles	(7-100 nm)	47 043	26 309	3720	126 246
	SMPS size range	(7-217 nm)	55 050	28 784	6326	143 547
	Lasair size range (Accumulation mode)	(100-2000 nm)	5316	1823	1956	12 090
summer	Nanoparticles	(7-50 nm)	23 049	15 228	1245	85 630
	Ultrafine particles	(7-100 nm)	29 302	18 357	1659	98 852
	SMPS size range	(7-217 nm)	37 182	23 119	2887	139 350
	Lasair size range (Accumulation mode)	(100-2000 nm)	2505	1104	478	6661

Table 6.3 Regression results from stepwise multiple linear regressions of ultrafine particles in winter (a) and summer (b).

Parameter	Standardized regression coefficient	Estimated regression coefficient	Estimated standard deviation	t^a	*P* value
(a) winter: regression coefficient R is 0.70 (n=77)					
(Constant)		b_0=12368.94	5323.71	2.32	0.02
Diesel-fueled vehicle (number)	0.70	b_1=21.06	2.46	8.56	0.00
Ultrafine particle mass concentration=b_0+b_1*[Number of diesel-fueled vehicle]					
(b) summer: regression coefficient R is 0.74 (n=76)					
(Constant)		b_0=9737.30	3748.86	2.60	0.01
Diesel-fueled vehicle (number)	1.10	b_1=22.64	2.57	8.81	0.00
Mixing height (m)	-0.60	b_2=-24.16	5.00	-4.83	0.00
Ultrafine particle mass concentration=b_0+b_1*[Number of Diesel-fueled vehicle]+b_2*[Mixing height]					

[a] Significant level of $t_{critical}$ is 95%

Chapter 7 Comparisons of $PM_{2.5}$ at Tunnel, Roadside, and Ambient Sites

7.1 Introduction

In order to obtain the accurate characterization of primary vehicle emissions and to evaluate the contributions of different vehicle categories, tunnel studies (e.g., Moeckli et al. 1996; Pierson et al. 1996; Weingartner et al. 1997; Fraser et al. 1998; Allen et al. 2001; Gillies et al. 2001; Schmid et al. 2001; Gertler et al. 2002; Jamriska et al. 2004; Lough et al. 2005) are commonly conducted, by measuring the pollutant concentrations simultaneously at the entrance and exit of a tunnel as well as monitoring traffic counts, vehicle speed, temperature, wind speed, and pressure in the tunnel. This method is believed to result in representative PM emission factor (or emission rate) for the on-road vehicles since individual vehicles by traditional dynamometer method have diverse emission profiles and cannot be representative of a specific fleet (Jamriska et al. 2004). On the other side, the resultant chemical profile for vehicles, based on the tunnel study, can serve as one important input to the CMB receptor model.

Although the emission factors from vehicles are fundamental parameters for

establishing the source profiles and emission inventories in a specific city, the information, based on real-world particulate emissions, is still unavailable in Hong Kong. All previous studies only include the emission factors from individual vehicles with particular emission characteristics, and the model-generated emission inventory as well.

In the present study, the one/two-hour $PM_{2.5}$ measurements are conducted in an urban highway tunnel, the Shing Mun Tunnel. A total of 16 runs were made during varying times that encompassed different traffic fractions of diesel-fueled vehicles. During the study, a total of 27310 vehicles traversed the tunnel, comprising approximately 50% diesel-fueled vehicles, 41% gasoline-fueled vehicles, and 9% LPG-vehicles.

The major aim of the tunnel study in the Shing Mun Tunnel was to determine the emission factors of $PM_{2.5}$ and its chemical compositions for vehicles; to evaluate the contributions of different vehicle types to the city pollution; and to obtain the typical source profile for vehicles that is significant for the source apportionment at PU Supersite. Besides the measurements in the tunnel, $PM_{2.5}$ was also collected at three roadside sites and one ambient site using the same sampling method as the tunnel measurement. Gravimetric and chemical analyses were performed. The results at each sampling station were compared, in order to understand how the vehicle exhausts

changed at roadside and urban environment as a major urban-scale plume.

7.2 Results and discussion

7.2.1 Emission factors for on-road vehicles

7.2.1.1 $PM_{2.5}$ emission factors for mixed vehicles

The measurements in the Shing Mun Tunnel have been conducted according to the method description in Chapter 3. The detailed sampling information can be found in Table 3.2. The emission factors were calculated based on the equation 3.4. The average $PM_{2.5}$ emission factor derived from the DRI sampler was 0.131±0.037 g veh^{-1} km^{-1}, ranging from 0.066 g veh^{-1} km^{-1} to 0.190 g veh^{-1} km^{-1} (Table 7.1). The seasonal difference of $PM_{2.5}$ was examined by *t*-tests. The result (*p*-values is larger than 0.05, *t*-test) showed that no statistical significance exists for $PM_{2.5}$. High $PM_{2.5}$ emission factors were found for samples taken during the time periods of 11:00-13:00 and 14:00-1600, which as mentioned in Chapter 3, recorded a high proportion of diesel-fueled vehicles. For the 4 runs (Run 6, 11, 12, 16) during 11:00-13:00 and 14:00-16:00, the average emission factor was the highest (0.173±0.019 g veh^{-1} km^{-1}). During rush hours (Run 1, 2, 3, 4, 5, 8, 9, 10, 14, and 15), the average emission factor was 0.126±0.033 g veh^{-1} km^{-1}. For the 2 runs (Run 7 and 13) in the evening, the average emission factor was the lowest, 0.090±0.034 g veh^{-1} km^{-1}, almost two times lower than

that for time periods of 11:00-13:00 and 14:00-16:00.

Comparisons of mean $PM_{2.5}$ emission factors for the present study and other recent tunnel studies conducted elsewhere are shown in Table 7.2. The mean $PM_{2.5}$ emissions for mixed on-road vehicles was the highest in the Shing Mun Tunnel, Hong Kong, followed by Tuscarora Tunnel, USA (Gertler et al. 2002), Sepulveda Tunnel, USA (Gillies et al. 2001), Kaisermuhlen Tunnel, Austria (Laschober et al. 2004), and Howell Tunnel, USA (Lough et al. 2005). The Tuscarora Tunnel (Gertler et al. 2002) has similar characteristics to the Shing Mun Tunnel, about 1.6 km in length and is relatively flat (an upgrade of 0.3% toward the middle from either end). The proportion of heavy-duty vehicles (or diesel-fueled vehicles) ranged from 11.6% to 86.5% during the sampling periods and the traffic speed was relatively constant. The average model year of traversing vehicles was 1991-1995, which is young, compared to the model year of most on-road vehicles in Hong Kong. This may partly explain the low $PM_{2.5}$ emissions in the Tuscarora Tunnel. For the other three tunnel studies mentioned above, the most important difference is the lower proportion of diesel-fueled vehicles: about 2.6% for Sepulveda Tunnel; 14.8% for Kaisermuhlen Tunnel; and 1.5-9.4% for Howell Tunnel. The low proportion of diesel-fueled vehicles in these tunnel studies may lead to low PM emissions.

7.2.1.2 Emission Factors of individual chemical species for mixed vehicles

Table 7.3 shows the emission factors of individual chemical species in $PM_{2.5}$ emissions. The chemical profiles of $PM_{2.5}$ from vehicles are illustrated in Figure 7.1. More than half of the $PM_{2.5}$ emissions were from the elemental carbon (65.819±18.429 mg veh^{-1} km^{-1}) and about one third were from the organic carbon fraction (35.685±11.727 mg veh^{-1} km^{-1}). The third most prominent species was sulfate, which accounted for 5.6±2.2% of the $PM_{2.5}$ emission, followed by ammonium (2.3±0.9%) and iron (1.0±1.3%). Typical crustal elements, including Mg, Al, K, Si, Ca, Ti and Mn, accounted for 2.2±0.7% of the $PM_{2.5}$ emissions. Inorganic ions (chloride, nitrate, and sodium), except for sulfate, ammonium, and potassium, contributed 1.5±0.4%, and the remaining trace elements and unidentified material made up 9.9±2.3% of the total $PM_{2.5}$ emissions. The seasonal difference was not significant statistically for $PM_{2.5}$ and its chemically speciated compositions (all of *p*-values are larger than 0.05, *t*-test).

Figure 7.2 shows the correlations of measured $PM_{2.5}$ emission factors and the sum of emission factors of individual species during 16 runs. On average, the composite sum was 10-20% lower than the emission factors derived from the Teflon filter. A similar result has been obtained by other researchers (Norbeck et al. 1998). This is due to the

fact that not all the species that contribute to the particle composition are measured (Norbeck et al. 1998), like oxygen, hydrogen, and sulfur from organic matter.

7.2.1.3 Annual emission flux of $PM_{2.5}$

In the present study, the annual vehicle-related $PM_{2.5}$ emission flux (1466.0±414.1 tonnes) during 2003 was roughly estimated as a product of average $PM_{2.5}$ emission factor (0.131±0.037 g veh^{-1} km^{-1}) and the total road travel distance in Hong Kong, 30.35 million vehicle kilometers per day (The Annual Traffic Census, 2003). This $PM_{2.5}$ emission flux was ~70% of PM_{10} as calculated by HKEPD using simulation method. The ratio is consistent with typical $PM_{2.5}/PM_{10}$ ratios at Hong Kong roadside environment, as shown in Chapter 4. This result further confirms the validation of measurement in the present study.

It should be noted that the tunnel measurements in this study are representative of 'normal' driving conditions, i.e. the vehicles were running in hot stable conditions and at relatively constant speeds on a nearly flat road. However, Hong Kong has a significant variation in terrain ranging from sea level to an elevation of several hundred meters or higher. The emissions from vehicles would therefore fluctuate with the variable speed, acceleration or deceleration in variable terrain outside the Shing Mun Tunnel. Therefore the estimated annual emission flux of $PM_{2.5}$ in the present

study can only provide a general guide with a relatively high degree of uncertainty.

7.2.1.4 Evaluation of particulate emissions from diesel- and gasoline-fueled vehicles

Regression analysis (Figure 7.3 a) was used to evaluate the $PM_{2.5}$ emission factors for diesel- and non-diesel-fueled vehicles. The emissions from non-diesel-fueled vehicles were assumed to represent those from gasoline-fueled vehicles since the LPG-taxis contribute little to particulate pollutions. The uncertainties estimate for the emission factors were determined from the regression statistics. The estimated $PM_{2.5}$ emission factor for diesel-fueled vehicles was 0.257±0.031 g veh^{-1} km^{-1}, which is similar to the results of Jamriska et al. (2004) in Woolloongabba Tunnel, Brisbane (Table 7.2). Allen et al. (2001) and Gertler et al. (2002) reported the $PM_{2.5}$ emission factor of 0.430±0.079 g veh^{-1} km^{-1} in Caldecott Tunnel, San Francisco Bay and 0.135±0.018 g veh^{-1} km^{-1} in Tuscarora Tunnel, respectively. Dynamometer studies usually show considerably higher values than tunnel study measurements. For example, the $PM_{2.5}$ emissions reported by Norbeck et al. (1998) and Lowenthal et al. (1994) exceeded the values in the present study by a factor of 1-3.

The emissions of individual species for diesel-fueled vehicles, estimated using the same method to mass, are listed in Table 7.4. The average organic carbon and elemental carbon emission factors for diesel-fueled vehicles was 67.873±10.192 mg

veh^{-1} km^{-1} and 130.955±14.410 mg veh^{-1} km^{-1}(see Figures 7.3 b and c for regression plots of OC and EC), which are comparable with Gertler et al. (2002)'s study in Tuscarora Mountain Tunnel, taking into consideration the high uncertainty in tunnel study. Carbonaceous aerosols comprised the largest fraction (77.5±9.7%) of $PM_{2.5}$ emissions from diesel-fueled vehicles. The previous reported proportion of carbonaceous aerosols (Norbeck et al. 1998; Lowenthal et al. 1994; Allen et al. 2001; Gertler et al. 2002) ranged from 71% (Norbeck et al. 1998) to 99.8% (Allen et al. 2001) for diesel-fueled vehicles. The chemical profiles of $PM_{2.5}$ from diesel-fueled vehicles are illustrated in Figure 7.4. The reconstructed mass emissions for diesel-fueled vehicles comprised 54.6±5.7% EC, 28.3±4.4% OC, and 9.1±2.8% sulfate. The other inorganic ions and elements made up 8.0±1.9% of total emissions. This chemical profile is similar to the results of the dynamometer studies by Kirchstetter et al. (1999) and Lowenthal et al. (1994). Hildemann et al. (1991) reported the 'best' case in terms of EC emissions through investigating two late model and low-mileage diesel-fueled vehicles, with results of about 41% EC and 39% OC for the fine aerosols. The percentage of EC was found to increase with increasing age of diesel vehicles (Hildemann et al. 1991).

It was noticed that sulfate accounted for a higher proportion in emissions of diesel-

fueled vehicles in the Shing Mun Tunnel study than studies in USA (Norbeck et al., 1998; Gertler et al., 2002). One of the most important reasons is the different sulfur content in diesel fuels because sulfate is emitted in direct proportion to the amount of sulfur in diesel fuel. In Hong Kong, the maximum sulfur content of 500 ppm was reduced to 50 ppm, commonly referred to as "low sulfur (LS)" diesel, since 2002. However, except for local vehicles, a number of goods vehicles from mainland, China also use the Shing Mun Tunnel. In China, the maximum sulfur content for Motor Vehicle Diesel is 2000 ppm, which is much higher than that in Hong Kong and USA.

The emission factors and chemical profile for gasoline-fueled vehicles showed distinctive differences with those for diesel-fueled vehicles (Table 7.5). The $PM_{2.5}$ emission factor for gasoline-fueled vehicles were 0.017±0.028 g veh^{-1} km^{-1}, which is about 15-fold lower than the estimated $PM_{2.5}$ emission factor for diesel-fueled vehicles. Elemental and organic carbon were the primary constituents for the emission of gasoline-fueled vehicles. On average, organic carbon composed a larger fraction of the total carbon, while elemental carbon represented the larger fraction of the total carbon for the diesel vehicles. The average percentage carbon breakdown was 62.0±67.4% organic carbon and 23.4±96.9% elemental carbon for the gasoline-fueled vehicles. Inorganic species, including ions and trace elements, composed an average of

12.1±18.7% of the total particulate composition. The most prominent inorganic species included ammonium, Na, Cl, P, Ba and Mg for gasoline vehicles. There was considerable variability for OC emission factors resulted from the three studies listed in Table 7.5, however, the EC emission factors were closely similar.

7.2.2 The comparisons of fine particulate matter ($PM_{2.5}$) at tunnel, roadside, and ambient sites

7.2.2.1 The $PM_{2.5}$ mass concentrations at tunnel

The average $PM_{2.5}$ mass concentration by DRI particulate sampler in the Shing Mun Tunnel, including the entrance and exit, was 229.1±90.1 μg m^{-3}. No significant seasonal variations were observed, with an average $PM_{2.5}$ mass of 204.2±75.1 μg m^{-3} in summer and 237.4±94.5 μg m^{-3} in winter. The average $PM_{2.5}$ concentration given by DustTrak after correction by the calculated factors was 157.3±90.2 μg m^{-3} at the tunnel entrance and 260.0±136.4 μg m^{-3} at the exit. This is comparable with the average $PM_{2.5}$ concentration using the DRI sampler, 172.7±45.1 μg m^{-3} and 285.4±89.2 μg m^{-3} for the entrance and exit, respectively.

Figure 7.5 shows the average diurnal variation of hourly average $PM_{2.5}$ mass concentrations collected using DustTrak at the tunnel entrance and exit, along with corresponding traffic counts of gasoline- and diesel-fueled vehicles. Both $PM_{2.5}$ curves

displayed distinct diurnal variation, with high values during the day and low values in the early morning. Low values in the early morning at the entrance and exit correspond well to the low traffic density during those time periods. During the day, $PM_{2.5}$ concentrations increased gradually starting from 5:00 due to increased morning traffic density. The diurnal patterns of $PM_{2.5}$ concentrations had a close relationship with the daily cycle of diesel-fueled vehicles, with a correlation coefficient (R) of 0.85 at the entrance and 0.70 at the exit, which is higher than the correlation coefficient of $PM_{2.5}$ and gasoline-fueled vehicles, with a correlation coefficient of 0.77 and 0.56 for the exit and entrance, respectively.

7.2.2.2 Aerosol mass and chemical composition in different environments

Except for tunnel measurements, the $PM_{2.5}$ samples were also collected at three roadside sites, including PU Supersite, MK, LMC, and one TW ambient station as part of the entire tunnel study. The sampling method and instruments were the same during the study. The sampling interval was two hours at roadside and six hours at TW. The average $PM_{2.5}$ mass concentrations are shown in Table 7.6. In terms of mass concentration levels and assigning the sites in descending order with site characteristics, it is observed that tunnel>roadside> ambient. The Shing Mun Tunnel south bore (the present study) had the highest $PM_{2.5}$ mass concentration (229.1±90.1

μg m^{-3}). The increase in the $PM_{2.5}$ emissions, at roadside environments, seemed to correlate with the increase in the percentage of passing diesel-fueled vehicles. For example, the percentage of diesel-fueled vehicles was ~90%, ~51%, and ~38% at LMC, MK, and PU roadside; the corresponding $PM_{2.5}$ mass concentration was 129.0±94.8, 69.3±11.9, 66.9±12.3 μg m^{-3}. The $PM_{2.5}$ level (49.3±17.5 μg m^{-3}) was lowest in an ambient atmosphere owing to the longer distance from emission sources.

Concentrations of individual chemical species in $PM_{2.5}$ collected in the tunnel, roadside, and ambient sites are presented in Table 7.6. The spatial distributions of OC and EC were similar to $PM_{2.5}$ mass concentrations, with relationship to the microenvironment and the percentage of diesel-fueled vehicles, suggesting primary vehicle emissions were dominant sources locally. The concentrations of sulfate and ammonium were evenly distributed outside the tunnel, namely at roadside and ambient sites, suggesting they are regional pollutions in Hong Kong, which is consistent with previous investigation on sulfate and ammonium in Chapter 4 and 5. Although the absolute values of sulfate and ammonium are high in the Shing Mun Tunnel, they only contribute ~10% and ~4% of the $PM_{2.5}$, meaning they are predominantly primary. The nitrate concentration was extremely high at LMC roadside, compared to all other sites. LMC roadside site was at the cross-border area between Hong Kong and Shenzhen,

with a considerable number of heavy goods vehicles from Mainland China passing this area, while both MK and PU roadside was typical roadside in Hong Kong. These vehicles from Shenzhen may use different fuels from the local vehicles in Hong Kong, thus showing some characteristics differ from local emissions.

7.2.2.3 The comparisons of OC/EC ratios in different environment

The OC/EC ratio, determined in different atmosphere environments, is an important factor for determining the relative amounts of scattering and absorption by aerosols and currently applied in the aerosol radiative forcing for regional and world warming and cooling (Novakov et al. 2005). Elemental carbon has been intensively used as a tracer of primary OC (Novakov, 1984; Gray et al. 1986; Turpin and Huntzicker, 1991). The OC/EC ratios exceeding 2.0 have been used to indicate the presence of secondary organic aerosols (Gray et al., 1986; Chow et al., 1996a). The OC/EC ratio was calculated for the samples collected in different environment. The average OC/EC ratio (0.6±0.2) at the Shing Mun Tunnel was lowest, while it (1.9±0.7) was highest in ambient atmosphere. The ratios at roadside sites were in the middle, 0.9±0.4 for LMC roadside, 0.7±0.2 for MK roadside, and 0.9±0.3 for PU roadside. The results agree with the expectation because aerosols measured at tunnel and roadside were supposed to be primary particles while those measured in ambient environment contain

secondary particles.

Figure 7.6 displays the percentage of major components in $PM_{2.5}$ at the Shing Mun Tunnel, PU and LMC roadside, and TW ambient station. The pie chart at MK roadside has not been shown because it was similar with that at PU roadside. As a closed microenvironment, the Shing Mun Tunnel represents the primary vehicle emissions, with the largest OM and EC fractions (~85%). PU and LMC roadside are typical roadside sites, with similar OM and EC fractions (~66%). TW ambient site has the lowest carbonaceous components, especially for EC, accounting for less than 50% of the total $PM_{2.5}$.

7.3 Summary

To be able to characterize to what extent the traffic or different vehicle types contribute to the city pollution, a detailed study on emission rates for vehicles with different fuels and attributes is needed. For the mixed vehicle types, the $PM_{2.5}$ emission factor ranged from 0.066 g veh^{-1} km^{-1} to 0.190 g veh^{-1} km^{-1} with an average of 0.131±0.037 g veh^{-1} km^{-1}, which is normally higher than that in other countries. More than half of the $PM_{2.5}$ emission was from elemental carbon (65.819±18.429 mg veh^{-1} km^{-1}) and about one third was from the organic carbon fraction (35.685±11.727 mg veh^{-1} km^{-1}). The third most prominent species was sulfate, which accounted for

5.6±2.2% of the $PM_{2.5}$ emission, followed by ammonium (2.3±0.9%) and iron (1.0±1.3%). No significant seasonal difference was detected for $PM_{2.5}$ and its chemically speciated compositions (all of *p*-values are larger than 0.05, *t*-test).

This study also found, as expected, that diesel engines emitted particles at a greater rate per kilometer than did gasoline engines and that the chemical profiles were different for both sources. Elemental and organic carbon were the primary constituents for the particulates emitted from gasoline- and diesel-fueled vehicles. On average, organic carbon composed a larger fraction of the total carbon for the gasoline-fueled vehicles, while elemental carbon represented the larger fraction of the total carbon for the diesel-fueled vehicles.

The annual vehicle-related $PM_{2.5}$ emission flux in Hong Kong was 1466.0±414.1 tonnes during 2003 based on the $PM_{2.5}$ emission factors in this tunnel study, which is ~70% of PM_{10} emission flux calculated by HKEPD using simulation method. The percentage is consistent with typical $PM_{2.5}/PM_{10}$ ratios at Hong Kong roadside environment. This result further confirms the validation of measurement in the present study and the model results by HKEPD.

The spatial distribution of $PM_{2.5}$ mass concentrations in Hong Kong was associated with the distance from the major roadway networks and the proportion of diesel-fueled

vehicles traveling on the road as well. The $PM_{2.5}$ mass concentrations were the highest in the Shing Mun Tunnel, followed by those measured at roadside sites and ambient site. In the Shing Mun Tunnel, $PM_{2.5}$ mass concentrations change with the fluctuation of diesel-fueled vehicles. Even at the three roadside sites, the increase in $PM_{2.5}$ emissions positively correlates with the increase in the percentage of passing diesel-fueled vehicles. For example, the percentage of diesel-fueled vehicles was ~90%, ~51%, and ~38% at LMC, MK, and PU roadside; the corresponding $PM_{2.5}$ mass concentration was 129.0±94.8, 69.3±11.9, 66.9±12.3 μg m^{-3}.

The characteristics of OC and EC in $PM_{2.5}$ were also associated with the microenvironments. The proportion of total carbonaceous aerosols (sum of OC and EC) in $PM_{2.5}$ was the highest in the tunnel, followed by the roadside and ambient sites; on the other hand, the OC/EC ratio was the lowest at tunnel, moderate at roadside, and the highest in ambient atmosphere. This is because the Shing Mun Tunnel is a relatively closed microenvironment and is capable of providing pure and fresh vehicle emissions, compared to the roadside, which in turn is a site with vehicle exhaust as the dominant source, by comparison with the ambient site.

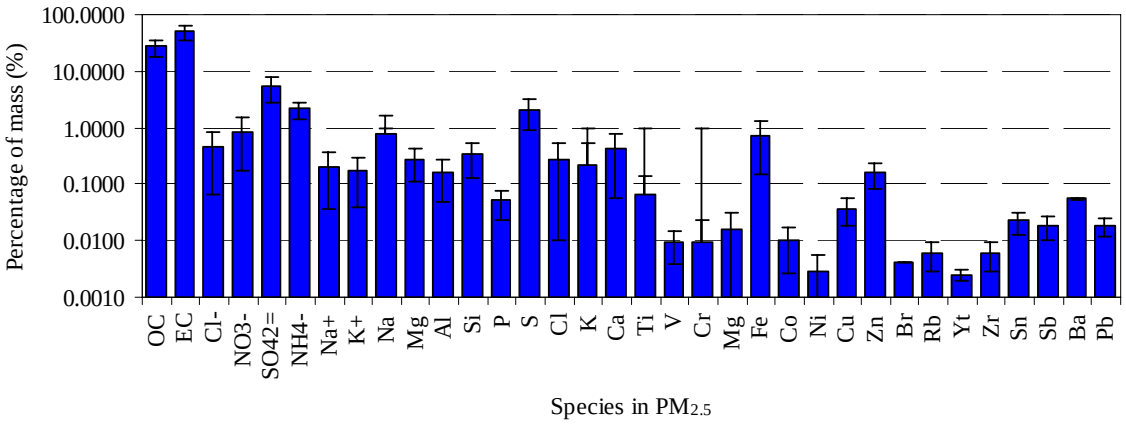

Figure 7.1 Chemical profile $PM_{2.5}$ for mixed vehicles in the Shing Mun Tunnel, Hong Kong.

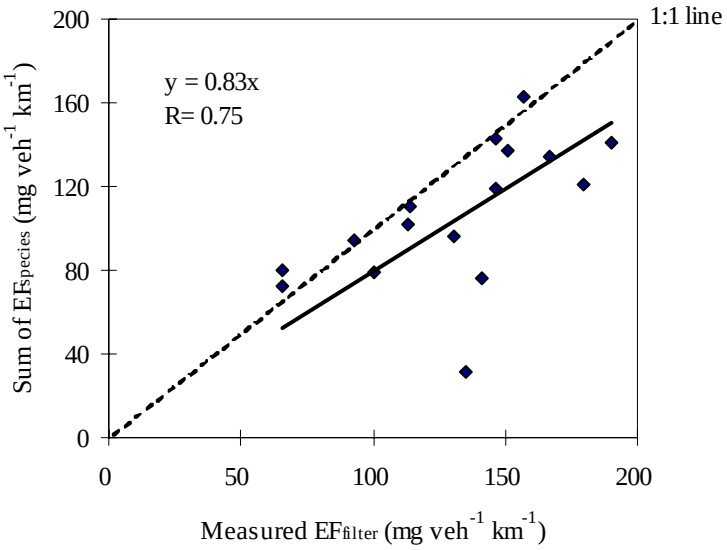

Figure 7.2 Scatter plot for measured EF and sum of individual EF of species.

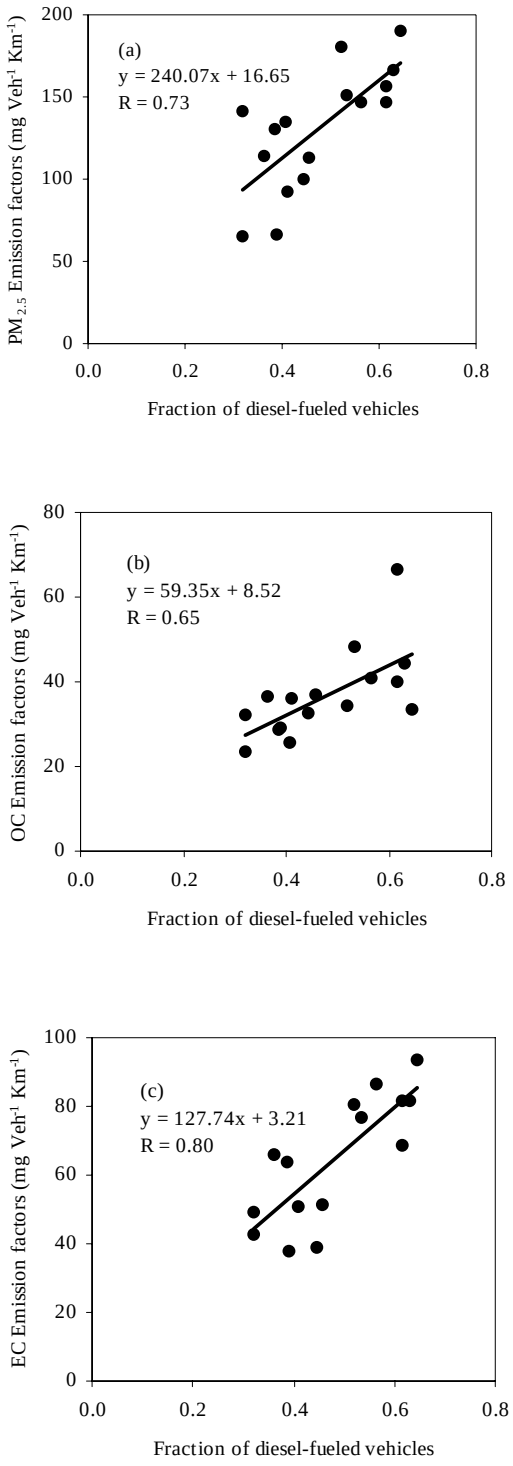

Figure 7.3 $PM_{2.5}$ (a), OC (b), EC (c) emission factors as a function of the fraction of diesel-fueled vehicles.

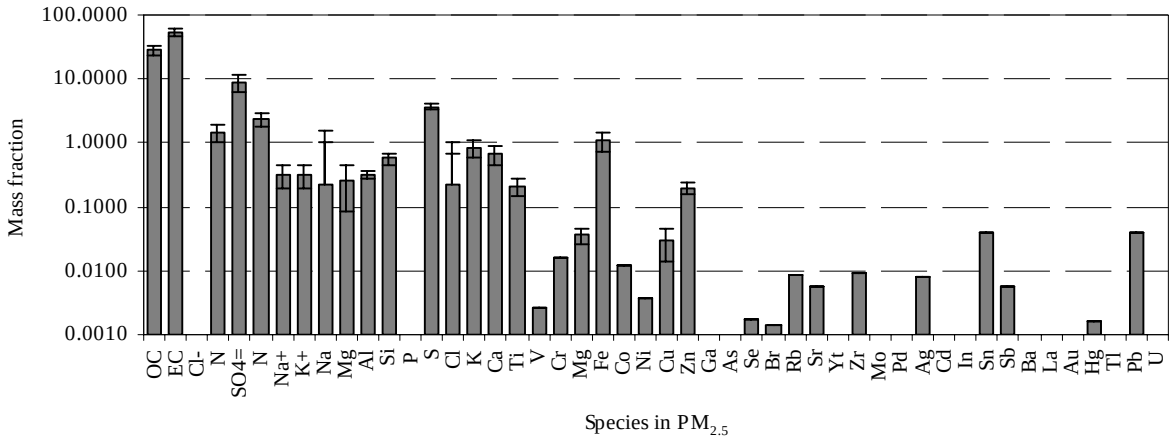

Figure 7.4 Chemical profiles of $PM_{2.5}$ from diesel-fueled vehicles derived from the Shing Mun Tunnel study.

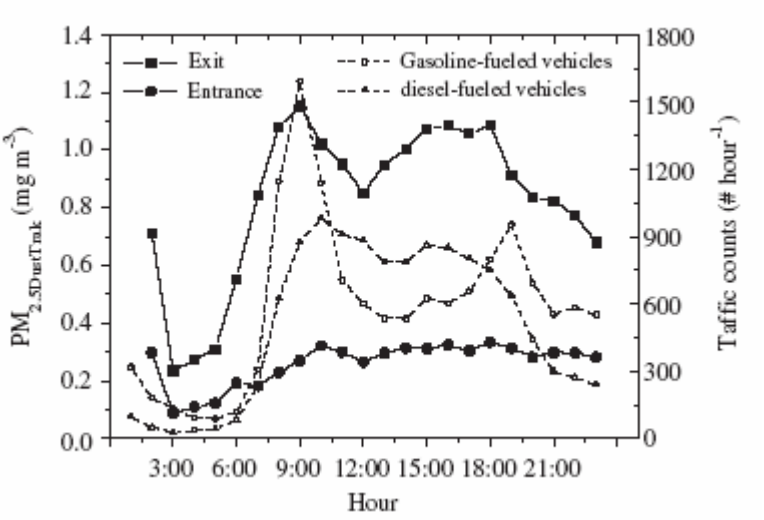

Figure 7.5 Hourly average $PM_{2.5}$ concentrations measured with two DustTrak units at the tunnel entrance and exit, along with corresponding average traffic counts of gasoline- and diesel-fueled vehicles. The data represents the average values from four sampling days on January 26, February 9, 11, 25.

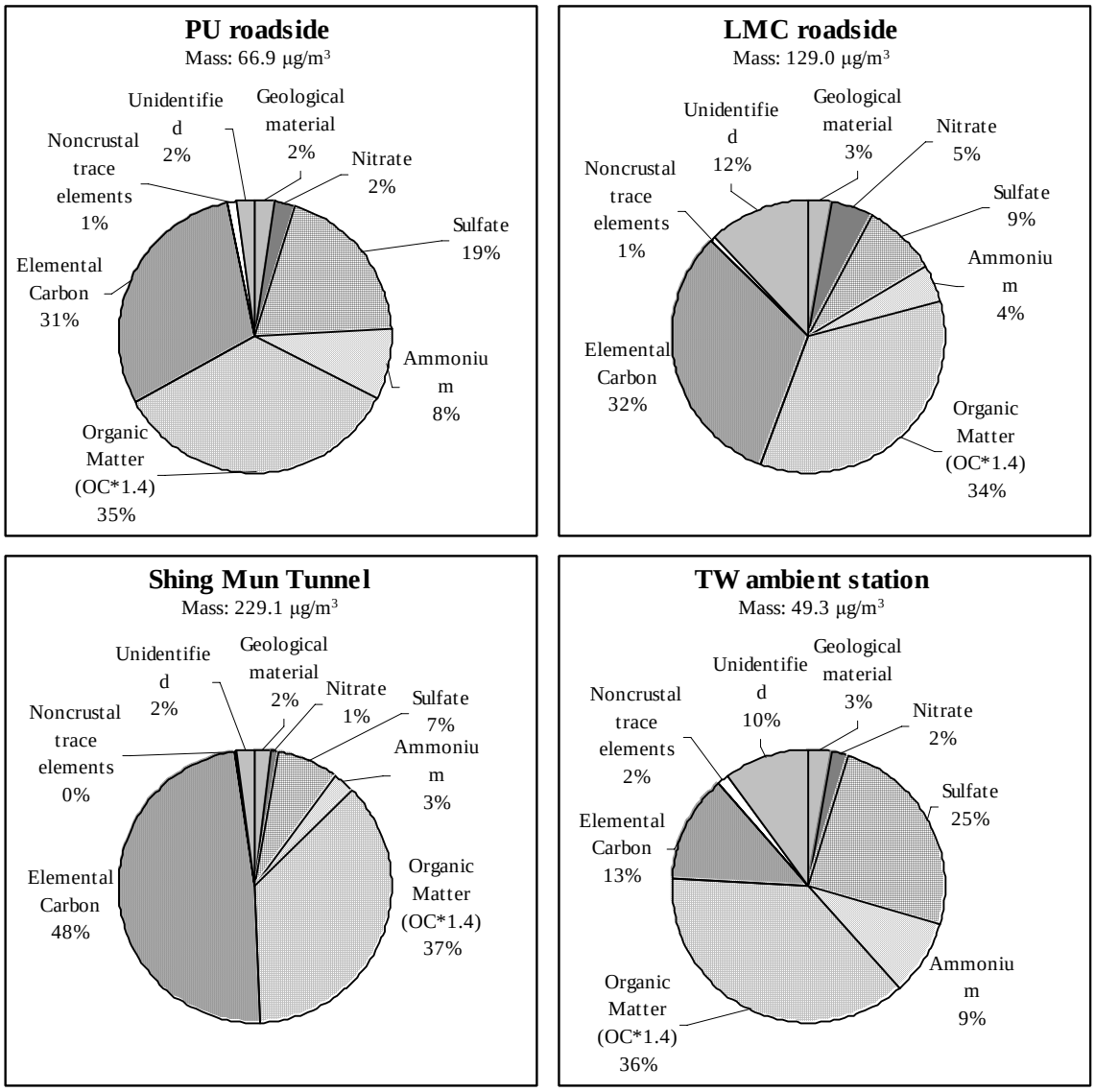

Figure 7.6 The $PM_{2.5}$ chemical compositions in various microenvironments.

Table 7.1 Emission factors of $PM_{2.5}$ in each run.

Run No.	Date	Day	Duration	Diesel Fraction	$PM_{2.5}$
					Emission factor (g $veh^{-1}km^{-1}$)
Run 1	Aug/13/03	Wed	1700-1900	0.52	0.180
Run 2	Aug/16/03	Sat	1700-1900	0.32	0.141
Run 3	Aug/17/03	Sun	0800-1000	0.41	0.135
Run 4	Aug/31/03	Sun	0800-1000	0.39	0.130
Run 5	Jan/12/04	Mon	1700-1800	0.53	0.151
Run 6	Jan/13/04	Tue	1400-1500	0.61	0.157
Run 7	Jan/14/04	Wed	2200-2300	0.36	0.114
Run 8	Feb/1/04	Sat	0800-0900	0.41	0.092
Run 9	Feb/9/04	Sun	0900-1000	0.44	0.100
Run 10	Feb/10/04	Mon	0800-0900	0.39	0.066
Run 11	Feb/11/04	Tue	1400-1500	0.61	0.147
Run 12	Feb/11/04	Tue	1500-1600	0.63	0.166
Run 13	Feb/14/04	Fri	2100-2200	0.32	0.066
Run 14	Feb/23/04	Sun	1700-1800	0.56	0.147
Run 15	Feb/23/04	Sun	1800-1900	0.46	0.113
Run 16	Feb/25/04	Tue	1100-1200	0.64	0.190

Table 7.2 PM emission factors in several recent studies.

Tunnel	Diesel-fueled vehicle fraction	Mode year/age	Vehicle speed (km h^{-1})	Instrument	PM emission factor (g $veh^{-1}km^{-1}$)
Shing Mun Tunnel, Hong Kong (this study)	30-60%		60-70	DRI portable sampler	
Tunnel measurements (mean)					0.131±0.037[a]
DV emission factors					0.257±0.031[a]
Tuscarora Tunnel, Pennsylvania (Gertler et al., 2002)	11.6-86.5%	1991-1995	33-38	IMPROVE sampler	
Tunnel measurements (mean)					0.062±0.042[a]
HD emission factors					0.135±0.018[a]
Sepulveda Tunnel, Los Angeles (Gillies et al., 2001)	2.60%	1985-1988	60.5±11.7	Medium-vol sampler	0.052±0.027[a]
Howell Tunnel, Milwaukee, WI (Lough et al., 2005)	1.5-9.4%				0.033±0.005[a]
Kaisermuhlen Tunnel, Vienna (Laschober et al., 2004)	14.80%		80[**]	Aerosol sampler	0.045±0.018[d]
Caldecott Tunnel, San Francisco Bay (Allen et al., 2001)				MOUDI	
HD emission factors					0.430±0.079[b]
Woolloongabba Tunnel, Brisbane (Jamriska et al., 2004)					
DV emission factors	100% bus	1-13 yr		TEOM	0.267±0.207[e]
Dynamometer, California. (Norbeck et al., 1998)		Pre-1981 to 1997		Designed sampler	
DV emission factor	100%				0.349±0.260[a]
Dynamometer (CBD cycle), South Phoenix. (Lowenthal et al., 1992)				DRI aerosol sampling apparatus	
DV emission factor	100% truck				0.785±0.353[a]

[a] $PM_{2.5}$; [b] $PM_{1.9}$; [c] PM_3; [d] PM size cut not stated; [e] TEOM $PM_{2.5}$ equivalent emission factor; [f] WVU truck cycle with No.2 diesel.

[**] the upper limit speed

Table 7.3 Emission factors of individual chemical species in $PM_{2.5}$ for mixed vehicles in this study and previous study.

Reference	This study		Gillies et al., 2001		Cadle et al., 1997		Laschober et al., 2004	
PM	$PM_{2.5}$		$PM_{2.5}$		PM_{10}		PM[a]	
Tunnel	Shing Mun Tunnel		Sepulveda Tunnel		Dynamometer		Kaisermuhlen Tunnel	
City	Hong Kong		Los Angeles		Costal Mesa and Santa		Vienna	
Year	2003-2004		1999		1995		2002	
Diesel Fraction	30-70%		2.60%				14.80%	
Mode year/age			1985-1988		6-22 yr			
Instrument	DRI portable sampler		Medium-vol sampler		Portable dynamometer		Aerosol sampler	
Emission factor	EF	SD[b]	EF	SD	EF[c]	SD	EF	SD
Unit	mg $veh^{-1}km^{-1}$		mg $veh^{-1}km^{-1}$		mg $veh^{-1}km^{-1}$		mg $veh^{-1}km^{-1}$	
Mass	130.992	36.886	52.500	27.000	0.068		45.300	17.500
OC	35.685	11.727	19.270	8.460			11.800[d]	
EC	65.819	18.429	25.500	4.980			27.900	4.000
Cl^-	0.595	0.509	0.670	0.990				
NO_3^-	1.081	0.859	3.270	1.170				
$SO_4^=$	7.051	3.295	1.770	2.060			2.400	0.900
NH_4^-	2.787	0.883	1.610	1.060			1.200	0.400
Na^+	0.263	0.215	0.350	0.160				
K^+	0.222	0.171	0.100	0.080				
Na	0.998	1.174	0.300	1.170	0.005	0.012		
Mg	0.350	0.208	0.260	0.290	0.047	0.043		
Al	0.216	0.153	0.220	0.150	0.070	0.201		
Si	0.446	0.274	0.560	0.120	0.791	2.255		
P	0.067	0.037	0.090	0.150	0.151	0.209		
S	2.749	1.559	0.320	0.560	0.169	0.184		
Cl	0.354	0.341	0.320	0.180	0.333	2.344		
K	0.286	0.418	0.080	0.070	0.009	0.016		
Ca	0.549	0.477	0.300	0.070	0.125	0.147		
Ti	0.084	0.099	0.090	0.500	0.001	0.002		
V	0.012	0.007	0.050	0.210	0.000	0.003		
Cr	0.013	0.018	0.020	0.050	0.003	0.007		
Mg	0.020	0.020	0.020	0.030	0.003	0.006		
Fe	0.950	0.758	2.790	0.290	0.171	0.400		
Co	0.013	0.009	0.000	0.100	0.000	0.000		
Ni	0.004	0.004	0.010	0.020	0.003	0.011	1.800	2.000
Cu	0.048	0.023	0.170	0.020	0.005	0.088	32.300	20.700
Zn	0.204	0.093	0.140	0.020	0.126	0.164	33.400	28.900
Ga*	0.005		0.010	0.040	0.000	0.000		
As*	0.004	0.004	0.000	0.050	0.000	0.000		
Se*	0.001	0.001	0.000	0.020	0.000	0.000		
Br	0.006	0.004	0.010	0.020	0.004	0.013		
Rb	0.008	0.013	0.000	0.020	0.000	0.000		
Sr*	0.007	0.010	0.020	0.020	0.000	0.000		
Yt	0.003	0.004	0.000	0.030	0.000	0.000		
Zr	0.008	0.009	0.010	0.030	0.000	0.000		
Mo*	0.000	0.000	0.010	0.060	0.001	0.003		
Pd*	0.009	0.003	0.020	0.180	0.001	0.002		
Ag*	0.006	0.004	0.040	0.200	0.000	0.000		
Cd*	0.013	0.012	0.020	0.220	0.001	0.002		
In*	0.008	0.004	0.060	0.250	0.000	0.000		
Sn	0.030	0.020	0.100	0.310	0.004	0.005		
Sb	0.024	0.016	0.150	0.370	0.003	0.004		
Ba	0.073	0.050	0.360	1.370	0.015	0.019		
La*	0.130	0.063	0.000	1.830	0.012	0.020		
Au*	0.000	0.000	0.000	0.060	0.000	0.000		
Hg*	0.003	0.002	0.010	0.050	0.000	0.000		
Tl*	0.001	0.000	0.000	0.050	0.000	0.000		
Pb	0.024	0.026	0.030	0.060	0.018	0.029	9.500	6.300
U*	0.000	0.000	0.000	0.050				

a PM size cut not stated; [b] Standard deviation; [c] average prepair value; [d] OC=TC-EC; * the concentrations below minimum detection limit.

Table 7.4 Emission factors of individual chemical species in $PM_{2.5}$ for diesel-fueled vehicles in this study and previous studies.

Reference	This study		Gertler et al., 2002		Norbeck et al., 1998		Lowenthal et al., 1994	
PM	$PM_{2.5}$		$PM_{2.5}$		$PM_{2.5}$		$PM_{2.5}$	
Tunnel	Shing Mun Tunnel		Tuscarora Moutain Tunnel		Dynamometer		Dynamometer	
City	Hong Kong		Pennsylvania		California		South Phoenix	
Year	2003-2004		1999		1996-1997		1992	
DV Fraction	30-70%		10%-80%		100%		100% truck	
Mode year/age			1991-1995		1981-1997			
Instrument	DRI portable sampler		IMPROVE sampler		Designed sampler		DRI sampling apparatus	
Emission factor	EF	SE[a]	EF	SE	EF	SE	EF	SE
Unit	mg $veh^{-1}km^{-1}$		mg $veh^{-1}km^{-1}$		mg $veh^{-1}km^{-1}$		mg $veh^{-1}km^{-1}$	
Mass	256.713	31.310					785.331	352.552
OC	67.873	10.192	111.747	42.955	153.914	332.869	213.356	127.130
EC	130.955	14.410	184.032	66.157	159.009	102.278	459.054	254.540
Cl^-	0.000	0.001			0.075	0.155	0.000	0.269
NO_3^-	3.570	1.118	2.268	3.143	0.249	0.385	0.538	0.362
$SO_4^=$	21.931	7.004	1.214	3.505	0.771	0.926	87.100	16.282
NH_4^-	5.549	1.298			0.454	0.528	5.179	2.574
Na^+	0.775	0.294	2.297					
K^+	0.759	0.299					0.043	0.075
Na	0.542	3.133	-0.411	-0.036	-0.155	0.043		
Mg	0.628	0.427	0.509	0.311	0.099	0.199		
Al	0.774	0.118	-0.077	-0.058	0.031	0.075	0.000	0.361
Si	1.381	0.301	0.874	0.881	0.826	0.435	0.075	0.563
P	0.000	0.031			0.423	0.789	0.048	0.734
S	8.942	0.962	0.267	0.152	1.056	1.050	20.156	6.441
Cl	0.540	1.102	2.350	2.069	0.398	0.795	0.003	0.108
K	2.039	0.568	0.519	0.694	0.050	0.174	0.001	0.038
Ca	1.614	0.561	0.701	0.402	0.646	0.926	0.242	0.137
Ti	0.504	0.146	0.250	0.109	0.000	0.000	0.002	0.078
V	0.006	0.000	0.009	0.006	0.000	0.000	0.000	0.040
Cr	0.038	0.000			0.006	0.012	0.000	0.014
Mg	0.088	0.023	2.768	0.862	0.006	0.006	0.007	0.008
Fe	2.619	0.891	1.985	0.861	0.833	1.025	0.193	0.103
Co	0.030	0.000			0.000	0.000	0.000	0.007
Ni	0.009	0.000			0.012	0.019	0.000	0.006
Cu	0.071	0.038	0.088	0.110	0.019	0.031	0.023	0.016
Zn	0.483	0.097	0.137	0.092	0.814	1.522	0.625	0.312
Ga	0.000	0.000			0.000	0.000	0.000	0.011
As	0.000	0.000			0.000	0.000	0.005	0.013
Se	0.004	0.000	-0.049	-0.026	0.000	0.000	0.004	0.007
Br	0.003	0.000	0.016	0.014	0.000	0.000	0.002	0.007
Rb	0.021	0.000			0.000	0.000	0.000	0.006
Sr	0.014	0.000	0.038	0.013	0.000	0.000	0.001	0.007
Yt	0.000	0.000			0.000	0.000	0.000	0.008
Zr	0.023	0.000			0.000	0.000	0.000	0.010
Mo	0.000	0.000			0.006	0.012	0.000	0.016
Pd	0.002	0.000			0.000	0.006	0.002	0.072
Ag	0.020	0.000			0.000	0.006	0.014	0.085
Cd	0.000	0.000			-0.012	0.006	0.027	0.085
In	0.000	0.000			0.000	0.006	0.020	0.094
Sn	0.097	0.000			0.000	0.006	0.030	0.126
Sb	0.014	0.000			0.000	0.012	0.000	0.149
Ba	0.001	0.000			0.068	0.075	0.063	0.518
La	0.000	0.000			-0.031	0.068	0.184	0.684
Au	0.000	0.000			0.000	0.000	0.000	0.032
Hg	0.004	0.000	0.011	0.003	0.000	0.000	0.000	0.015
Tl	0.001	0.000			0.000	0.000	0.001	0.014
Pb	0.093	0.000	0.037	0.026	0.019	0.062	0.005	0.019
U	0.000	0.000			0.000	0.000	0.000	0.014

[a] standard error.

Table 7.5 Emission factors of individual chemical species in $PM_{2.5}$ for gasoline-fueled vehicles in this study and previous studies.

Reference	This study		Gertler, et al. 2002		Norbeck et al. 1998	
PM	$PM_{2.5}$		$PM_{2.5}$		$PM_{2.5}$	
Tunnel	Shing Mun Tunnel		Tuscarora Moutain Tunnel		Dynamometer	
City	Hong Kong		Pennsylvania		California	
Year	2003-2004		1999		1996-1997	
DV Fraction	30-70%		10%-80%		100%	
Mode year/age	1981[a]		1991-1995		1981-1997	
Instrument			IMPROVE sampler		Designed sampler	
Emission factor	EF	SE[b]	EF	SE[b]	EF	SE[b]
Unit					mg $veh^{-1}km^{-1}$	
Mass	16.646	28.450				
OC	8.521	9.262	2.827	1.087	16.547	31.504
EC	3.213	13.316	3.306	1.187	3.480	4.840
Cl^-	0.000	0.001			0.050	0.255
NO_3^-	0.000	1.007			0.006	0.025
$SO_4^=$	0.000	6.256			0.093	0.193
NH_4^-	0.573	1.209			0.068	0.149
Na^+	0.000	0.257				
K^+	0.000	0.256				
Na	0.356	2.016	2.383	0.210	0.000	0.025
Mg	0.055	0.509	0.290	0.177	0.025	0.031
Al	0.000	0.114	0.544	0.404	0.019	0.037
Si	0.000	0.264	0.738	0.744	0.317	0.702
P	0.162	0.025			0.056	0.075
S	0.000	0.890	1.169	0.664	0.087	0.143
Cl	0.166	0.895	0.559	0.492	0.075	0.311
K	0.000	0.462	0.275	0.369	0.000	0.006
Ca	0.000	0.499	0.280	0.160	0.081	0.118
Ti	0.000	0.116	0.052	0.023	0.000	0.000
V	0.019	0.000	0.007	0.005	0.000	0.000
Cr	0.000	0.000			0.000	0.006
Mg	0.000	0.020	0.400	0.125	0.000	0.006
Fe	0.000	0.793	0.221	0.090	0.280	0.684
Co	0.000	0.000			0.000	0.000
Ni	0.000	0.000			0.006	0.012
Cu	0.027	0.030	0.015	0.018	0.006	0.006
Zn	0.000	0.086	0.046	0.030	0.112	0.174
Ga	0.000	0.000			0.000	0.000
As	0.013	0.000			0.000	0.000
Se	0.000	0.001	0.011	0.006	0.000	0.000
Br	0.008	0.000	-0.001	-0.001	0.000	0.000
Rb	0.000				0.000	0.000
Sr	0.000	0.000	-0.002	-0.001	0.000	0.000
Yt	0.019	0.000			0.000	0.000
Zr	0.000	0.000			0.000	0.000
Mo	0.000	0.000			0.000	0.000
Pd	0.016	0.000			0.000	0.000
Ag	0.000	0.000			0.000	0.000
Cd	0.048	0.000			0.000	0.000
In	0.022	0.000			0.000	0.000
Sn	0.000	0.000			0.000	0.000
Sb	0.035	0.000			0.000	0.000
Ba	0.135	0.000			0.000	0.006
La	0.352	0.000			0.000	0.006
Au	0.000	0.000			0.000	0.000
Hg	0.003	0.000	0.002	0.000	0.000	0.000
Tl	0.001	0.000			0.000	0.000
Pb	0.000	0.000	0.011	0.008	0.025	0.093
U	0.000	0.000			0.000	0.000

Table 7.6 The comparison of $PM_{2.5}$ mass and chemical compositions in various microenvironments.

Site	TW Ambient (μg m^{-3})			LMC Roadside (μg m^{-3})			MK Roadside (μg m^{-3})			PU Supersite (μg m^{-3})			SM Tunnel (μg m^{-3})		
	Mean	N	S.D.	Mean	N	S.D.	Mean	N	S.D.	Mean	N	S.D.	Mean	N	S.D.
Diesel-fueled vehicle % of total traffic counts				90%			51%			38%			50%		
Mass	49.31	20	17.90	128.95	11	94.77	69.26	16	11.85	66.89	13	12.26	229.06	32	90.05
Cl^-	0.17	18	0.12	0.62	11	1.01	0.29	16	0.07	0.32	12	0.12	0.87	30	0.61
NO_3^-	0.79	20	0.59	5.67	11	10.82	1.71	16	0.84	1.60	13	0.84	3.13	32	2.54
SO_4^{2-}	11.62	20	5.68	10.44	11	11.47	11.05	16	5.59	13.33	13	5.84	23.69	32	9.35
NH_4^+	4.33	20	2.06	4.98	11	6.81	4.38	16	2.02	5.46	13	2.31	8.31	32	3.10
Na^+	0.26	20	0.08	0.27	11	0.17	0.33	16	0.12	0.29	13	0.17	0.46	32	0.35
K^+	0.67	20	0.57	0.62	11	0.91	0.56	16	0.48	0.53	11	0.31	0.73	32	0.52
OC1	1.16	20	0.47	7.13	11	4.55	2.41	16	1.31	2.81	13	1.02	14.63	32	8.29
OC2	2.14	20	0.84	6.89	11	4.10	4.51	16	1.15	3.13	13	1.04	13.62	32	6.49
OC3	6.20	20	3.34	12.09	11	7.09	6.58	16	1.46	6.38	13	1.59	14.45	32	5.40
OC4	4.84	20	2.38	11.65	11	10.16	6.41	16	2.61	5.26	13	1.94	14.94	32	9.41
EC1	5.78	20	2.44	31.70	11	17.19	21.64	16	4.68	16.19	13	4.04	67.14	32	30.98
EC2	0.90	20	0.47	8.85	11	8.61	6.38	16	4.19	3.82	13	2.77	47.53	32	32.59
EC3	0.10	13	0.09	0.15	9	0.08	0.10	11	0.06	0.18	8	0.13	0.30	24	0.25
OC	13.78	20	6.48	37.46	11	24.86	19.43	16	4.03	17.59	13	3.45	58.49	32	25.21
EC	7.31	20	3.03	43.89	11	21.10	28.38	16	2.88	20.11	13	4.25	114.08	32	39.92
TC	21.08	20	7.09	81.34	11	43.24	47.81	16	5.32	37.70	13	6.01	172.57	32	62.51
Na	0.27	14	0.21	0.68	8	0.49	0.59	9	0.42	0.58	12	0.41	1.37	27	1.12
Mg	0.05	17	0.03	0.10	4	0.08	0.12	14	0.07	0.11	10	0.06	0.15	23	0.16
Al	0.06	19	0.06	0.19	11	0.11	0.07	13	0.06	0.08	12	0.07	0.26	32	0.33
Si	0.32	20	0.23	0.88	11	0.65	0.35	15	0.22	0.34	13	0.16	0.99	32	1.22
P	0.01	2	0.00	0.00	0	0.00	0.01	2	0.01	0.01	1	0.00	0.04	22	0.05
S	4.45	20	2.37	4.12	11	4.26	4.39	16	1.90	5.38	13	2.47	9.01	32	4.16
Cl	0.07	5	0.04	0.60	8	1.26	0.12	12	0.06	0.08	5	0.04	0.19	28	0.26
K	0.74	20	0.67	0.66	11	0.88	0.57	16	0.51	0.56	13	0.27	0.77	32	0.63
Ca	0.13	20	0.05	0.35	11	0.21	0.19	16	0.09	0.16	13	0.06	0.69	32	0.60
Ti	0.01	16	0.01	0.04	11	0.03	0.02	11	0.01	0.02	12	0.01	0.05	25	0.05
V	0.02	17	0.01	0.02	9	0.03	0.01	12	0.00	0.01	11	0.01	0.01	21	0.01
Cr	0.00	10	0.00	0.01	8	0.01	0.00	5	0.00	0.00	6	0.00	0.01	25	0.01
Mn	0.02	20	0.01	0.03	11	0.02	0.01	16	0.01	0.01	13	0.01	0.03	32	0.02
Fe	0.20	20	0.11	0.65	11	0.41	0.30	16	0.14	0.32	13	0.10	1.14	32	1.11
Co	0.00	12	0.00	0.00	6	0.00	0.00	5	0.00	0.00	5	0.00	0.01	25	0.01
Ni	0.01	17	0.00	0.01	9	0.01	0.01	8	0.00	0.01	8	0.00	0.01	24	0.00
Cu	0.03	20	0.01	0.02	11	0.02	0.02	15	0.01	0.03	13	0.01	0.06	32	0.04
Zn	0.31	20	0.21	0.39	11	0.35	0.31	16	0.14	0.21	13	0.09	0.43	32	0.26
Ga	0.00	6	0.00	0.00	3	0.00	0.00	1	0.00	0.00	3	0.00	0.00	0	0.00
As	0.01	14	0.01	0.01	6	0.02	0.01	10	0.01	0.01	10	0.00	0.01	20	0.01
Se	0.00	15	0.00	0.01	4	0.01	0.00	5	0.00	0.00	5	0.00	0.00	4	0.00
Br	0.01	20	0.01	0.01	11	0.02	0.02	14	0.01	0.01	13	0.01	0.01	31	0.01
Rb	0.01	18	0.01	0.01	10	0.01	0.01	9	0.01	0.00	9	0.00	0.00	20	0.01
Sr	0.00	11	0.00	0.00	4	0.00	0.00	5	0.00	0.00	3	0.00	0.00	17	0.00
Y	0.00	0	0.00	0.00	1	0.00	0.00	0	0.00	0.00	1	0.00	0.00	6	0.00
Zr	0.00	7	0.00	0.00	5	0.00	0.00	4	0.00	0.00	6	0.00	0.00	17	0.00
Mo	0.00	0	0.00	0.00	6	0.00	0.00	4	0.00	0.00	6	0.00	0.00	2	0.00
Pd	0.00	5	0.00	0.00	5	0.00	0.00	1	0.00	0.00	2	0.00	0.00	11	0.00
Ag	0.00	5	0.00	0.00	3	0.00	0.00	4	0.00	0.00	5	0.00	0.00	3	0.00
Cd	0.00	7	0.00	0.00	5	0.00	0.00	5	0.00	0.00	1	0.00	0.00	10	0.01
In	0.00	3	0.00	0.00	2	0.00	0.00	0	0.00	0.00	3	0.00	0.00	11	0.00
Sn	0.02	17	0.01	0.03	9	0.04	0.02	12	0.01	0.02	8	0.01	0.02	22	0.02
Sb	0.01	10	0.00	0.01	6	0.00	0.01	4	0.00	0.01	6	0.00	0.01	20	0.01
Ba	0.02	6	0.01	0.03	9	0.02	0.03	6	0.01	0.03	3	0.01	0.04	22	0.04
La	0.01	8	0.01	0.04	2	0.00	0.04	6	0.03	0.05	1	0.00	0.01	5	0.03
Au	0.00	2	0.00	0.00	2	0.00	0.00	2	0.00	0.00	3	0.00	0.00	1	0.00
Hg	0.00	8	0.00	0.00	3	0.00	0.00	1	0.00	0.00	2	0.00	0.00	3	0.00
Tl	0.00	6	0.00	0.01	3	0.01	0.00	2	0.00	0.00	1	0.00	0.00	7	0.00
Pb	0.08	20	0.08	0.07	11	0.10	0.06	16	0.05	0.05	13	0.04	0.07	31	0.06

Chapter 8 Source Apportionments for Particles at PU Supersite

8.1 Introduction

One of the main aims in air pollution management is to determine the quantitative relationship between ambient air quality and pollutant sources. Receptor models use the chemical characteristics of particles measured at source and receptor to identify and quantify source contributions to receptor concentrations. PMF has been shown to be a powerful tool for airborne particulate matter source identification (Willis, 2000; Song et al. 2001) and has been used to assess particle source contributions in the Arctic (Xie et al. 1999), Hong Kong (Lee et al. 1999), Thailand (Chueinta et al. 2000), Vermont (Polissar et al. 2001), and cities in U.S. (Kim et al. 2003; 2004; Song et al. 2000).

Although the previous application of PMF to ambient atmosphere in Hong Kong (Lee et al. 1999; Qin et al. 2002; Yuan et al. 2006) tend to keep abreast with the improvement of sampling technique and chemical analyses, the source apportionments are still focused on the PM_{10} data, which has been found to be a mix of fine and coarse particles. As described previously in this thesis, USEPA has suggested that it is better

to treat the $PM_{2.5}$ and PM_{coarse} as bases for two separated air quality standards. Thus we need to advance the progress of source apportionment from PM_{10} to two separated fractions, $PM_{2.5}$ and PM_{coarse}, in order to develop an in-depth understanding of the nature of particles.

The CMB receptor model is another tool for source apportionments and it has been applied to PM_{10} and $PM_{2.5}$ problems throughout the western United States with generally acceptable success (e.g., SCAQMD, 1996). $PM_{2.5}$ chemical profiles for local sources, such as vehicle exhaust (see Chapter 7), cooking (HKEPD, 2006), and fugitive dust (Ho et al. 2003) etc., has been developed for Hong Kong in recent years, which makes source apportionments by the CMB possible.

In this study, the PMF receptor model was applied to available data to estimate the contribution of each of the various source categories to the particulate mass concentration, e.g., $PM_{2.5}$ and PM_{coarse}, respectively. In order to make comparison with the PMF, the CMB was also applied to the $PM_{2.5}$ data sets in this study. EPA-CMB 8.2 modeling software used is directly available from the website of USEPA. The PM_{coarse} data was not apportioned by CMB receptor model since the source profiles for coarse particles are unavailable.

8.2 Results and discussion

8.2.1 Source apportionments for $PM_{2.5}$ and PM_{coarse} using PMF receptor model

8.2.1.1 Input data

The PMF was applied to apportion source contributions to $PM_{2.5}$ and PM_{coarse} measured at PU Supersite, separately. For input data for the PMF, two files are needed, one file with the concentrations and one with the uncertainties associated with those concentrations. In this study, the measured concentration values were used directly, and the uncertainty took account of both sampling and chemical analytical errors. Species that are always below their detection limit or species that have a lot of error in their measurements relative to the magnitude of their concentrations degrade the solution of PMF (Paatero and Hopke, 2003). The signal-to-noise ratios can be used as good indicator for those species; smaller signal-to-noise ratios indicate that the species is noisier. Thus those with small signal-to-noise ratios were identified in PMF by labeling a species as “Weak” or “Bad”. Species that are labeled “Bad” are removed from the analysis and species that are labeled “Weak” have their uncertainties increased by a factor of 3 prior to modeling. Finally, about twenty-seven species were included in the PMF, e.g., Cl^-, NO_3^-, SO_4^{2-}, NH_4^+, K^+, OC, EC, Na, Mg, Al, Si, K, Ca, Ti, V, Mn, Fe, Ni, Cu, Zn, As, Br, Rb, Sn, Sb, Ba, Pb.

8.2.1.2 Determination of the number of sources

In the PMF, different numbers of factors need to be tested and the optimal number is the one that adequately fits the data with the most physically meaningful results. Analysis of the goodness of model fit, Q, as defined in Equation 3.7, can be used to help determine the optimal number of factors. Two types of Q values are reported by PMF, one called robust and one called true. Generally, using the robust Q is preferable for understanding how well the model fit the data because the robust Q value is the one for which the impact of outliers has been reduced, efficiently preventing over-fitting of the extreme values. The true Q value is impacted by extreme values. If the model is appropriate for the data and if the uncertainties specified are truly reflective of the uncertainties in the data, then the robust Q should be approximately equal to the number of data points in the concentration data set. In this study, the PMF was initially run several times to find out a factor number, with which the objective function Q values are close to the number of data points in the concentrations data set. The final acceptable rotations were determined by trail and error and banded on the evaluation of the resulting source profiles.

Explained variation (EV) value is an important parameter resulting from the PMF analysis, which is a measure of the contribution of each chemical species in each

source. The loading of each chemical species in each factor is normalized to 1. Profiles of EV values are useful reference for initial qualitative identification of the sources and the mass profiles are the final criteria for source identification (Lee et al. 1999).

8.2.1.3 Source profiles and contributions for $PM_{2.5}$

Seven factors were resolved for $PM_{2.5}$ data, with robust Q value almost equaling to the data numbers in the input mass concentrations file. The EV profiles of each source are shown in Figure 8.1 for $PM_{2.5}$. The corresponding average mass concentrations for individual species can be found in Figure 8.2. The annual mass concentrations and percentages of each factor to the measured total $PM_{2.5}$ mass are shown in Figure 8.3. For $PM_{2.5,}$ the resolved seven factors are identified as diesel- and gasoline-fueled vehicle, secondary aerosol and biomass burning, coal combustion, residual oil combustion, paved soil dust, and tire wear.

Among the seven source categories for $PM_{2.5}$, vehicle is the most important contributor to fine particles, with ~26% from diesel-fueled vehicle and ~13% from gasoline-fueled vehicle. The EV profile of diesel-fueled vehicle by PMF is characterized with high proportion of EC, followed by OC, and trace elements (e. g. Mg, Fe, Cu, Ba), and the source profile of gasoline-fueled vehicle is characterized

with high proportion of OC, followed by EC, and trace elements (e. g. K, As, Rb, Pb), as shown in Figure 8.1. The properties of these EV profiles are identical with the tunnel study in Chapter 7 and previous studies on vehicle emissions (Norbeck et al. 1998; Gertler et al. 2002): both diesel- and gasoline-fueled vehicles generate large amount of carbonaceous compounds but the ratios of OC to EC in the emission profile can be quite different, with low OC/EC ratio (<1) for diesel-fueled vehicles and high OC/EC ratio (>1) for gasoline-fueled vehicles. Moreover, good agreement was observed by comparing the chemical profile of diesel-fueled vehicles derived from the PMF factors with that obtained from the tunnel study, as shown in Figure 8.4.

The second important source, amounting for ~20% of $PM_{2.5}$, was distinguished by large EV values for nitrate, sulfate, ammonium, and soluble potassium, suggesting its association with secondary aerosols and biomass burning (Louie et al. 2005b). It has been shown through previous analyses in this thesis (see Chapters 4 and 5) that long-range transported secondary aerosols and biomass burning impact the air quality at the sampling site when the air mass traveled over China before reaching Hong Kong.

The third source, coal combustion, was ~13% of total $PM_{2.5}$ mass, characterized by multi-elements related with the coal components. The coal combustion is mainly generated from several power-plants located at the north and southwest of Hong Kong

territory. The fourth source identified by PMF is residual oil combustion (~8% of $PM_{2.5}$), distinguished by Ni and V, which are good indicator for residual oil combustion used for ships or utility at container terminal (Yu et al. 2003; Yuan et al. 2006). The spatial variations of Ni and V in Hong Kong have been found to have linkage with the location of container ports in the study of Yu et al. (2003). The paved soil dust profile is represented by Mg, Al, Si, Ca, and Ti in this study, which is similar with the chemical profiles obtained by Ho et al. (2003b). The paved soil dust contributes ~7% of total $PM_{2.5}$ mass and caused by vehicle- and wind-generated turbulence. The last identified source is tire dust, characterized by Zn. Tire wear has been reported to be a main source of Zn in atmosphere (Adachi and Yoshiaki, 2004; Councell et al. 2004;). Finally, ~10% of $PM_{2.5}$ mass can not be explained by the PMF, which may be related to some undetermined compounds in particles, such as oxides related to metals, and material burning.

8.2.1.4 Source profiles and contributions for PM_{coarse}

Five factors were resolved for PM_{coarse} data, with robust Q value almost equaling to the data numbers in the input mass concentrations file. The EV profiles of each source are shown in Figure 8.5 for PM_{coarse}. The corresponding average mass concentrations for individual species can be found in Figure 8.6. The annual mass concentrations and

percentages of each factor to the measured total $PM_{2.5}$ mass are shown in Figure 8.3. For PM_{coarse}, the resolved six factors are tire dust, paved soil dust, marine aerosols, vehicle, and secondary aerosol and biomass burning.

Four out of the five sources for PM_{coarse} data are common with those for $PM_{2.5}$ data, such as vehicle, paved soil dust, tire wear, and secondary and biomass burning. The gasoline- and diesel-fueled vehicles are combined into one single vehicle in PM_{coarse}, perhaps because the low proportions of vehicle emission in coarse particles. The corresponding profile of EV values for each source also has similar indicators, but the contributions of each source to PM mass are different; they are ~20% for tire dust, ~17% for paved soil dust, ~13% for secondary aerosol and biomass burning, ~11% for vehicle in PM_{coarse}. An extra source is marine aerosols, characterized with Cl and Na, occupying ~17% of total PM_{coarse} mass.

8.2.1.5 Previous studies on source apportionments in Hong Kong

In recent years, several groups have tried to apportion source contributions to the ambient atmosphere in Hong Kong using the PMF model. Lee et al. (1999) applied PMF to PM_{10} compositional data collected between 1992 and 1994 in Hong Kong. Unfortunately, as nitrate and carbon were excluded in their PMF trials, a large fraction of their aerosol mass (~31%) remained unexplained because of data quality issues. Qin

et al. (2002) used the PM_{10} compositional dataset from 1986 to 1995 to compare the result between PMF and convenient factor analyses (CFA). Qin et al. (2002) did not make specific comments on the relative importance of different sources, but concluded that PMF was better than CFA. More recently, Yuan et al. (2006) reanalyzed the PM_{10} data in Hong Kong with more accurate carbon data using PMF and Unmix receptor model.

Although the application of PMF to the ambient atmosphere in Hong Kong tends to keep abreast with the improvement of sampling technique and chemical analyses, the source apportionments are still focused on the PM_{10} data, which has been found to be a mix of fine and coarse particles. As described previously in this thesis, USEPA has suggested that it is better to treat the $PM_{2.5}$ and PM_{coarse} as two separate air quality standards. Thus we need to advance the progress of source apportionment from PM_{10} to two separated fractions, $PM_{2.5}$ and PM_{coarse}, in order to develop an in-depth understanding of the nature of particles.

Although the data set was for PM_{10} in the study of Yuan et al. (2006), we still observe reasonable agreement for the $PM_{2.5}$ regional source concentrations with the present study because particles with regional sources are in fine size ranges rather than coarse size ranges. It is found that Yuan and his colleagues reported slightly higher regional

source concentrations, 18.5 μg m^{-3} by Unmix and 14.6 μg m^{-3} by PMF, than the present study. This is reasonable because of the different size fractions used in these two studies. On the other hand, the lower concentrations were observed for the local sources in the previous study than those in this study, which is because the receptor is ambient site in the former study, while it is a source-dominated site in the latter study.

8.2.2 Source apportionments for $PM_{2.5}$ using CMB receptor model

8.2.2.1 Source profiles

The selected potential sources are comprised of vehicle emission, paved soil dust, tire wear, brake lining, cooking fumes, biomass burning, residual oil combustion, marine aerosols, coal combustion from plants, and secondary aerosol, based on the preliminary analyses on chemical characteristics of particles at PU Supersite. It is apparent that the vehicle emission, paved soil dust, tire wear, and brake lining were vehicle-related local sources. The chemical profile of mixed vehicle emissions determined in the Shing Mun Tunnel study was used to represent vehicle exhaust. The paved soil dust profile was based on the resuspended soil dust composition at the Hong Chong road near the PU Supersite, which was determined by Ho et al. (2003b). This study used a tire wear (Hildemann et al. 1991) and a brake lining profile (Ondov et al. 1981) from other studies.

Except for the nearby primary profiles described above, two categories of point source profiles in PRD region (including Hong Kong), namely biomass burning (Core et al. 1989) and coal combustion (Klein et al. 1975) were also included. These kinds of point sources may influence the Hong Kong atmosphere according to the suitable wind direction (Liu et al. 2003, Louie et al. 2005b). In addition, marine aerosols (Watson, 1979) and cooking fumes (HKEPD, 2007) were added as potential sources due to the location of sampling site. Residual oil combustion profile was also included because the occasional contribution of ship emissions to ambient atmosphere has been reported previously (Yu et al. 2003, Lee et al. 2006).

Secondary ammonium sulfate and ammonium nitrate cannot be explained by the primary emissions profiles. Therefore, secondary source profiles representing pure ammonium sulfate, ammonium bisulfate, and ammonium nitrate were constructed (Watson et al. 1994a). These profiles account for sulfate and nitrate formed by gas to particle conversion between the source and receptor. Based on the previous description in Chapter 4 and 5, most secondary aerosol observed in Hong Kong, especially ammonium sulfate, was mainly formed during the transport from mainland to Hong Kong regardless of seasonal difference.

8.2.2.2 Source apportionments

The chemical species, including carbonaceous aerosols, water-soluble ions, and elements, in $PM_{2.5}$ aerosols collected from Oct 2004 to Sep 2005 at PU Supersite served as input ambient database, applied to the CMB modeling. All the results of the CMB model calculations were examined in terms of several performance indices, such as r^2, Chi square, percent mass explained, and calculated/measured ratio, as well as residual/uncertainty ratio according to Watson et al. (2004). The function of 'Source elimination' was active to eliminate negative source contributions from the calculation by EPA-CMB8.2, one at a time. After each fit attempt, if any sources had negative contributions, the source with the largest negative contribution was eliminated and another fit is attempted. This process is repeated until EPA-CMB8.2 finds no sources with negative contributions. Invocation of this option affects the fit obtained by effectively removing collinear sources.

Since some potential sources were influenced by wind direction, the CMB results were taken as average for days with similar back trajectories of air masses. Two cases are summarized here. Case I mainly occurred in summer, with air masses traveling over the South China Sea before reaching Hong Kong. Case II mainly occurred in the rest of the seasons, presenting the air masses traveling over south east China or over the

marine surface along the southeast coast.

Average source contribution by mass and percentage calculated by the CMB model are tabulated in Table 8.1. Except for cooking fume, all sources present in the lists of estimated sources. The cooking fume was deleted automatically during processes by the EPA CMB8.2, perhaps due to collinearity between cooking fume and biomass burning.

According to the CMB results, vehicle emission was the most significant source in the PU Supersite, accounting for ~72% and ~54% of mass concentration for Case I and Case II, respectively. Secondary aerosols, e.g., ammonium sulfate, ammonium bisulfate and ammonium nitrate, were the second contributors, occupying ~14% for Case I and ~20% for Case II. Ammonium bisulfate was the most important secondary aerosols at PU Supersite in either of Cases. Among the four point sources, the most significant source was coal combustion from plants, especially power plants, contributing ~10% and ~14% of total $PM_{2.5}$ mass concentrations, respectively. This is because several power plants and a number of plants are located on the south and north to the Hong Kong territory, respectively. Biomass burning mainly occurred in rural area of PRD region (Hong Kong exclusive) in winter, thus easily transported to Hong Kong, accounting for ~9% to $PM_{2.5}$ mass under northern winds (Case II).

Contributions from residual oil combustion were quite small in this study, which may be due to the limited sample sizes. Paved soil dust, brake lining, tire wear, and marine aerosols were minor contributors, accounting for less than 3% of total $PM_{2.5}$, and they were insignificant in statistics.

Most estimated sources had high contributions (in $\mu g\ m^{-3}$) to $PM_{2.5}$ mass concentration when air masses were from the continent (Case II), compared to when air mass was from marine (Case I), indicating obvious impact of continental aerosols on Hong Kong air quality. As shown in Table 8.1, the concentrations of both local and regional sources increase when air masses are from the continent (Case II) compared with cases when air masses are from marine, but the increased magnitudes are different, with a factor of 1.5 for local sources and 3.3 for regional sources (Table 8.1). The contributions of regional sources to the $PM_{2.5}$ at PU Supersite increase from less than 30% in Case I to nearly 50% in Case II, and even higher at ambient atmosphere (Yuan et al. 2006). This suggested that besides the local vehicle exhausts elimination, regional air quality management strategies are quite important for Hong Kong.

Beside the contributions by species, another report that may be of interest is the Modified Pseudo-Inverse Normalized (MPIN) Matrix for each run. The MPIN matrix identifies which fitting species have the largest influence on the source contribution

estimates from each profile. MPIN is normalized in such a way that it takes on values from -1 to 1. Species with MPIN absolute values of 0.5 to 1.0 are considered influential species. Non-influential species have MPIN absolute values of 0.3 or less. MPIN values obtained in this study indicated the same marker species with the chemical profiles for each sources. Moreover, characteristics of MPIN profile derived from the CMB is similar with the EV profile derived from the PMF. For example, we found MPIN values between 0.5-1.0 were OC and EC for vehicle emission, Al, Si, Ca and Fe for paved soil dust, Mg for brake lining, Zn for tire dust, Cl, Na and Br for marine aerosols, V and Ni for residual oil combustion, K^+ for biomass burning, and Mg, Ca, and Br for coal combustion.

8.2.3 Comparison between PMF- and CMB-derived $PM_{2.5}$ source contributions

Source contribution by mass and percentages calculated by the two models are tabulated in Table 8.2. Overall, the PMF underestimated the $PM_{2.5}$ mass by ~10% (equaling 5.5 μg m^{-3}), while the CMB overestimated by ~7% (equaling 3.7 μg m^{-3}). This is not surprising because the PMF and CMB use different input data and calculation method. For all $PM_{2.5}$ data set (annual), both PMF and CMB identified vehicle, secondary aerosol, and coal combustion as the first three top sources for $PM_{2.5}$ at PU Supersite. The three sources almost dominate the total $PM_{2.5}$ mass. The

concentration and contributions of secondary aerosol and coal combustion are comparable between the PMF- and CMB-generated results, but it is not true for vehicles' contributions. The concentration and contribution of vehicles derived from PMF was lower than those from CMB. It is also noticed that PMF generate high concentrations of 5 μg m^{-3} (~10% of $PM_{2.5}$) for paved soil dust, tire dust, brake lining, while CMB estimate those vehicle-related sources as only 0.6 μg m^{-3} (less than 2% of $PM_{2.5}$). If we combine all vehicle-related sources, including vehicle, paved soil dust, tire dust, brake lining, into one mixed vehicle-related source, we could see the difference between PMF and CMB eliminated. In addition, the underestimation of $PM_{2.5}$ by PMF and overestimation of $PM_{2.5}$ by CMB could be one of important reasons for the difference. Minor sources, including paved soil dust, residual oil combustion, tire dust, brake lining, and marine aerosols, can/can't be detected by PMF and CMB since their low concentrations and contributions to $PM_{2.5}$.

Overall, the contributions from the local, regional, and marine sources showed similar results between CMB and PMF method, as shown in Table 8.2. Therefore, for our data set, it is hard to conclude which method is able to better resolve the sources, but the CMB does provide more details on source contributions on days with different air mass in origin.

Since the underestimation of PMF and the overestimation of CMB, we assumed the source concentrations derived from the two models represent the minimal and maximal concentrations, respectively. Thus, the annual concentrations of local sources ranged from 31.1 to 37.2 μg m^{-3}, contributing to 56-67% of $PM_{2.5}$, and the regional sources ranged from 18.3 to 21.3 μg m^{-3}, contributing to 33-38% of $PM_{2.5}$. Marine aerosols ranged from 0 to 0.6 μg m^{-3}, only accounting for 0-1% of $PM_{2.5}$.

8.3 Summary

This study has reported above an application of two advanced receptor models, the PMF and CMB, for source identification of $PM_{2.5}$ at PU Supersite using chemical composition measurements. Although the PMF and CMB calculate potential factors based on totally different principles, both identified three major underlying factors for fine particles at PU Supersite. The most important factor is vehicle emissions, with EC and OC as indicative species. The secondary factor is secondary aerosols, with high proportions of sulfate, ammonium, and nitrate. The third factor is coal combustion, with multi-elements related to the coal. Overall, the local sources are major sources for $PM_{2.5}$, contributing 56-67% on annual basis and vehicle exhaust is dominant contributor among the local sources. The regional sources contribute 33-38% of $PM_{2.5}$, including secondary aerosol, biomass burning, and coal combustion. The

concentrations of both local and regional sources increase when air masses are from the continent compared with when air masses are from marine. However the increased magnitudes are different, with a factor of 1.5 for local sources and 3.3 for regional sources. The contributions of regional sources to the $PM_{2.5}$ at PU Supersite are less than 30% when air masses are from marine direction, while they increase to nearly 50% when air masses are from continent direction.

The coarse particles observed at PU Supersite are mainly from local sources, ~20% from tire dust, ~17% from paved soil dust, ~11% from vehicles. Reginal source, like secondary aerosol and biomass burning, only contribute ~13% of total coarse mass. In addition, marine aerosols occupy ~17% of total PM_{coarse} mass.

The chemical profile for each resolved source, derived from the two models, reflects a mixture of local and regional sources. OC and EC provide indicators of vehicle emission; ammonium bisulfate, ammonium sulfate, and ammonium nitrate represent secondary aerosol; elements such as Al and Si are associated with paved soil dust, Cl and Na are indicators of marine aerosols, V and Ni reflect residual-oil combustion (ship), Zn for tire dust, Mg for brake lining, K for biomass burning, and coal combustion have multi-elements in it.

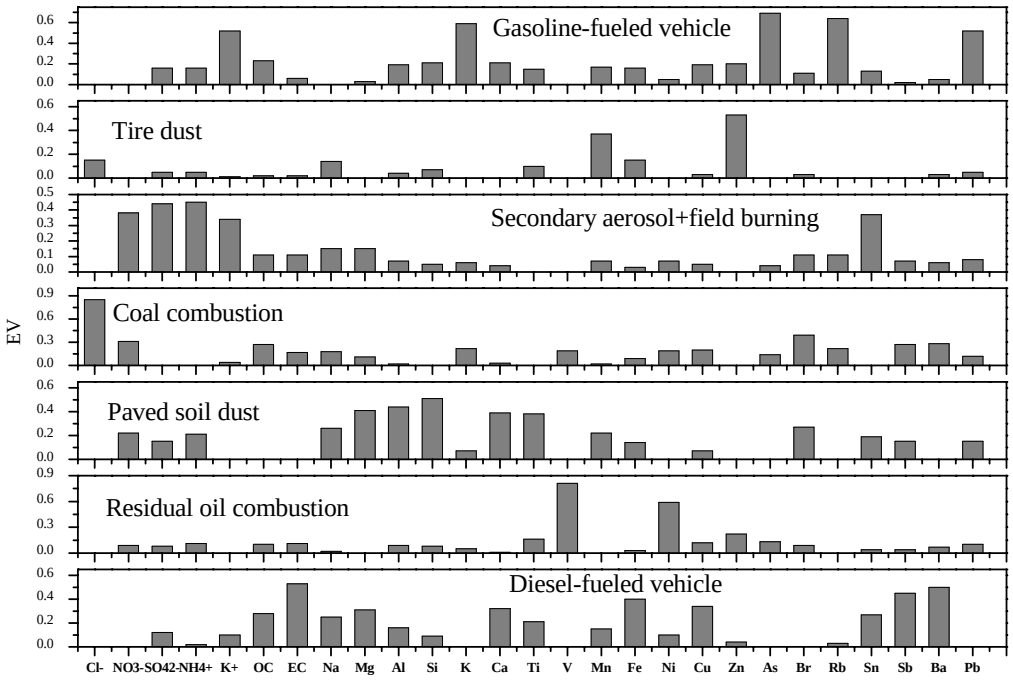

Figure 8.1 Source profiles for $PM_{2.5}$ in EV values.

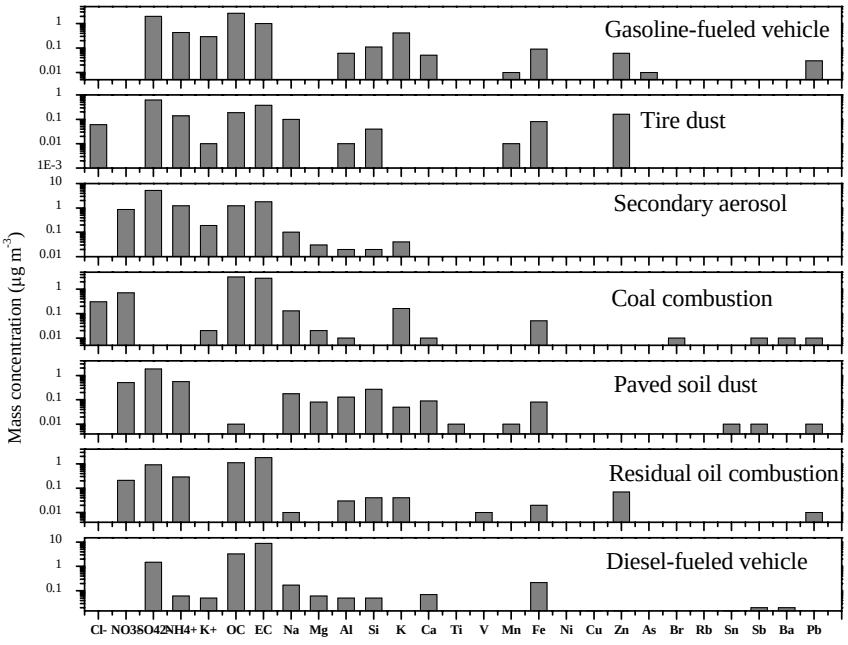

Figure 8.2 Source profiles for $PM_{2.5}$ in mass concentration.

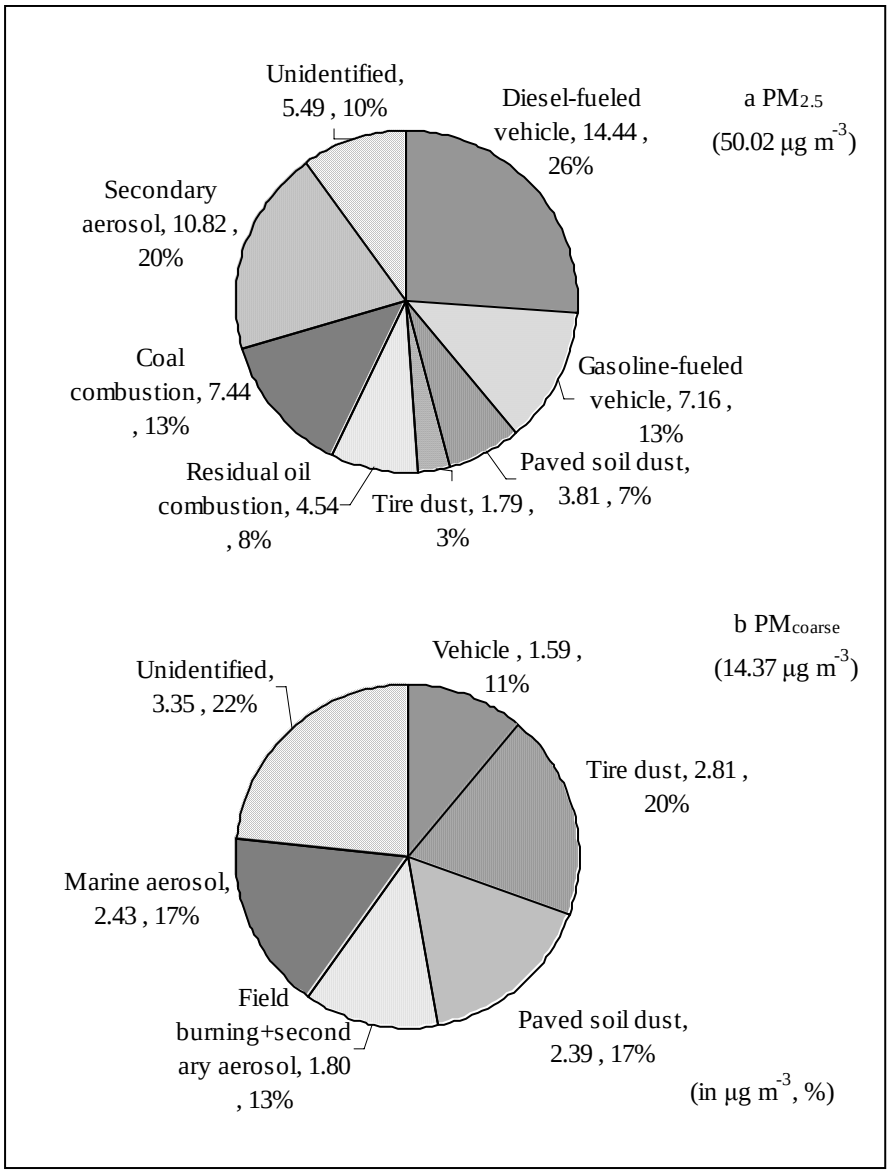

Figure 8.3 The average mass concentrations and percentages of identified sources for $PM_{2.5}$ (a) and PM_{coarse} (b).

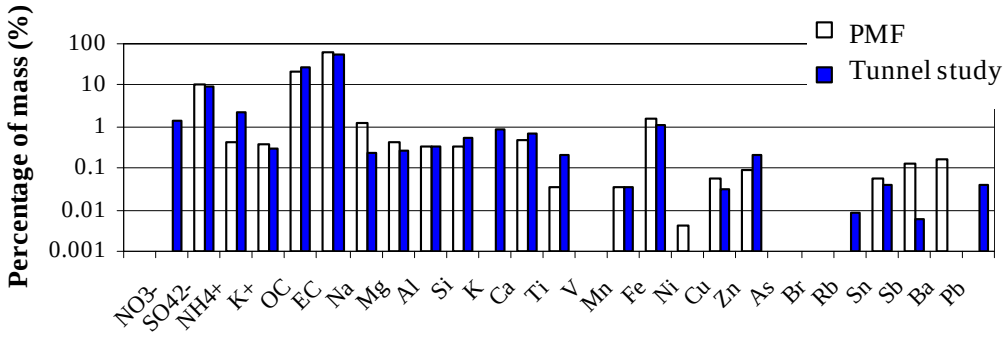

Figure 8.4 The comparison of chemical profiles for $PM_{2.5}$ in percentage between PMF and measurements.

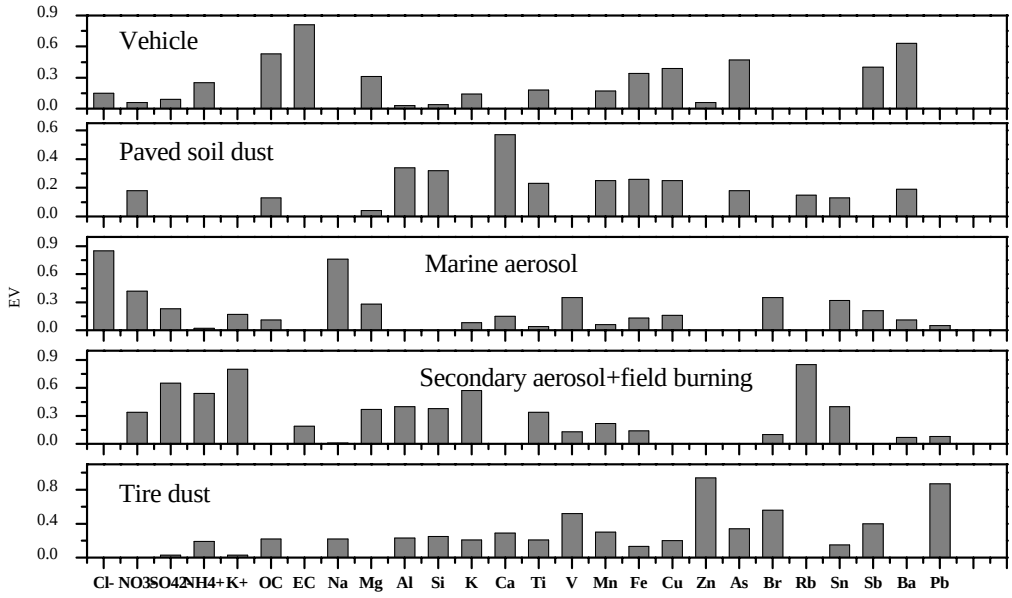

Figure 8.5 Source profiles for PM_{coarse} in EV values.

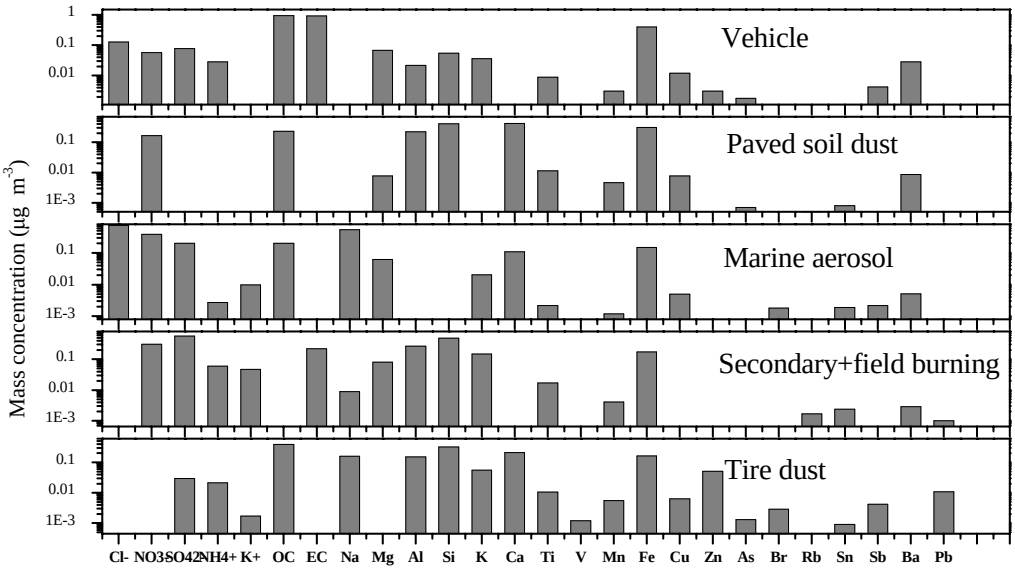

Figure 8.6 Source profiles for PM_{coarse} in mass concentration.

Table 8.1 $PM_{2.5}$ source contribution derived from CMB model.

Source	Case I Marine sector		Case II Continent sector	
	μg m^{-3}	% of mass	μg m^{-3}	% of mass
Vehicle emission	28.9 ± 7.7	72	42.9 ± 13.2	55
Paved road dust	0.0 ± 0.0	0	0.7 ± 2.5	1
Brake lining	0.3 ± 0.4	1	0.2 ± 0.0	0
Tire wear	0.0 ± 0.0	0	0.0 ± 0.0	0
Ammonium sulfate	0.2 ± 0.8	1	0.0 ± 0.0	0
Ammonium bisulfate	4.3 ± 1.9	11	11.0 ± 2.2	14
Ammonium nitrate	0.9 ± 0.4	2	4.5 ± 0.8	6
Coal combustion	3.9 ± 1.9	10	10.9 ± 2.7	14
Field burning	0.8 ± 0.7	2	7.2 ± 1.6	9
Residual oil combustion	0.0 ± 0.1	0	0.1 ± 0.1	0
Marine aerosol	0.4 ± 0.4	1	0.8 ± 1.0	1
Calculated mass	39.9 ± 6.2		78.3 ± 10.0	
Local sources[a]	29.3	73	43.9	56
Regional sources[b]	10.2	26	33.6	43
Unidentified	-3.0	-8	-4.4	-6
R	0.9		1.0	
Chi square	1.2		1.5	
Percent mass	108.1		104.2	

[a] Local sources include vehicle exhaust, paved road dust, brake lining, tire dust, and residual oil combustion.

[b] Regional sources include secondary aerosol, field burning, and coal combustion.

Table 8.2 $PM_{2.5}$ source contributions derived from two models for the entire analysis period.

Model	Annual			
	PMF		CMB	
	μg m^{-3}	%	μg m^{-3}	%
Vehicle emission	21.6	39	35.9	64
Paved road dust	3.2	7	0.3	0
Brake lining	0.0	0	0.3	1
Tire dust	1.8	3	0.0	0
Residual oil combustion	4.5	8	0.1	0
Secondary+field burning	10.8	20	14.5	22
Coal combustion	7.4	13	7.4	12
Marine aerosol	0.0	0	0.6	1
Local sources[a]	49.4	56	59.1	67
Regional sources[b]	18.3	33	21.9	39
Unidentified	5.5	10	-3.7	-7
Predicted $PM_{2.5}$ mass	67.6		81.0	
Measured $PM_{2.5}$ mass	55.5		55.5	

[a] Local sources include vehicle exhaust, paved road dust, brake lining, tire dust, and residual oil combustion.

[b] Regional sources include secondary aerosol, field burning, and coal combustion.

Chapter 9 Conclusion

This thesis employs several approaches to investigate the characteristics, influencing factors, and sources of airborne aerosols in the roadside environment in Hong Kong. Most of the field sampling is conducted at PU Supersite. A few sets of samples are collected at the Shing Mun Tunnel and HT station.

The sampling plan for this study is designed to obtain information on: 1) the chemical characteristics of fine and coarse particles with 24-hour chemically speciated $PM_{1.0}$, $PM_{2.5}$, and PM_{coarse} samples; 2) the effects of different vehicle categories, large-scale weather systems, and synoptic systems on Hong Kong aerosols with semi-continuous measurements for $PM_{2.5}$, BC and chemically speciated aerosols; 3) the chemical compositions and size distributions of ultrafine particles with size-fractioned particulates; 4) the emission factors and chemical profiles of on-road vehicles with the tunnel study; and 5) the contributions of various local and regional sources to fine and coarse particles at PU Supersite. Key findings of this study are summarized as below.

Investigation on the aerosol mass, chemical composition and OC/EC ratios at PU Supersite shows that fine particles have distinctive properties of vehicle emissions, while coarse particles have typical properties of marine aerosols and resuspensions

from road surface. On the other hand, PM_{10} is a poor indicator for coarse particulate pollution because PM_{10} reflects the properties of $PM_{2.5}$ rather than PM_{coarse}. With a high density of traffic and population in Hong Kong, the concentrations of atmospheric aerosols are higher than those in Europe and the USA.

The diurnal variations of fine aerosol mass are influenced by nearby sources at micro scale, namely the vehicle exhausts. The seasonal variations are affected by long-range-transported pollutants at continental scale under the prevailing winter monsoon. In addition, fine particulate episodes are formed sometimes due to the regional or long-range transport of air pollution under unfavorable synoptic systems. For PM_{coarse}, the hourly mass concentrations have positive relationships with both traffic volume and wind speed; the seasonal variations are less important because continental aerosols transported from Asian continent are enriched in the fine size fraction.

The study of aerosol chemical compositions in each scenario indicated substantial variations. Secondary aerosols such as sulfate, nitrate, and ammonium, are formed in the atmosphere, showing high loading when air masses are from the Asian continent. EC is mainly from the local vehicular exhaust, but the concentrations increase in summer due to combined effects of the local and transported pollutants from the container terminals in Hong Kong, and also occasionally from the PRD region. The

concentrations of fine mode OC indicate increase trend in cold seasons. On the other hand, coarse mode OC are evenly distributed through the whole year, suggesting there are stable local/regional sources. High concentrations of fine mode Cl^- are found in winter and low in summer, while the seasonal pattern is opposite for coarse mode Cl^-.

By examining the chemical composition and size distributions of ultrafine particles in summer and winter with size-fractionated samples, the typical properties of combustion coupled with insignificant seasonal variations are found. The concentration of ultrafine particle number at PU Supersite is very large, accounting for almost 85% of the total particle counts (7-217 nm). In addition, it is found that the elimination of PM_{10} or $PM_{2.5}$ mass only leads to the reduction of accumulation mode particle numbers rather than ultrafine particle numbers.

The number concentrations of ultrafine particle are influenced by the adjacent sources (exhausts from diesel-fueled vehicles in particular) at the micro scale, indicating good correlations with BC concentrations on a daily cycle basis. Mixing height is another influencing factor on the daily fluctuations of ultrafine particle number concentrations. The seasonal variations of ultrafine particle number appear to associate with the temperature, in which higher levels in winter and lower in summer.

To study the particulate emissions from vehicles with different fuels, the emission rates are calculated based on the tunnel measurements. It is found that the $PM_{2.5}$ emission rate for diesel-fueled vehicles is about 15-fold of the emission rate for gasoline-fueled vehicles. By comparing the chemical profiles between diesel- and gasoline-fueled vehicles, it is found that EC is the main component in particulate emissions from diesel-fueled vehicles, while OC is the major constituent in emissions from gasoline-fueled vehicles.

By using the PMF receptor model, the source contributions to $PM_{2.5}$ at PU Supersite are similar to the results estimated by the CMB receptor model. The majority of fine particulate mass (56-67%) is from the local source, including particulate emissions from motor vehicles, paved soil dust, brake lining, tire dust, and ships. The rest of particulate mass (33-39%) can be explained by the regional-scale transport of pollutants from Asian continent, including secondary aerosol, coal-combustion power plant, and field burning. When air masses are from the Asian continent, the contributions of regional sources could increase to about 50% even at the roadside environment. This indicates great impact of continental aerosols on Hong Kong air quality.

The source contributions to PM_{coarse} at PU Supersite are quantified by PMF receptor model. PM_{coarse} are mainly from local sources, about 20% from tire dust, 17% from paved soil dust, 11% from vehicles. Regional sources, like secondary aerosol and biomass burning, only contribute 13% of total coarse mass. In addition, marine aerosols occupy approximately 17% of total PM_{coarse} mass.

In summary, this study presents the characteristics and sources of the particulate emissions in different size ranges and their driven mechanism at the roadside environment in Hong Kong. Information on aerosol mass and chemical composition for ultrafine and coarse particles, which are quite limited resources in the past in Hong Kong, has been achieved in this study. Moreover, emission factors and chemical profiles are first established based on the local on-road vehicles during the Shing Mun tunnel study. Consequently the new chemical profiles for vehicles make the results of source apportionments by CMB model more scientifically reasonable. Although there are some weaknesses such as limited data sets during the summer case studies and several non-local source profiles existing in the CMB modeling, it has achieved its main objectives and shed light on the air pollution improvement in Hong Kong.

References

Aalto, P., Hameri, K., Paatero, P., Kulmala, M., Bellander, T., Berglind, N., Bouso, L., Castano-Vinyals, G., Sunyer, J., Cattani, G., Marconi, A., Cyrys, J., Klot, S., Peters, A., and Zetzsche, K., Lanki, T., Pekkanen, J., Nyberg, F., Sjovall, B., and Forastiere, F., 2005. Aerosol particle number concentration measurements in five European cities using TSI-3022 condensation particle counter over a three-year period during health effects of air pollution on susceptible subpopulations. Journal of Air & Waste Management Association 55, 1064-1076.

Adachi, K. and Yoshiaki T., 2004. Characterization of heavy metal particles embedded in tire dust. Environment International 30, 1009-1017.

Alam, A., Shi, J. P., and Harrison, R. M., 2003. Observations of new particle formation in urban air, Journal of Geophysics Research 108, doi:10.1029/2001JD001417.

Alander, T. J. A., Leskinen, A. P. Raunemaa, T. M., and Rantanen, L., 2004. Characterization of diesel particles: effects of fuel reformulation, exhaust aftertreatment, and engine operation on particle carbon composition and volatility. Environmental Science and Technology 38, 2707-2714.

Allen, G., Sioutas, C., Koutrakis, P., Reiss, R., Lurmann, F. W., and Roberts, P. T., 1997. Evaluation of theTEOM method for measurement of ambient particulate mass in urban areas. Journal of Air & Waste Management Association 47, 682-689.

Allen, J. O., Mayo, P. R., Hughes, L. S., Salmon, L. G., and Cass, G. R., 2001. Emissions of size-segregated aerosols from on-road vehicles in the Caldecott Tunnel. Environmental Science and Technology 35 (21), 4189-4197.

Arhami, M., Kuhn, T., Fine, P. M., Delfino, R. J., and Sioutas, C., 2006. Effects of sampling artifacts and operating parameters on the performance of a semicontinuous particulate elemental carbon/organic carbon monitor. Environmental Science and Technology 40, 945-954.

Ashbaugh, L. L., 1983. A statistical trajectory technique for determining air pollution source regions. Journal of Air Pollution Control Association 33, 1096-1098.

Ayers, G. P.; Keywood, M. D.; Gras, J. L., 1999. TEOM vs manual gravimetric methods for determination of $PM_{2.5}$ aerosol mass concentrations. Atmospheric Environment 33, 3717-3721.

Bassett, M. E. and Seinfeld, J. H., 1984. Atmospheric equilibrium model of sulfate and nitrate aerosols-II. Particle size analysis. Atmospheric Environment 18, 1163-1170.

Blando, J. D. and Turpin, B. J., 2000. Secondary organic aerosol formation in cloud and fog droplets: a literature evaluation of plausibility. Atmospheric Environment 34, 1623-1632.

Bruynseels, F. and Van Grieken R., 1985. Direct detection of sulfate and nitrate layer on sampled marine aerosol by laser microprobe mass analysis. Atmospheric Environment 19, 1969-1970.

Bukowiecki, N., Dommen, J., Prevot, A. S. H., Weingartner, E., and Baltensperger, U., 2003. Fine and ultrafine particles in the Zurich (Switzerland) area measured with a mobile laboratory: an assessment of the seasonal and regional variation throughout a year. Atmospheric Chemistry and Physics 3, 1477-1494.

Burnett, R. T., Brook, J., Dann, T., Delocla, C., Philips, O., Cakmak, S., Vincent, R., Goldberg, M. S., Krewski, D., 2000. Association between particulate- and gas-phase components of urban air pollution and daily mortality in eight Canadian cities. Inhalation Toxicology 12, 15-39.

Cabada, J. C., Rees, S., Takahama, S., Khlystov, A., Pandis, S. N., Davidson, C. I., and Robinson, A. L., 2004. Mass size distributions and size resolved chemical composition of fine particulate matter at the Pittsburgh Supersite. Atmospheric Environment 38, 3127-3141.

Cachier, H., Bremond,M.-P., and Buat-Menard, P., 1989. Carbonaceous Aerosols from different tropical biomass burning sources. Nature 340, 371-373.

Cadle, S.H., Mulawa, P.A., Ball, J., Donase, C., Weibel, A., Sagebiel, J.C., Knapp, K.T., and Snow, R., 1997. Particulate emission rates from in-use high-emitting vehicles recruited in Orange County, California. Environmental Science and Technology 31, 3405-3412.

Cao, J. J., Lee, S. C., Ho, K. F., Zhang, X. Y., Zou, S. C., Fung, K., Chow, J. C., and Watson, J. G., 2003. Characteristics of carbonaceous aerosol in Pearl River Delta Region, China during 2001 winter period. Atmospheric Environment 37, 1451-1460.

Cass, Glen R., Hughes, Lara A., Bhave, Prakash, Kleeman, Michael J., Allen, Jonathan O., and Salmon, and Lynn G., 2000. The chemical composition of atmospheric ultrafine particles. Philosophical Transactions of The Royal Society of London Series A 358, 2581-2592.

Chang, C. T., Tsai, C. J., Lee, C. T., Chang, S. Y., Cheng, M. T., and Chein, H. M., 2001. Differences in PM_{10} concentrations measured by β-gauge monitor and hi-vol sampler. Atmospheric Environment 35 (33), 5741–5748.

Chang, W. L. and Koo, E. H., 1986. A study of visibility trends in Hong Kong. Atmospheric Environment 20(10), 1847-1858.

Charlson, R. J., Lovelock, J. E., Andreae, M. O., and Warren, S. G., 1987. Oceanic phytoplankton, atmospheric sulfur, cloud albedo and climate. Nature 326, 655-661.

Charlson, R. J., Schwartz, S. E., Hales, J. M., Cess, R. D., Coakley, J. A., Hansen, J. E., and Hofmann, D. J., 1992. Climate forcing by anthropogenic aerosols. Science 255, 423-430.

Charron, A., Harrison, R.M., Moorcroft, S., and Booker, J., 2004. Quantitative interpretation of divergence between PM_{10} and $PM_{2.5}$ mass measurement by TEOM and gravimetric (Partisol) instruments. Atmospheric Environment 38(3), 415-423.

Charron, A., and Harrison, R. M., 2003. Primary particle formation from vehicle emissions during exhaust dilution in the roadside atmosphere. Atmospheric Environment 37 (29), 4109-4119.

Cheng, M. T. and Tsai, Y. I., 2000. Characterization of visibility and atmospheric aerosols in urban, suburban, and remote areas, The Science of Total Environment 263, 101-114.

Cheng, M. D., Hopke, P. K., Barrie, L., Rippe, A., Olson, M., Landsberger, S., 1993. Qualitative determination of source regions of aerosol in Canadian High Arctic. Environmental Science Technology 27, 2063-2071.

Cheng, Y., Lee, S. C., Ho, K. F., Wang, Y. Q., Cao, J. J., Chow, J. C., and Watson, J. G., 2006. Black carbon measurement in a coastal area of South China, Journal of Geophysical Research 111(D12310) doi:10.1029/2005JD006663.

Cheng, Z. L., Lam, K. S., Chan, L. Y., Wang, T., and Cheng, K. K., 2000. Chemical characteristics of aerosols at coastal stations in Hong Kong. I. Seasonal variation of major ions, halogens and mineral dusts between 1995 and 1996. Atmospheric Environment 34, 2771-2783.

Chin, P. C., 1986. Climate and weather. in A Geography of Hong Kong, edited by T. N. Chiu and C. L. So, pp. 69-85, Oxford University Press, New York.

Chow, J. C., Watson, J. G., Pritchett, L. C., Pierson, W. R., Frazier, C. A., and Purcell, R. G., 1993. The DRI thermal/optical reflectance carbon analysis system:

description, evaluation and applications in US air quality studies. Atmospheric Environment 27A (8), 1185-1201.

Chow, J. C., Watson, J. G., Lu, Z., Lowenthal, D. H., Frazier, C. A., Solomon, P.A., Thuillier, R. H., and Magliano, K. L., 1996a. Descriptive analysis of $PM_{2.5}$ at regionally representative locations during SJVAQS/AUSPEX. Atmospheric Environment 30(12), 2079-2112.

Chow, J. C., Watson, J. G., Lowenthal, D. H. and Countess, R. J., 1996b. Sources and chemistry of PM_{10} aerosol in Santa Barbara County, CA. Atmospheric Environment 30 (9): 1489-1499.

Chow, J. C. and Watson, J. G., 1998. Guideline on speciated particulate monitoring. Report, Prepared to Office of Air Quality Planning and Standards (MD-14), U.S. Environmental protection Agency, Reasrearch Triangle Park, NC 27711.

Chow, J. C. and Watson, J. G., 1999. Ion chromatography in elemental analysis of airborne particles. In Landsberger S.; Creatchman, M., eds. Elemental Analysis of Airborne Particles. Gordon and Breach Science, Amsterdam. 1:97-137.

Chow, J. C., Watson, J. G., Chen, L. W. A., Arnott, W. P., Moosmüller, H., and Fung, K., 2004. Equivalence of elemental carbon by thermal/optical reflectance and

transmittance with different temperature protocols. Environmental Science and Technology 38(16), 4414-4422.

Chow, J. C., Watson, J. G., Louie, P. K. K., Chen, L. W. A., and Sin, D., 2005. Comparison of $PM_{2.5}$ carbon measurement methods in Hong Kong, China. Environmental Pollution 137(2), 334-344.

Chueinta, W., and Hopke, P.K., 2001. Beta gauge for aerosol mass measurement. Aerosol Science and Technology 35(4), 840-843.

Chueinta, W., Hopke, P. K., and Paatero, P., 2000. Investigation of source of atmospheric aerosol at urban and suburban residential areas in Thailand by positive matrix factorization. Atmospheric Environment 34, 3319-3329.

Claes, M., Gysels, K., Grieken, R. V., and Harrison, R. M., 1998. Inorganic composition of atmospheric aerosols, In Atmospheric Particles, edited by Harrison, R. M. and Grieken, R. Van, John Wiley&Sons Ltd.

Cohen, D. D., Garton, D., Stelcer, E., Hawas, O., Wang, T., Poon, S., Kim, J., Choi, B. C., Oh, S. N., Shin H. J., Ko, M. Y., and Uematsu, M., 2004. Multielemental analysis and characterization of fine aerosols at several key ACE-Asia sites, Journal of Geophysics Research 109(D19S12), doi:10.1029/2003JD003569.

Core, J. E., et al., 1989. Receptor modeling source profile development for the Pacific Northwest States; The Pacific Northwest Source Profile Library, Volume 3 - Project Final Report. State of Oregon Department of Environmental Quality, Portland, Oregon.

Councell, T. B., Duckenfield, K. U., Landa, E. R., and Callender, E., 2004. Tire-wear particles as a source of Zinc to the environment. Environmental Science and Technology 38, 4206-4214.

Countess, R. J., Wolff, G. T., and Cadle, S. H., 1980. The Denver winter aerosol: A comprehensive chemical characterization. Journal of Air Pollution Control Association 30, 1194-1200.

Dockery, D. W., Arden, P. C., Xu, X. P., Spengler, J. D., Ware, J. H., Fay, M. E., Ferris, B. G., and Speizer, F. E., 1993. An association between air pollution and mortality in six U.S. cities. The New England Journal of Medicine 329(24), 1753-1759.

Dockery, D.W., Schwartz, J., and Spengler, D., 1992. Air pollution and daily mortality: associations with particulates and acid aerosols. Environmental Research 59, 362-373.

Donaldson, K., Li, X. Y., and MacNee, W., 1998. Ultrafine (nanometre) particle mediated lung injury. Journal of Aerosol Science 29(5/6), 553-560.

Draxler, R. R. and Hess, G. D., 1997. Description of the HYSPLIT_4 Modeling System. Report No. NOAA Technical Memorandum ERL ARL-224. National Oceanic and Atmospheric Administration, Air Resources Laboratory, Silver Spring, MD, (http://www.arl.noaa.gov/data/models/hysplit4/win95/arl-224.phf).

Draxler, R. R. and Hess, G. D., 1998. An overview of the HYSPLIT-4 modeling system for trajectories, description, and deposition. Australian Meteorological Magazine 47, 295-308.

Eldering, A. and Cass, G. R., 1996. Source-oriented model for air pollutant effects on visibility. Journal of Geophysical Research, 101(D14), 19343-19370.

Engelbrecht, J. P., Swanepoel, L., Chow, J. C., Watson, J. G., and Egami, R. T., 2001. $PM_{2.5}$ and PM_{10} concentrations from the Qalabotjha low-smoke fuels macro-scale experiment in South Africa. Environmental Monitoring and Assessment 69(1), 1-15.

Facchini, M. C., Mircea, M., Fuzzi, S., and Charlson, R. J., 1999. Cloud albedo enhancement by surface-active organic solutes in growing droplets. Nature 401, 257-259.

Ferin, J., Oberdorster, G., and Penney, D. P., 1992. Pulmonary retention of ultrafine and fine particles in rats. American Journal of Respiratory Cell and Molecular Biology 6, 535-542.

Fine, P. M., Shen, S., and Sioutas, C., 2004. Inferring the sources of fine and ultrafine particulate matter at downwind receptor sites in the Los Angeles Basin using multiple continuous measurements. Aerosol Science and Technology 38(S1), 182-195.

Fitz, D. R., 1990. Reduction of the positive organic artifact on quartz filters. Aerosol Science and Technology 12(1), 142-148.

Fitzgerald, J. W., 1991. Marine aerosols: a review. Atmospheric Environment 25A(3/4), 533-545.

Fraser, M. P., Cass, G. R., and Simoneit, B. R. T., 1998. Gas-phase and particle-phase organic compounds emitted from motor vehicle traffic in a Los Angeles roadway tunnel. Environmental Science and Technology 32, 2051-2060.

Fung, Y. S. and Wong, L. W. Y., 1995. Apportionment of air pollution sources by receptor models in Hong Kong. Atmospheric Environment 29, 2041-2018.

Gao, N., Cheng, M.D., Hopke, P.K., 1994. Receptor modeling for airborne ionic species collected in SCAQSs, 1987. Atmospheric Environment 28, 447-1470.

Gao, N., Hopke, P.K., Reid, N.W., 1996. Possible sources for some trace elements found in airborne particles and precipitation in Dorset, Ontario. Journal of the Air and Waste Management Association 46, 1035-1047.

Gauderman, W. J., McConnell, R., Gilliland, F., London, S., Thomas, D., Avol, E., Vora, H., Berhane, F., Margolis, H. G., and Peters, J., 2000. Association between air pollution and lung function growth in Southern California Children. American Journal of Respiratory Cell and Molecular Biology 162 (4 Pt 1), 1383-1390.

Geller, M. D., Kim, S., Misra, C., Sioutas, C., Olson, B. A., and Marple, V. A., 2002. A methodology for measuring size-dependent chemical composition of ultrafine particles. Aerosol Science & Technology 36(6), 748 - 762.

Gertler, A. W., Wittorff, D. N., Mclaren, R., Belzer, W., and Dann, T., 1997. Characterization of vehicle emissions in Vancouver BC during the 1993 lower FRASER valley oxidants study. Atmospheric Environment 31(14), 2107-2112.

Gertler, A. W., Gillies, J. A., Pierson, W. R., Rogers, C. F., Sagebiel, J. C., Abu-Allaban, M., Coulombe, W., Tarnay, L., Cahill, T. A., Grosjean, D., and Grosjean E., 2002. Emissions from diesel and gasoline engines measured in highway tunnels. Health Effects Institute, Boston MA USA. Capital City Press,

Montpelier VT.

Gillies J. A., Gertler A. W., Sagebiel J. C., and Dippel, W. A., 2001. On-road particulate matter ($PM_{2.5}$ and PM_{10}) emissions in the Sepulveda Tunnel, Los Angeles, California. Environmental Science and Technology 35 (6), 1054-1063.

Goyer, R. A., 1986. Toxic effects of metals, in Toxicology, Klaassen, C.D., Amdur, M.O., Doull, J. Eds., New York: Macmillan, 582-635.

Graham, B., Guyon, P., Taylor, P. E., Artaxo, P., Glovsky, M. M., Glagan, R. C., and Andreae, M. O., 2003. Organic compounds present in the natural Amazonian aerosol: Characterization by gas chromatography-mass spectrometry. Journal of geophysical research 108 (D24).

Gray, H. A., Cass, G. R., Huntzicker, J. J., Heyerdahl, E. K. and Rau, J. A., 1986. Characteristics of atmospheric organic and elemental carbon particle concentrations in Los Angeles. Environmental Science and Technology 20, 580-589.

Gray, H. A. and Cass, G. R., 1998. Source contributions to atmospheric fine carbon particle concentrations. Atmospheric Environment 32, 3805-3825.

Grosjean D. and Friedlander S. K., 1975. Gas-particle distribution factors for organic and other pollutants in Los-Angeles atmosphere, Journal of Air Pollution Control Association 25 (10), 1038-1044.

Gundel, L. A., Dod, R. L., Rosen, H., and Novakov, T., 1984. The relationship between optical attenuation and black carbon concentration for ambient and source particles, The Science of Total Environment 36, 197-202.

Hamilton, R. S. and Mansfield, T. A., 1991. Airborne particulate elemental carbon: its sources, transport and contribution to dark smoke and soiling. Atmospheric Environment 25A(3/4),715-723.

Hansen, A. D. A., Bodhaine, B. A., Dutton, E. G. and Schnell, R. C., 1988. Aerosol black carbon measurements at the South Pole: initial results 1986-1987. Geophysical Research Letters 15(11), 1193-1196.

Hansen, A. D. A. and Rosen, H., 1990. Individual measurements of the emission factor of aerosol black carbon in automobile plumes. Journal of Air Waste Management Association 40, 1645-1657.

Harris, S. J. and Maricq M. M., 2001. Signature size distributions for diesel and gasoline engine exhaust particulate mater, Journal of Aerosol Science 32, 794-764.

Harrison, R. M., Jones, M., and Collins G., 1999. Measurements of the physical properties of particles in the urban atmosphere. Atmospheric Environment 33, 309-321.

Harrison, R. M., Shi, J. P., Xi, S. H., Khan, A., Mark, D., Kinnersley R., and Yin, J. X., 2000. Measurement of number, mass and size distribution of particles in the atmosphere. Philosophical Transactions of The Royal Society of London Series A 358, 2567-2580.

Harrison, R. M., 2004. Key pollutants-airborne particles, The Science of the Total Environment 334-335, 3-8.

Harvey, L. D. D., 1988. On the role of high latitude ice, snow, and vegetation feedbacks in the climatic response to external forcing changes. Climatic Change 13(2), 191-224.

Haywood, J. M. and Shine, K. P., 1995. The effect of anthropogenic sulfate and soot aerosol on the clear sky planetary radiation budget. Geophysics Research Letter 22(5), 603-606.

Heintzenberg, J. and Winkler, P., 1984. Elemental carbon in the urban aerosol: results of a seventeen month study in Hamburg, FRG. The Science of the Total Environment 36, 27-38.

Hering, S. V. and Friedlander, S. K., 1982. Origins ofaerosol sulfur size distributions in the Los Angeles basin. Atmospheric Environment 16, 2647-2656.

Hering S., Eldering A., and Seinfeld J. H., 1997. Bimodal character of accumulation mode aerosol mass distributions in Southern California. Atmospheric environment 31 (1), 1-11.

Hildemann, L. M., Markowski, G. R., Jones, M. C., and Cass, G. R., 1991a. Submicrometer aerosol mass distributions of emissions from boilers, fireplaces, automibiles, diesel trucks, and meat-cooking operations. Aerosol Science and Technology 14, 138-152.

Hildemann, L. M., Markowski, G. R., and Cass, G. R., 1991b. Chemical composition of emissions from urban sources of fine organic aerosol. Environmental Science and Technology 25, 744-759.

Hitzenberger, R., Berner, A., Galambos, Z., Maenhaut, W., Cafmeyer, J., Schwarz, J., Muller, K., Spindler, G., Wieprecht, W., Acker, K., Hillamo, R., and Makela, T., 2004. Intercomparison of methods to measure the mass concentration of the atmospheric aerosol during INTERCOMP2000-Influence of instrumentation and size cuts. Atmospheric Environment 38, 6467-6476.

HKEPD, 2007. A study on profiles of cooking fumes in Hong Kong. 2007.

Ho, K. F., Lee, S. C., Chan, C. K., Yu, J. C., Chow, J. C., and Yao, X. H., 2003a. Characterization of chemical species in $PM_{2.5}$ and PM_{10} aerosols in Hong Kong. Atmospheric Environment 37, 31-39.

Ho, H. F., Lee, S. C., Chow, J. C., and Watson, J. G., 2003b. Characterization of PM_{10} and $PM_{2.5}$ source profiles for fugitive dust in Hong Kong. Atmospheric Environment 37, 1023-1032.

Hogrefe, O., Schwab, J. J., Drewnick, F., Lala, G. G., Peters, S., Demerjian, K. L., Rhoads, K., Felton, H. D., Rattigan, O. V., Husain, L., and Dutkiewicz, V. A., 2004. Semicontinuous $PM_{2.5}$ sulfate and nitrate measurements at an urban and a rural location in New York: PMTACS-NY Summer 2001 and 2002 Campaigns. Journal of Air & Waste Management Association 54(9), 1040-1060.

Hopke, P.K., Barrie, L.A., Li, S.-M., Li, C., Cheng, M.-D., Xie, Y., 1995. Possible sources and preferred pathways for biogenic and non-seasalt sulfur for the high Arctic. Journal of Geophysical Research 100, 16595-16603.

Horak Jr., F., Frischer, T., Studnicka, M., Gartner, C., Hauck, H., and Preining, O., 2001. The chemical composition of particulate matter has a short term effect on

the lung-function of pre-school children. European Respiratory Journal 18 (Suppl. 33), 128.

Howes, J. E., Cooper, J. A., and Houck, J. E., 1983. Sampling and analysis to determine source signatures in the Philadelphia area. Draft Final Report to U. S. Environmental Protection Agency, ESRL, Research Triangle Park, NC. NEA, Inc.

Hughes, L. S., Cass, G. R., Gone, J., Ames, M., and Olmez, I., 1998. Physical and chemical characterization of atmospheric ultrafine particles in the Los Angeles Area. Environmental Science and Technology 32(9), 1153-1161.

Hussein, T., Puustinen, A., Aalto, P. P., Makela, J. M., Hameri, K., and Kulmala, M., 2003. Urban aerosol number size distributions. Atmospheric Chemistry and Physics Discussion 3, 5139-5184.

Jacobson, M. Z., 2001. Strong radiative heating due to the mixing state of black carbon in atmospheric aerosols. Nature 409(6821), 695-697.

Jacobson, M. Z., 2002. Control of fossil-fuel particulate black carbon and organic matter, possibly the most effective method of slowing global warming. Journal of Geophysics Research 107(D19), 4410.

Jamriska, M., Morawska, L., Thomas, S., and He, C. R., 2004. Diesel bus emissions

measured in a tunnel study. Environmental Science and Technology 38 (24), 6701-6709.

John, W., Wall, S. M., Ondo, J. L., and Winklmayr, W., 1990. Modes in the size distributions ofatmospheric inorganic aerosol. Atmospheric Environment 24A, 2349-2359.

Jones, A. M. and Harrison, R. M., 2005. Interpretation of particulate elemental and organic carbon concentraitons at rural, urban and kerbside sites. Atmospheric Environment 39(37), 7114-7126.

Kaneyasu, N. and Murayama, S., 2000, High concentrations of black carbon over middle latitudes in the North Pacific Ocean, Journal of Geophysics Research 105(D15), 19881-19890.

Katsouyanni, K., Touloumi, G., Samoli, E., Gryparis, A., Le Terte, A., and Monopolis, Y., 2001. Confounding and effect modification in the short-term effects of ambient particles on total mortality: results from 29 European cities within the APHEA2 project. Epidemiology 12, 521-531.

Kerminen, V. M. and Wexler, A. S., 1995. Growth laws for atmospheric aerosol particles: an examination of the bimodality of the accumulation mode. Atmospheric Environment 29, 3263-3275.

Ketzel, M. and Berkowicz, R., 2004. Modelling the fate of ultrafine particles from exhaust pipe to rural background: an analysis of time scales for dilution, coagulation and deposition. Atmospheric Environment 38, 2639-2652.

Keywood, M. D., Ayers, G. P., Gras, J. L. Gillett, R. W., and Cohen, D. D., 1999. Relationships between size segregated mass concentration data and ultrafine particle number concentrations in urban areas. Atmospheric Environment 33, 2907-2913.

Kim E., Hopke, P. K., and Edgerton, E. S., 2003. Source identification of Atlanta aerosol by positive matrix factorization. Journal of Air & Waste Management Association 53, 731-739.

Kim, E., Hopke, P. K., Larson, T. V., and Covert, D. S., 2004. Analysis of ambient particle size distributions using Unmix and Positive matrix Factorization. Environmental Science and Technology 38, 202-209.

Kim, S., Shen, S., Sioutas, C., Zhu, Y. F., and Hinds, W. C., 2002. Size distribution and diurnal and seasonal trends of ultrafine particles in source and receptor sites of the Los Angeles Basin. Journal of Air & Waste Management Association (52), 297.

Kirchstetter, T. W., Corrigan, C. E., and Novakov, T., 2001. Laboratory and field investigation of the adsorption of gaseous organic compounds onto quartz filters, Atmospheric Environment 35(9), 1663-1671.

Kirchstetter, T., Novakov, T., Hobbs, P. V., and Magi, G., 2003. Airborne measurements of carbonaceous aerosols in southern Africa during the dry biomass burning season. Journal of Geophysics Research 108 (D13), 8476, doi:10.1029/2002JD002171.

Kittelson, D. B., 1998. Engines and nanoparticles: a review. Journal of Aerosol Science 29(5/6), 575-588

Kittelson, D. B., Watts, W. F., and Johnson, J. P., 2004. Nanoparticle emissions on Minnesota highways. Atmospheric Environment 38, 9-19.

Klingenberg, H. and Winneke, H., 1990. Studies on health effects of automotive exhaust emissions, how dangerous are diesel emissions? The Science of Total Environment 93, 95-105.

Köhler, I., Dameris, M., Ackermann, I. and Hass, H., 2001. Contribution of road traffic emissions to the atmospheric black carbon burden in the mid-1990s. Journal of Geophysics Research 106(D16), 17997-18014.

Kupiainen, K. J., Tervahattu, H., Raisanen, M., Makela, T., Aurela, M., and Hillamo, R., 2005. Size and composition of airborne particles from pavement wear, tires, and traction sanding. Environmental Science and Technology 39 (3), 699-706.

Lam, G. C. K., Leung, D. Y. C., Niewiadomski, M., Pang, S. W., Lee, A. W. F., and Louie, P. K. K., 1999. Street level concentrations of nitrogen dioxide and suspended particulate matter in Hong Kong. Atmospheric Environment 33, 1-11.

Langner, J. and Rodhe, H., 1991. A global three-dimensional model of the tropospheric sulfur cycle. Journal of Atmospheric Chemistry 13, 225-264.

Laschober C., Limbeck A., Rendl. J., and Puxbaum H., 2004. Particulate emissions from on-road vehicles in the Kaisermühlen-tunnel (Vienna, Austria). Atmospheric Environment 38, 2187-2195.

Lee S. C., Cheng, Y., Ho, K. F., Cao, J. J., Louie P. K-K., Chow, J. C., and Watson, J. G., 2006. $PM_{1.0}$ and $PM_{2.5}$ characteristics in the roadside environment of Hong Kong. Aerosol Science and Technology 40, 157-165.

Lee, E., Chan, C. K., and Paatero, P., 1999. Application of positive matrix factorization in source apportionment of particulate pollutants in Hong Kong. Atmospheric Environment 33, 3201-3212.

Li, N., Sioutas, C., Cho, A., Schmitz, D., Misra, C., Sempf, J., Wang, M. Y., Oberley, T., Froines, J., and Nel, A., 2003. Ultrafine particulate pollutants induce oxidative stress and mitochondrial damage. Environmental Health Perspectives 111, 455-460.

Lin, C. C., Chen S. J., Huang, K. L., Hwang, W. I., Chang-chien G. P., and Lin, W. Y., 2005. Characteristics of metals in nano/ultrafine/fine/coarse Particles collected beside a heavily trafficked road. Environmental Science and Technology 39 (21), 8113-8122.

Lough, G. C., Schauer, J. J., Park, J. S., Shafer, M. M., Deminter, J. T., and Weinstein, J. P., 2005. Emissions of metals associated with motor vehicle roadways. Environmental Science and Technology 39, 826-836.

Louie, P. K. K., Chow, J. C., Chen, L. W. A., Watson, J. G., Leung G. and Sin, D. W. M., 2005a. $PM_{2.5}$ chemical composition in Hong Kong: urban and regional variations. The Science of Total Environment 338, 267-281.

Louie, P. K-K., Leung, G. S. P., Yeung, B. T. W., Sin D. W. M., Yu J. Z., Lau A., Bergin, M., Zheng, M., Chow J., and Watson , J., 2002. Twelve-month particulate matter study in Hong Kong, Final report to Hong Kong Environmental Protection Department.

Louie, P. K-K. Watson, J. G., Chow, J. C., Chen, L-W. A., D. Sin, W-M., and Lau, A. K-H., 2005b. Seasonal characteristics and regional transport of $PM_{2.5}$ in Hong Kong, Atmospheric Environment 39(9), 1695-1710.

Lowenthal, D. H., Zielinska, B., Chow, J. C., Watson, J. G., Gautam, M., Ferguson, D. H., Neuroth, G. R., and Stevens, K. D., 1994. Characterization of heavy-duty diesel vehicle emissions. Atmospheric Environment 28(4), 731-743.

Mage, D., Ozolins, G., Peterson, P., Webster, A., Orthofer, R., Vandeweerd, V., and Gwynne, M., 1996. Urban air pollution in megacities of the world. Atmosphere Environment 30, 681-686.

Malm, W. C., Johnson, C. E. and Bresch, J. F., 1986. Application of principal component analysis for purposes of identifying source-receptor relationships in receptor methods for source apportionment, Pace, T.G., ed., Air Pollution Control Association Pittsburgh, PA, 127-148.

Mamane, Y., Stevens, R. K., and Dzubay, T. G., 1990. On the sources of fine and coarse carbon particles in the Great Lakes. Journal of Aerosol Science 21, S353-S356.

Manoli, E., Voutsa, D., and Samara, C., 2002. Chemical characterization and source identification/apportionment of fine and coarse air particles in Thessaloniki, Greece. Atmospheric Environment 36, 949-961.

Mar, T. F., Larson, T. V., Stier, R. A., Claiborn, C., and Koenig, J. Q., 2004. An analysis of the association between respiratory symptoms in subjects with asthma and daily air pollution in Spokane, Washintong. Inhalation Toxicology 16, 809-815.

Mar, T. F., Norris, G. A., Koenig, J. Q., and Larson, T. V., 2000. Associations between air pollution and mortality in Phoenix, 1995-1997. Environmental Health Perspectives 108, 347-353.

Maricq, M. M., Podsiadlik, D. H., and Chase, R. E., 2000. Size distributions of motor vehicle exhaust PM: a comparison between ELPI and SMPS measurements. Aerosol Science and Technology 33, 239-260.

Marple, V. A., Rubow, K. L., and Behm, S. M., 1991. A microorifice uniform deposit impactor (MOUDI): description, calibration, and use. Aerosol Science and Technology 14, 434-446.

Mathis, U., Mohr, M., and Forss, A. M., 2005. Comprehensive particle characterization of modern gasoline and diesel passenger cars at low ambient temperatures. Atmospheric Environment 39, 107-117.

McMurry, P. H. and Wilson, J. C., 1983. Droplet phase (heterogeneous) and gas phase (homogeneous) contribution to secondary ambient aerosol formation as functions of relative humidity. Journal of Geophysics Research 88, 5101-5108.

Meng Z. and Seinfeld J. H., 1994. On the source of the submicrometer droplet mode of urban and regional aerosols. Aerosol Science and Technology 20, 253-265.

Meng, Z., Seinfeld, J., Saxena, P., and Kim, Y., 1995. Contribution of water to particulate mass in the South Coast Air Basin. Aerosol Science and Technology 22, 111-123.

Metzger, K. B., Tolbert, P. E., Klein, M., Peel, J. L., Flanders, W. D., Todd, K., Mulholland, J. A., Ryan, P. B., and Frumkin, H., 2004. Ambient air pollution and cardiovascular emergency department visits. Epidemiology 15, 46-56.

Moeckli, M. A., Fierz, M., and Sigrist, M. W., 1996. Emission factors for ethene and ammonia from a tunnel study with a photoacoustic trace gas detection system. Environmental Science and Technology 30 (9), 2864-2867.

Molnár P., Janhall, S., and Hallquist, M., 2002. Roadside measurements of fine and ultrafine particles at a major road north of Gothenburg. Atmospheric Environment 36(25), 4115-4123.

Moosmuller, H., Arnott, W. P., Rogers, C. F., Bowen, J. L., Gillies, J. A., Pierson, W. R., Collins, J. F., Durbin, T. D., and Norbeck, J. M., 2001. Time resolved characterization of diesel particulate emissions. 1. instruments for particle mass measurements. Environmental Science and Technology 35, 781-787.

Morawska, L., Bofinger, N. D., Kocis, L., and Nwankwoala, A., 1998. Submicrometer and supermicrometer particles from diesel vehicle emissions. Environmental Science and Technology 32, 2033-2042.

Mulawa, P. A., Cadle, S. H., Knapp, K., Zweidinger, R., Snow, R., Lucas R., and Goldbach, J., 1997. Effect of ambient temperature and E-10 fuel on primary exhaust particulate matter emissions from light-duty vehicles. Environmental Science and Technology 31, 1302-1307.

Natusch, D. F. S. and Wallace, J. R., 1974. Urban aerosol toxicity: the influence of particle size. Science 186(4165), 695-699.

Novakov, T., Chang, S. G., and Harker, A. B., 1974. Sulfates as pollution particulates: catalytic formation on carbon (soot) particles. Science 186(4160), 259-261.

Novakov, T., 1984. The role of soot and primary oxidants in atmospheric chemistry. The Science of Total Environment 36, 1-10.

Novakov, T. and Penner, J. E., 1993. Large contribution of organic aerosols to cloud-condensation-nuclei concentrations. Nature 365, 823-826.

Norbeck, J. M., Durbin, T. D., and Truex, T. J., 1998. Measurement of primary particulate matter emissions from light-duty motor vehicles. Report to the coordinating research council under CRC Project No. E-24-2, by Center for Environmental Research and College of Engineering Technology (CE-CERT), U.C., Riverside, CA.

Novakov, T., Menon, S., Kirchstetter, T. W., Koch, D., Hansen, J. E., 2005. Aerosol Organic Carbon to Black Carbon Ratios: Analysis of Published Data and Implications for Climate Forcing. Journal of Geophysical Research 110, D21205, doi:10.1029/2005JD005977.

Nriagu, J. O. and Pacyna, J. M., 1988. Quantitative assessment of worldwide contamination of air, water and soils by trace metals. Nature 333, 134-139.

Oberdörster, G., Gelein, R., Ferin, J. and Weiss, B., 1995. Association of particulate air pollution and acute mortality: involvement of ultrafine particles. Inhalation Toxicology 71, 111-124.

Oberdörster, G., 2001. Pulmonary effects of inhaled ultrafine particles. International Archives of Occupational and Environmental Health 74, 1-8.

Oberdörster, G., Oberdörster, E., and Oberdörster, J., 2005. Nanotoxicology: An studies of ultrafine particles. Environmental Health Perspectives 113(7), 823-839.

Ogren, J. A., Groblicki, P. J., and Charlson, R. J., 1984. Measurement of the removal rate of elemental carbon from the atmosphere. The Science of Total Environment 36, 329-338.

Ogren, J. A. and Charlson, R. J., 1983. Elemental carbon in the atmosphere: cycle and lifetime. Tellus 35B, 241-254.

Paatero, P. and Hopke, P. K., 2003. Discarding or downweighting high-noise variables in factor analytic models. Analytica Chimica Acta 490(1), 277-289.

Pakkanen, T. A., Kerminen, V. M., Korhonen, C. H., Hillamo, R. E., Aarnio, P., Koskentalo, T., and Maenhaut, W., 2001. Urban and rural ultrafine ($PM_{0.1}$) particles in the Helsinki area. Atmospheric Environment 35, 4593-4607.

Pandis, S. N., Harley, R. A., Cass, G. R., and Seinfeld, J. H., 1992. Secondary organic aerosol formation and transport. Atmospheric Environment 26A(13), 2269-2282.

Pandis, S. N., Wexler, A. S., and Seinfeld, J. H., 1993. Secondary organic aerosol formation and transport-II, predcting the ambient secondary organic aerosol size distribution. Atmospheric Environment 27A(15), 2403-2416.

Park, K., Kittelson, D. B., Zachariah, M. R., and McMurry, P. H., 2004. Measurement of inherent material density of nanoparticle agglomerates. Journal of Nanoparticle Research 6, 267-272.

Pathak, R. K., Yao, X. H., Lau, A. K.H., and Chan, C. K., 2003. Acidity and concentrations of ionic species of $PM_{2.5}$ in Hong Kong. Atmospheric Environment 37, 1113-1124.

Patterson, C. C. and Gillette, D. A., 1977. Commonalities in measured size distributions for aerosols having a soil-derived component. Journal of Geophysics Research 82, 2074-2082.

Penner, J. E., Dickinson, R. E., O'Neill, C. A., 1992. Effects of aerosol from biomass burning on the global radiation budget. Science 256, 1432-1433.

Pierson, W. R. and Brachaczek, W. W., 1983. Particulate matter associated with vehicles on the road II. Aerosol Science and Technology 2, 1-40.

Pierson, W. R., Gertler, A. W., Robinson, N. F., Sagebiel, J. C., Zielinska, B., Bishop, G. A., Stedman, D. H., Zweidinger, R. B., and Ray, W. D., 1996. Real-world

automotive emissions-summary of studies in the fort McHenry and Tuscarora mountain tunnels. Atmospheric Environment 30(12), 2233-2256.

Polissar, A. V., Hopke, P. K., and Poirot, R. L., 2001. Atmospheric aerosol over vermont: chemical composition and sources. Environment Science and Technology 35, 4604-4621.

Polissar, A. V., Hopke, P. K., Malm, W. C., and Sisler, J. F., 1998. Atmospheric Aerosol over Alaska: 2. Elemental Composition and Sources, Journal of Geophysical Research 103, 19045-19057.

Pope III, C. A. and Dockery, D. W., 2006. A summary of the 2006 critical review: health effects of fine particulate air pollution. EM, A&WMA's Magazine for Environmental Managers June 2006, 30-35.

Puxbaum, H. and Wopenka, B., 1984. Chemical composition of nucleation and accumulation mode particles collected in Vienna, Austria. Atmospheric Environment 18(3), 573-580.

Qin, Y., Chan, C. K., and Chan, L.Y., 1997. Characteristics of chemical compositions of atmospheric aerosols in Hong Kong: spatial and seasonal distributions. The Science of the Total Environment 206, 25-27.

Qin, Y., Oduyemi, K., and Chan, L. Y., 2002. Identification of sources of Phoenix aerosol by positive matrix factorization. Journal of Air and Waste Management Association 50, 1308-1320.

Reisen, F. and Arey, J., 2005. Atmospheric reactions influence seasonal PAH and nitro-PAH concentrations in the Los Angeles basin. Environmental Science and Technology 39, 64-73.

Ristovski, Z. D., Morawska, L., Bofinger, N. D., and Hitchins, J., 1998. Submicrometer and supermicrometer particulate emission from spark ignition vehicles. Environmental Science and Technology 32(24), 3845-3852.

Ristovski, Z. D., Morawska, L., Hitchins, J., Thomas, S., Greenaway, C., and Gilbert, D., 2000. Emissions from compressed natural gas engines. Journal of Aerosol Science 31(4), 403-413.

Rodhe, H., 1999. Clouds and climate. Nature 401, 223-225.

Rogers, C. F., Watson, J. G., Day, D., and Oraltay, R. G., 1998. Real-time liquid water mass measurement for airborne particulates. Aerosol Science and Technology 29, 557-562.

Rogge, W. F., Hildemann, L. M., Mazurek, M. A., and Cass, G. R., 1993a. Sources of fine organic aerosol 3. Roaddust, tire debris and organometallic brake lining dust:

roads as sources and sinks. Environmental Science and Technology 27, 1892-1904.

Rogge, W. F., Hildemann, L. M., Mazurek, M. A., and Cass, G. R., 1993b. Sources of fine organic Aerosol 4. Particulate abrasion products from leaf surfaces of urban plants. Environmental Science and Technology 27, 2700-2711.

Rosen, H. and Hansen, A. D. A., 1984. Role of combustion generated carbon particles in the absorption of solar radiation in Arctic haze. Geophysical Research Letters 11, 461-464.

Russell, A. G., McRae, G. J., and Cass, G. R., 1983. Mathematical modeling of the formation and transport of ammonium nitrate aerosol. Atmospheric Environment 17, 949-956.

Salter, L. F. and Parsons, B., 1999. Field trials of the TEOM and partisol for PM_{10} monitoring in the St Austell china clay area, Cornwall, UK. Atmospheric Environment 33, 2111-2114.

SCAQMD, 1966. Modeling an attainment demonstrations, South Coast Air Quality Management District, Diamond Bar, California.

Schauer, J. J., Kleeman, M. J., Cass, G. R., and Simoneit, B. R. T., 1999. Measurement of emissions from air pollution sources 2. C1 through C30 organic

compounds from medium duty diesel trucks, Environmental Science and Technology 33, 1578-1587.

Schauer, J. J., Rogge, W. F., Hildemann, L. M., Mazurek, M. A., Cass, G. R., 1995. Source apportionment of airborne particulate matter using organic compounds as tracers. Atmospheric Environment 30, 3837-3855.

Schlesinger, R. B., 1990. The interaction of inhaled toxicants with respiratory tract clearance mechanisms, Critical Reviews in Toxicology 20, 257-286.

Schmid, H., Pucher, E., Ellinger, E., Biebl, P., and Puxbaum, H., 2001. Decadal reductions of traffic emissions on a transit route in Austria—results of the Tauern tunnel experiment 1997. Atmospheric Environment 35, 3585-3593.

Schult, I., Feichter, J., and Cooke, W. F., 1997. Radiative forcing by BC and sulfate effect of black carbon and sulfate aerosols on the global radiation budget. Journal of Geophysics Research 102(D25), 30107-30118.

Schwartz, J., Dockery, D. W., and Neas, L. M., 1996. Is daily mortality associated specifically with fine particles? Journal of Air & Waste Management Association 46, 927-939.

Seaton, A., MacNee, W., Donaldson, K., and Godden, D., 1995. Particulate air pollution and acute health effects. The Lancet 345, 176-178.

Seinfeld, J. H. and Pandis, S. N., 1998. Atmospheric chemistry and physics from air pollution to climate change. Wiley Interscience, New York, 337-407.

Seinfeld, J. H., 1986. Atmospheric chemistry and physics of air pollution. Wiley, New York, 378-382.

Shah, S. D., Cocker III, D. R., Miller, J. W., and Norbeck, J. M., 2004. Emission rates of particulate matter and elemental and organic carbon from in-use diesel engines. Environmental Science and Technology 38, 2544-2550.

Shen, S., Jaques, P. A., Zhu, Y. F. Geller, M. D., and Sioutas, C., 2002. Evaluation of the SMPS–APS system as a continuous monitor for measuringPM2.5, PM10 and coarse (PM2.5-10) concentrations. Atmospheric Environment 36, 3939-3950.

Shi, J. P., Evans, D. E., Khan, A. A., and Harrison, R. M., 2001. Sources and concentration of nanoparticles (<10 nm diameter) in the urban atmosphere. Atmospheric Environment 35, 1193-1202.

Solomon, P. A., Fall, T., Salmon, L., Cass, G. R., Gray, H. A., and Davidson, A., 1989. Chemical characteristics of PM_{10} aerosols collected in the Los Angeles Area. Journal of Air Pollution Control Association 39, 154-163.

Song, X. H., Polissar, A. V., and Hopke, P. K., 2001. Sources of fine particle composition in the northeastern US. Atmospheric Environment 35, 5277-5286.

Soutar, A., Watt, M., Cherrie, J. W., and Seaton, A., 1999. Comparison between a personal PM_{10} sampling head and the tapered element oscillating microbalance (TEOM) system. Atmospheric Environment 33, 4373-4377.

Stanier, C. O., Khlystov, A. Y., and Pandis, S. N., 2004. Ambient aerosol size distributions and number concentrations measured during the Pittsburgh Air Quality Study (PAQS). Atmospheric Environment 38, 3275-3284.

Stein, S. W., Turpin, B. J., Cai, X. P., Huang, P. F., and Mcmurry, P. H., 1994. Measurements of relative humidity-dependent bounce and density for atmospheric particles using the DMA-impactor technique. Atmospheric Environment 28(10), 1739-1746.

Stern, J. E., Flagan, R. C., Grosjean, D., and Seinfeld, J. H., 1987. Aerosol formation and growth in atmospheric aromatic hydrocarbon photooxidation. Environment Science Technology 21, 1224-1231.

Streets, D. G., Bond, T. C., Carmichael, G. R., Fernandes, S. D., Fu, Q., He, D., Klimont, Z., Nelson, S. M., Tsai, N. Y., Wang, M. Q., Woo, J. H., and Yarber, K. F., 2003. An inventory of gaseous and primary aerosol emissions in Asia in the year 2000. Journal of Geophysics Research 108(D21) 8809, doi:10.1029/2002JD003093.

Streets, D. G., Bond, T. C., Lee, T., and Jang, C., 2004. On the future of carbonaceous aerosol emissions. Journal of Geophysics Research 109(D24212), doi:10.1029/2004JD004902.

Streets, D. G., Gupta, S., Waldhoff, S. T., Wang, M. Q., Bond, T. C., and Bo, Y. Y., 2001. Black carbon emissions in China. Atmospheric Environment 35, 4281-4296.

Tanner, P. A. and Law, P. T., 2002. Effects of Synoptic Weather Systems Upon the Air Quality in an Asian Megacity. Water, Air, & Soil Pollution 136(1-4), 105-124.

Tanner, P. A., 1999. Relationships Between Rainwater Composition and Synoptic Weather Systems Deduced from Measurement and Analysis of Hong Kong Daily Rainwater Data. Journal of Atmospheric Chemistry 33(3), 219-240.

Tanner, R. L., Bairai, S. T., Olszyna, K. J., Valente, M. L., and Valente, R. J., 2005. Diurnal patterns in $PM_{2.5}$ mass and composition at a background, complex terrain site. Atmospheric Environment 39(21), 3865-3875.

Taylor, K. E. and Penner, J. E., 1994. Response of the climate system to atmospheric aerosols and greenhouse gases. Nature 369, 734-737.

Taylor, S. R. and McLennan, S. M., 1995. The geochemical evolution of the continental crust. Reviews of Geophysics 33, 241-265.

The Annual Air Quality Report, 2004. Prepared by Environmental Protection Department.

The Annual Traffic Census, 2005. Prepared by traffic and transport survey division, the government of the Hong Kong special administrative region.

Turpin, B. J. and Huntzicker, J. J., 1991. Los Angeles summer midday particulate carbon: primary and secondary aerosol. Environmental Science and Technology 25, 1788-1793.

Turpin, B. J. and Huntzicker, J. J., 1994. Investigation of organic aerosol sampling artifacts in the Los Angeles Basin. Atmospheric Environment 28(19), 3061-3071.

Turpin, B. J. and Huntzicker, J. J., 1995. Identification of secondary organic aerosol episodes and quantitation of primary and secondary organic aerosol concentrations during SCAQS. Atmospheric Environment 29(23), 3527-3544.

Turpin, B. J. and Lim, H. J., 2001. Species contributions to PM2.5 mass concentrations: revisiting common assumptions for estimating organic mass. Aerosol Science and Technology 35, 602-610.

U.S. Environmental Protection Agency, 1989. An acid aerosols issue paper: Health effects and aerometrics, U.S. Environmental Protection Agency, Research Triangle Park, NC.

Vallius, M. J., Ruuskanen, J., Mirme, A., and Pekkanen, J., 2000. Concentrations and estimated soot content of PM_1, $PM_{2.5}$, and PM_{10} in a Subarctic urban atmosphere. Environmental Science and Technology 34, 1919-1925.

Vasiliou, J. G., Sorensen, D., McMurry, P. H., 1999. Sampling at controlled relative humidity with a cascade impactor. Atmospheric Environment 33, 1049-1056.

Van der Wal, J. T. and Janssen, L. H. J. M., 2000. Analysis of spatial and temporal variations of PM_{10} concentraitons in the Netherlands using Kalman filtering. Atmospheric Environment 34, 3675-3687.

Van Vaeck, L. and Van Cauwenberghe, K., 1978. Cascade impactor measurements of the size distribution of the major classes of organic pollutants in atmospheric particulate matter. Atmospheric Environment 12, 2229-2239.

Vanderpool, R., Hanley, T., Dimmick, F., and Hunike, E., 2005. Multi-site evaluations of candidate methodologies for determining coarse particulate matter (PM_c) concentrations. Updated Report Regarding Second-Generation and New $PM_{10-2.5}$ Samplers. USEPA.

Vignati, E., Berkowicz, R., Palmgren, F., Lyck, E. and Hummelshj, P., 1999. Transformation of size distribution of emitted particles in streets. The Science of Total Environment 235, 37-49.

Wall, S. M., John, W., and Ondo, J. L., 1988. Measurement of aerosol size distributions for nitrate and major ionic species. Atmospheric Environment 22, 1649-1656.

Wang, J. T., Lam, K. S., Xie, M., Wang, X. M., Carmichael, G., and Li, Y. S., 2006. Integrated studies of a photochemical smog episode in Hong Kong and regional transport in the Pearl River Delta of China. TELLUS (B) 58 (1), 31-40.

Wang, T., Lam, K. S., Chan, L. Y., and Lee, A. S. Y., 1997. Trace gas measurements in coastal Hong Kong during the PEM-West B. Journal of Geophysics Research 102, 28575-28588.

Wang, T., Vincent, T. F., Lam, K. S., Kok, G. L., and Harris, J. M., 2001. The characteristics of ozone and related compounds in the boundary layer of the South China coast: Temporal and vertical variations during autumn season. Atmospheric Environment 35, 2735-2746.

Wang, T., 2003. Study of visibility reduction and its causes in Hong Kong (Tender Ref. AS 01-286), Final report to The Environmental Protection Department of HKSAR.

Wang, T., Ding, A. J., Blake, D. R., Zahorowski, W., Poon, C. N., and Li, Y. S., 2003. Chemical characterization of the boundary layer outflow of air pollution to Hong Kong during February-April 2001. Journal of Geophysics Research 108 (D20), 8787, doi:10.1029/2002JD003272.

Wang, W. G., Lyons, D. W., Clark, N. N., and Gautam, M., 2000. Emissions from nine heavy trucks fueled by diesel and biodiesel blend without engine modification. Environmental Science and Technology 34, 933-939.

Watson, J. G., 1979. Chemical element balance receptor model methodology for sources of fine and total suspended particulate matter in Portland, Oregon. Ph.D. Thesis, Oregon Graduate Center.

Watson, J. G., Robinson, N. F., Chow, J. C., Henry, R. C., Kim, B. M., Pace, T. G., Meyer, E. L. and Nguyen, Q., 1990. The USEPA/DRI chemical mass balance receptor model, CMB 7.0. Environmental Software 5, 38-49.

Watson, J. G., Chow, J. C., Lu, Z., Fujita, E. M., Loweothal, D. H. and Lawson, D. R., 1994a. Chemical mass balance apportionment of PM during the Southern California Air Quality Study. Aerosol Science and Technology 21, l-36.

Watson, J. G., Chow, J. C., Lowenthal, D. H., Pritchett, L. C., Frazier, C. A., Neuroth, G. R., Robbins, R., 1994b. Differences in the carbon composition of source profiles for diesel- and gasoline-powered vehicles. Atmospheric Environment 28(15), 2493-2505.

Watson, J. G., Chow, J. C., Frazier, C. A., 1999. X-ray fluorescence analysis of ambient air samples. In Elemental Analysis of Airborne Particles, Vol. 1, S. Landsberger and M. Creatchman, Eds. Gordon and Breach Science Amsterdam, 67-96.

Watson, J. G. and Chow, J. C., 2001a. Source characterization of major emission sources in the imperial and Mexicali valleys along the US/Mexico border. Science of the Total Environment 276(1-3), 33-47.

Watson, J. G. and Chow, J. C., 2001b. Estimating middle-, veighborhood-, and urban-scale contributions to elemental carbon in Mexico city with a rapid response Aethalometer. Journal of Air & Waste Management Association 51, 1522-1528.

Watson, J. G. and Chow, J. C., 2002a. Comparison and evaluation of in-situ and filter carbon measurements at the Fresno Supersite. Journal of Geophysics Research doi:10.1029/2001JD000573.

Watson, J. G. and Chow, J. C., 2002b. A wintertime $PM_{2.5}$ episode at the Fresno, CA, Supersite. Atmospheric Environment 36, 465-475.

Watson, J. G., et al., 2004. Protocol for applying and validating the CMB model for $PM_{2.5}$ and VOC. Prepared for: C. Thomas Coulter and Charles W. Lewis, Project Officers U.S. Environmental Protection Agency, Contract No. 5D1808NAEX.

Watson, J. G., Chow, J. C., Lowenthal, D. H., Kreisberg, N. M., Hering, S. V. and Stolzenburg, M. R., 2006. Variations of nanoparticle concentrations at the Fresno Supersite. The Science of Total Environment 358(1-3), 178-87.

Weingartner, E., Keller, C., Stahel, W. A., Burtscher, H., and Baltensperger, U., 1997. Aerosol emission in a road tunnel. Atmospheric Environment 31(3), 451-462.

Whitby, K. T., 1978. The physical characteristics of sulfur aerosols. Atmospheric Environment 12, 135-159.

WHO, World Health Organization, 2000. Guidelines for Air Quality; Geneva.

Willeke, K. and Whitby, K. T., 1975. Atmospheric aerosol: size distribution interpretation. Journal of the Air Pollution Control Association 25(5), 529-534.

Willis, R. D., 2000. Workshop on Unmix and PMF as applied to $PM_{2.5}$. EPA 600-A-00-048.

Xie, Y. L., Hopke, P. K., Paatero, P., Barrie, L. A., and Li, S. M. J., 1999. Identification of source nature and seasonal variations of Arctic aerosol by Positive Matrix Factorization. Journal of Atmospheric Science 56, 249-260.

Yao, X. H., Fang, M., and Chan, C. K., 2001. Experimental study of the sampling artifact of chloride depletion from collected sea salt aerosols. Environmental Science and Technology 35 (3), 600-605.

Yu, J. Z., Tung, J. W. T., Wu, A. W. M., Lau, A. K. H., Louie, P. K. K., and Fung, J. C. H., 2004a. Abundance and seasonal characteristics of elemental and organic carbon in Hong Kong PM_{10}. Atmospheric Environment 38(10), 1511-1521.

Yu, J. Z., Yang, H., Zhang, H. Y. and Lau, A. K. H., 2004b. Size distributions of water-soluble organic carbon in ambient aerosols and its size-resolved thermal characteristics. Atmospheric Environment 38(7), 1061-1071.

Yuan Z. B., Lau A. K. H., Zhang H. Y., Yu J. Z., Louie, P. K. K., Fung, J. C. H., 2006. Identification and spatiotemporal variations of dominant PM_{10} sources over Hong Kong. Atmospheric Environment 40(10), 1803-1815.

Zanobetti A., Schwartz. J., Samoli E., Gryparis A., Touloumi G., Peacock J., Anderson

R. H., Tertre A. L., Bobros J., Celko M., Goren A., Forsberg B., Michelozzi P., Rabczenko D., Hoyos S. P., Wichmann H. E., and Katsouyanni K., 2003. The temporal pattern of respiratory and heart disease mortality in response to air pollution. Environmental Health Perspectives 111, 1188-1193.

Zhang, K. M. and Wexler, A. S., 2004. Evolution of particle number distribution near roadways-Part I: analysis of aerosol dynamics and its implications for engine emission measurement. Atmospheric Environment 38, 6643-6653.

Zhang, Q., Canagaratna, M. R., Jayne, J. T., Worsnop, D. R., and Jimenez, J. L., 2005. Time- and size-resolved chemical composition of submicron particles in Pittsburgh: Implications for aerosol sources and processes. Journal of Geophysics Research 110(D07S09), doi:10.1029/2004JD004649.

Zhang, X. Q., Turpin, B. J., McMurry, P. H., Hering, S. V., and Stolzenburg, M. R., 1994. Mie Theory evaluation of species contributions to wintertime visibility reduction in Grand Canyon. Journal of Air Waste Management Association 44, 153-162.

Zheng, M., Fang, M., Wang, F., and To, K. L., 2000. Characterization of the solvent extractable organic compounds in $PM_{2.5}$. Atmospheric Environment 33, 783-795.

Zhuang, H., Chan, C. K., Fang, M., and Wexler, A. S., 1999a. Size distributions of particulate sulfate, nitrate, and ammonium at a coastal site in Hong Kong. Atmospheric Environment 33, 843-853.

Zhuang, H., Chan, C. K., Fang M., and Wexler, A. S., 1999b. Formation of nitrate and non-sea-salt sulfate on coarse particles. Atmospheric Environment 33, 4223-4233.

Appendix A: List of Abbreviations

BC	Black Carbon
CMB	Chemical Mass Balance
CPC	Condensation Particle Counter
D_p	Aerodynamic Diameter of Particles
DV	Diesel-fueled Vehicles
EC	Elemental Carbon
EF	Emission Factors
EPA	Environmental Protection Agency
FID	Flame Ionization Detector
HK	Hong Kong
HKEPD	Hong Kong Environment Protection Department
HKUST	Hong Kong University of Science and Technology
HT	Hok Tsui
IC	Ion Chromatography
IMPROVE	Interagency Monitoring of Protected Visual Environments
KT	Kwun Tong
LMC	Lok Ma Chou
MDL	Minimum Detection Limit
MK	Mong Kok
MOUDI	Micro-Orifice Uniform Deposit Impactor
NAAQS	National Ambient Air Quality Standards

OBC	Optical Black Carbon
OC	Organic Carbon
OM	Organic Material
OPC	Optical Particle Counter
PAH	Polycyclic Aromatic Hydrocarbons
PM	Particulate Matter
PMF	Positive Matrix Factorization
PRD	Pearl River Delta
PSCF	Potential Source Contribution Function
PU	Hong Kong Polytechnic University
QC	Quality Control
RSP	Respirable Suspended Particle or PM_{10}
SMPS	Scanning Mobility Particle Sizer
SOA	Secondary Organic Aerosol
TC	Tung Chung
TEOM	Tapered Element Oscillating Microbalance 1400a $PM_{2.5}$ Monitor
TOR	Thermal Optical Reflectance
TOT	Thermal Optical Transmittance
TSP	Total Suspended Particle
TW	Tsuen Wan
WHO	World Health Organization
WSOC	Water-soluble Organic Compounds
XRF	X-ray Fluorescence

Appendix B: Photos of Sampling Equipments & Monitors

Photo 3.1 PU Supersite

Photo 3.2 Hong Chong road

Photo 3.3 Background station (HT)

Photo 3.4 URG ABC3000 sampler

Photo 3.5 RP2025 sequential sampler

Photo 3.6 MOUDI 110 impactor

Photo 3.7 Nano-MOUD 115 impactor

Photo 3.8 Kimoto SPM-613D monitor

Photo 3.9 SMPS3936

Photo 3.10 PMS OPC 1003

Photo 3.11 Aethalometer AE-42 at HT

Photo 3.12 DRI particulate sampler

Photo 3.13 DustTrak air monitors